Effect of Groundwater on Landslide Triggering

PAR

Cornelia Sara BRÖNNIMANN

ÉCOLE POLYTECHNIQUE
FÉDÉRALE DE LAUSANNE

Suisse
2011

Abstract

Landslides belong to the most important natural hazards in all mountainous regions. It is well-known that water is one of the major triggers of landslides. Numerous landslide studies discuss different effects that water may have on slope stability: decreasing suction, rising groundwater table and subsequent increasing pore water pressure, groundwater exfiltration from the bedrock, seepage erosion, hydraulic uplift pressure from below the landslide, and influence of water on the plasticity of the landslide. Geological and hydrogeological characteristics such as permeability and saturation of the landslide and the substratum determine to a large extent, which of those processes are dominant in causing triggering.

The first objective of this study is to investigate the origin, flow paths and effect of groundwater in three different slopes and landslides in Switzerland. These are 1) an artificially triggered shallow landslide in Rüdlingen located in the distal Molasse in the North of Switzerland; 2) the active Pont Bourquin landslide located in a tectonically complex zone in the Western Swiss Prealps; and 3) the Rufiberg, a slope prone to shallow landslides located in the Subalpine Molasse in Central Switzerland. Hydrochemical analyses, groundwater monitoring in observation wells and geophysical profiling are found to be promising methods to trace the origin and flow paths of groundwater in these three slopes and landslides. Based on hydrogeological, hydrochemical and geophysical data, three conceptual hydrogeological models are constructed which show the different effects groundwater may have on landslide triggering: Large joints in the bedrock are draining the loose soil cover in Rüdlingen, which has a stabilizing effect on the slope. At Pont Bourquin, groundwater flow through the fractured bedrock and the formation of perched groundwater in the heterogeneous highly-plastic landslide mass is found to be crucial for the triggering. And at Rufiberg, artesian or uplift pressure that builds up in the bedrock below the potential landslide may influence the triggering. These different case studies show how diverse and complex the hydrogeological pattern in landslides may be.

So far, no classification system exists that is based on the dominant hydrogeological characteristics of landslides and slopes prone to landslides. Therefore, the second objective of this study is to develop a classification for the hydrogeological categorisation of landslides and slopes prone to landslides. This classification is based on the parameter "permeability contrast" between the landslide and the substratum (hydrogeological predisposition) and the time dependent parameter "saturation" of the different geological layers.

The classification provides a tool to describe the hydrogeology of landslides and to evaluate the potential hydrogeological triggering mechanisms. It can be applied to illustrate the evolution of the saturation of the different geological layers during rainfall and snowmelt. This classification may be applied to estimate, whether a slope is in a critical equilibrium stage depending on the saturation. In the present study, the classification is applied to the three landslides and slopes investigated (Pont Bourquin, Rüdlingen and Rufiberg) and on seven other well-known landslides

in the Alps.

The classification supports the understanding of complex hydrogeological processes occurring in landslides. It is a framework for the construction of conceptual hydrogeological models of landslides and can be applied as a tool for planning further investigations, numerical modelling and mitigation measures.

Zusammenfassung

Rutschungen gehören zu den meist gefürchteten Naturgefahren in gebirgigen und hügeligen Regionen. Wasser ist einer der häufigsten Auslöser für Rutschungen. Die verschiedenen Auswirkungen, welche das Wasser auf die Stabilität eines Hanges haben kann, wurden in der Literatur ausführlich diskutiert: Verminderte Saugspannung, steigender Grundwasserspiegel und dadurch erhöhter Porenwasserdruck, Exfiltration aus dem Fels, Strömungsdruck und innere Erosion, Aufbau von Wasserüberdruck unter der Rutschung und Mechanismen im Zusammenhang mit einem hohen Plastizitätsindex. Geologische und hydrogeologische Eigenschaften wie die Durchlässigkeit und Sättigung der Rutschmasse und des Felsuntergrundes bestimmen in grossem Masse, welcher dieser Mechanismen für die Auslösung der Rutschung dominant ist.

Das erste Ziel dieser Doktorarbeit ist, den Ursprung, die Fliesswege und die Auswirkungen des Grundwassers in drei verschiedenen Hängen und Rutschungen in der Schweiz detailliert zu untersuchen. Dies sind 1) eine künstlich ausgelöste flachgründige Rutschung in Rüdlingen (SH) in der distalen Molasse im Norden der Schweiz, 2) die aktive Rutschung Pont Bourquin (VD), welche in einer tektonisch komplexen Zone in den westlichen Schweizer Präalpen liegt und 3) der Rufiberg (SZ), ein Hang der anfällig ist für Rutschungen in der Subalpinen Molasse in der Zentralschweiz. Hydrochemische Analysen, kontinuierliche Überwachung des Grundwassers in Bohrlöchern und geophysikalische Profile erweisen sich als hilfreiche Methoden, um den Ursprung des Wassers und seine Fliesswege in diesen Hängen und Rutschungen aufzuzeigen. Basierend auf diesen Untersuchungen wurden drei konzeptuelle hydrogeologische Modelle erstellt, welche verschiedene hydrogeologische Charakteristiken aufzeigen: In Rüdlingen haben grosse Klüfte im Fels eine drainierende Wirkung auf das Lockergestein. In Pont Bourquin ist das Grundwasser, welches durch den tektonisch geprägten Fels und die mit Rissen durchzogene Rutschmasse fliesst, sowie das lokal gespannte Grundwasser in der heterogenen hoch-plastischen Rutschmasse entscheidend für die Instabilität. Und auf dem Rufiberg bildet sich wegen des hohen Felswasserspiegels ein Überdruck unter der potentiellen Rutschung. Diese drei Fallstudien zeigen, wie vielfältig und komplex hydrogeologische Prozesse in Rutschungen sein können.

Bis heute existiert keine Klassifikation, welche auf den dominanten hydrogeologischen Eigenschaften von Rutschungen und potentiell instabilen Hängen aufgebaut ist. Deshalb ist das zweite Ziel dieser Doktorarbeit, eine Klassifikation für die hydrogeologische Kategorisierung von Rutschungen und potentiell instabilen Hängen zu erstellen. Die Klassifikation basiert auf dem Parameter "Permeabilitätskontrast" zwischen der Rutschung und dem darunterliegenden Fels (hydrogeologische Prädisposition) und auf dem zeitabhängigen Parameter "Sättigung" der verschiedenen geologischen Schichten.

Die entwickelte Klassifikation ist ein Instrument zur Beschreibung der Hydrogeologie von Rutschungen und zur Abschätzung der potentiellen hydrogeologischen Auslösemechanismen. Sie findet Anwendung, um die Entwicklung der Sättigung während Regenfall und Schneeschmelze zu illustrieren und um abzuschätzen, ob sich ein Hang je nach dem Sättigungsgard in einem kri-

tischen Stabilitätszustand befindet. Im Rahmen dieser Doktorarbeit wird die Klassifikation für die drei Fallbeispiele Rüdlingen, Pont Bourquin und Rufiberg sowie für sieben weitere bekannte Rutschungen in den Alpen angewendet.

Diese Klassifikation unterstützt das Verständnis der hydrogeologischen Prozesse, welche in Rutschungen ablaufen. Sie ist ein Instrument zur Konstruktion von hydrogeologischen konzeptuellen Modellen, schafft eine Grundlage für Numerische Modellierungen und ist ein Hilfsmittel für die Planung von weiterführenden Untersuchungen und Massnahmen gegen Rutschungen.

Schlüsselwörter: Hangrutschungen, Auslösemechanismen, Grundwasser, Permeabilitätskontrast, Klassifikation.

Résumé

Les glissements de terrain font partie des dangers naturels les plus graves dans les régions de montagnes. L'eau est connue pour être un déclencheur principal des glissements. Les différentes influences de l'eau sur la stabilité d'une pente, tels que la diminution de la succion, l'augmentation du niveau d'eau et des pressions interstitielles, l'exfiltration d'eau du rocher, la surpression hydraulique sous le glissement et l'effet de l'eau sur la plasticité sont bien décrits dans la littérature. Les caractéristiques géologiques et hydrogéologiques, comme la perméabilité et la saturation de la masse glissée et du substratum, déterminent quels sont les mécanismes importants pour le déclenchement.

Le premier objectif de cette étude est d'examiner l'origine et les effets de l'eau souterraine dans trois différents versants et glissements en Suisse qui sont 1) un glissement peu profond déclenché artificiellement, situé à Rüdlingen dans la Molasse distale au Nord de la Suisse; 2) le glissement actif au lieu-dit Pont Bourquin, situé dans une zone tectoniquement complexe des Préalpes occidentales de la Suisse; et 3) Rufiberg, un versant sensible aux glissements de terrain situé dans la Molasse subalpine en Suisse centrale. Des analyses hydrochimiques, un suivi de la nappe phréatique dans des forages et des profils géophysiques s'avèrent des méthodes utiles pour montrer l'origine et l'écoulement de l'eau souterraine dans ces versants et glissements. Basés sur ces investigations, trois modèles conceptuels, montrant chacun des caractéristiques hydrogéologiques particulières, sont élaborés. À Rüdlingen, de grandes fractures dans le rocher drainent les roches meubles ce qui représente un effet plutôt stabilisant. À Pont Bourquin, les écoulements de l'eau souterraine dans le rocher tectonisé et dans la masse glissée, la formation de nappes perchées dans le glissement ainsi que la haute plasticité du glissement sont déterminants pour le déclenchement. Enfin, à Rufiberg, une surpression se produit dans les fractures du rocher sous le glissement potentiel. Ces comportements différents montrent la variété et la complexité de la structure hydrogéologique dans les glissements de terrain.

Jusqu'à aujourd'hui, il n'existait aucune classification basée sur les caractéristiques hydrogéologiques dominantes des glissements et versants potentiellement instables. Pour cette raison, le deuxième objectif de ce travail est d'élaborer une classification pour la catégorisation hydrogéologique des glissements et des versants potentiellement instables. Cette classification respecte le contraste des perméabilités entre le glissement et le substratum (prédisposition hydrogéologique) et la saturation des différentes unités géologiques, variable dans le temps.

Cette classification est un outil pour décrire l'hydrogéologie des glissements et les mécanismes de déclenchement potentiels. Elle peut être utile pour décrire l'évolution de l'hydrogéologie d'un glissement pendant un événement de pluies ou de fonte des neiges. De plus, la classification est un moyen d'évaluer si la stabilité d'une pente est dans un état critique selon la saturation. Dans le travail présenté ici, la classification a été appliquée aux trois cas d'études Rüdlingen, Pont Bourquin et Rufiberg et pour sept autres glissements connus dans les Alpes.

Cette classification permet une meilleure compréhension des processus hydrogéologiques observés dans les glissements. Dans ce sens, la classification présente une base pour l'élaboration des modèles conceptuels avant la phase de modélisation numérique. De plus, c'est un outil permettant d'évaluer les mécanismes de déclenchement potentiels, ce qui est particulièrement important pour la planification des mesures contre les glissements de terrain.

Mots-clefs: Glissement de terrain, mécanisme de déclenchement, eau souterraine, contraste de perméabilité, classification.

Acknowledgement

Contents

Chapter 1

Introduction

1.1 Objectives

Landslides are one of the most widespread natural hazard on earth (Kjekstad and Highland, 2009). The *Center for Research on the Epidemiology of Disasters (CRED)* reported that 17% of fatalities due to natural hazards are caused by landslides (http://www.cred.be). Each year landslides cause thousands of deaths and injuries and billions of dollars in economic losses. For example in the countries Switzerland, Italy, France, and Austria the annual costs are estimated to 1-5 billion US Dollars (Kjekstad and Highland, 2009). In August 2005, heavy rainfalls triggered over 5'000 landslides in Switzerland, which caused damages of 100 million of Swiss Francs (Bezzola and Hegg, 2007). 3.7 million km^2 and 5% of the world population (300 million people) are exposed to landslides, whereof 66 million people live in high risk areas (Dilley, 2005).

It seems that the occurrence of landslide disasters is increasing. This is a result of the increased vulnerability and exposure of the population and infrastructure due to growing urbanization. More extensive human interaction, uncontrolled land-use and enhanced forest clearing increase the susceptibility of surface soil to instability (Sidle and Ochiai, 2006). Furthermore, the actual intensity, frequency and location of the hazard areas may change over the globe as a result of changing precipitation patterns and migration due to climate change. More frequent high intensity rainfall events and higher winter precipitations may increase the risk for landslides (Parriaux, 2011).

Precipitation, subsequent infiltration and groundwater flow are some of the most important landslide triggering factors (Johnson and Sitar, 1990; Leroueil et al., 1996; Noverraz et al., 1998; Van Asch et al., 1999). In 2007, 89.6 % of world-wide fatalities were the result of landslides caused by intense and/or prolongated precipitation (Petley, 2008). Increasing pore water pressure decreases the shear strength of the soil which may lead to slope failure (Iverson, 2000; Van Asch et al., 2007). Many slope stability studies concentrate on the saturated and partly saturated near-surface soil and assume the bedrock to be an impermeable boundary (Uchida et al., 2003). This might be true in certain cases, but depending on the bedrock geology, the degree of fracturing and weathering, and saturation, the bedrock might act as a sink or as a source for groundwater in the overlying landslide and should therefore be taken into account for slope stability analyses. Some studies show that especially the altered bedrock between the fresh bedrock and the unconsolidated sediment may play an important role for infiltration-exfiltration processes (Montgomery et al., 1997; Onda et al., 2004).

Landslide triggering mechanisms related to hydrogeology are very complex. Every landslide has a unique groundwater flow pattern. It is often difficult to trace the origin of groundwater and

the water flow paths in landslides. This is because on the one hand hydrogeological processes take place in the underground and are hardly accessible. On the other hand, the permeability of the landslide mass, which controls to a large extent the groundwater flow, may be very heterogeneous (Guglielmi et al., 2002). Preferential flow paths and local formation of confined and perched aquifers complicate the hydrogeology of a landslide (Debieche et al., 2011). Furthermore, the groundwater flow pattern may change in time because of landslide activity, formation of cracks and increased permeability due to soil saturation. Because of this complexity, still many uncertainties exist about the hydrological processes occurring in landslides.

The first aim of this work is to investigate the hydrogeology of three different landslides and slopes and to construct a conceptual model of each of these three landslides. For this purpose, different approaches are used: (1) a real scale triggering experiment,(2) monitoring of an active landslide and (3) monitoring of a slope prone to landsliding. The three case studies were carried out in three different regions of Switzerland:

1. Slope scale landslide triggering experiment in Rüdlingen, Canton Schaffhausen: In this area, the horizontally layered Molasse sediment composed of fractured sandstone and marlstone is overlaid by weathered bedrock and silty colluvium. The aim of this study is to understand the hydrogeological reaction of the slope to heavy rainfall. Is groundwater mainly percolating through unconsolidated sediment, flowing along bedrock discontinuities or through permeable bedrock layers?

2. Monitoring of the active Pont Bourquin landslide, Canton Vaud: The different lithologies in this tectonically complex zone between the Prealps and the Helvetic nappes are Flysch, cellular dolomite, and Aalenian black shale overlaid by low permeable moraine. The main interest in this study is to trace the origin and groundwater flow paths in the landslide (exfiltration from the bedrock and lateral groundwater flow).

3. Investigation of a slope prone to shallow landslides at Rufiberg, Canton Schwyz: The Subalpine Molasse in this area is composed of fractured conglomerate, sandstone, and marlstone overlaid by low permeable clayey silt. The main focus of this study is to find out if overpressure in the fractured bedrock below the landslide may be a triggering mechanism.

For the three studies, the role of the substratum is investigated and the potential hydrogeological triggering mechanisms are discussed: Is the bedrock draining or feeding the landslides? What are the effects of groundwater on the landslide triggering? Furthermore, the applied field methods to trace the origin of groundwater in the investigated landslides are evaluated. These case studies illustrate nicely the diversity of hydrogeological processes occurring in landslides (infiltration, exfiltration, groundwater flow along preferential paths, and the formation of local perched and confined water bodies) and resulting triggering mechanism.

The second aim of the present study is to create a classification that takes into account dominant hydrogeological characteristics (permeability contrasts and saturation) and potential triggering mechanisms for the categorisation of landslides and slopes prone to landslides and for creating conceptual models. So far, no classification system exists which is based on the hydrogeological characteristics and mechanisms of landslids.

Finally, the three investigated landslides and slopes are put in the framework of the developed hydrogeological classification. Additionally, the classification is applied to several other well-known landslides which are described based on literature.

1.2   Content

Chapter 2 gives an overview of the state of the art in hillslope hydrology and hydrogeology as well as landslide research and slope stability analyses. The concept and the application of the hydrogeological classification for landslides is explained in Chapter 3. Chapter 4 describes the applied field methods. In the following three chapters, the data from the case studies Rüdlingen (Chapter 5), Pont Bourquin (Chapter 6) and Rufiberg (Chapter 7) is presented and discussed and put in the framework of the hydrogeological classification. In Chapter 8, the classification is applied for several other landslides which are described based on literature work. Finally, the application of the classification system is discussed in Chapter 9 and the findings of the three field case studies and the additional landslide studies are summarised and compared.

1.3   Context

The landslide triggering experiment in Rüdlingen and the investigations on the Rufiberg slope were carried out within the framework of the four-year project *Triggering of Rapid Mass Movements in Steep Terrain (TRAMM)* founded by the *Competence Center Environment and Sustainability (CCES)* (2006-2010). The monitoring of the Pont Bourquin landslide was a collaboration with the *Institute of Geomatics and Risk Analysis, University of Lausanne (IGAR)* and the *Laboratory of Internal Geophysics and Tectonophysics, University Joseph Fourier, Grenoble (LGIT)* in the framework of the *Mountain Risks-Project*, a *Marie Curie Research Training Network*. Figure 8.1 shows the location of the three case studies.

1.4   Definitions and notations

In this section, some technical terms, which are frequently used in the present sudy, are listed. For the definitions, it is referred to the corresponding sections in which the terms are described.

Bedrock exfiltration:	see Sections 2.6 and 3.5
Criticality:	see Section 3.7
Landslide:	see Section 2.3.1
Percolation:	see "seepage"
Pipes, piping:	see Section 2.5.4
Piston flow:	"Old" groundwater that is pushed out of pores by infiltrating "new" precipitation water.
Plasticity:	see Section 2.5.7
Predisposing factor:	see Section 2.3.1
Seepage:	see Section 2.5.3
Soil:	Section 3.3.1
Substratum:	Immobile formation below the landslide, in most cases the bedrock.
Subsurface storm flow:	see Section 2.2.2
Trigger:	see Section 2.3.1
Triggering mechanism:	see Section 2.5
Unconsolidated sediment:	see Section 3.3.1
Weathered bedrock:	see Section 3.3.3

In the following list, the parameters used in the present work are explained.

A Section [m^2], used in Darcy's law.

c' Effective cohesion [kPa]. Cohesion is the strength in the soil (or rock) that keeps the particles together independent from the normal force. Time, weathering and desiccation contribute to true cohesion (Lambe and Whitman, 1979). Cohesion is caused by electrostatic forces between clay particles and cementation due to secondary mineralization between soil clasts. Apparent cohesion can be caused by the strength of interpenetrating roots of plants or by capillarity due to moisture. Especially in coarse grained soil suction causes apparent cohesion which is lost when the soil is saturated.

e Void ratio [-], $e = V_v/V_s$ (see Figure 1.2).

F_s Seepage forces [Newton], $F_s = V\gamma_w i$.

g Gravitational acceleration, 9.81 m/s2.

h Hydraulic potential (or head potential, hydraulic head, piezometric head) [m], $h = \psi + Z$. The hydraulic potential is usually measured as height of the groundwater level. The hydraulic potential is the gravitational potential of water expressed in energy per unit weight.

i Hydraulic gradient [-], $i = \frac{dh}{L}$. If i = 1 (vertical downwards flow) then it can be assumed that k is equal the apparent velocity v_a. But in practice, $i < 0.1$ and $k < 10$ m/d so that $v < 1$ m/d.

K Permeability [m^2], $K = \frac{Q\eta l}{\Delta p A} = \frac{k\eta}{\rho g}$. The permeability depends on the density, dynamic viscosity and temperature of the fluid and the size, shape and distribution of pores and fractures of the soil or rock. The permeability is a constant for a specific soil or rock type and has to be distinguished from the hydraulic conductivity k.

k Hydraulic conductivity [m/s], $k = \frac{QL\rho g}{A\Delta p} = \frac{vL}{\Delta h}$. The hydraulic conductivity is a property of soil and rock that describes the resistance against a through-flowing fluid. It is an important parameter because it controls the water flow in slopes. The hydraulic conductivity is the proportionality constant in Darcy's law (see Figure 1.1): $v = -k\frac{dh}{L}$ or $Q = -kAi$. Darcy's law is an empirical law that says that the flux Q flowing through a section A is directly proportional to the hydraulic gradient **i**. The hydraulic conductivity depends on the soil's saturation and thus is a function of the pressure head ψ. Figure 1.3 shows this relationship between k and ψ for uniform sand, silty sand and silty clay (Modified after Kirkby (1978)). If the suction becomes very large in unsaturated soils, the hydraulic conductivity for clays is larger than for sands. The k-values used in the present work refer to the saturated hydraulic conductivity.

L Length [m], distance in the direction of groundwater flow, used in Darcy's law.

n Porosity [-], $n = \frac{V_v}{V}$ (see Figure 1.2). The effective porosity that condributes to darcy flow is equal the total porosity minus the water retained by te grains. As the surface of clay is very large, clay retains a large amount of water and the effective porosity is $< 5\%$. See table 3.1.

S_r Degree of soil saturation [-], $S_r = V_w/V_v$ (Lambe and Whitman, 1979), see Figure 1.2. Sr=0 when the soil is completely dry and $0 < S_r < 1$ when the soil is unsaturated. Unsaturated soil is defined as soil with negative pore water pressure and as soil whose pores are filled with water and air and (Nuth, 2009). $S_r = 1$ when the pores are completely filled with water (saturated). Figure 1.4 shows schematically the different saturation phases below and above the groundwater table (saturated-unsaturated zones) under hydrostatic conditions in relation with the hydraulic potential h, the soil depth Z and the pore water pressure u_w, modified after Lu (2010). The saturation of the soil is influenced by evapotranspiration.

u_a Pore air pressure [Pa].

u_w Pore water pressure [Pa], $u = z\gamma_w$. The pore water pressure rises linearly with water depth (see Figure 1.4). At the groundwater surface u and z are equal 0. At a depth z [m] below the groundwater table, the pore water pressure u becomes $z\gamma_w$ and is positive. Above the groundwater table, u is negative and is called suction ψ.

v_a Apparent velocity of the groundwater [m/s] = hydraulic flux q = Darcy velocity.

V_g: Volume of gas [m^3].

V_v: Volume of voids [m^3], $V_v = V_g + V_w$.

V_w: Volume of water [m^3].

Z Height above geodetic datum or depth in soil [m].

z Depth below groundwater table [m].

α Inclination of the slope and the slip surface in infinite slope analyses.

Δp Applied pressure difference [Pa], used in the definition for k.

ϕ Angle of internal friction [°]. Friction is the dominant shear resistance between soil particles and depends on the normal force acting between soil particles. The friction angle is a way to express the frictional resistance. Water can act as a lubricant that decreases the friction angle (Lambe and Whitman, 1979). The friction angel has to be distinguished from the angle of repose which is the angle of the slope of loose material. The angle for repose is increasing with little saturation but decreasing with further saturation (Hustrulid et al., 2000). It depends mainly on the roughness of the material and the grain size (about 25° for fine grained soil and 35° for angular sand).

ϕ' Effective angle of internal froction [°]. If material is submerged (completly saturated and without flow), ϕ' is equal the slope angle of respose measured with respect to the horizontal α.

γ_d: Specific weight of dry soil [kN/m^3], $\gamma = \rho g$.

γ':   Effective specific weight of soil [kN/m^3], $\gamma' = \gamma_{sat} - \gamma_w$.

γ_s: Specific weight of the solid [kN/m^3].

γ_{sat}:   Saturated specific weight of soil [kN/m^3] $\gamma_{sat} > \gamma_d$.

γ_w Specific weight of water, $\approx$ 10 kN/m^3, $\gamma_w = \rho_w\, g$.

η Dynamic viscosity of the fluid [Pa s].

λ Direction of seepage measured from the normal to the ground surface [°].

ϕ Osmotic suction [Pa]. The presence of ions in the pore water leads to osmotic suction (Nuth, 2009).

Θ Volumetric water content [m^3/m^3].

ρ Density of soil [kg/m$^-$3].

ρ_w Density of water, 1000 kg/m^3.

σ Total stress [Pa], $\sigma = \gamma z$. The total stress is the sum of all forces, including those transmitted through particle contacts and those transmitted through water pressure, divided by total area (Duncan and Wright, 2005).

σ' Effective stress [Pa], $\sigma' = \sigma - u_w$. Terzaghi's effective stress principle says that when a rock is subjected to a stress, it is opposed by the fluid pressure of pores in the rock (Terzaghi, 1925). The effective stress is the force transmitted through particles contacts, divided by total area (Duncan and Wright, 2005).

τ Shear stress [Pa]. The shear stress is equal to the shear force divied by the area.

τ_f Shear strength [Pa]. The shear strength is the maximum value of shear stress that soil can withstand. It is controlled by effective stress and defined by the Mohr-Coulomb criterion.

ψ Fluid potential (or pressure potential, pressure head) at altitude Z [m], $\psi = \frac{u}{\rho_w g} = \frac{u}{\gamma_w}$. The fluid potential is the gravitational potential of water expressed in energy per unit volume.

ψ Total suction [Pa], $\psi = \psi_m + \phi$. In unsaturated soils, the pores are filled with air (non-wetting fluid relative to water) and water (wetting fluid relative to air) which are separated by the contractile skin, a purely elastic membrane-like interface that can sustain surface tension (Nuth, 2009). The surface tension results from the balance of energy between the water and the air molecules by creating a curved interface between the two that is called meniscus. The action of the interphase due to air and water pressure is called capillarity and leads to a rise of the water in porous media above the water table.

ψ_m Matric suction, [Pa], $\psi_m = u_a - u_w = f(\Theta)$. Matric suction is directly linked to the surface tension property of the contractile skin, thus to capillarity and the size of the pores in the soil. In fine grained soil, the capillary force is higher, thus the matric suction is higher and the water due to capillarity will rise higher than in soils with larger pores. Matric suction is a function of the volumetric water content Θ and depends on the grain size of the soil as seen in Figure 1.3.

General references for this notations are Lambe and Whitman (1979) and Hoelting and Coldewey (2009).
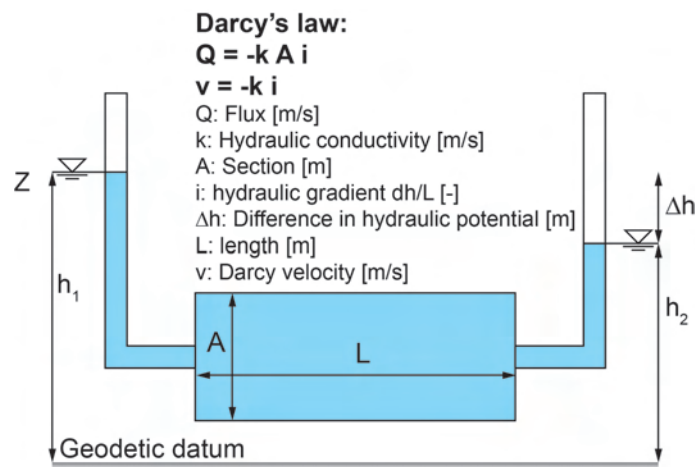
Figure 1.1: Experiment set up for Darcy's law.
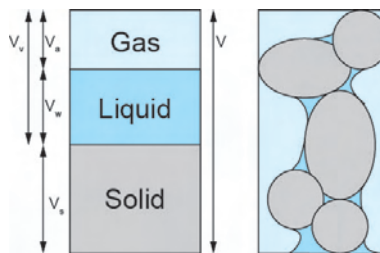
Figure 1.2: Scheme of the relationship between the volumes of the different phases in a soil element (modified after Lambe and Whitman (1979)).

Chapter 2

State of the art

2.1 Overview

Studying the origin and role of groundwater in landslides needs knowledge of both, hillslope hydrology/hydrogeology and landslides. Therefore, in this chapter hydrology research and landslide research are briefly discussed, followed by a review about slope stability and hydrogeological triggering of landslides. Figure 2.1 shows a scheme of the content of this chapter.
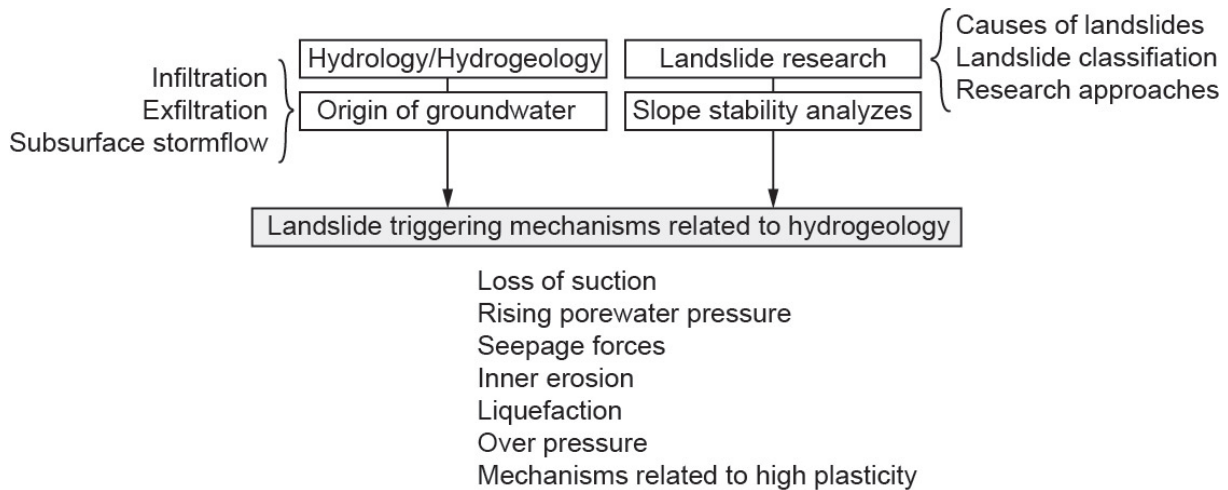
Figure 2.1: *Scheme of the content of this chapter.*

2.2 Hillslope hydrology and hydrogeology

The main aim of hillslope hydrology is to study the flow paths and residence time of rainwater from a catchment to a receiving stream. Water from precipitation and snow melt does either flow as surface runoff or does infiltrate into the soil. Figure 2.2 shows different flow paths of water on and in a hillslope.

2.2.1 Surface runoff

Two types of surface runoff are distinguished. Hortonian overland flow occurs when precipitation exceeds infiltration rate. Saturated overland flow occurs when the soil has reached complete saturation.
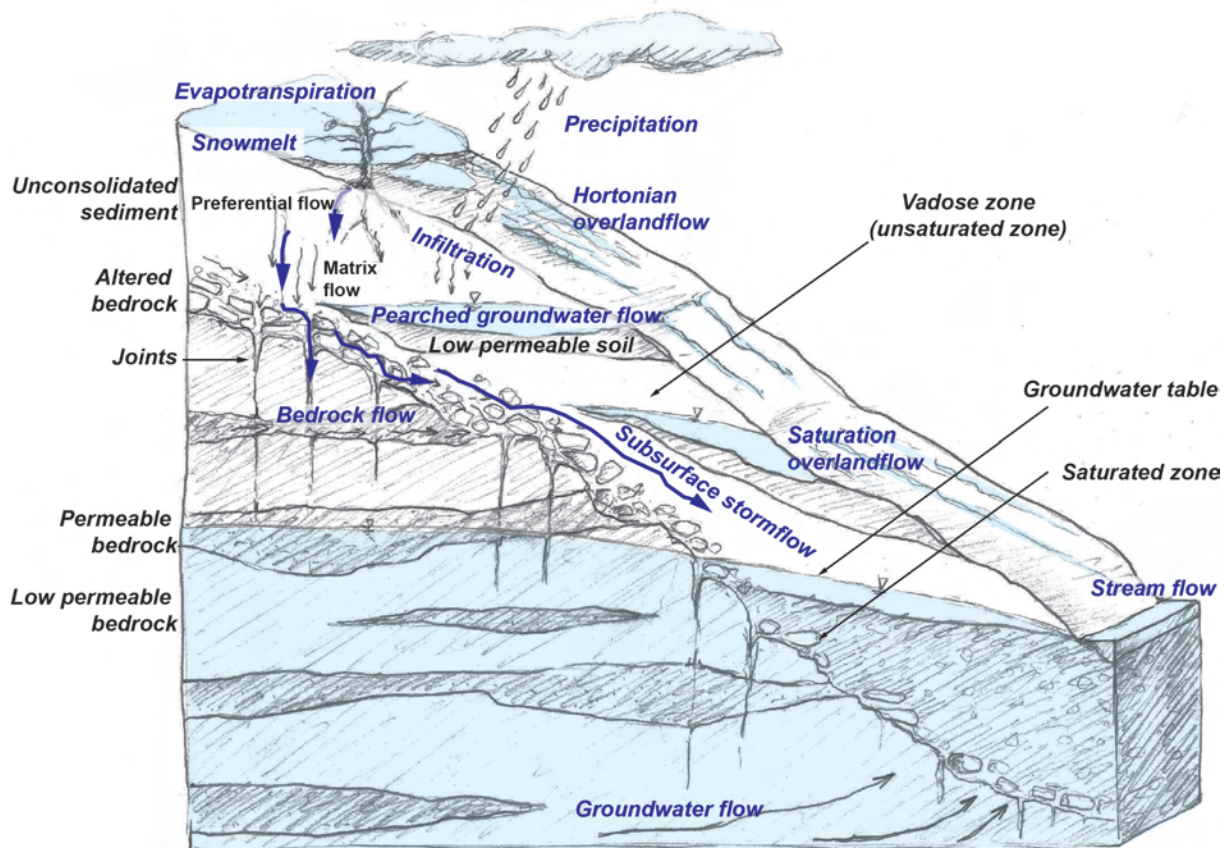
Figure 2.2: *Illustration showing the different components of surface and subsurface water flows on a hillslope. Surface runoff occurs as saturated overland flow when the soil is completely saturated and as Hortonian overland flow when precipitation exceeds infiltration. The runoff below surface is called subsurface stormflow.*

2.2.2 Subsurface stormflow

Subsurface stromflow is water that infiltrates and percolates through unsaturated and saturated underground (Weiler et al., 2006). The underground can be unconsolidated sediment, weathered bedrock or massive bedrock. The water flow is mainly driven by gravity and capillarity. Subsurface stormflow occurs either as homogeneous matrix flow through micropores or as preferential flow through macropores like animal burrow holes, tree roots, or fractures (McDonnell et al., 2007). Subsurface stormflow was first described by Engler (1919) (see Figure 2.3). The formation of subsurface stormflow depends on

1. The pre-event saturation of the soil

2. The bedrock topography

3. The geometry, depth and permeability of different soil and bedrock layers

4. The rain intensity and duration

Subsurface stormflow is more important in saturated or nearly saturated soil and in macropores than in unsaturated soil and micropores because of the connectivity (Beven and Germann, 1982). Kienzler (2007) observed that during high precipitation intensities, saturation occurred first within the top soil (top-down saturation) and during low precipitation at the base of the soil along an impermeable layer (bottom-up saturation).
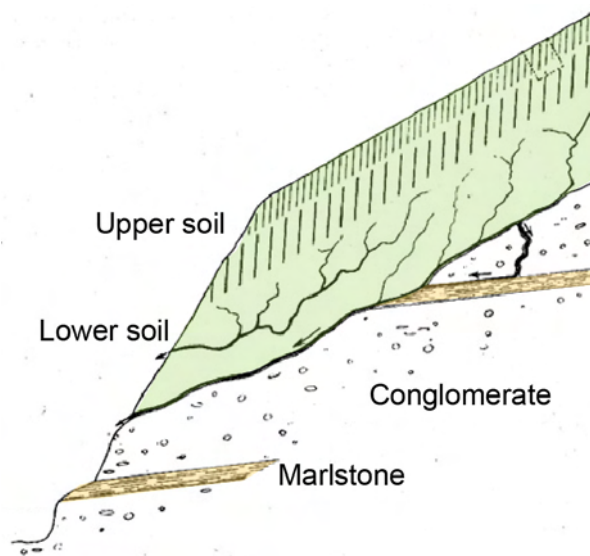
Figure 2.3: *First conceptual model of subsurface stormflow through a profile of soil and weathered bedrock on a forested hillslope (Engler, 1919). In the upper soil, the water is uniformly infiltrating whereas in the lower soil, distinct flow along water courses develops.*

2.2.3 Bedrock infiltration and exfiltration

Bedrock is often assumed to be an impermeable boundary below the unconsolidated sediment (Beven and Germann, 1982; Brammer and McDonnell, 1996), but different studies have shown that bedrock permeability controls to a large extent the hydrological response of catchments (Wilson and Dietrich, 1987). Bedrock flow may also contribute to runoff in most environments (Onda et al., 2001).

Especially, the subsurface flow along the altered bedrock layer (between the fresh bedrock and the unconsolidated sediment cover) may be important because permeability in this layer can be larger than in the overlaying soil. In granitic catchments in central Japan, the formation of soil mantle groundwater was investigated by Asano et al. (2003), Katsuyama et al. (2005) and Katsura et al. (2008). They found that bedrock groundwater flowing in permeable weathered and fractured bedrock seeps semi-perennially into the overlaying unconsolidated sediments (see Figure 2.4).
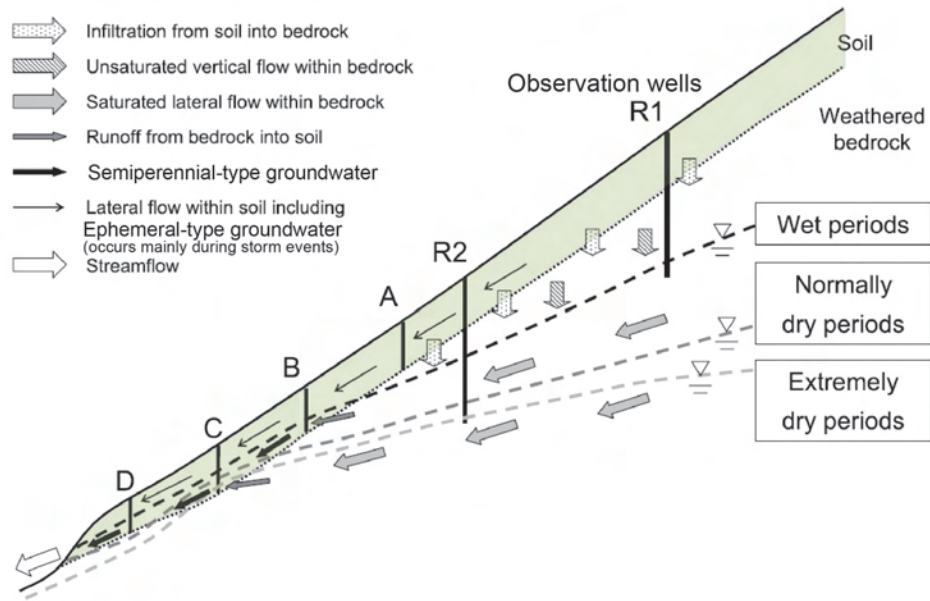
Figure 2.4: *Depending on the season, groundwater seeps from weathered and fractured bedrock into the overlaying unconsolidated sediments (Katsura et al., 2008).*

Uchida et al. (2003) studied the size of the area where bedrock groundwater seeped into the soil layer and the rate of water flowing out of the bedrock. They found that the seepage from granitic bedrock into the soil was considerable (between 50 and 95% of total streamflow) even though the size of the seepage area was small (0.5 - 2 % of the catchment).

The amount of bedrock groundwater that contributes to the formation of transient groundwater varies with the rainfall duration and intensity (Uchida et al., 2002). Uchida et al. (2002) found that only after heavy rainfall events, bedrock exfiltration played an important role in a steep headwater catchment in Paleozoic sediments in central Japan.

An opposite situation was described by Anderson et al. (1997) who observed rapid bedrock flow exfiltrating into the colluvium and mixing with water that is percolating in the vadose zone [1] in an unchannelled catchment in the Oregon Coast Ranges. They found that the more it rains, the smaller the portion of bedrock groundwater in the saturated zone is. In this catchment, the interaction of flow in near-surface weathered and fractured sandstone bedrock with overlaying colluvium during high-intensity rainfall was described by Montgomery et al. (1997) (see Figure 2.5).

Subsurface stormflow, whether it occurs only in the soil or in both, the bedrock and the soil, can lead to enhanced and positive pore water pressure in steep terrain which may trigger landslides

---

[1]Vadose zone is the unsaturated zone above the groundwater table, see Figure 2.2.
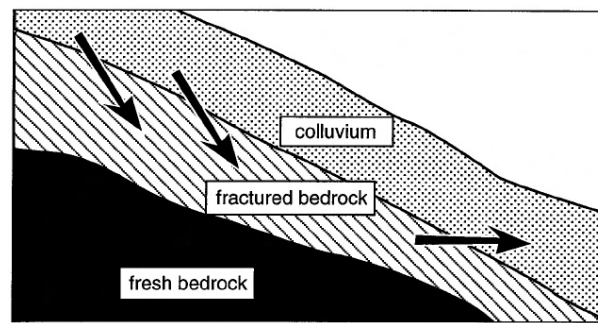
Figure 2.5: *Conceptual model from Montgomery et al. (1997) showing groundwater flow trough altered bedrock layers and subsequent bedrock exfiltration.*

(Weiler et al., 2006; Montgomery et al., 1997). In the following section, the causes and triggering of landslides and study approaches are reviewed.

2.3 Landslide research

2.3.1 Landslide hazards and causes of landslides

A very general definition of a **landslide** was given by Cruden and Varnes (1996): A landslide is "a mass of rock, debris or earth sliding down a slope". Important geomorphological features and definitions of a landslide are indicated on Figure 2.6.
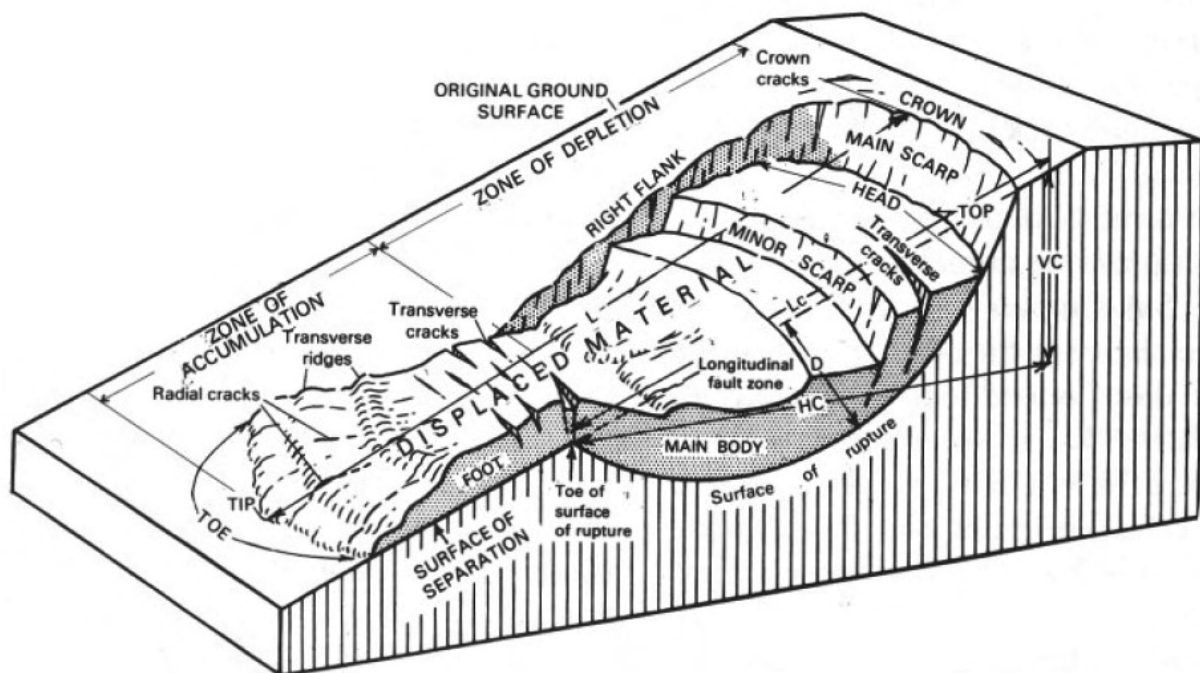
Figure 2.6: *Block diagram of an idealised rotational earth slide-earth flow (Cruden and Varnes, 1996).*

Landslides belong to the most frequent natural hazards all over the world where the landscape shows a relief (Center for Research on the Epidemiology of Disasters (CRED), International Disaster Database, http://www.emdat.be/). On Figure 2.7 a map is shown with the worldwide distribution of landslide fatalities in the years 2006, 2007 and 2008. Often, landslides occur

as secondary natural hazards triggered by earthquakes, volcanic eruptions in combination with earthquakes, or flood events. This explains the worldwide distribution of landslides along tectonically active zones and mountain ranges (see Figure 2.7). It has to be distinguished between landslide trigger and primary-causes or pre-dispositions. A landslide trigger is a sudden event which changes the force equilibrium in a slope and leads to failure. Natural landslide **triggers** are earthquakes, volcanic eruptions, high-intensity rainfall, long-term precipitation and rapid or late snowmelt. Rainfall triggered landslides related to flood events are among the most severe natural hazards because they occurred typically very rapidly and have a large damage potential. Also in Switzerland, landslides are often related to flood events (Hilker et al., 2009; Lateltin et al., 1997; Bezzola and Hegg, 2007, 2008). Nevertheless, landslides do not always occur instantaneously. Large deep seated landslides can also be a slow and long term process for example due to glacier retirement (Noverraz et al., 1998) or erosion. Additionally, landslides can be triggered by human impact when steep slopes are constructed for example along roads or dams (Sidle and Ochiai, 2006).
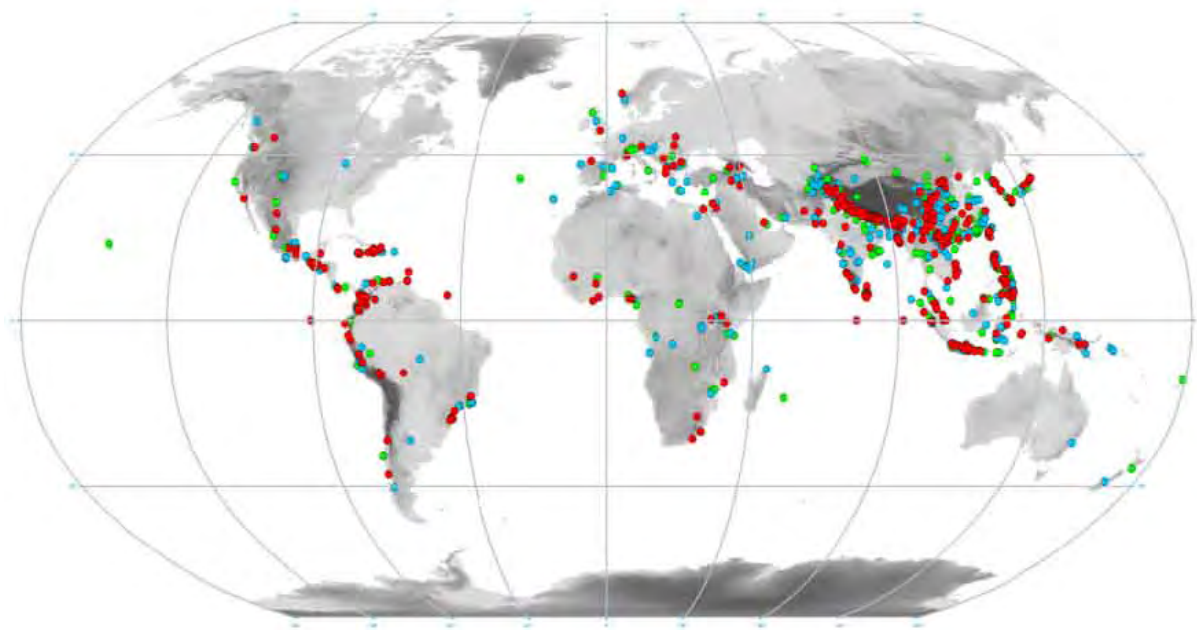
Figure 2.7: *Map showing the landslide fatalities from the years 2006 (green), 2007 (blue) and 2008 (red) (Petley, 2010). It can be seen that landslides are mostly distributed along tectonically active zones. The darker colours in the background image indicate higher elevation.*

Pre-dispositions are geological, hydrogeological, hydrological, chemical, mechanical, biological, geomorphological characteristics which define if a certain slope is susceptible for landslides. Most pre-dispositions do not change in short-term but can change over a longer time span for example due to erosion (Popescu, 1996). Long-term predispositions are: slope angle, aspect (slope orientation), altitude, slope shape (convex or concave topography), vegetation, climate, rock and soil type (lithology, tectonic, structures).

Other pre-dispositions, especially when related to hydrology, can change more rapidly: permeability (depending on saturation and macropores for example caused by landslide movements), type of aquifer (free or confined), and soil saturation related to snowmelt, long-term rainfall or evapotranspiration.

Thus if a slope is prone to landslides due to an unfavourable combination of predisposing factors, a trigger with a certain intensity can release a landslide. The triggering mechanisms that explains the changes in force equilibrium in the slope will be discussed in Section 2.5.

2.3.2 Landslide classifications

Landslide classifications are important to avoid misunderstandings and to structure the different processes (Cruden and Varnes, 1996). They are based on specific parameters depending on what information the classification should bring. Depending on the purposes, specific landslide characteristics are important and therefore numerous landslide classifications exist. The most established landslide classifications are based on criteria like morphology, movement, activity and material:

- Hutchinson (1988) puts focus on the morphology of slope movements, taking also into account the mechanism, material and rate of the movement.

- Cruden (1991) and Cruden and Varnes (1996) defined landslide as "a mass of rock, debris or earth sliding down a slope" and classified landslides in terms of their movement (fall, slide, flow, spread) and material.

- Hungr et al. (2001) deepened the classification for flow-type landslides taking into account soil saturation and referring to the classification of Cruden and Varnes (1996).

- In a report of the Swiss Federal Office for the Environment, it was proposed to categorise landslides according to the depth of the slip surface: 0 - 2 m below surface: shallow landslide, 2 - 10 m below surface: medium seated and > 10 m below surface: deep seated landslide (Lateltin et al., 1997).

Other relevant parameters for landslide classifications are landslide activity, geotechnical parameters, slope angle and aspect, vegetation cover, and geometry. The groundwater was taken into account in the classifications by quantifying the saturation of the landslide materials (Hungr et al., 2001). But as far as known to the author, no classification combines the permeability contrast of the material, the origin of the groundwater and the hydrogeological triggering mechanism.

In the present work it will be referred to the classification of Cruden and Varnes (1996) if there are no other specifications. In the following the landslide classification from the Swiss Federal Office for the Environment (Lateltin et al., 1997) is described in more detail, because the landslide depth will be used in the next chapter as main criteria for the landslide classification.

Landslide types according to the depth of the slip surface

Shallow landslides (slip surface <2 m deep) are often rainfall triggered rapid debris slides (Cruden and Varnes, 1996) which develop into unchannelized debris flows with long run out distance. In Switzerland they are called "Hangmure". The slip surface of shallow landslides often represents the interface between the bedrock and the soil material that is a zone of weathered bedrock which can reach more than one meter of thickness. Rapid/very rapid earth/debris slides may reach speeds of several meters per second and are characterized by sudden occurrence. Therefore they are difficult to spatially and temporally forecast. They are more dangerous to both people and infrastructure than large slow moving deep seated landslides, which cause mainly material damage.

Medium seated landslides (slip surface 2 - 10 m deep) are often triggered due the development of positive pore water pressure along a distinct slip surface.

Deep seated landslides (slip surface >10 m deep) are often slow moving and caused due to glacier retirement in large valleys of the Alps. Large deep seated and medium seated landslides and the effect of groundwater on their movement have been studied in detail, for example in Switzerland and Lichtenstein: La Frasse (VD) landslide (Bonnard et al., 1987; GEOLEP and GEOMOD, 2007; Tacher et al., 2005), Stein-Mumpf (AG) landslide (Parriaux et al., 2008), Triesenberg landslide, Fürstentum Lichtenstein, (François et al., 2007; Tullen, 2002) and Cuolm Da Vi(GR) instability (Amann et al., 2006) which will be discussed in Chapter 8.

2.3.3   Landslide studies and investigative approaches

Studying landslides is very interdisciplinary and knowledge from different research fields have to be combined. Figure 2.8 summarizes the different research fields, study aims and investigation approaches. Due to their economic and social risk, landslides have been studied extensively in terms of several study aims shown in Figure 2.8. The present study puts focus on the hydrological and hydrogeological landslide characteristics and triggering mechanisms. The response of slopes to intense rainfall has been studied by different approaches shown on Figure 2.8, These approaches are discussed in the following section. In the present study, focus was put on the approaches "monitoring real landslides" and "landslide triggering experiment".
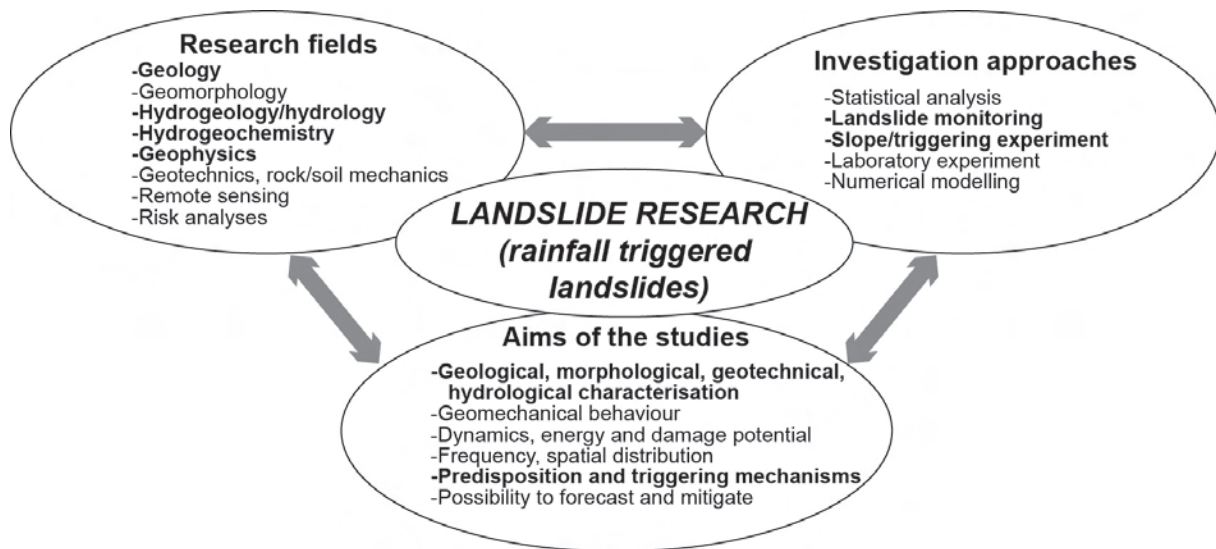
Figure 2.8: *Scheme showing the different research fields, study aims and investigation approaches of rainfall triggered landslide research. In bold the focus of the present study.*

Statistical analyses based on landslide inventories

Statistical analyses are made of entire mountainous regions for landslide hazard mapping (Guzzetti et al., 1999). The aim of these studies is to establish thresholds for critical antecedent and daily rainfall that trigger landslides and to forecast location and time of landslide occurrence. With the aid of GIS software, large landslide inventories, rain hydrographs and parameters like local geology, geomorphology, vegetation and topography are statistically analysed. In the last decade, several intense rainfall events, which triggered thousands of landslides have also been recorded and analyzed in Switzerland. Due to temporal and spatial rainfall distribution, these events are geographically clearly defined:

- 1997: Sachseln (Petrascheck et al., 1998) and Obwalden (Rickli, 2001),

- 2000: Vallis (Petrascheck and Hegg, 2002)

- 2002: Appenzell and Napf (Rickli and Bucher, 2003)

- 2005: Napf, Entlebuch, Prättigau (Rickli et al., 2008) and Obwalden (Berwert-Lopes and Spichtig, 2006) (see Section 2.6 and Chapter8)

Back analyses generally have to deal with the disadvantage that the exact conditions at the initial stage of landslides are unknown. The landslide inventory made by Rickli and Bucher (2003) and Rickli et al. (2008) for example has been made three to four months after the respective events. Other disadvantages of landslide inventories analyses are, on the one hand that a large amount of precipitation data and dated landslide events are needed. This is often not available or incomplete. On the other hand, the study areas are rarely homogeneous in terms of lithology, landslide type, vegetation etc. (Van Asch et al., 1999). This makes it difficult to compare the different landslides with each other. Therefore, more detailed studies are necessary which focus on local geomechanical and hydrological characteristics of landslides (which could be representative for the study area).

Investigation and monitoring of active landslides and slopes prone to landsliding

As seen in Figure 2.8, the investigation of landslides includes methods from different geo-research fields. These methods will be described in more detail in Chapter 4. Monitoring of active landslides is possible if they are slow or if it is known where they will occur (for example debris flows). Numerous large deep seated slow moving landslides (after-glaciations-landslides) have been monitored over large time spans (Noverraz et al., 1998; Corominas et al., 2005; Bonnard, 2006). But the triggering of unchannelised, rapid shallow debris slides is more difficult to investigate because they are not easy to temporally and spatially forecast (Montgomery et al., 2009). Therefore, slope experiments are performed to study the triggering mechanism and the evolution of such rapid events.

Slope and sprinkling experiment

In order to investigate the hydrologic regime of slopes prone to landslides, they have been either equipped densely with different sensors (Montgomery et al., 2002) or equipped with both, instruments and artificial irrigation (Montgomery et al., 1997). Instruments may include tensiometer to measure soil water tension/suction, TDR[2] to measure water content, decagon to measure soil moisture, piezometers or pressure sensors to measure piezometric level and water pressure respectively and pluviometer to measure rain intensity. Sprinkling experiments have been carried out in order to either trigger a landslide (Broennimann and Tacher, 2009; Ochiai et al., 2004) or to investigate the subsurface water flow and runoff without reaching the critical saturation to trigger the slope (Kienzler and Naef, 2008; Kienzler, 2007; Debieche et al., 2011). Such slope scale sprinkling experiments are very expensive and it is not evident to obtain permission at accessible locations with sufficient infrastructure. Therefore, it can be easier to study the landslide triggering in laboratory tests like flume[3] (Ching-Chuan et al., 2009; Wang and Sassa, 2003) or centrifuge experiments [4] (Take et al., 2004).

Numerical modelling

Slope monitoring and slope experiments are often combined with numerical modelling. Numerous geomechanical slope stability models have been developed for the assessment of shallow landslides

---

[2]Time-domain reflectometer

[3]Inclined channel in meter-scale to perform mass movements in the laboratory for example with different materials and under different saturation conditions.

[4]Centrifuge experiments allow to downscale real slope experiments by increasing the gravitational acceleration of the earth. This is achieved by rapid rotation of the experiment box.

(Borga et al., 2002; Montgomery and Dietrich, 1994). Parameters like slope angle, curvature and lithology were taken into account. Van Asch et al. (2007) stated that the quality of the hydrological model had a greater influence on the general performance of landslide models than the geomechanical model. A main limitation of hydro-geomechanical coupled models is the need for reliable pore pressure measurements along the slip surface (Cascini et al., 2008a). Pore pressure values are calculated using physically based flow models for the saturated and unsaturated zones. Especially the flow in the unsaturated zone and transient regimes remains still a big challenge to model. Often slope stability models assume the bedrock to be an impermeable boundary and concentrate on the water infiltration at the ground surface. Other models tested a local inflow from underlying bedrock into the landslide (Cascini et al., 2006) whereas Borja and White (2010) neglected the occurrence of exfiltration processes by using a hydro-mechanical slope stability model. Numerical flow modelling can be an aid to compare different scenarios of the groundwater origin and flow in landslides. Nevertheless, hydrological modelling does not replace field investigations.

2.4 Slope stability analyses

Slope stability analyses deal with calculation, investigation, modelling and design of natural and artificial rock and soil slopes. A common method to calculate the slope stability for slip failure is called "Limit equilibrium analyses". The principles of this method are reviewed in the following section. This will serve as base for the theory of landslide triggering mechanisms related to hydrology that will be discussed afterwards.

2.4.1 Limit equilibrium analyses

Limit equilibrium analyses are based on the principle that a slope is stable if the resisting forces exceed the driving forces that is if the factor of safety SF is equal or larger than 1:

$$SF = \frac{Resisting\ forces}{Driving\ forces} = \frac{Shear\ strength\ \tau_f}{Shear\ stress\ \tau} \geq 1 \qquad (2.1)$$

τ is the equilibrium shear stress which depends on the soils weight, porewater pressure and slope angle. The equilibrium shear stress is the shear stress required to maintain a just-stable slope (Duncan and Wright, 2005).

τ_f is the available shear strength which depends on the soils weight, cohesion, friction angle and pore water pressure. The shear strength is equal to the maximum shear stress which can be absorbed by the slope without failure and can be defined by the Mohr-Coulomb criterion:

$$\tau_f = c + \sigma \tan \varphi \qquad (2.2)$$

τ_f: shear strength at the rupture surface [kPa]
c: cohesion [kPa]
σ: normal stress at rupture surface [kPa]
φ: angle of internal friction [°]

Including equation 2.2 in 2.1 leads to the following equation for the factor of safety:

$$SF = \frac{c + \sigma \tan \varphi}{\tau} \qquad (2.3)$$

The factor of safety is assumed to be the same at all points along the slip surface. In reality a continuous shear surface develops and the slope fails if sufficient soil elements along a potential

slip surface are in the state of failure. This can be a newly forming or a reactivated slip surface. A slope becomes unstable when the shear stress exceeds the shear strength in the soil and the factor of safety becomes smaller than one (Duncan and Wright, 2005). This can occur when:

1. The resisting forces are reduced, i.e. the shear strength of the soil is reduced.

2. The driving forces are increased, i.e. the shear stress τ acting on a soil particle is increased.

Two factors are crucial for the stability of a slope: The water and clay content. On the one hand, rising water table and adverse seepage destabilises the slope due to increased pore water pressure. On the other hand, water in clay soils can have chemical and physical effects on the stability of a slope. The landslide triggering mechanisms related to water and clay will be discussed in more detail in Section 2.5.

To calculate the factor of safety, a certain slip surface has to be assumed. The forces acting on this slip surface are calculated with one or more equations of static equilibrium. The complete static equilibrium considers forces in horizontal and vertical direction and moments at any point. Depending on the analysing method, not all forces are taken into account and different assumptions are made. The forces are then calculated for several assumed slip surfaces in order to find the critical slip plane with the minimum factor of safety. Two different approaches exist:

1. Method of a single mass: The equilibrium is considered for a single mass of soil (the mass between the slip plane and the slope surface). Different methods are: Infinite slope, Swedish slip circle, and Logarithmic spiral.

2. Method of slices: The soil mass is divided into a number of vertical slices and the equilibrium is considered for each slice. Methods to calculate the equilibrium for a circular slip surface are for example: Ordinary method of slices, Simplified Bishop, Complete Bishop. Methods to calculate the equilibrium for a non-circular slip surface consider either only the force equilibrium (example: Janbu's Generalized Procedure of Slices) or the complete equilibrium procedure (example: Spencer's Procedure, Morgenstern and Price method).

The factor of safety can be calculated by charts, spread sheet software, slope stability computer programs or simple equations (Duncan and Wright, 2005). In the following, the Infinite slope method is described in more details. This is a simple equation method which is suitable for the analysis of shallow landslids. The introduction to this method is a base for the understanding of the landslide triggering mechanisms which will be discussed afterwards.

2.4.2 Infinite slope theory

The infinite slope theory is a simplified method to analyse the translational slope failure (Lambe and Whitman, 1979). As the name says, the slope is assumed have an infinite extent in all directions. The slip surface is assumed to be shallow, except in the case of cohesionless soil where the factor of safety does not depend on the depth of the slip plane. The soil is assumed to be homogeneous and isotropic, and the slip surface has to be parallel to the slope so that the inclination of the slope and the slip surface is α. Figure 2.9, 1) shows such a block. The lateral forces acting on the two ends of the block are identical in magnitude but in opposite direction and therefore cancel each other and can be ignored in the equilibrium equation. So only the sum of the forces acting parallel and perpendicular on the slip surface are taken into account for the equilibrium equation and the moment equilibrium is implicitly satisfied. Figure 2.9, 1) shows the shear force F_S and the normal force F_N of a weight $F = \gamma V$ of the block acting on the slip plane. The thickness in the direction perpendicular to the plane of cross section is assumed to
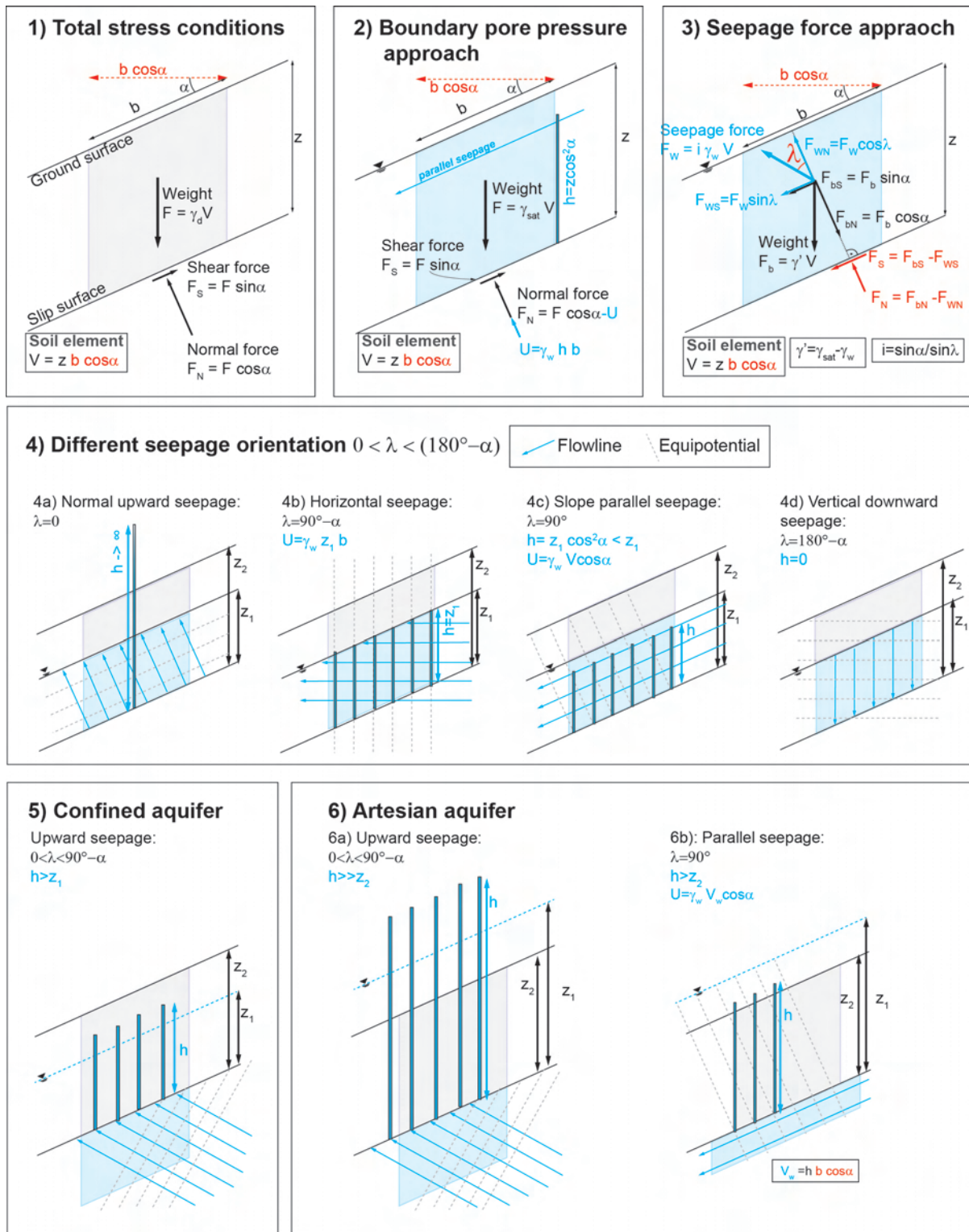
Figure 2.9: *Different schemas showing the forces acting on a soil element in an infinite slope under dry conditions 1) and saturated conditions 2), boundary pore pressure approach. 3) shows the forces acting in the volume including the seepage force. The weight of the soil and the seepage forces can be divided in a normal and a shear component. 4) shows the flow lines, equipotential and hydraulic potential h for different seepage angles. 5) shows the situation of a confined aquifer below a dry layer and 6) an artesian aquifer below a dry layer. V is the volume of the soil element. λ is the angle of seepage and α is the slope angle.*
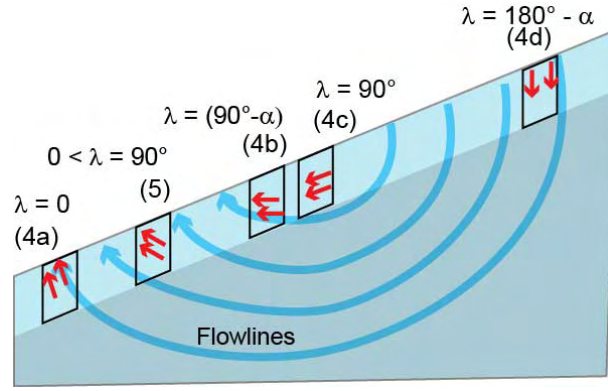
Figure 2.10: *Profile showing the idealised flow and equipotential lines through a saturated slope. The locations of downward, parallel and upward flow described in Figure 2.9 are indicated.*

be unity. γ is the total unit weight of soil, b is the distance between the two ends of the block and z is the vertical depth to the shear plane. Thus the Volume $V = zb\cos\alpha 1$ (the thickness of the section is assumed to be unity). So the shear force F_S and the normal force F_N are (Duncan and Wright, 2005):

$$F_S = \gamma bz \cos\alpha \sin\alpha \tag{2.4}$$

$$F_N = \gamma bz \cos^2\alpha \tag{2.5}$$

Dividing the shear force and normal force by the area of the plane (is equal b because the thickness of the section is assumed to be unity) gives the shear and normal stress:

$$\tau = \gamma z \cos\alpha \sin\alpha \tag{2.6}$$

$$\sigma = \gamma z \cos^2\alpha \tag{2.7}$$

Including equations 2.6 and 2.7 in equation 2.3, leads to the following factors of safety (see Figure 2.11):

Factor of safety for total stress conditions

The factor of safety for total stresses is used under the assumption that the soil is dry and that capillary effects are not considered (see Figure 2.9, 1):

$$SF = \frac{c + (\gamma_d z \cos^2\alpha)\tan\varphi}{\gamma_d z \cos\alpha \sin\alpha} \tag{2.8}$$

c: Cohesion [kPa]
γ_d: Specific weight of dry soil, [kN/m^3]
φ: Angle of internal friction [°]
α: Slope angle [°]
z: Soil thickness [m]

For cohesionless soil ($c = 0$), the factor of safety is reduced to:

$$SF = \frac{tan\varphi}{tan\alpha} \tag{2.9}$$

In cohesionless soil, if $tan\alpha \geq tan\varphi$, failure occurs simultaneously in all depth. On the contrary, if cohesion is not zero, Mohr-Coulomb failure can only occur at a specific depth.

Rogers and Selby (1980) showed that the factor of safety is very sensitive to changes in h and c', moderately sensitive to z and α, and rather insensitive to ϕ' and γ.

Factor of safety for effective stresses

The pore water pressure u is determining for slope stability and is taken into account by calculating with the effective normal stress (Terzaghi, 1925):

$$\sigma' = \sigma - u \tag{2.10}$$

Thus for effective stresses, the factor of safety is:

$$SF = \frac{c' + (\gamma_{sat}z\cos^2\alpha - u)\tan\varphi'}{\gamma_{sat}z\cos\alpha\sin\alpha} \tag{2.11}$$

If the soil is saturated, it is calculated with the saturated specific weight of the soil γ_{sat}.

In unsaturated soil the interaction between water and air pressure in the pores causes capillarity which increases the effective strength of the soil (see Section 1.4 for definition of suction). Thus suction has to be taken into account in unsaturated soil and the effective stress is defined as Bishop (1959):

$$\sigma' = (\sigma - u_a) + \chi(u_a - u_w) \tag{2.12}$$

u_a: Air pressure [kPa]
u_w: Pore water pressure [kPa]
χ: Effective stress parameter, varies between 0 (perfectly dry) and unity (completely saturated) [kPa]
$(\sigma - u_a)$: Normal stress [kPa]
$(u_a - u_w)$: Matric suction [kPa] (see Section 1.4)

If χ is equal unity, equation 2.12 is reduced to equation 2.10. If χ is between 0 and unity, the term $\chi(u_a - u_w)$ represents the contribution of matric suction to effective stress.

As the calculation of unsaturated conditions exceeds the aim of this work, in the following the effect of suction will only be mentioned qualitatively.

The porewater pressure u depends also on the orientation of the groundwater flow λ (angle between the normal to the slip surface and the seepage vector). In the infinite slope analysis, it is assumed that u is constant along the shear plane. In reality the groundwater flow patterns are much more complex and u is preferably calculated with numerical finite element groundwater flow models.

Factor of safety including seepage force

Two approaches exist to take the seepage force into account (see Figure 2.12): The boundary pore pressure approach and the seepage force approach (Ghiassian and Ghareh, 2008). In the boundary pore pressure approach, pore water pressure u is assumed to be an external force acting on the shear surface (Figure 2.9, 2). In the seepage force approach, the seepage forces F_s acting
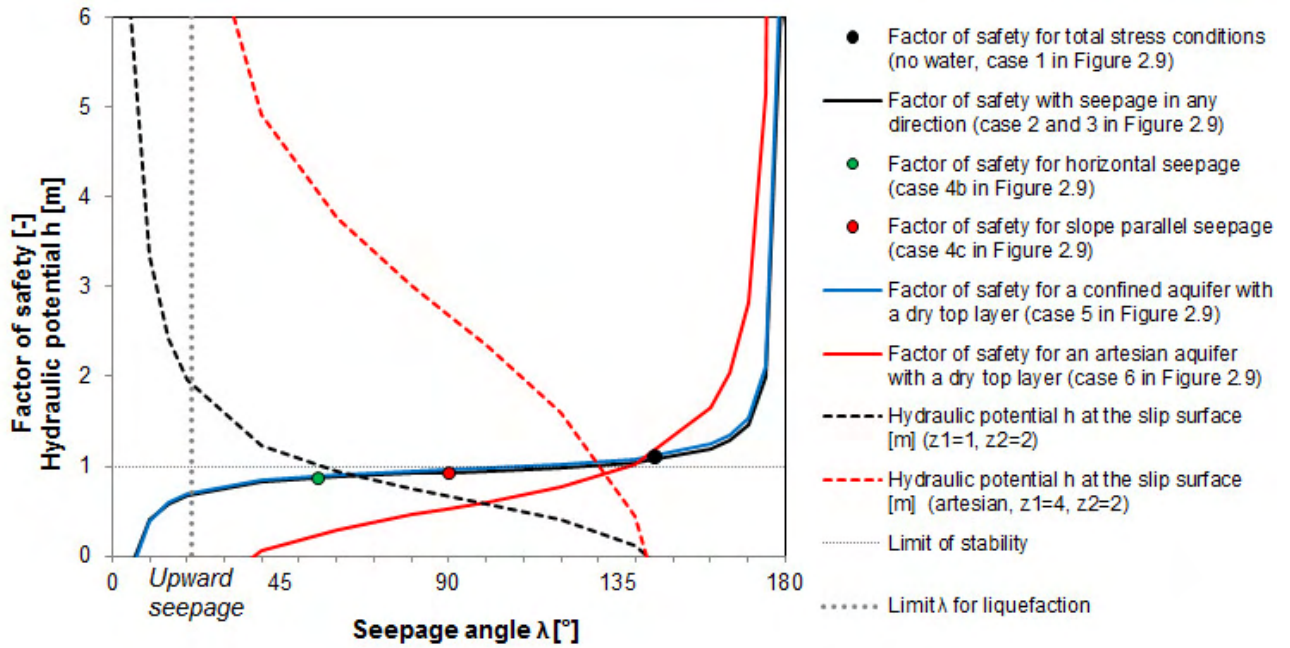
Figure 2.11: *Graph showing different factors of safety for different hydraulic conditions and for varying seepage angle λ, for a steep slope (α=35°) and soil composed of sandy silt with little clay (γ_{sat}=21 kN/m³, γ_{dry}=18 kN/m³, c'=10 kN, ϕ'=20°, z_1=1 m, z_2= 2 m, z_1(artesian)=4 m). λ is the angle between the normal on the slope and the seepage direction (see Figure 2.9, 3). Additionally, the hydraulic potential h [m] is displayed. A factor of safety = 1 represents the limit of stability. The limit angle λ for liquefaction will be discussed in Section 2.5.5, equation 2.20. If the seepage direction is vertically downwards (180°-α) the stability is equivalent to that under total stress conditions. The most unfavourable seepage direction is oriented upward.*
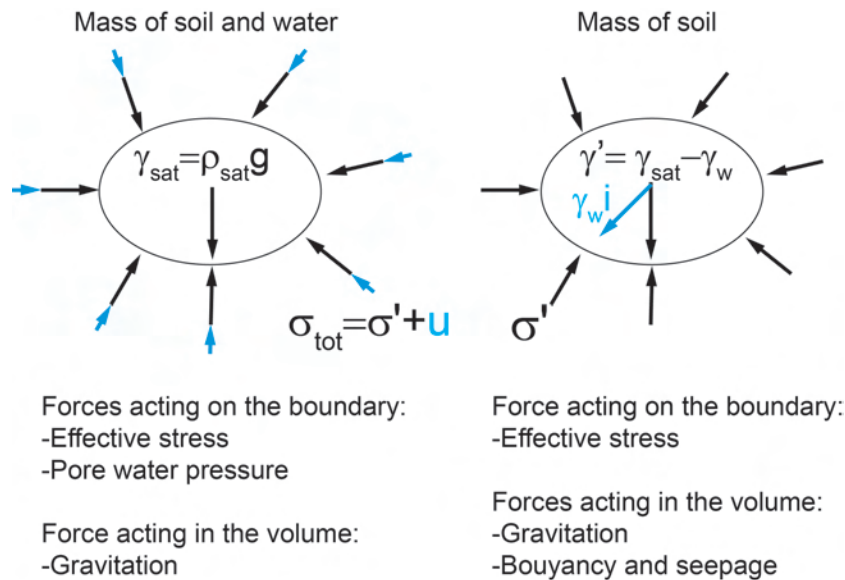
Figure 2.12: *The two approaches to calculate the influence of porewater pressure and seepage forces on a mass of soil.*

on the soil particles in the soil element are taken into account (Figure 2.9, 3). Seepage forces are defined as (Lambe and Whitman, 1979):

$$F_s = V\gamma_w i \tag{2.13}$$

γ_w: Specific weight of water, 10 kN/m^3
i: Hydraulic gradient [-]
V: Volume of the soil [m^3]

The gradient is assumed to be (Ghiassian and Ghareh, 2008):

$$i = \frac{\sin\alpha}{\sin\lambda} \tag{2.14}$$

The orientation of the seepage force (λ, angle measured from the normal to the slope, see Figure 2.9) is crucial for the slope stability. It is assumed that the seepage force can act in directions from vertically downward ($\lambda = 180$ ° - α, Figure 2.9, 4d) over slope parallel ($\lambda = 90°$, Figure 2.9, 4c) to slope-normal upward ($\lambda = 0°$, Figure 2.9, 4a). On Figure 2.11 it can be seen that the most unfavourable seepage direction is perpendicular upward ($\lambda = 0$).

With the seepage force approach, the factor of safety for seepage with a direction λ is (see Figure 2.9, 3), the water table is always at the surface):

$$SF = \frac{c' + ((\gamma_{sat} - \gamma_w)z\cos^2\alpha - \gamma_w z\cos\alpha\frac{\sin\alpha}{\sin\lambda}\cos\lambda)\tan\varphi'}{\gamma_{sat}z\cos\alpha\sin\alpha} \tag{2.15}$$

With the boundary pore pressure approach for a slope where the water table is in a depth z_2 - z_1 below surface (equal to a height z_1 above the slip surface), the factor of safety is (modified after Springman and Mayor (2008)):

$$SF = \frac{c' + ((\gamma_{sat}z_1 + \gamma_d(z_2 - z_1))\cos^2\alpha - u)\tan\varphi'}{(\gamma_{sat}z_1 + \gamma_d(z_2 - z_1))\cos\alpha\sin\alpha} \tag{2.16}$$

with the pore water pressure $u = \gamma_w h$. The hydraulic potential h is equal (see Figure 2.13):

$$h = \frac{z_1 cos\alpha}{cos\lambda}tan(90 - \lambda)cos(90 - \alpha - \lambda) \tag{2.17}$$

If seepage is parallel to the slope and slip surface (see Figure 2.9, 2) the factor of safety is (Springman and Mayor, 2008):

$$SF = \frac{c' + (\gamma_d(z_2 - z_1) + (\gamma_{sat} - \gamma_w)z_1)\cos^2\alpha\tan\varphi'}{(\gamma_d(z_2 - z_1) + \gamma_{sat}z_1)\cos\alpha\sin\alpha} \tag{2.18}$$

Factor of safety in the case of a semi-confined aquifer

A semi-confined aquifer is formed if the upper limit is low permeable and if the hydraulic potential h is higher than the upper limit of the aquifer (Figure 2.9, 5). If the upper layer is considered as saturated, Equation 2.16 can be used to calculate the factor of safety. If the upper layer is considered as dry, the factor of safety with the "boundary pore pressure approach" is:

$$SF = \frac{c' + ((\gamma_d z_2\cos^2\alpha - u)\tan\varphi'}{\gamma_d z_2\cos\alpha\sin\alpha} \tag{2.19}$$

An artesian aquifer is a semi-confined aquifer with a hydraulic potential h above the ground surface (Figures 2.9, 6). In such a situation, buoyancy forces can lead to overpressure.
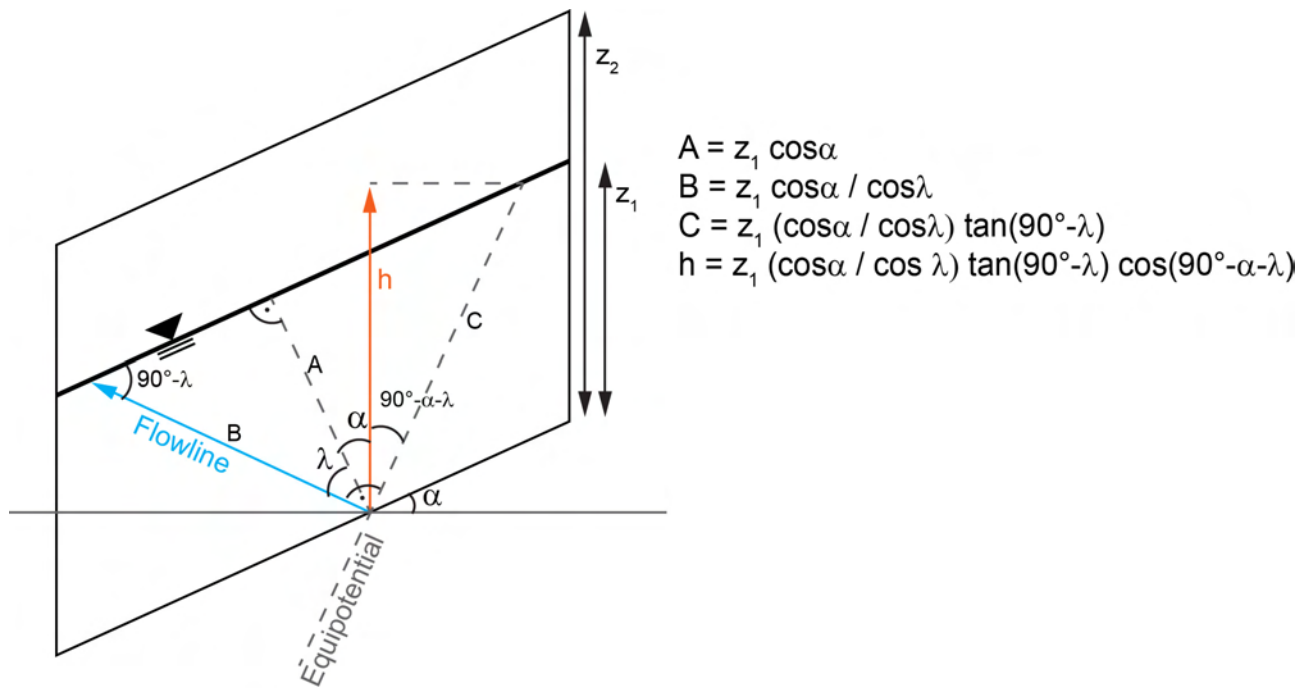
Figure 2.13: *Calculation of the hydraulic potential h in an infinite slope.*

2.4.3 Summary infinite slope theory

Shallow landslides are often translational and slide parallel to the slope and the bedrock surface. Therefore the infinite slope method is often suitable for this type of landslides. On the contrary, the assumptions of the infinite slope theory are rarely applicable for deep landslides. Rock slides for example often underlie local lateral porewater pressures due to saturated fractures. Thus forces acting on the side of the landslide do not cancel each other. It cannot be assumed that the landslide material is homogeneous and the slip surface is often complex and not slope parallel. Nevertheless, the infinite slope theory gives a good base to understand the forces acting on soil mass. In this section the different parameters like pore water pressure and seepage which influence the slope stability were discussed. This is the base for the understanding of the hydrogeological landslide triggering mechanisms described in the following section.

2.5 Landslide triggering mechanisms related to hydrogeology

It should be distinguished between "trigger", "triggering mechanism" and "cause". A trigger is a sudden event (Wieczorek, 1996) such as an earthquake, volcanic eruption, water-level change, intense rainfall, rapid snowmelt or human impacts that releases or reactivates the landslide (see Section 2.3.1). On the contrary, the triggering mechanism describes the physical, chemical and mechanical function of the triggering process that is connected with the loss of strength of the soil (Duncan and Wright, 2005). In literature, the term "landslide causes" is often used for long term processes leading to slope instabilities (Sowers, 1979). Cruden and Varnes (1996) distinguished between geological, morphological, physical and human causes. "Triggering mechanisms" described in this section do not refer to any time span. The increase in pore water pressure for example may be very slowly during a long-term low-intensity rainfall (cause) or it may be rapid as a consequence of an intense short rainstorm (trigger). Furthermore, in the present work, the term "pre-dispositions" is used to distinguish different characteristics of a slope which are crucial

for stability and which may change over a long time span (see Section 2.3.1).

As discussed above, water influences the stability of slopes in many ways (decreasing suction, positive pore water pressure, and seepage forces reduce the shear strength of soil). It is often impossible to isolate one effect of water and identify it as a single cause of failure (Duncan and Wright, 2005). Sowers (1979) stated: "In most cases, several "causes" exist simultaneously; therefore, attempting to decide which one finally produced failure is not only difficult but also technically incorrect. Often the final factor is nothing more than a trigger that sets a body of earth in motion that was already on the verge of failure. Calling the final factor the cause is like calling the match that lit the fuse that detonated the dynamite that destroyed the building the cause of the disaster."

Thus different processes operate always simultaneously and it is always an interaction between several factors that lead to the triggering of a landslide. Nevertheless it is important to evaluate the potential causes and to take into account the potential changes in time (Duncan and Wright, 2005). In this Section, the effect of water on the landslide triggering will be discussed qualitatively in terms of the increasing saturation, pore water pressure, seepage and plasticity.

2.5.1 Loss of suction

Additional water content leads to decreasing soil suction (for the definition of suction see Section 1.4) and thus to decreasing apparent cohesion. A reduction of the suction in unsaturated or partly saturated soil may be sufficient to trigger shallow landslides even if the soil is not completely saturated (Fourie et al., 1999; Godt et al., 2009). According to Equation 2.12, decreasing suction decreases the soil's effective stress. Thus the shear strength is reduced, which destabilizes the slope. The additional weight of water has an extra destabilizing effect on the soil. The moisture content of the soil may remain below saturation if the rainfall infiltration rate is below the hydraulic conductivity (Iverson et al., 1997). When the percolating wetting front reaches a critical depth in the soil, the slope may become unstable. This depth depends on the cohesion and the slope angle and is typically between 1 m and 2 m (Van Asch et al., 1999). Especially steep slopes with cohesionless soil are susceptible to fail before they are saturated (Iverson et al., 1997).

2.5.2 Positive pore water pressure

A rising groundwater table ("bottom up" saturation) within the saturated zone leads to a gradual growth of porewater pressure in the soil (Iverson et al., 1997). This process is frequently observed during heavy rainfall. As seen in Equation 2.10, an increase in the porewater pressure decreases the effective stresses in the soil (the total stress remains constant under drained conditions). This reduces the shear strength and destabilizes the slope. All types of soil are affected and the response time depends on the permeability of the soil: More permeable soil underlies more rapid changes. It has been shown that also in clayey soil pore water pressure can change rapidly due to secondary permeability as cracks, fissures, lenses of more permeable material (Rogers and Selby, 1980; Duncan and Wright, 2005). A rising positive water pressure can lead to the failure of slopes. Especially deeper landslides (5 m - 20 m deep) are triggered by raising groundwater level and thus positive pore water pressure on the slip surface (Van Asch et al., 1999). The factor of safety is very sensitive to a raising hydraulic potential (Rogers and Selby, 1980).

Like in unsaturated conditions, the increase in soil weight due to the water has an additional destabilizing effect, depending on the slope angle and if the cohesion is $\neq 0$. According to equa-

tion 2.16 the factor of safety increases with additional weight if cohesion is equal 0.

Cracks formed due to landslide activity or desiccation may be an additional destabilising element. Hydrostatic pressure can build up in cracks. This additionally loads the soil within the slope and thus destabilise it (Rogers and Selby, 1980).

Saturation of the soil may also occur "top down". Prolonged rainfall with intensity $\geq k$ can lead to vertical downwards steady state infiltration without development of positive porewater pressure even if saturation is reached. This is because the downward gradient $\mathbf{i} = dh/dz$ is assumed to be equal -1 what implies zero pore water pressure and the downward flux q equals the saturated hydraulic conductivity k. A saturated zone develops in the top soil and propagates downwards. Iverson et al. (1997) described a mechanism that after a first rainfall event, the soil can remain tension saturated and a subsequent high intensity rainfall can lead to an instantaneous rise in pore water pressure.

Lastly, the pore water pressure can also be increased if the total volume of the pores decreases. Consolidation due to settlement (especially in weakly bounded soil) and swelling (namely in clayey soil) can decrease the total volume of pores. As the total stresses remain constant, the effective stresses are reduced, which destabilizes the slope.

2.5.3   Seepage force

Seepage is the water flow through the soil that occurs when parts of the soil are saturated and when the hydraulic gradient is not equal zero. Seepage has basically two effects on the soil strength of the soil: Seepage force and seepage erosion.

The seepage force acts on the volume of the soil mass. The viscous drag of water flowing through the soil mass imposes pressure acting on the soil particles in the direction of flow. Thus seepage leads to an additional increase (or decrease) in the pore water pressure what affects the shear strength of the soil. Depending on the direction of the seepage, this fluid pressure may act against the restraining forces and decreases the factor of safety (Ghiassian and Ghareh, 2008). The direction of the water flow in a regional scale depends for example on the location in the slope (see Figure 2.10). The flow direction may change locally due to permeability heterogeneities. Figure 2.11 displays the slope stability for varying seepage directions for a soil with cohesion. The seepage force is minimal in slope parallel direction ($\lambda = 90$). The shear strength is maximal when the seepage is oriented downward. The most adverse seepage condition is oriented upward vertically to the slip surface. If the hydraulic head in the bedrock is higher than in the overlaying soil, water flows in an upward direction and leads to an upward pressure on the soil particles, which reduces the effective shear stresses in the soil. Discontinuities like bedrock fractures help to channel the groundwater into the overlaying soil (Wilson and Dietrich, 1987; Mathewson et al., 1990; Montgomery and Dietrich, 1994; Iverson et al., 1997). Upward seepage does not only enhance the potential for slope failure (hydraulic shear failure), but also for liquefaction (Section 2.5.5). Overpressure in a semi-confined aquifer favours upward seepage (Section 2.5.6).

If cracks in the upper part of a slope are filled with water, additional seepage may occur. Furthermore, seepage forces my locally be increased when the hydraulic gradient is increased. This is for example at the foot of landslides where the flow section is reduced (see Figure 2.14).
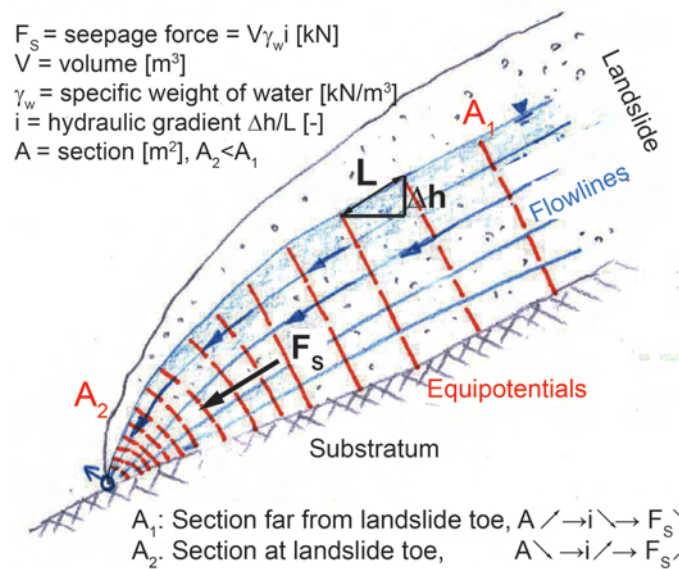
Figure 2.14: *At the toe of a landslide, the hydraulic gradient is larger because the section is reduced. This leads to larger seepage forces which favours seepage erosion. See Equation 2.13. Illustration modified after Parriaux et al. (2010).*

2.5.4   Seepage erosion

Seepage erosion (also named inner or internal erosion) is the dragging effect induced by seeping water in granular material (Lourenco et al., 2006). Water that seeps in the soil can lead to a mechanical displacement of soil particles trough the soil matrix or to regressive erosion and the formation of pipes. **Pipes** are preferential flow paths which have a higher permeability than the surrounding material. These processes loosen the soil. Seepage erosion is more efficient in sandy soils where the fine-grained components are washed out. Silt and clay-size fraction of the soil are deposited, eroded, redeposited within the flow network. This can continually change the permeability and flow path within the slope (Harp et al., 1990). Piping can reduce the contact between grains. This decreases the cohesion and the shear strength can decrease even though the pore water pressure does not rise. This process is particularly active at locations with high permeability and thus high flow velocity. It is not possible to calculate the effect of seepage erosion as it strongly depends on the local characteristics of the soil.

2.5.5   Liquefaction

When a saturated soil completely loses the strength, it collapses entirely and behaves like a fluid because high pore water pressure can not be relieved. This failure mechanism is called static liquefaction. Liquefaction occurs in both, coarse grained material (silty-clayey sand or gravel) with low plasticity and fine-grained high plastic material. Poorly sorted, loosely compacted, or cohesionless soils are especially sensitive to liquefaction. Overpressure, upward seepage and strong inner erosion favours liquefaction. If the vertical component of the seepage force is equal or greater than the saturated weight of the cohesionless soil, the effective stresses between the particles becomes zero and thus the frictional strength as well (Iverson and Major, 1986; Budhu and Gobin, 1996; Ghiassian and Ghareh, 2008). Cohesive soil will only liquefy if the cohesive bounds are broken, for example due to earthquake or landslide (dynamic liquefaction). Dynamic liquefaction may be caused when the porosity of the soil is reduced during failure. A reduced porosity leads to an increase of porewater pressure. The porosity may either be reduced due to contraction of the soil mass or if the soil particles dilate (Iverson et al., 1997).

If the failure of a landslide is governed by the Mohr-Coulomb mechanism or both, Mohr-Coulomb and liquefaction, strongly depends on the cohesion and the direction of the seepage vector λ (Iverson and Major, 1986; Budhu and Gobin, 1996; Ghiassian and Ghareh, 2008). The critical seepage direction λ for liquefaction in a slope with the inclination α is (Ghiassian and Ghareh, 2008):

$$\lambda_{crit} \leq tan^{-1}(tan\alpha/2tan^2\alpha + 1) \tag{2.20}$$

The limit seepage angle λ is displayed on Figure 2.11.

2.5.6 Overpressure

Overpressure (also named upthrust pressure, buoyancy forces, uplift) acting on the slip surface from below a landslide builds up if the hydraulic potential in the aquifer below the landslide is higher than in the landslide. This may happen if the permeability of the landslide is smaller than the permeability of the geological unit below the landslide. If an aquifer is limited on the upper boundary by a low permeable or impermeable horizon, it is named semi-confined or confined, respectively. If the hydraulic potential is higher than the ground surface, it is an artesian aquifer. An example of a locally confined aquifer is shown in Figure 2.16. Overpressure from below the landslide can act as a trigger mechanism (Rogers and Selby, 1980; Mikos et al., 2004) and may favour upward seepage and liquefaction.

2.5.7 Effect of water on high plastic soil

Water has an important effect on the strength properties of clays, especially of high plastic clays (Rogers and Selby, 1980; Duncan and Wright, 2005). The plasticity is a characteristic of the soil that describes how deformable it is without the soil particles loose the contact between each other (Lambe and Whitman, 1979). In other words, the plasticity describes how strong the particles in the soil stick together. This depends on the amount of water that can be absorbed by the soil. Only fine grained soil, especially clay-minerals can absorb sufficient water to become plastic because their particles have a large (electric charged) specific surface. Therefore the plasticity depends a lot on the soils mineralogical composition. The structure of Smectite (Montmorillonite, which is common in the Molasse rocks) can absorb more water than for example Kaolinite or Illite (also found in Molasse rocks). High plastic soils are generally cohesive.

The plasticity can be defined with the Plasticity Index IP = WL - WP (see Figure 2.15). The Liquid limit WL and the Plastic limit PW are consistence boundaries which can be defined by laboratory tests. The consistence describes the actual state of the soil depending on the actual water content. Different types of clays have different specific surface areas which controls how much wetting is required to cross the liquid limit or the plastic limit. The larger the IP of a soil, the higher is the plasticity (Lambe and Whitman, 1979). The Plasticity Index divided by the percentage of clay-sized particles gives the activity A of a soil (Lambe and Whitman, 1979). From the activity one can predict the dominant clay type present in a soil sample. High activity signifies large volume change when wetted and large shrinkage when dried. Soils with high activity are chemically very reactive. Normally, the activity of clay is between 0.75 and 1.25. In this range clay is called normal. It is assumed that the plasticity index is approximately equal to the clay fraction (A = 1). When A is lower than 0.75, it is considered as inactive. When it is larger than 1.25, it is considered as active.

Plastic soil tends rather to slow landslides than rapid movements. Nevertheless rapid movements could occur for example when a large amount of water infiltrates under pressure from below the
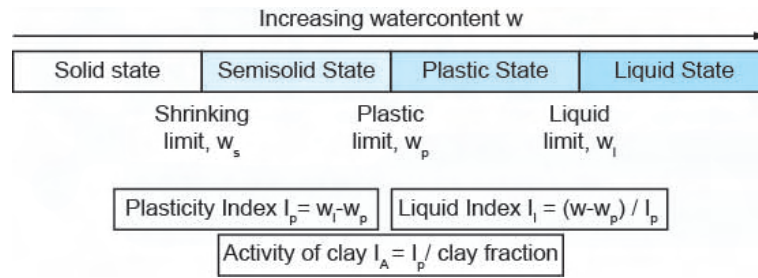
Figure 2.15: *Definition of the plasticity index IP. The plasticity index shows the range of water contents where soil exhibits plastic property. This is important for quantifying how much a soil expands and shrinks. In sand, the IP is zero. An IP of 5-10% is considered as low (silt) and IP > 40% is high (clay) Lambe and Whitman (1979).*

landslide which liquefies the soil and triggers a rapid liquid flow. On the contrary, when the groundwater table rises slowly, the clay is swelling and no landslide is triggered. Silt and sand are not plastic and, depending on the slope angle, can become unstable even when the groundwater table is rising slowly.

The mechanical behaviour of clay is affected by the physico-chemical interaction between particles, the water in the voids and the ions in the water. The following mechanisms can be distinguished:

- Chemical processes and weathering: Water that seeps through pores in the soil changes the chemical composition of pore water. In marine clays for example, salt can be leached out. Such chemical processes reduce the shear strength in clay (Duncan and Wright, 2005).

- Slickensides: Slickensides develop in clayey soil, especially high plastic clays, as a result of shear along distinct planes (Duncan and Wright, 2005). Plate-like clay particles reorientate along slickenside surfaces, which reduces drastically the shear strength of the soil. The residual friction angle on the slickenside surface may be 5 - 6° whereas the peak friction angle of the same soil without slickensides may be 20 - 30°. Sand and silt size particles inhibit the formation of slickensides.

- Swelling: High plastic clay is sensitive to swelling when in contact with water (especially when over consolidated and under confining pressure). Swelling increases the void ratio which decreases the shear strength (De Gaff, 1978; Duncan and Wright, 2005).

- Shrinkage and formation of cracks: Capillary tension can cause extension cracks in clay. These cracks increase drastically the permeability of the soil and if they are filled with water, high hydrostatic pressure is acting against the soils strength (De Gaff, 1978).

- Wetting-drying cycles: Periodically wetting and drying favour the continuous and irreversible downhill creep of clays under sustained load. A failure plane can develop (Duncan and Wright, 2005).

2.6   Effect of bedrock infiltration and exfiltration

Many authors put focus on the in-situ infiltration of rainwater into the soil as main triggering mechanism of landslides (Onda et al., 2004). They did not take into account a possible exfiltration of bedrock groundwater into the overlaying soil which may contribute to slope failure. Infiltration and exfiltration are described in Section 3.5. A first aim of studying in-situ infiltration (Iverson, 2000; Wang and Sassa, 2003) is to model the soils shear strength depending on

saturation. A further aim is to apply the models over large areas where the parameters slope angle, curvature, soil properties and rain intensity were known. Bedrock infiltration and exfiltration are rather local processes which were rarely taken into account for regional slope stability models, even these processes may be good indicators of landslide susceptibility (Onda et al., 2004; Kosugi et al., 2006). Assuming the bedrock to be an impermeable model boundary may lead to large errors by simulating pore water pressure development in slopes (Ebel et al., 2007).

Bedrock infiltration depends strongly on the lithology and is determinant for resulting landforms (Onda et al., 2004). The draining effect of different lithologies influences the landslide triggering (Matsushi and Matsukura, 2007) and the type of landslide (Onda et al., 2004), because fissures, fractures and permeable bedrock layers can act as drains for landslides if the bedrock is not saturated (Van Asch et al., 1999).

Depending on predispositions of a landslide, water circulating in rock fissures and joints can control the triggering of landslides (Rickli et al., 2008). An overcharged bedrock aquifer can lead to increased pore water pressure in the unconsolidated sediment at locations of bedrock springs and seeps. This increased pressure from below results in localized slope failures (Mathewson et al., 1990). Temporary springs issuing from bedrock in fresh landslide scarps can be important indicators for flow through bedrock fractures (Calcaterra and Santo, 2004; Cascini et al., 2008b; Di Crescenzo and Santo, 2005).

One of the first authors who mentioned these processes was Everett (1979). He studied the triggering of debris avalanches in the Appalachian region. He found out that water from heavy rainstorms was moving downwards through extensively fractured silty shale and coal beds to the surface of the relatively less jointed sandstone beds. The flow was lateral to the soil mantle of the hillslope, where it increased pore pressure and consequently triggering debris avalanches (see scheme on Figure 2.16). The shallow groundwater flow in fractured bedrock and the landslide triggering effect was also investigated by Montgomery et al. (2002) and Montgomery et al. (2009) in unchannelled valleys in the Oregon Coast Range. They monitored local upward flow from the bedrock into overlying colluvium and showed that exfiltration from bedrock fractures related to heavy rainfall is connected with landslide initiation. Water exfiltration from the bedrock in scar areas that influences the failure of slopes was also observed by Johnson and Sitar (1990).
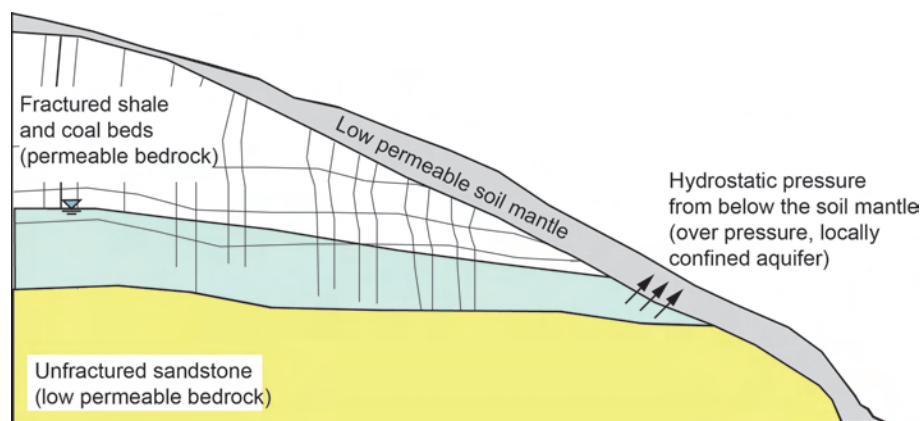
Figure 2.16: *Scheme of the landslide triggering mechanism described by Everett (1979). Water is infiltrating in heavily fractured bedrock and percolates downwards to a low permeable horizon where positive pore water pressure is build up. The increased pore pressure below the soil cover destabilizes the slope and triggered landslides.*

In Switzerland the phenomena of bedrock exfiltration was observed for example during the rainstorm event 2005 mentioned in Section 2.3.3 in the Prättigau area (Canton Graubünden), where "fountain like" water outlets have been observed along the slopes, which indicated the extreme pore water pressures in the soil. During the same rain event, extremely high water pressures causing earthquakes were observed in the karstic formations of the Bürgenstock, central Switzerland, where water outburst triggered several landslides (Liniger, 2006). Groundwater exfiltration from the bedrock under high pressure has been observed also during the rainstorm event 2005 in the region of Napf (Canton Bern). From the rainstorm event in Canton Obwalden, 2000, it is known that middle to deep seated landslides (Lateltin et al., 1997) were governed by groundwater originating in the bedrock (Berwert-Lopes and Spichtig, 2006). But it is not known, to what extent this phenomena can be explained by a high water table in the mountain (Rickli et al., 2008).

2.7 Summary and open questions

The water content in unconsolidated sediment and bedrock is crucial for different chemical, physical and mechanical processes that influence slope stability, especially in clayey soil. Thus, saturation and pore water pressure are key factors for landslide triggering. But it is difficult or impossible to define one distinct triggering mechanism for a landslide, because several processes are often involved. Nevertheless, it is important to evaluate potential triggering mechanisms.

What are potential hydrogeological landslide triggering mechanisms and how can they be defined? Which geological and hydrogeological units should be taken into account and which parameters are determinant? Would a concept for the hydrogeological classification of landslides be useful to answer these questions and to better understand the hydrogeological behaviour of landslides?

Based on the knowledge of landslide research, slope hydrology and hydrogeology, and slope stability, these potential triggering mechanisms have to be analysed for a better understanding of landslides. In the following Chapter, a tool is presented (based on the two factors saturation and permeability) to evaluate the triggering processes related to the hydrology and hydrogeology. For this purpose, it is important to look at the system in a large scale by considering the hydrogeological interaction with the substratum. Thus flow through bedrock, infiltration and exfiltration are assumed to be important processes.

Chapter 3

Hydrogeological classification of landslides

3.1 Aim of the classification

As discussed in the previous chapter, numerous landslide classifications exist for different purposes, but as far as known by the author, none of them is based on the hydrogeological characteristics of landslides. Therefore the question arises, if it is possible to classify landslides in a reasonably simple way depending on their hydrology and hydrogeology. In this chapter, such a hydrogeological landslide classification is proposed. The aims of the classification are:

- Cover the dominant hydrogeological characteristics for different geological contexts and landslides.

- Describe the hydrogeological interaction between substratum and unconsolidated sediment cover for different geological contexts and landslides.

- Evaluate potential hydrogeological triggering mechanisms for different geological contexts and landslides.

- Provide a tool to better compare the hydrogeology of different geological contexts and landslides.

- Provide a tool to describe the evolution of the landslide hydrogeology in time (based on changes in the saturation).

- Evaluate, if a slope is in a critical equilibrium stage depending on the saturation of the landslide and the substratum (criticality).

- Put the three case studies in a common frame.

At the end of this work, the classification will be applied for several cases and it will be discussed if the concept is useful in practice. Knowing that the hydrology and the hydrogeology of landslides is very complex, this classification should remain relatively simple and applicable. In the following, the classification will be named "Hydrogeological classification for landslides" aware that also the hydrology is taken into account. In the next section the classification is described.

3.2 Structure of the classification

On Figure 3.1 the hydrogeological classification is shown. The classification is based on:

- Permeability contrast between 2 or 3 geological layers: high permeable and low permeable (rows in Figure 3.1).

- Saturation of the different geological layers: unsaturated, saturated and confined (columns in Figure 3.1).

A main assumption of the classification is that the landslide affects only the upper layer (or the two upper layers in the three-layer model) and that the slip surface is along the interface between the layers. Furthermore it is assumed that three dimensional geology and groundwater flow patterns can be reduced to two dimensions. This is because it is assumed that the conditions along the interface between the two layers is particularly important (see Section 9.3). All possible combinations of the two parameters "permeability contrast" and "saturation" are illustrated on Figure 3.1. Crosses signify unrealistic or impossible combinations. As function of the two parameters permeability contrast and saturation, the following processes can be described:

- Dominant origin of the groundwater (infiltration at the surface, lateral flow through unconsolidated sediment, exfiltration from bedrock).

- Potential hydrological triggering mechanisms.

In the following it will be explained why the permeability contrast and the saturation are chosen as main characteristics (Sections 3.3 and 3.4). Furthermore, the origin of the groundwater, the triggering mechanisms and the criticality for shallow, medium and deep seated landslides will be described (Sections 3.5, 3.6 and 3.7). In Section 3.8 the application of the classification will be explained.

3.3 Permeability

In Section 1.4 the parameters "permeability" (K) [m^2] and "hydraulic conductivity" (k) [m/s] were defined. In landslide research usually only the "hydraulic conductivity" (k), which is the proportionality constant in Darcy's law, is used as a material property. But in practice often the term "permeability" is used for the "k"-value. Therefore also in the present work, the term "permeability" will be used for the "k"-value. As described in Section 1.4, the permeability is determinant for the groundwater flow. Therefore it was chosen as a key parameter for the hydrogeological classification. Characteristics of the permeability of geological material are:

- Anisotropy: In an anisotropic soil, the permeability depends on the direction of water flow. Anisotropy is caused for example due to horizontal structures like layering or vertical structures related to vegetation and bioactivity. Anisotropy can be crucial for example when it impedes vertical flow and favours lateral flow in a succession of horizontally layered sediments. Anisotropy is not directly taken into account in the classification. Generally, the permeability in the direction of the groundwater flow is assumed to be determinant and representative for one layer.

- Temporal variations: As the permeability depends on the soil saturation (see Figure 1.3, B and D), it is subject to temporal variations. These variations can be seasonal for example due to infiltration of rain water and snow melt water or evapotranspiration of plants. Seasonal variations are more pronounced in montmorillonitic and smectitic clay soils with swelling and shrinking properties (Oosterbaan and Nijland, 1994). In some cases, reduced saturation can also lead to enhanced hydraulic conductivity. For example in clayey soils desiccation cracks can be formed (Rogers and Selby, 1980). Additionally, bioactivity or extension cracks can enhance the permeability. In the classification, changes in time can be illustrated by drawing the path from one "permeability - saturation type" to an other until failure (see Section 3.4).
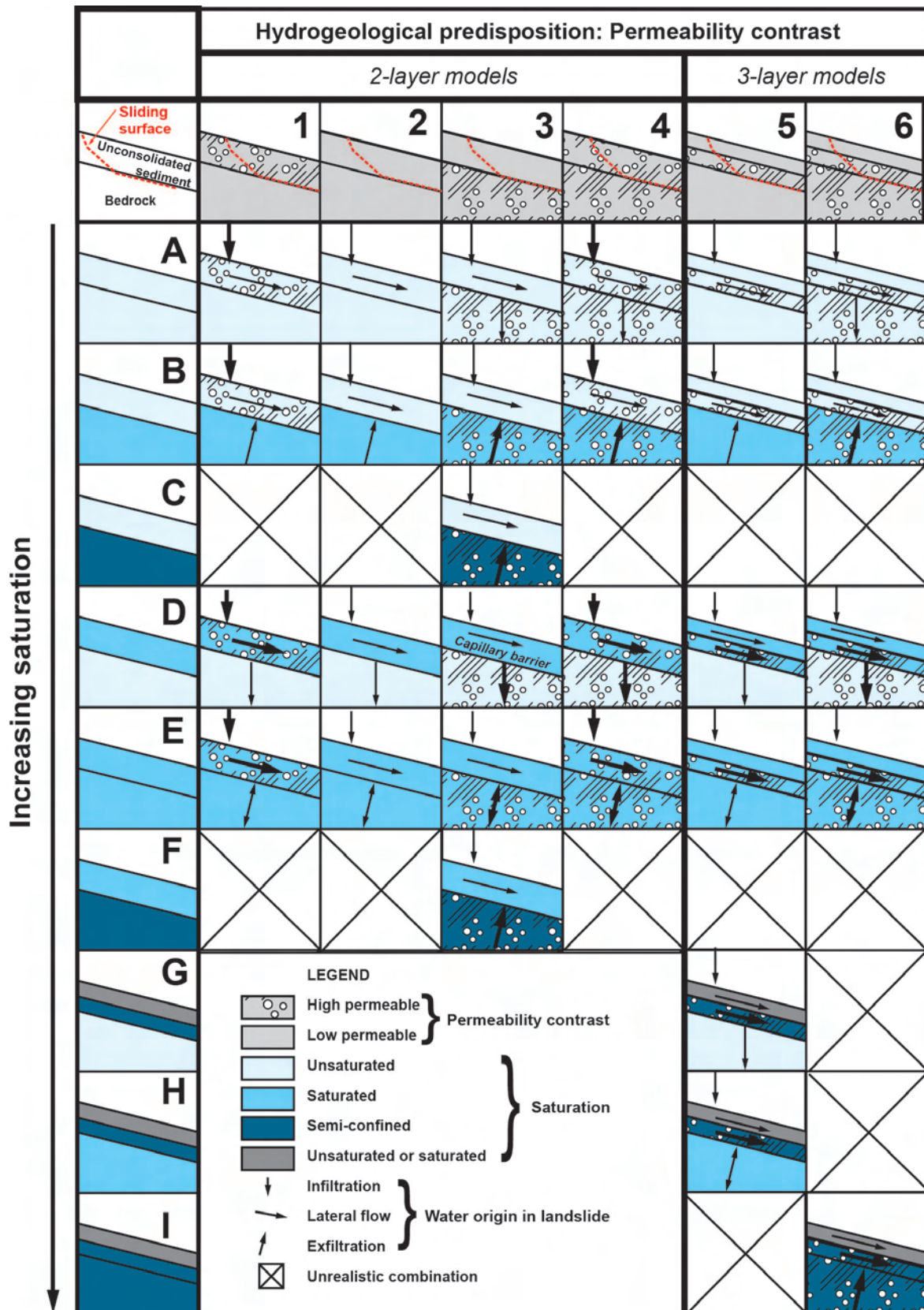
Figure 3.1: *Hydrogeological classification for landslides. The classification is based on the permeability contrast between two or three layers (rows, see Section 3.3.4) and the saturation of the different layers (columns). A permeability contrast of two orders of magnitude (or larger) that occur abruptly (in between less than one meter of profile) is significant (Rogers and Selby, 1980; Carvalho Vieira and Ferreira Fernandes, 2004). The combinations of the three parameters gives information about the potential hydrogeological triggering mechanisms of landslides (see Figure 3.6).*

- Primary and secondary permeability: Primary and secondary permeability refer to the time of formation of the permeability. Primary permeability are the micro pores that arose during the formation of the soil or rock. Secondary permeability are macro pores that formed afterwards due to external forces like tectonic (joints and fractures), vegetation (roots), animals (borrows) or water and erosion (cracks and fissures caused by slope instability or dryness). Matrix flow occurs through micro pores and is often several orders of magnitude smaller than flow through macro pores. Macro pores play a very important role for preferential groundwater flow (Van Asch et al., 1999). Most high permeable layers are characterised by macro pores. The effect of macro pores on slope stability is not evident: On the one hand, they are draining the slope and have a rather stabilising effect. On the other hand, they favour preferential flow what can lead to inner erosion and favour local formation of positive pore water pressure (Van Asch et al., 1999). In the classification it will not be distinguished if the permeability is primary or secondary.

- Heterogeneity: Different studies have shown that the permeability in landslides is very heterogeneous because of to the complexity of landslide bodies (Matti, 2008; Johnson and Sitar, 1990; Debieche et al., 2011). To simplify the complex permeability pattern of landslides, in the classification a two-layer or a three-layer situation with two different permeabilitiy (high permeable, low permeable) is assumed: A top layer of unconsolidated sediments, a bottom layer which is usually the fresh bedrock and in some cases, an intermediate third layer. This intermediate layer usually consists of altered bedrock, but could also represent a second unit of unconsolidated sediments, for example alluvial deposits[1] below moraine. Lateral heterogeneity is neglected in this assumption because often too many uncertainties exist.

In the following, the three possible layers "unconsolidated sediment", "fresh bedrock" and "altered bedrock" are described more precisely.

3.3.1 Permeability of unconsolidated sediments

Unconsolidated sediment is the loose material above the bedrock for example quaternary moraine, colluvium [2] or eluvium[3]. In literature, these sediments are named "soil mantle", "regolith" or just "soil". In this work the term "soil" is used either in the context of soil mechanics and slope stability or referring to the pedologic soil layer. In the context of geological lithologies, the term "unconsolidated sediments" will be used.

Unconsolidated sediment is classified according to the grain size as clay, silt or sand with gravel or stones (Table 3.1). The grain size distribution of soil is determinant for the water retention (high for fine grained soil, small for coarse grained soil) and the water storage capacity (fine grained soil can hold more water than coarse grained soil).

Primary permeability of unconsolidated sediment mainly depends on the grain size distribution, porosity and moisture content. Secondary permeability for example due to extension cracks and preferential flow due to heterogeneities (described in the previous section) can increase drastically the overall permeability of the unconsolidated sediment and should be taken into account. Table 3.1 shows the grain size, porosity and hydraulic conductivity for different soils.

---

[1]Alluvium is unconsolidated sediment eroded and deposits by non-marine water.

[2]Colluvium: Product of erosion or ancient mass movement deposits on slopes.

[3]Eluvium: Unconsolidated sediment that was washed out in-situ and thus is depleted in easily dissolvable minerals.

Soil type	Grain size [mm]	Total porosity [%]	Effective porosity [%]	Hydraulic conductivity k [m/s]
Clay	≤ 0.002	> 50	< 5	$< 10^{-9}$
Clayey silt		40 - 55	3 - 8	10^{-6}-10^{-9}
Silt	0.002 - 0.063	45 - 50	5 - 15	10^{-6}-10^{-7}
Silty sand		33 - 40	8 - 12	10^{-5}-10^{-7}
Sand	0.063 - 2	40 - 45	15 - 35	10^{-3}-10^{-5}
Sandy gravel		25 - 35	20 - 25	10^{-2}-10^{-4}
Gravel	2 - 63	30 - 40	20 - 35	10^{-1}-10^{-2}

Table 3.1: Total porosity, effective porosity and hydraulic conductivity (Hoelting and Coldewey, 2009) for different grain size/soil types. The porosity depends on the grain size composition, the shape of the grains and the consolidation of the soil, therefore this table gives only general values of porosities. Total porosity is high for fine grained soil but relatively low in coarse grained soil. The effective porosity is generally small for fine grained soil and large for coarse grained soil because clay minerals retain a large amount of water. Total porosity is equal effective porosity + water retained by soil grains. Only the effective porosity participates to the Darcy groundwater flow.

3.3.2 Permeability of bedrock

In most cases, the bottom layer (substratum) in the classification is the bedrock which can be sedimentary, magmatic or metamorphic rocks. The primary permeability in bedrock is usually small except for example in porous volcanic rocks or little-lithified sandstones. Sediment layers with higher permeability are for example found in Molasse formations and Flysch rocks in "layer-aquifers" (see Figure 3.2). The hydraulic conductivity of the rock depends mainly on the secondary permeability. Depending on the tectonic history of the rock it is fractured and may form a "joint-aquifer" (see Figure 3.2). The hydrogeology of crystalline massifs in the Alps was studied in several tunnels (Maréchal and Etcheverry, 2003). Discharges from less than 1 litre per minute in the Great Saint Bernard to several hundreds of litres per minute in the Mont Blanc tunnel were recorded. Unloading fractures are assumed to reach a depth in the rock massif of about 500 m forming the more permeable "decomprssion zone" (Maréchal and Etcheverry, 2003). Carbonate rocks are often karstified due to the dissolution of $MgCO_3$ and $CaCO_3$ in contact with water and form "karst-aquifers" (Clemens et al., 1997; Einsiedl, 2005; Ford and Williams, 2007). In a karst aquifer the conduit permeability is usually more important than matrix and fracture permeability. If the rock has a permeability $>10^{-5}$ m/s it is considered as an aquifer, if the permeability is between 10^{-5} and 10^{-9} m/s it is an aquiclude and if the permeability is $<10^{-9}$ m/s it is an aquitard (Hoelting and Coldewey (2009), see Table 3.2). If permeable bedrock is not saturated it can act as a sink for the groundwater in the overlaying soil. If permeable bedrock is saturated or even confined, it can act as a source of groundwater in the overlaying soil.
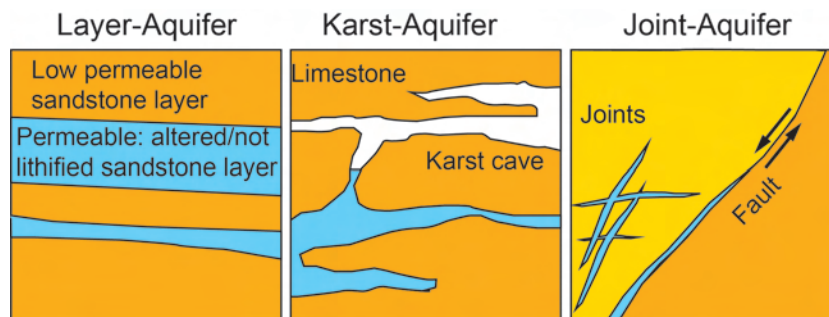
Figure 3.2: Different types of bedrock-aquifers.

Rock type	Aquifer	Aquitard	Aquiclude
Limestone, primary permeability			x
Limestone, fissured	x		
Sandstone, primary permeability		x	x
Sandstone, fissured	x		
Basaltic igenous rock	x	x	x
Gypsum, primary permeabilty			x
Gypsum, karstified	x		
Claystone, small scale			x
Claystone, rock formation	x	x	x

Table 3.2: *Disposition of some rock types in aquifer (k >10^{-5} m/s), aquitard ($10^{-5} < k < 10^{-9}$ m/s) and aquiclude (k <10^{-9} m/s), modified after Hoelting and Coldewey (2009).*

3.3.3 Permeability of weathered bedrock

The transition between the bedrock and the unconsolidated sediment is rarely sharp. The upper part of the bedrock is often altered. Therefore there is a change in permeability compared to the fresh bedrock. The layer of altered bedrock can be crucial for the groundwater flow pattern of a slope and the triggering of landslides. Therefore in the classification (in the three-layer case) it is considered as a separate layer.

The altering process depends on the availability of water, the chemical composition, and the rock type. On the one hand, physical weathering (fracturing) and chemical weathering (dissolution, for example dissolution of the calcitic cement between grains in sandstone) increase the permeability. If the weathered bedrock is highly permeable, it can act as preferential flow path. Due to irregularities in the low permeable bedrock surface, this can lead to the development of local positive pore water pressure in hollows. In karstic areas, the formation of epikarst[4] and dolines favours the infiltration (Clemens et al., 1999).

On the other hand, initially fractured or porous rock that contains clay minerals may become less permeable. The weathered bedrock in this case may be a low permeable clayey layer and initial pores or fractures become clogged with unconsolidated clayey sediment. If the layer of weathered bedrock has a low permeability, it can act as a barrier either for groundwater flowing in the overlying unconsolidated sediment or for groundwater exfiltrating from the bedrock beneath. This can either lead to the formation of a perched groundwater table above or a confined aquifer below the weathered layer. Both situations are unfavourable for the slope stability. These two processes are equal in a three-layer situation and a two-layer situation, because only two layers are affected. Therefore the case of a low permeable intermediate layer is not specified in the classification.

In some cases it may be difficult to determine if a rock is weathered or not. In the classification from Hoek and Brown (1997), which provides a tool to the estimate the strength of rocks in the field, "Highly weathered or altered rock" is defined as: "The rock crumbles under firm blows with point of a geological hammer. It can be peeled by a pocket knife." In the classification from Hoek and Brown (1997), "Highly weathered or altered rock" has a strength of of 1-5 MPa and is specified as "very weak". In the hydrogeological classification it is assumed that a rock is weathered when the permeability changed significantly (at least for one order of magnitude) in comparison with fresh bedrock.

---

[4]Epikarst may be formed at the top of a limestone formation. It is permeable due to dissolution of calcite.

3.3.4 Permeability contrast classes 1-6

Determinant for the groundwater flow pattern in landslides is the relative and not the absolute permeability. The permeability contrast controls preferential flow and the formation of positive pore water pressure. These are both important processes for the triggering of landslides. Therefore the permeability contrast and not the absolute permeability is used in the hydrogeological classification. Because of the horizontal layering, the vertical permeability contrast is assumed to be dominant and the lateral permeability contrast is neglected in the classification. On Figure 3.1 the contrast of permeability is displayed with a signature for high permeable layers. A permeability contrast of two orders of magnitude (or larger) that occur abruptly (in between less than one meter of profile) is significant (Rogers and Selby, 1980; Carvalho Vieira and Ferreira Fernandes, 2004).

If two layers are assumed, four different combinations of high and low permeable are possible (classes 1-4 in Figure 3.1). In a three-layer situation, it would be a total of eight combinations[5]. Nevertheless, the three-layer cases can be reduced to two classes (class 5 and class 6 in Figure 3.1)). The other three-layer combinations are already taken into account by the two-layer cases. (For example if the unconsolidated sediment and the weathered bedrock are high permeable over low permeable bedrock, the implications on the landslide triggering are similar to the case where there is only one high permeable layer over low permeable bedrock). The six classes are:

1) High permeable top layer over low permeable bottom layer:

- Example: Horizontal beds of permeable ash overlying impermeable mudflow deposits, Nishigo Village, Japan (Chigira, 2002). Often, the top soil is more permeable due to macro pores than the subsoil and thus plays an important role for the infiltration and lateral drainage of the soil (Van Asch et al., 1999).

- Hydrogeology: Rainwater infiltrates in the unconsolidated sediment and percolates downwards to the impeding layer where a groundwater table is formed. Mainly in the saturated zone, water is flowing parallel to the slope towards the toe of the slope. The subsurface storm flow theory (see Section 2.2.2) is based on the assumption of a permeable layer over one or more impeding layers or a progressive decrease in permeability with depth (Kirkby, 1978). Depending on the rain intensity, the saturation can occur bottom up or, by transient water-table perching, top down (Iverson et al., 1997; Lourenco et al., 2006; Kienzler, 2007).

- Landslides: The situation of permeable unconsolidated sediment over an impermeable substratum is very frequent in the case of shallow landslides. Convergent topography (hollows) favour saturated flow and make a slope additionally susceptible for the local accumulation of groundwater and thus for landsliding (Iverson et al., 1997; Chigira, 2002; Montgomery et al., 2002).

2) Low permeable top layer over low permeable bottom layer:

- Example: Fine grained moraine covering fresh granite or clayey silt covering Flysch (Trisenberg landslide, see Section 8.3).

- Hydrogeology: The in-situ infiltration capacity of the low permeable top layer is small and water percolates slowly as subsurface stormflow in the top layer. Long-term rainfall is needed to saturate the unconsolidated sediment. During precipitation, the saturation of the soil can occur top-down and perched groundwater tables are formed inside the low permeable top layer (Iverson et al., 1997; Lourenco et al., 2006).

---

[5]Variation with repetition: $n^k = 2^3$

- Landslides: In low permeable unconsolidated sediment, especially when high plastic, landslides are rather continuous and slowly creeping than rapid movements.

3) Low permeable top layer over high permeable bottom layer:

- Example: Morainic material over a relatively high permeable dolomite (Mikos et al., 2004).

- Hydrogeology: The capacity of in-situ infiltration is small and little water percolates through the low permeable top layer. If the bottom layer is unsaturated, a capillary barrier may form at the transition between the two layers (Lu, 2010) and only little water infiltrates into the bottom layer. If the bottom layer is saturated a confined or an artesian aquifer can be formed, which increases the pore water pressure on the potential landslide slip surface. If the bottom layer is semi-confined, little water exfiltrates into the top layer (aquitard). This is common for example in deposits of river deltas or coastal plains, where low permeable clay overlies high permeable sand or gravel beds. In this case, the flow in the aquitard is mainly vertical (Oosterbaan and Nijland, 1994). The bottom layer may be fed further upslope by infiltration of rain water and it is likely that the hydrogeological catchment is larger than the hydrological catchment.

- Landslides: When the bottom layer is semi-confined, confined or artesian, a very unfavourable situation for the triggering of landslides can develop. High porewater pressure and seepage forces from below can lead to inner erosion and liquefaction and a hydraulic shear failure can occur.

4) High permeable top layer over high permeable bottom layer:

- Examples: Silty little clayey sand over Molasse sandstone (Bollinger et al., 2000).

- Hydrogeology: Water infiltrates easily at the surface and percolates trough the unconsolidated sediment. If the bottom layer is saturated, groundwater can exfiltrate into the top layer. If it is unsaturated, it acts as a sink and water infiltrates. But no confined groundwater can be formed.

- Landslides: If the hydraulic head in the bottom layer is higher than in the top layer, groundwater flow is upward which is unfavourable for the triggering of landslides. Inner erosion and liquefaction may occur.

5) Low permeable top layer and high permeable middle layer over low permeable bottom layer:

- Example: Low permeable colluvium material and volcanic ash (silty clay) over strongly weathered greywacke with jointing pattern (sandy silt, silty sand) over fresh low permeable greywacke. (Rogers and Selby, 1980).

- Hydrogeology: Water infiltrates (for example through cracks in the top layer, at the top of the slope) into the middle layer which has considerably higher hydraulic conductivities than the overlying horizons. Flow takes place through the permeable middle layer. This can lead to semi-confined or artesian aquifers, especially if the bedrock shows an irregular topography and hollow structures (Figure 3.3) or at the toe of a landslide.

- Landslides: If the lower soil horizon is more permeable than the surface horizon, an upward pressure may develop. This favours sallow landsliding (Rogers and Selby, 1980). Water penetrating downwards in the permeable horizon can create upthrust and buoyancy effects. The formation of confined aquifer and preferential water flow in

the permeable middle layer enhances the potential for inner erosion and liquefaction. On the contrary, a permeable middle layer can act as a sink which would rather stabilize the slope.
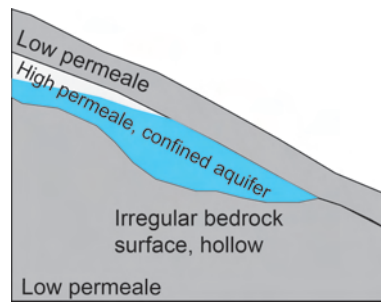
Figure 3.3: Irregular bedrock surface and hollow structures can locally lead to the formation of positive pore water pressure and confined aquifers.

6) Low permeable top layer and high permeable middle layer over high permeable bottom layer:

- Example: Fine grained moraine over fractured and weathered conglomerate (Ruffberg, Chapter 7).
- Hydrogeology: Little precipitation water infiltrates in-situ. If the bottom layer is saturated, groundwater may exfiltrate into the middle layer.
- Landslides: Like in case 5), preferential flow and confined groundwater enhances the potential for inner erosion and liquefaction.

It is often impossible to define a single permeability contrast class for a certain landslide. For example if the bedrock underlying a large landslide has a draining function in the upper part but a feeding function in the lower part of the landslide. Thus, it is possible to combine several classes with respect to the location on the landslide. Nevertheless, it should be possible to choose on class that is determinant for the triggering mechanisms. In this example, the feeding function of the lower landslide part should be considered.

3.4 Saturation

Landslide triggering mechanisms related to decreasing suction and rising groundwater level (see Section 2.5) depend on the saturation and thus on the porewater pressure (see Figures 1.4 and 1.3). Furthermore, with the parameter saturation, the evolution of the hydrogeology in time is taken into account. Therefore, the saturation has been chosen as second key parameter for the classification (see Figure 3.1).

In the previous section it has been discussed that the influence of the permeability contrast on the landslide triggering depends on the saturation of the different layers. For example when a permeable bottom layer is saturated it acts as a source for the groundwater in the landslide. When it is unsaturated, it acts as a sink, which has a rather stabilizing effect on the hillslope. If the substratum is effectively draining the overlying layer, it is difficult to build up a positive pore water pressure in this upper layer. Therefore, the saturation has to be concerned separately for each layer. For example if the top layer is saturated, the bottom layer can be unsaturated and vice versa. This strongly influences the triggering mechanism.

In the classification, three saturation stages are distinguished: unsaturated (negative por water pressure, suction), saturated (positive pore water pressure) and semi-confined. Unsaturated means, that the entire layer is not saturated. The upper layer is assumed to be saturated if a groundwater table exists, (even the layer is not saturated up to the ground surface). The lower layer is assumed to be saturated if the groundwater table is about at the slip surface. A semi-confined aquifer is formed if the upper limit is defined by a low permeable layer and the hydraulic potential in the aquifer lies higher than this boundary. A confined aquifer would be formed, if the upper layer is completly impermeable, which is rarely the case in nature. Therefore, in the classification the term "semi-confined" is used. A special case is the artesian aquifer which occurs when the hydraulic potential lies above the ground surface and an overpressure from below is formed.

With the parameter "saturation", the dimension of time is taken into account in the classification because of the transient character. For analysing the changes from the initial saturation to the saturation during the landslide triggering, the path of increasing saturation can be drawn in the classification. This can be done for both the reactivation of a landslide and a newly formed landslide. Additionally, the delay of the reaction of a slow moving landslide to a precipitation event can be discussed. Nevertheless, for the final triggering mechanisms (as defined in the classification) it is not of interest how long it took to saturate the landslide or to reach a semi-confined situation.

For landslides it is determinant how much and how rapidly water can be stored. The rain intensity and the rate of infiltration are crucial for the timing when an aquifer will be saturated. If the saturation front of a perched groundwater patch that is seeping downwards and reaches a water table or an impeding layer, the saturation conditions can change immediately from unsaturated (suction) to saturated (positive pore water pressure) (Iverson et al., 1997). The response time of an aquifer to a rain event or snow melt depends on several parameters shown in Table 3.3.

Parameter	Favours slow and smoothed reaction	Favours fast reaction
Initial saturation*	Low	High
Water retention**	Small	Large
Effective porosity	Large	Small
Aquifer type***	Unconfined	Confined
Permeability****	Low	High
Rainfall	Low intensity and long-term	High intensity and short-term
Snowmelt	Slow and early	Fast and late

Table 3.3: *Qualitative influence of important hydrological and hydrogeological parameters on the response time of aquifers (slow/fast) to precipitation events. *For example after snowmelt, the soil is more saturated and a rain event can trigger a landslide more easily than the same event occurring before snow melt. Especially the saturation of the top soil is of interest which is controlled by evapotranspiration. **The water retention influences the initial saturation and is higher in fine grained soil. Fine grained soil can hold more water than coarse grained soil. ***In a confined aquifer, the specific storage coefficient is much smaller and thus the hydraulic potential rises faster than in an unconfined aquifer. ****Low permeability avoids rapid infiltration and thus favours rather slow movements.*

It is assumed that the reaction of deep landslides involving large aquifers with a favourably high storage capacity (not confined aquifers) is delayed and smoothed after a long-term rain event. Short but intense events have little impact on such systems. Furthermore, if the permeability of to top layer is small, only prolonged (low intensity) rainfall can lead to saturation. On the

contrary, shallow landslides with high permeability will response fast to a heavy rain event of short duration. Thus deep landslides are more sensitive for long-term precipitation periods and shallow rapid landslides are more sensitive for short-term storm events.

3.5   Origin of groundwater

It is assumed that the origin of groundwater in landslides can be in-situ infiltration, lateral flow, or exfiltration from the bedrock:

- In-situ infiltration at the surface: The higher the permeability of the top layer is, the higher the capacity for in-situ infiltration of rain water (Iverson, 2000; Wang and Sassa, 2003) or snowmelt water is (Mathewson et al., 1990). The lower the permeability is, the more water runs off at the surface. Thus in-situ infiltration is more important for the permeability classes 1 and 4. The topography and the vegetation influence to a large extent the amount of water that infiltrates. For example water ponding in hollows or flowing along trees and tree roots can infiltrate more efficiently.

- Lateral subsurface storm flow through the layer of unconsolidated sediments: Water can also arrive through the unconsolidated sediments by lateral subsurface stormflow (see Section 2.2.2) especially above a low permeable boundary. Thus lateral flow is important for permeability classes 1, 4, 5 and 6. The water can arrive from further upslope or from the sides of the landslide for example when the topography forms rather a hollow structure (convergent flow). For example at La Frasse landslide, it has been shown that two-thirds of the water input was coming laterally from fractured bedrock (Tacher et al., 2005). Also in unsaturated conditions, flow can be lateral (Iverson et al., 1997).

- Exfiltration from bedrock (exfiltration from the substratum): Exfiltration from bedrock occurs either from a permeable layer (layer-aquifer, see Figure 3.2) or from fractures and joints (Joint-aquifer, karst-aquifer, see Figure 3.2). When the hydraulic potential in the bedrock is higher than in the top layer, groundwater may exfiltrate from the bedrock into the landslide (Johnson and Sitar, 1990; De Montety et al., 2007; Fifer Bizjak and Zupancic, 2009; Mikos et al., 2004). If the groundwater in the bedrock is semi-confined due to a low permeable top layer, only little groundwater exfiltrates but a pore water overpressure may build up below the potential slip surface. A semi-confined aquifer does not necessarily lead to upward seepage/overpressure. The piezometric level in the upper layer may be higher than in the lower layer and natural downward drainage occurs instead of upward seepage.

  Two cases should be distinguished: Either the groundwater exfiltrates directly below the landslide and contributes to the triggering by upward seepage and overpressure. Or the groundwater exfiltrates from the bedrock further upslope or at the side of the landslide and contributes as lateral flow through the unconsolidated sediment layer on the triggering. In this second case, bedrock exfiltration acts indirectly as lateral flow. This is for example the case for the active Triesenberg landslide (see Section 8.3).

  In the classification, several permeability contrast types could be used to illustrate groundwater exfiltration from the bedrock: Types 3, 4 and 6 may be used if the bedrock is permeable or shows many discontinuities like fractures and joints. Type 5 could be used to illustrate sporadic altered or fractured layers in the shallow bedrock or for the weathered bedrock layer below the unconsolidated sediment.

Exfiltration from the bedrock typically appears when the hydrogeological catchment is larger than the hydrological catchment. This could be observed for example at the Triesenberg landslide (François et al., 2007). An important indicator for bedrock exfiltration are springs (De Gaff, 1978; Onda et al., 2004). Springs can also originate in the unconsolidated sediment, but many spring types originate from the deeper bedrock as shown in Figure 3.4 (Springs B-F). If no springs are observed, the tectonic setting, fractures and joints observed on outcrops and the type of bedrock can give information about potential bedrock exfiltration.
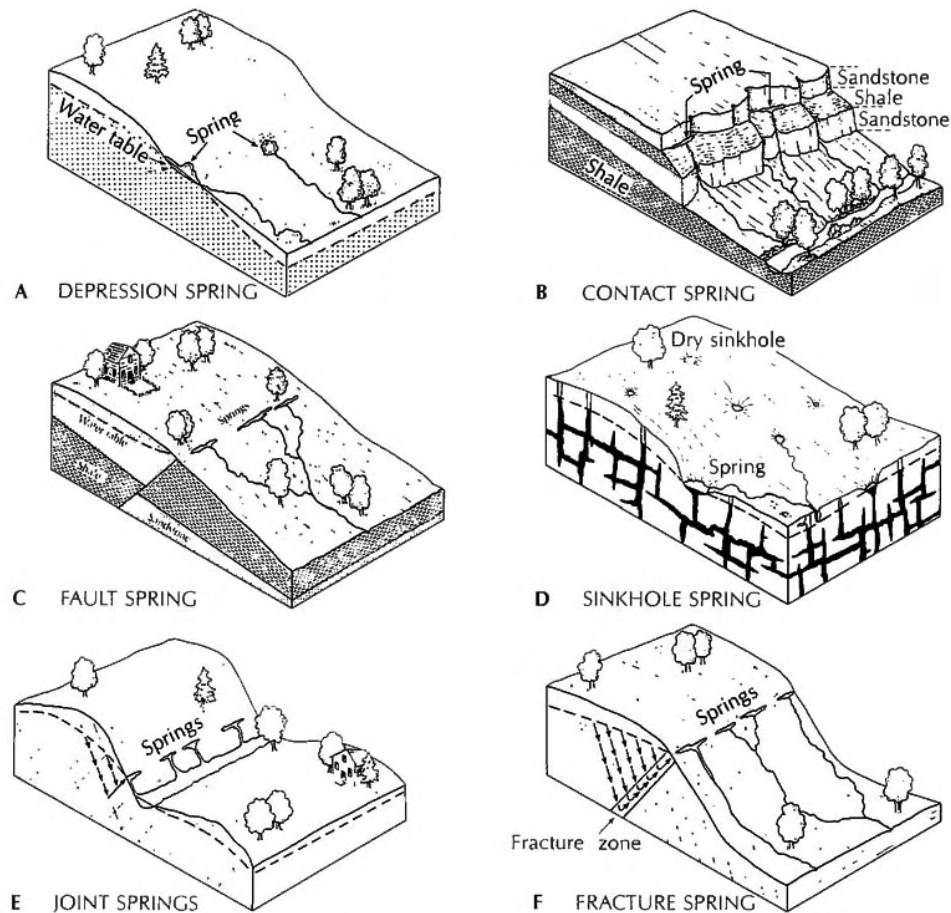
Figure 3.4: *Different types of springs depending on the geology and geomorphology according to Fetter (2001).*

In the classification (Figure 3.1), it is assumed that "unsaturated" and/or "low permeability" imply little flow, thus a thin arrow. On the contrary, "high permeable" and "saturated" conditions imply large flow, thus a thick arrow (see Figure 3.5).

A horizontal arrow in the classification (Figure 3.1) does not strictly mean lateral flow. In such a case, upward and downward flows are not excluded. The arrow only indicates the main origin of the water (bedrock, rain water infiltration, lateral input), and not the strict flow direction. The flow direction depends on the hydraulic potential h which is not quantified in the classification.
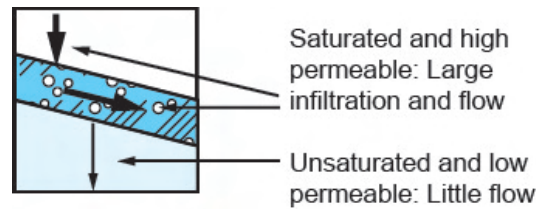
Figure 3.5: *Thick and thin arrows indicate large and little flow and the main origin of the groundwater in the potential landslide.*

Flow due to suction is neglected. Thus if the substratum is unsaturated (conditions A and D), it is assumed that no bedrock exfiltration occurs.

3.6 Potential hydrogeological triggering mechanisms

An aim of the classification is to define potential landslide triggering mechanisms related to hydrology and hydrogeology. In the case of slow moving landslides like the La Frasse landslide (see Section 8.2) it is more logical to talk about "acceleration mechanism" or "reactivation mechanism" than "triggering mechanisms". Nevertheless, in the classification the term "triggering mechanism" is used. In Section 2.5, the following seven mechanisms have been described:

- $\psi \downarrow$: Suction decrease. This mechanism is chosen if the upper layer is unsaturated.

- $u \uparrow$: Pore water pressure rise. This mechanism is important if the upper layer is (partly) saturated.

- E: Seepage erosion. This mechanism is important if the upper (or intermediate) layer is saturated and high permeable.

- L: Liquefaction. This phenomenon depends strongly on the soil type. Theoretically, liquefaction can occur whenever a soil is saturated. Upward seepage and overpressure may favour liquefaction.

- $\uparrow F_s$: Upward seepage force. This mechanism may be important when both, the upper and the lower (or intermediate) layer are saturated. If a regional scale is concerned, upward seepage depends on the location in the slope (see Figure 2.10). If only a part of the slope is concerned, upward seepage may depends on the local hydraulic potential and the hydraulic gradient in relation to local heterogeneities in permeability.

- OP: Overpressure. This mechanism is taken into account when the lower (or intermediate) layer is semi-confined. To produce overpressure, the hydraulic potential has to be higher in the lower layer than in the upper layer.

- PI: Mechanisms related to a high Plasticity Index. It is assumed that the upper layer may be plastic if the permeability is rather small.

As these mechanisms mainly depend on the permeability contrast and saturation, they can be classified for the different permeability-saturation types. On Figure 3.6, symbols for the different mechanisms are assigned to each type. For example loss of suction occurs in unsaturated conditions, positive pore water pressure in saturated conditions and overpressure occurs in the case of a confined aquifer. The mechanisms refer in each case to the upper (or middle) layer in which the landslide occurs.
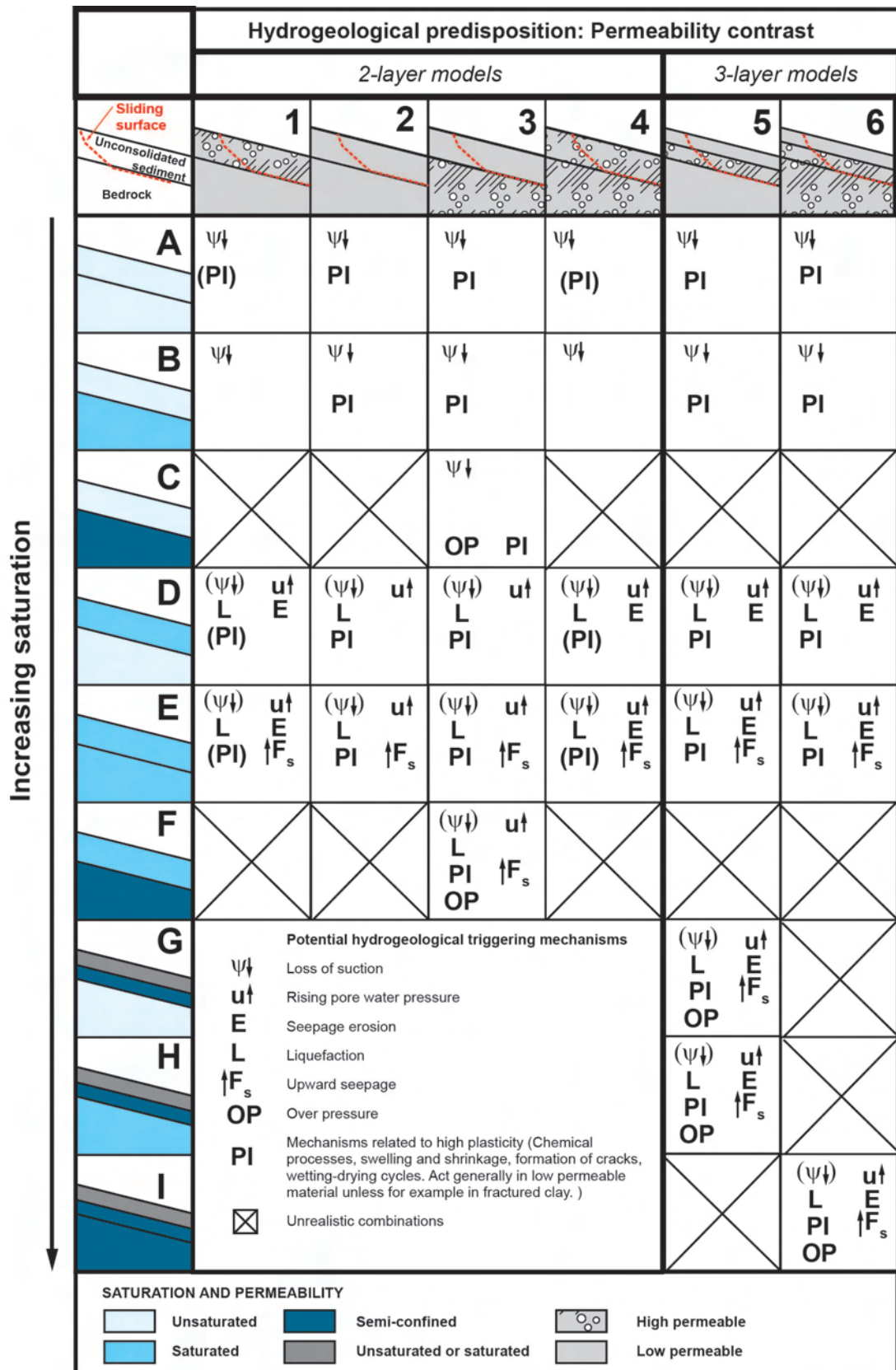
Figure 3.6: *Hydrogeological classification showing potential landslide triggering mechanisms. For the understanding of a landslide, it is important to evaluate potential triggering mechanisms. Mechanisms related to high plasticity (PI) should be considered in every case by determining or evaluating the Plasticity Index of the unconsolidated sediment. In the case of a permeable top layer, the plasticity is normally less important (PI in brackets).*

Generally, only low permeable unconsolidated sediment have a high IP. This is not completely true because clayey plastic soil can become permeable due to cracks.

It is possible that a landslide is divided into parts where different triggering mechanisms are dominant. For example inner erosion can be stronger at the toe of a landslide where the section is reduced and thus the seepage increased (Figure 2.14). So it is possible to combine different permeability-saturation types for a single landslide.

3.7 Types of landslides and the criticality

The developed classification may be used to estimate, if a slope is in a critical equilibrium stage according to the hydrogeology. The term "susceptibility" of a slope to landslides is often used to describe, if a certain slope is prone to landslides independent of changing conditions. Therefore, the term "criticality" is used in the present work to describe the hazard that a slope may become unstable at a certain stage depending on the hydrogeological parameters saturation and permeability contrast. Other parameters such as slope angle, vegetation and altitude are not taken into account in this estimation of the criticality.

On Figure 3.1, the landslide slip surface is indicated schematically. In the present classification, different types of landslides are defined according to their depth:

- 0-2 m: shallow landslide.

- 2 - 10 m: medium seated landslide.

- >10 m: deep landslide.

The criteria of landslide depth has been chosen because typical landslide types can be distinguished with the slip surface depth (Lateltin et al. (1997), Van Asch et al. (1999), for example rapid shallow landslide or deep seated creeping landslide, see Section 2.3.2).

It is assumed that the slip surface is along the boundary of permeability contrast. In most cases, this will be the interface between the bedrock or weathered bedrock and the overlaying unconsolidated sediment. Nevertheless, other cases are not excluded.

On Figure 3.7, the criticality for the three landslide types is shown. It is distinguished between high (red), medium (orange), low criticality (yellow) and the situation when it is unrealistic or impossible that a landslide will occur (grey). The criteria for this arrangement are qualitatively and based on experience and literature (Van Asch et al., 1999) and not on a specific method. This should indicate which combinations are not realistic and which combinations are unfavourable for the triggering of landslides. The following criterion were used:

- In unsaturated conditions, only shallow landslides can be triggered.

- In saturated conditions, landslides are possible at all depth.

- Deep landslides are unlikely if the bedrock is not saturated.

- A semi-confined aquifer leads to high criticality unless for deep-seated landslides. For these landslides, semi-confined conditions lead only to medium criticality because it is assumed, that a higher hydraulic potential has to build up below the landslide than for shallower mass movements to produce an over pressure. The probability for a hydraulic potential of about 10 meters is assumed to be smaller than for a hydraulic potential of a few meters.
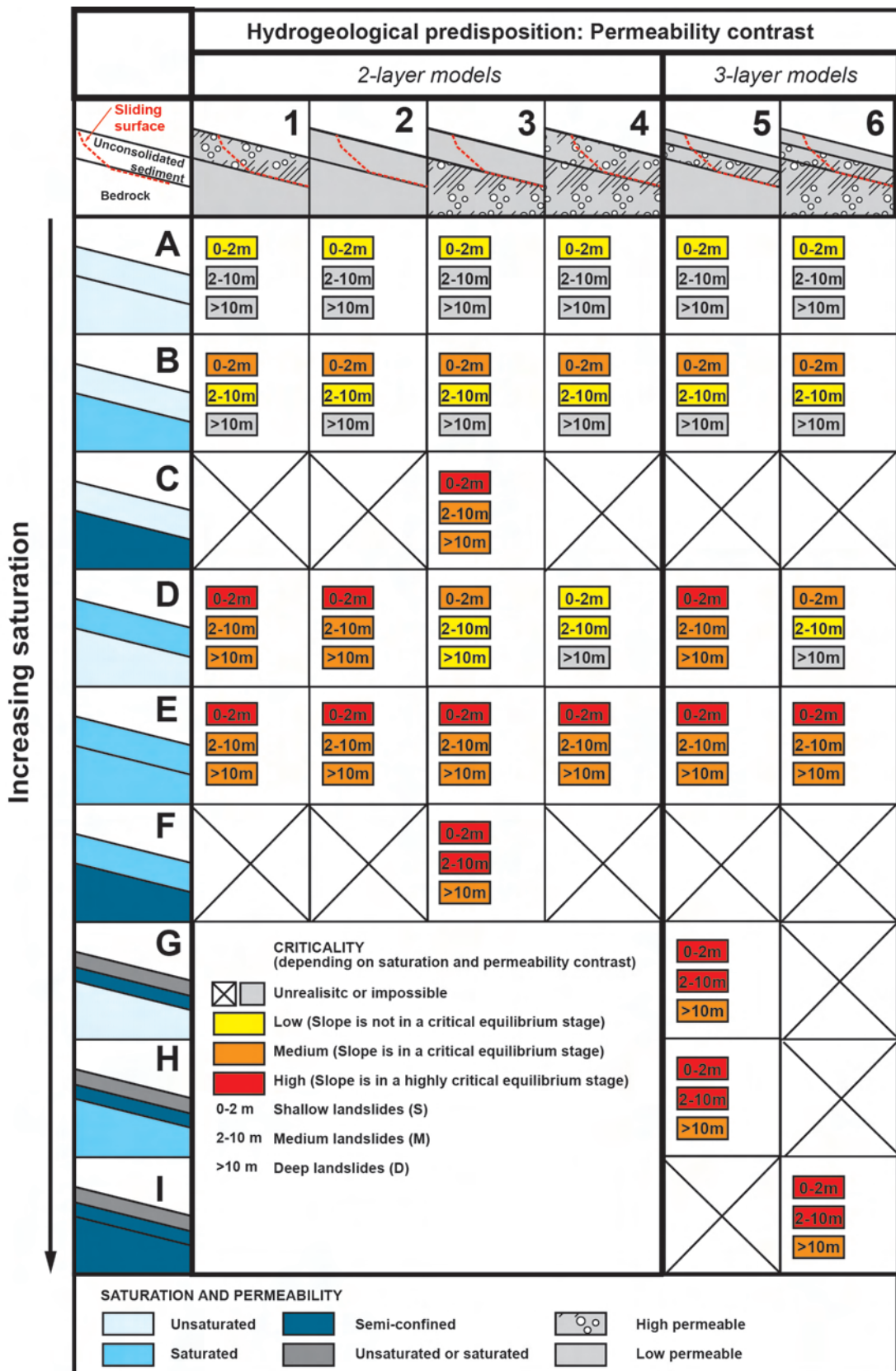
Figure 3.7: *Criticality of the permeability contrast-saturation types to shallow, medium and deep landslides.*

- Type C3 is only realistic, if the confined aquifer builds up rapidly. Otherwise, the upper layer becomes also saturated.

3.8 How to use the classification

To classify a landslide, the following steps have to be followed:

1) Determine the permeability contrast pattern (two- or three-layer model, Figure 3.1) → chose a permeability contrast 1-6 (rows). The three-layer cases where the intermediate layer (e.g. weathered bedrock) has the same permeability like the top layer are treated as two-layer class. If the intermediate layer is low permeable, it is considered as a mixture of class 1 and 3 (Section 3.3.4).

2) Determine the saturation of the different layers during the triggering → chose a saturation class A - I (columns) on Figure 3.1 (Section 3.4).

3) Read the dominant origin of the groundwater water (Figure 3.1) → in-situ infiltration, lateral flow or bedrock exfiltration (Section 3.5).

4) Define or estimate the plasticity of the upper layer (see Section 2.5.7).

5) Read the potential triggering mechanism (Figure 3.6)→ Suction decrease, positive pore water pressure, seepage force, seepage erosion, overpressure, liquefaction, high plasticity (Section 3.6).

6) Determine the depth of the landslide: → shallow, medium or deep (Figure 3.7).

7) Determine the criticality of the landslide → red: high, orange: medium, yellow: low, grey: unrealistic (Section 3.7, Figure 3.7).

8) Analyse temporal variations: Determine the initial saturation and permeability (see Section 3.4). Draw the path of increasing saturation until triggering. The system reacts fast or slow on rainfall (use table 3.3).

9) Analyse spatial variations: Determine if different permeability patterns are necessary for different parts of the landslide (Section 3.3.4).

10) Comparison of different landslides: If several landslides have been classified, groups of different types can be formed, for example according to the geology or climate, in order to better compare the hydrological and hydrogeological characteristics of the landslides.

The classification will be applied for the three landslides presented in Chapters 5, 6 and 7. Each of the three case studies shows a specific permeability contrast and thus is representative for a certain type in the hydrogeological landslide classification. Furthermore, several other well studied landslides in Switzerland were described to further apply the hydrogeological classification (Chapter 8). Figure 8.1 shows a map of Switzerland with the locations of the case studies and the additional landslides. Nevertheless, the classification can also be used outside of Switzerland.

Chapter 4

Applied field methods

4.1 Introduction

The investigation of landslides is complex and it is important to combine methods from different research fields (see Figure 2.8). In this study, different methods were chosen to characterise the geometry, geology, and hydrology/hydrogeology of landslides. This served as base for the discussion about the potential hydrogeological triggering mechanisms. In this chapter, the field methods applied for the three case studies, which were carried out in the frame of the present work, are described. Advantages and disadvantages of the applied methods are discussed. Table 4.1 gives an overview of the different methods including their aim (geological or hydrological/hydrogeological), interest (potential of the method), and case study for which the method was applied.

Section	Method	Aim			Case study			Interest for this study
		Geo	Hydro	M	Rue	PB	Rufi	
4.2	Mapping	x	x		x	x	x	++
4.3	ERT	x	x		x	x	x	+
4.4	Seismic refraction tomography	x				x		
4.5	Ambient seismic noise correlation			x		x		
4.6	Borehole drilling	x	x	x	x	x	x	++
4.7	Soil penetration tests	x			x	x		+
4.8	Piezometric measurements		x		x	x	x	++
4.9	Infiltration and pumping tests		x		x	x	x	+
4.10	Hydrological water balance		x		x	x		
4.11	Hydrogeochemical analyses		x		x	x	x	+
4.12	Tracer experiment		x		x			
4.13	Sulphur isotope analysis		x			x		+
4.14	Extensometer			x		x		
4.15	Time-domain reflectometer (TDR)		x		x			+
4.16	Tensiometer		x		x			+
4.17	Remote Sensing			x	x	x		

Table 4.1: *Overview of the methods applied for each case study. Aims: Geometry and geology of the landslide (Geo), Groundwater flow regime in the landslide, reaction to precipitation and snowmelt, origin of the groundwater (Hydro), and landslide movements (M). Case studies: Rüdlingen (Rue), Pont Bourquin (PB), Rufiberg (Rufi). Interest: positive and helpful results (+), important results (++).*

4.2 Mapping

Mapping is important for landslide studies. Without a detailed map, it is difficult to investigate a landslide. Three different types of maps are distinguished: Geological, geomorphological and hydrological maps. In this study, the geology, geomorphology and hydrogeology of the landslides and the surrounding areas have been mapped with the aid of a GPS Garmin eTrex Vista® HCx and blow ups of the 1:25'000 maps of Swisstopo.

4.2.1 Geological mapping

Geological mapping is the base for every landslide study and if possible should be completed with lithological data from drill hole logs. Geological maps should contain outcrops, lithological units, dip and strike of bedding planes and structural features like folds, foliation, lineation and faults. Tectonic boundaries and quaternary sediments can be included. Different lithologies and rock formations are drawn with different colours and it should be indicated, where they are exposed at the surface (outcrops) and where they are interpreted. Depending on the complexity of the geology and the size of the landslide, different scales for the geological maps are chosen. In a geological homogeneous terrain, the scale can be larger than in a zone where the lithology changes several times. The different lithologies may be described directly in the field (Bilgot, 2011) or rock samples are collected to analyse in more detail in the laboratory.

Advantages of the method: Mapping is not costly and no special equipment is needed. Geological maps are the base for landslide studies. A detailed map of the surface allows making extrapolations of the geology in the underground.

Disadvantages of the method: Mapping needs experience. A difficulty in mapping is that the bedrock is often covered by Quaternary sediments and vegetation. Thus uncertainties of lithological boundaries often exist. Sometimes, landslides expose bedrock which makes the mapping easier. In some cases with complex geology, the maps should be verified with drill holes.

Application of the method in the present study: The rock formations and quaternary sediments were described macroscopically from outcrops in the field. First, a map of the outcrops was drawn. This map was then geologically interpreted for zones where the bedrock was covered by vegetation or quaternary sediment.

4.2.2 Geomorphological mapping

Geomorphological maps describe surface forms and the material. Furthermore they provide information about the age of landforms and processes that created the landforms. Mapped features for landslides are scarps, cracks, rills and the micro topography like hollows, concave or convex hill slopes. Figure 2.6 shows the typical geomorphological features of a landslide. For a better understanding of the complexity of a landslide, a geomorphological map should always be made in combination with a geological map.

Advantages of the method: Geomorphological maps are important to define the limits of the landslide. Furthermore they can give information about the activity of a landslide.

Disadvantages of the method: The difficulty of a geomorphological map can be that the landslides evolve rapidly and the map has to be adapted regularly. It can be difficult to define the age of features which is important in landslide research.

Application of the method in the present study: Main, secondary and side scarps have been mapped as well as location and orientation of extension cracks. Additionally, superficial movements and deposition zones have been drawn on the map.

4.2.3 Hydrological/hydrogeological mapping

Hydrological maps may include features as rivers, streams, lakes and groundwater units, characteristics like aquifer productivity, vulnerability and circulation, springs and wells, and information about infiltration and exfiltration zones. In this study, the hydrological features creeks, springs and swamps were included in the geomorphological map.

Advantage of the method: Hydrological maps are often used for exploration or protection of ground- and surface water. Important information for landslide research is the size of aquifers, the location of infiltration and exfiltration zones and the location of springs.

Disadvantages of the method: Due to the activity of the landslide the water flow paths may change. Springs and swamps may dislocate or dry up. According to the season, the hydrology may additionally change and ephemeral springs may disappear.

Application of the method in the present study: Springs, creeks and humid areas were mapped.

4.3 Electrical resistivity tomography (ERT)

Electrical resistivity tomography (ERT) is a geophysical method. Geophysical methods (also seismic and ground penetration radar) are powerful tools to obtain information about the underground. This are either profiles in 1D, results of inversion processes in 2D or 3D, or time and space imaging in 4D (Jongmans and Garambois, 2007). Geophysical methods are based on the interpretation of contrasts in specific physical properties of the subsurface. These methods gives a picture of lithological boundaries, the limits of the landslide, the slip surface, internal structures and the saturation pattern of the soil and rock bodies.

For measuring the electrical resistivity of the underground, electrical potentials between electrode pairs are measured while a direct current is transmitted between another electrode pair. Figure 4.1 shows resistivity values for different rock, soil and water. According to Ohm's law, the electrical resistivity R can be calculated by knowing the induced current I and the measured voltage U. Different configurations of the electrode pairs are possible to record the apparent resistivity in order to obtain a 2D pseudo section of the underground (Lowrie, 2000):

- The Wenner and vertical electrode sounding (VES) configuration is best adapted to resolve vertical changes, thus to detect horizontal layers.

- The Schlumberger method is best to observe lateral inhomogeneities.

- The Wenner-Schlumberger method is suitable to record horizontal structures, such as the slip surface of landslides, and is better than the Wenner configuration to also detect vertical structures at the same time.

- The Dipol-dipol configuration is useful for the determination of spatially confined objects in shallow subsurface.

The recorded 2D pseudo section has then to be inverted. To create a 2D section of the subsurface resistivity, several iterations are performed to minimise the deviation between the initial
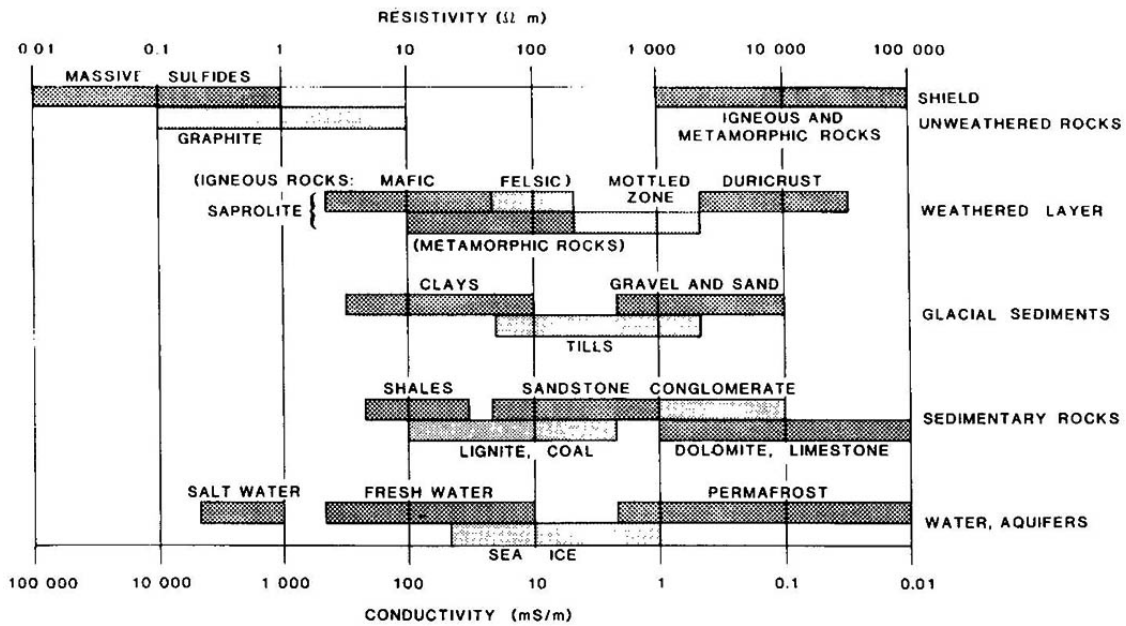
Figure 4.1: *Typical ranges of electrical resistivity of earth materials. Note the large differences in resistivity between unweathered and weathered rocks and also between water and frozen ground (Palacky, 1987).*

pseudo section of measured apparent resistivity and the simulated apparent resistivity values calculated from the subsurface model. The inversion models can be carried out with two different constraints:

- Standard least-square constraints (RMS): The standard method attempts to minimise the square of the difference between the observed and calculated apparent resistivity.

- Robust constraints (Abs): The robust method minimises the absolute difference between the measured and calculated apparent resistivity values. The robust inversion constraint method is less sensitive to very noisy data points and it is more suitable for sharp boundaries.

Advantage of the method: Geophysical methods are very helpful because they avoid expensive excavating or drilling works. Furthermore they may be used for the monitoring of landslide movements and groundwater flow. Advantages of ERT are that the electrode spacing and configuration can be adapted according to the investigation. The penetration depth ranges from some decimetres to several hundreds of meters and thus the resolution of the profiles can be adapted. Furthermore, there exist almost no restriction regarding topography, surface features, vegetation (Schrott and Sass, 2008).

Disadvantages of the method: The difficulty of geophysical methods is that the measured physical characteristics of the underground have to be interpreted into geological and hydrogeological materials and structures, which is not always evident. The inversed data is always an integration of the properties of a certain volume. Therefore the accuracy of the model decreases with depth. There is never a unique solution, especially if the contrast between the physical properties is not large enough. To avoid misinterpretation, it is recommended to combine different geophysical methods and to check the results with outcrops and drillings (Schrott and Sass, 2008). Another disadvantage of ERT is that dry soil or rock may impede good data acquisition. The interpretation of the tomography images may be difficult because the ranges of resistivity overlap

for different material and because the water content and fractures have a big influence on the resistivity.

Application of the method in the present study: In Rüdlingen, the ERT method was very useful to image preferential water flow paths in the altered bedrock and the changing saturation of the soil during the experiment. On Pont Bourquin landslide, ERT helped to localise the slip surface of the landslide and lithological boundaries in the bedrock. Additionally, ERT gave evidence for the existence of groundwater and saturation pattern. At Rufiberg, ERT profiles helped to estimate the thickness of the unconsolidated sediment, location of lithological boundaries and saturation patterns.

Data inversion was made with the software Res2DINV. The following settings and parameters were used:

- Constraint method: In the Pont Bourquin landslide (see Chapter 6) a sharp horizontal boundary (slip surface) as well as sharp sub-vertical boundaries (lithological boundaries) were expected. Therefore robust inversion method was chosen (see Figure 4.2).

- Robust data constraint cut-off factor: 0.05.

- Robust model constraint cut-off factor : 0.005.

- Cell size: Because large resistivity variations appeared near the surface, a model with cell width half the unit electrode spacing was chosen.

- Bad data points: Bad data points were removed manually.

- Number of iterations: Iterations were performed until the difference between two iterations was smaller than 5%.
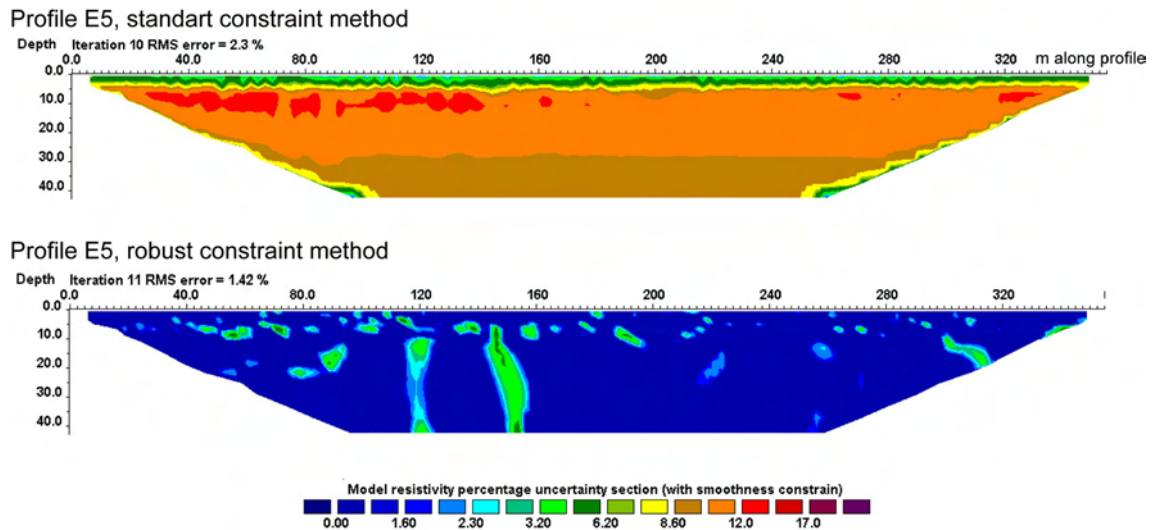
Figure 4.2: *Uncertainty of profile E5 for the standard constraint and the robust constraint method. The uncertainty of different models was used to find the best model parameters. For the standard constraint inversion, the uncertainty is more than 10% and for the robust constraint it is less than 1%. Because of the better result for the robust method and because sharp boundaries were expected in the profiles of the Pont Bourquin landslide, the robust constraint inversion method was chosen for all tomography profiles.*

4.4 Seismic refraction tomography

Two different elastic waves exist that can travel through the subsurface:

- P-wave: Longitudinal, compression or primary waves are deformation parallel to the direction of wave propagation.

- S-wave: Transverse, shear or secondary waves are particle motion perpendicular to the direction of wave propagation.

The velocity of the waves depends on the elastic modulus and the density of the material. Figure 4.3 shows values for P-wave velocities in different materials. It is assumed that the velocity in the landslide mass is minor than in the unaffected ground and increases with depth (Jongmans and Garambois, 2007). The propagation is determined by reflection and refraction of the waves at boundaries between layers: A part of the wave is reflected to the surface, a part is refracted along the boundary and a part is refracted into the lower layer. At a certain distance from the seismic source (crossover distance), waves that travel through deeper layers will overtake the direct waves. They will arrive faster at the surface because the velocity is increasing with depth.

Nature de la formation	Vitesse des ondes de compression m/s		Masse spécifique en T/m³	
	Hors nappe	Sous nappe	Hors nappe	Sous nappe
Terre végétale	250-350			
Éboulis	300-700	1500-2500	1,5-2	2-2,3
Sable fin	300-700	1450-1700	1,4-1,6	1,9-2
Graves	500-900	1700-2300	1,6-2,1	2-2,3
Argile	500-1400	1400-1700	1,3-1,7	1,8-2,1
Marnes	1800-2100	2100-3000	1,5-2,1	1,9-2,3
Grès	800-3000	2000-4000	1,6-1,9	2-2,2
Craie fracturée	800-1500	1700-2300	1,7-1,9	2,1-2,2
Craie saine	1800-2500	2300-3200	1,9-2,1	2,2-2,3
Calcaire fracturé	900-2000	1700-3000	2-2,2	2,2-2,5
Calcaire compact	3000-5000	3500-5000	2,3-2,4	2,4-2,5
Granite fracturé	1000-2500	2500-4500	1,8-2,1	2,1-2,3
Granite sain	4500-5500	4500-5500	2,3-2,5	2,4-2,6
Gneiss fracturé	1000-2500	2500-4500	1,9-2,2	2,2-2,5
Gneiss sain	5000-6000	5000-6000	2,3-2,6	2,5-2,7
Basalte fracturé	800-2500	2300-4500	1,7-2,1	2,1-2,3
Basalte sain	5500-6000	5500-6000	2,5-2,8	2,6-3
Quartzite fracturé	700-2500	1800-3500	1,6-2,1	2-2,3
Quartzite sain	3000-4500	3500-5000	2,3-2,4	2,4-2,5
Schiste altéré	500-2000	1700-2500	1,3-2,2	1,8-2,4
Schiste sain	2500-4500	3000-4500	2,1-2,5	2,3-2,6
Gypse	1000-3500		1,8-2,4	
Glace	3500-4000	3500-4000	0,95	
Nappe d'eau libre	1450-1500	1450-1500	1	

Figure 4.3: Seismic velocities for main geological units (Magnin and Bertrand, 2005).

The seismic signals are recorded with geophones placed into the ground with regular spacing. To detect a layer within the time-distance plot (see Figure 4.4), the geophone spacing must be smaller than the difference between two following crossover distances (Schrott and Sass, 2008). Depending on the velocity contrast between the layers, the penetration depth of the seismic waves is 3-5 times less than the profile length. The seismic signal is usually made by hitting a

sledge hammer on a plate placed on the ground. For distances larger than 50-100 m between source and geophone it is recommended to use explosives to impact enough energy.
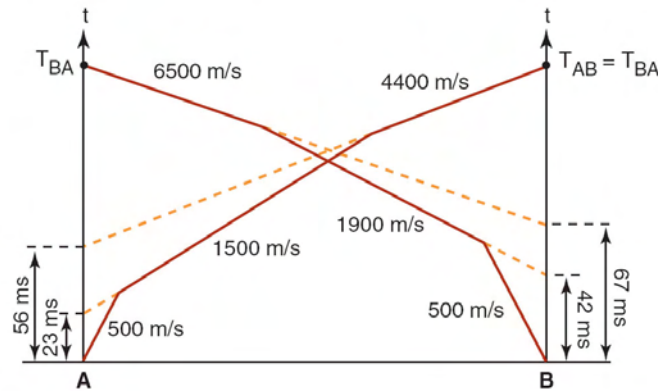
Figure 4.4: *Example of a travel time diagram for a model with three layers with different P-wave velocity (Magnin and Bertrand, 2005). The x-axis represents the distance along the seismic profile. A and B are two locations of the geophone and the source of the seismic signal along the profile. The y-axis is the travel time in milliseconds. T_{AB} and T_{BA} is the travel time of the wave from the source to the geophone.*

The seismic refraction method is based on the interpretation of the first arrivals of P-waves. The travel time of a wave between the seismic source and the geophone is used to make time-distance plots (see Figure 4.4). Anomalies in the travel time are cause by irregularities of the interface and varying velocities within different layers. Different methods exist to interpret the recorded travel times (Schrott and Sass, 2008): intercept time method, wave front inversion method, network ray tracing, and seismic tomography. Seismic tomography is based on inverting first-arrival times to get an image of P-wave velocity distribution in the ground (Jongmans and Garambois, 2007).

Advantages of the method: Horizontal bedding can be detected if the difference in P-wave velocity of the layers is strong enough. The main objective of the application of seismic refraction in landslide research is the assessment of depth to bedrock and the detection of the slip surface. Seismic refraction tomography allows determining also lateral P-wave variations. As advantage of seismic refraction, the large range of observed velocity values 400-6500 m/s can be mentioned.

Disadvantages of the method: Seismic refraction tomography requires more travel-time data than classical seismic refraction. Like in the resistivity method, velocity values for different material overlap and the weathering and fracturing of the rock influences the velocity. Another problem is that intermediate layers with low velocity are not detectable. Additionally, it can be difficult to detect exactly the first onset of seismic waves. Noise in the seismic record due to wind, torrents, rainfall, or traffic makes the interpretation more difficult (Schrott and Sass, 2008). Seismic refraction tomography smoothes velocity contrasts and is therefore best adapted for near surface investigations of the progressive transition between unconsolidated sediment and bedrock. For sharp contrasts in the lithologies, other refraction methods like the delay or plus-minus method are more adapted. With those methods, vertical structures can also be detected, whereas with travel-time analyses, mainly horizontal layers are detected.

Application of the method in the present study: In this study, seismic tomography was made with the software Sardine (Demanet, 2000).To test the robustness of the inversion model, it was helpful to use different initial models for the tomography. P-wave velocities were estimated for different geological units by dividing the travel-distance by the travel-time. Based on the

obtained layers with different P-wave velocities, initial models for the seismic tomography were created. With the seismic tomography software Sardine, the best results were obtained by using a homogeneous initial P-wave velocity model (Demanet, 2000).

A cell size of half of the geophone spacing was found to give best results: 2.5 m for the long profile and 1.5 m for the short profiles. With a cell size of 5 m, the tomography shows less detail. The optimal number of iterations was 5 - 7. With more iteration, artefacts started to develop and the RMS[1] error didn't decrease further.

With seismic refraction, the slip surface of the Pont Bourquin landslide (which corresponds most likely to the bedrock surface), lateral variation in the landslide thickness, and lateral variations in the lithology of the bedrock could be determined. These results correspond well with the ERT data but provide no additional information and needed more effort for both, field work and data processing.

4.5 Ambient seismic noise correlation

Ambient seismic noise correlation is a method to monitor landslides by measuring the evolution of the seismic surface wave velocity within the subsurface (Mainsant et al., 2011). The seismic wave propagation is directly related to the mechanical properties of the soil, i.e. density and shear modulus. The shear wave velocity in clayey landslide significantly decreased due to breaking in the landslide mass previously to the triggering. Ambient noise is continuously acquired by two passive sensors as if one of them was a source. Frequency-dispersion analysis allows to locate the change in shear wave velocity at the base of the sliding layer.

Advantages of the method: The reproducibility of the seismic source, which is necessary for ensuring that seismic response changes actually result from changes in the soil, is difficult. Ambient noise correlation overcomes this problem. It is possible to measure apparent relative velocity changes of the material with a precision lower than 0.1%.

Disadvantages of the method: Pre-cursors like cracking and braking in the landslide mass are necessary to predict the ultimate landslide.

Application of the method in the present study: The noise correlation technique was applied for detecting mechanical property changes in the Pont Bourquin landslide.

4.6 Bore hole drilling

Shallow drill holes are performed by hand with a hand auger, engine auger or a tripod hammer rig. Deeper holes are performed with a drilling rig. According to the drilling depth, hole diameter, soil and rock type, and accessibility, different drilling rigs are used. It is drilled constructive or destructive. By constructive drilling, soil and rock cores are evacuated to the surface and the geological material is analysed. By destructive drilling, the material is destroyed during drilling.

Advantages of the method: In landslide research, drill holes provide very important information about the lithological profile, the slip surface depth, the movements and the groundwater level. Additionally, geophysical, geomechanical and hydrological test can be carried out in drill holes.

---

[1]The root mean square error (RMS) is a measure of precision for the model. It is the differences between values predicted by the model and the observed values.

For examples inclinometers can be installed in drill holes. Rock and soil samples from the cores can be described and used for strength parameter analyses in the laboratory.

Disadvantages of the method: The installation of boreholes is costly and can be complicated on steep slopes, and they can be sheared rapidly on active landslides.

Application of the method in the present study: In the three case studies, the following rigs were used:

- Rüdlingen: Hand auger (drill hole depth 1 - 2.5 m, sediment samples were evacuated to the surface and could be analysed), engine auger (drill hole depth 2 - 4 m, sediment samples were evacuated), TerrBohr Bohranlage MC 400 device (drill hole depth 3 and 23 m, cored, see Figure 4.5).

- Pont Bourquin: hand auger (drill hole depth 1 - 3 m), tripod hammer rig (drill hole depth 2 - 4 m, sediment samples were evacuated to the surface, see Figure 4.6), Geotool GTR crawler drilling rig (drill hole depth 5 - 9 m, cored).

- Rufiberg: Flexible 1.5-tonne drilling rig operated by *Gasser Felstechnik AG* Gasser rig (see Figure 4.7, drill hole depth 2 - 9 m). Diameter was 11 cm for destructive drilling with a Mitsubishi hammer system and 7 cm for coring with a rotating diamond drilling head.

When it was cored, the soil and rocks were described macroscopically according to colour, grain size, and organic components, structures like layering and fractures, heterogeneity, plasticity, consistence. The strength of rock samples was tests with a geological hammer by counting the blows until breakage. Special attention was paid on signatures from water circulations like coloured and altered fractures. Photographs were taken from all cores.

Figure 4.5: *Photograph of the drilling platform and drilling rig located above the test site, March 2009.*

4.7 Soil penetration tests

For the dynamic penetration test with variable energy, a conical wedge is driven into the soil by manual hammering. Based on the penetration rate, the mechanical resistance of the soil can be

Figure 4.6: *Photograph of the tripod hammer rig used on the Pont Bourquin landslide, June 2009.*

Figure 4.7: *Photograph of the drilling rig used on the Rufiberg slope, November 2010.*

calculated by counting the number of blows for a defined penetration depth (for example 10 cm).

Advantage of the method: Penetration tests are a low-cost and fast method to obtain information about the in-situ soil strength properties. This is complementary to borehole information. Lithological boundaries, especially the bedrock surface can be localised with this method.

Disadvantage of the method: The difficulty is that single rock blocks can be interpreted as bedrock. Also, the transition to bedrock may be continuous instead of a sharp boundary and thus is not easily detected.

Application of the method in the present study: On the Pont Bourquin landslide several penetration test have been performed. On the Rüdlingen triggering experiment, DPL data were provided by the *Institute for Geotechnical Engineering* (IGT), ETH Zürich. An energy of 50 kJ was applied with a 10 kg-weight that was dropped for 0.5 m in order to drive the probe into the soil (Springman et al., 2009). The diameter of the cone was 35.7 mm and the dip angle 90° which gives a cross section of 10 cm^2. The number of blows was calculated for each 10 cm. The criterion for bedrock was 30 blows per 10 cm penetration. With a grid of 2 m spacing, the depth of the bedrock was investigated over the test site. This data was then refined with drill hole information and measurements of the bedrock that was exposed after the landslide triggering experiment. With ESRI GIS this data was interpolated over the entire test site using a grid of 1 m spacing (see Figure 5.6).

4.8 Piezometric measurements

Observation wells are essential to understand the hydrological functioning of a landslide. Monitoring the groundwater level in drill holes provides information about the water flow pattern in the landslide and the response of the aquifers to precipitation. To monitor the groundwater level in the bore hole, either a piezometer has to be installed or a water pressure sensor has to be placed directly into the soil. A third system is a mixture of this two methods which allows to measure directly the water pressure without losing the sensor[2]. For this purpose, tubes were constructed to place the sensor in rills which seals it upwards. The sensors were placed 0.5 m above the bottom of the drill holes.

In any case, the piezometric tube has to be installed with caution. The tube should be slotted only at depth of interest, for example at 1 m from the bottom. In order to avoid up-silting, the slotted section should be protected by geotextile and refilled with coarse sand. Above the sand, the hole should be refilled with an impermeable material, for example bentonite pellets, in order to avoid bypass. It is possible to install several piezometer tubes with small diameter and different length in a single drill hole in order to monitor the groundwater at different levels (they should be separated for a few meters to avoid bypass). It is recommended to fill the tubes with water during the installation to avoid the inflow of dirty drilling water which is often trapped at the bottom of the bore hole.

Monitoring the groundwater level and pore water pressure gives information about daily and seasonal fluctuations in the aquifer, about the reaction of the aquifer to precipitation events and the environment (for example evapotranspiration):

- Pressure sensors in open piezometers give information about the permeability of the geological layer after pumping water or adding water into the well.

---

[2]Such a system was developed by *Solexperts* AG, Mönchaltdorf (Piezo Press System).

- If the water storage capacity is small, the pore water pressure will rise a lot faster than if the water storage capacity is large.

- Confined or unconfined aquifer: Changes in the ambient air pressure give a different response in confined or unconfined aquifers. In confined aquifers, rising air pressure is pushing the ground water table downwards, which results in a lower water pressure. In unconfined aquifers, the additional air pressure is added to the water pressure which leads to a higher groundwater pressure even the groundwater level remains constant.

- Also the vegetation has an influence on the groundwater table, during the growing season, the groundwater is lower. Also daily fluctuation in the evapotranspiration can have an influence on the groundwater table.

- Landslide movements and opening or closing of cracks can lead to sudden draining of the piezometer.

Advantage of the direct installation of the sensor: The sensor will react fast on pore water pressure fluctuations. The sensors can be easily installed at several depths. This is particularly of interest if different aquifers are separated by impeding layers. In such a case it is important to seal the sensors in order to avoid by bass of groundwater.

Disadvantage of the direct installation of the sensor: A sensor installed directly in the soil cannot be evacuated. This is a problem if it should be repaired or if it is not used any more.

Advantage of the piezometer: Advantages of a piezometer is that the sensor is accessible and the ground water can be sampled and chemically analysed.

Disadvantage of the piezometer: The groundwater table in a piezometric tube can react with a delay in low permeable soil.

Advantage Piezo Press System: The advantage of the Piezo Press System is that the response of variations in the pore water pressure is much faster than in open water piezometers, which is particularly useful in low permeable material.

Disadvantage Piezo Press System: This system is more expensive than the other two variants and special equipment is needed.

Application of the method in the present study: In the 23-m deep drill hole in Rüdlingen, 4 Piezo Press Systems were installed. Also At Rufiberg, several Piezo Press Systems were installed. In all other observation wells, open water piezometric tubes were installed. Periodically, the groundwater level in the observation wells was measured manually with an acoustic piezometric senor. Additionally, several piezometers were equipped with pore water pressure sensors.

4.9 Infiltration and pumping tests

Infiltration tests are methods based on Darcy's law to determine the saturated hydraulic conductivity k of the soil above the groundwater table. The hydraulic conductivity is a very important parameter because it determines the subsurface drainage systems. It controls the rate of water infiltration. An overview of different infiltration tests is given on Figure 4.8. Detailed descriptions of different methods to measure the saturated hydraulic conductivity can be found in Oosterbaan

and Nijland (1994).

The hydraulic conductivity of the geological layers can also be calculated by extracting water from the observation wells.
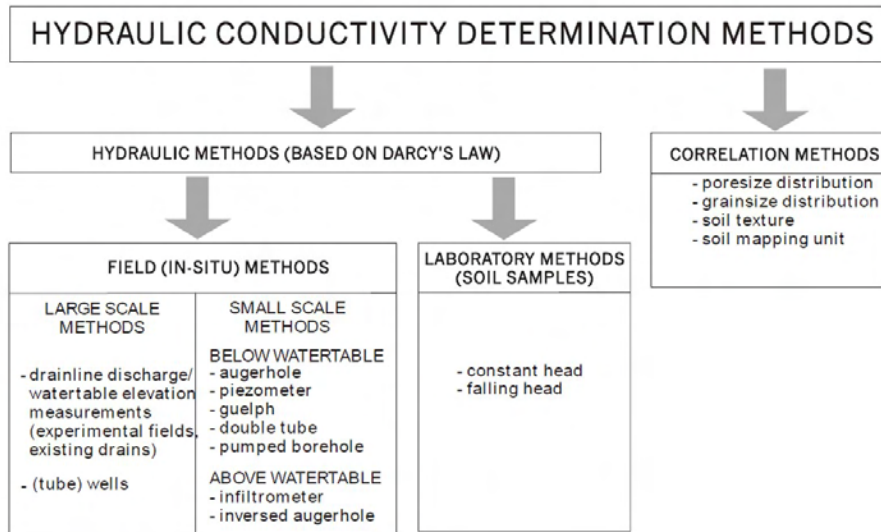
Figure 4.8: *Different field methods to determine the hydraulic conductivity of geological layers above and below the groundwater table (Oosterbaan and Nijland, 1994).*

Advantages of the infiltration tests: Infiltration tests are conducted in-situ. Therefore they are representative for a larger scale than laboratory tests made with small soil samples. In landslide research the heterogeneities of the soil can be crucial and therefore in-situ tests are necessary.

Disadvantages of the infiltration tests: In sandy soils the measured k-value can be too small because of clogging. In clayey soils the augering and drilling may change the structure of the soil along the wall of the auger and drill hole which could lead to too small k-values. Horizontal and vertical k-values cannot be distinguished. Another disadvantage is that the availability of water for infiltration is not always guaranteed.

Advantages of the pumping tests: Pumping tests are useful to calculate k below the natural groundwater table.

Disadvantages of the pumping tests: In clayey soil, it can take days or weeks until the water is flowing back into the well.

Application of the method in the present study: In all three case studies, infiltration and tests were performed to measure and estimate the hydraulic conductivity. The decreasing water pressure that was monitored after rainfall events was used like an infiltration test. The rising water table after water sampling was used like a pumping test. For this purpose, the water was extracted with hand samplers fixed at a solid cord. Guelph penetrometer tests have been performed only on the Pont Bourquin landslide.
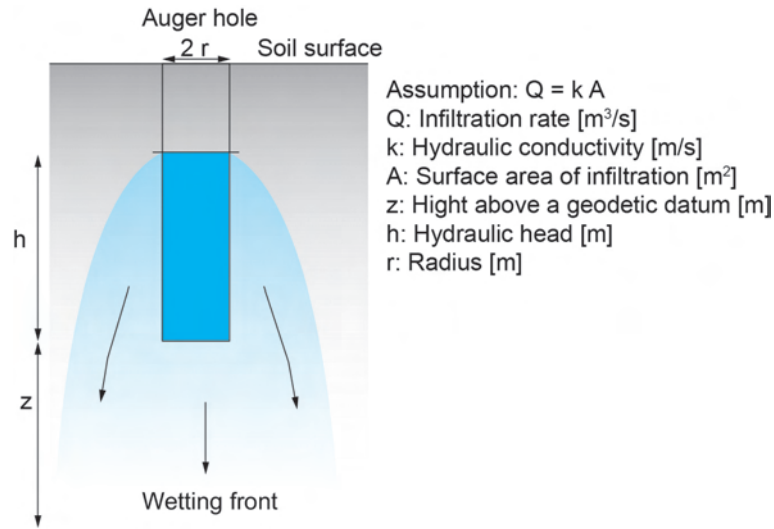
Figure 4.9: *Setting of the inverse auger hole infiltration test (modified after Oosterbaan and Nijland (1994)).*

4.9.1   Inverse auger hole test

For the inverse auger hole test, a hole has to be drilled with an auger in the unsaturated soil. Sufficient water has to be filled in the hole so that near-saturated conditions can be reached around the hole. Figure 4.9 shows an auger hole and the wetting front. The drop of water in the hole has to be measured at distinct time steps. The interpretation of the test is based on the relationship between the measured infiltration rate Q $[m^3/\text{s}]$ and the hydraulic head h [m] to calculate the hydraulic conductivity k [m/s]. The assumption is made that according to Darcy's law (see Figure 1.1) the hydraulic gradient **i** approximates unity if z is large enough and hence the flow velocity approaches the value of k (v = k). It is assumed that $Q = k\,A$, where A is the surface area of infiltration which leads to the following equation for k Oosterbaan and Nijland (1994):

$$k = 1.15r\frac{log(h_0 + \frac{1}{2}r) - log(h_t + \frac{1}{2}r)}{t - t_0} \tag{4.1}$$

k: Hydraulic conductivity [m/s]
r: Radius of auger hole [m]
t_0: Time at the start [s]
t: Time since start of measuring [s]
h_0: Water level in the hole at time t = 0 [m]
h_t: Water level in the hole at time t [m]

Advantages of the method: Inverse auger hole tests can be conducted easily and no installations are needed.

Disadvantages of the method: With this infiltration test, the saturated hydraulic conductivity is measured in the unsaturated zone. Therefore it may be not very accurate.

4.9.2   Guelph Penetrometer test

The Guelph Penetrometer method is a constant head method that can be carried out above the groundwater table. Based on the measured water flow in defined time steps, the permeability

of the saturated soil k_s can be calculated with the following equation (Soilmoisture-Equipment-Corp, 2008).

$$k_s = \frac{C_1 Q_1}{2\pi H_1^2 + \pi a^2 C_1 + 2\pi \frac{H_1}{\alpha*}} \tag{4.2}$$

H : Well height [cm]
$\alpha*$: Alpha Parameter, depends on the soil structure, obtained from site analyses (Soilmoisture-Equipment-Corp, 2008)
Q_1: Soil water pressure head [cm]
C_1: Factor corresponding to H/a ratio
a: Well radius [cm].

Advantages of the method: The constant head method may be more precise than the inverse auger hole test.

Disadvantages of the method: The installation of the Guelph penetrometer apparatus is more complicate than to perform an inverse auger hole test.

4.9.3 Lefranc test (slug test)

With the Lefranc test (or slug test), the hydraulic conductivity can be estimated with little effort above or below the groundwater table in observation wells by adding or pumping water, respectively. The same formulas can be used for both ways. After adding or pumping water, the falling or rising groundwater level has to be measured in defined time intervals (Tacher, 2010). The hydraulic conductivity is calculated with the following formulas:

$$k = \frac{G}{\Delta t} ln(\frac{P_i - P_r}{P_{i+1} - P_r}) \tag{4.3}$$

$$G = \frac{\pi d^2}{4C} \tag{4.4}$$

$$C = 2\pi d + 1 \tag{4.5}$$

d: Well diameter [m]
P_r: Water level of repose [m]
P_0: Water level [m] at time $t = 0$ [s]
P_i: Water level [m] at time i [s]
l: Length of slotted piezometer
Δt: Time step between P_i and P_{i+1}

Advantages of the method: Slug tests are easy to perform. In observation wells, where bypass occurs along the piezometric tube during rain events, the falling water level in the piezometer can be considered like an infiltration test.

Disadvantages of the method: Depending on the location (on a hill slope), depth and diameter of the observation well, pumping may be complicate. This method is not representative for large depth (Tacher, 2010).

4.10   Calculation of the hydrological water balance

The hydrological water balance is made with the hydrologic equation (Hoelting and Coldewey, 2009):

$$P = ET + R + \Delta S \qquad (4.6)$$

P: Precipitation rate, mm/year
ET: Evapotranspiration rate, mm/year
R: Surface run off rate, mm/year
ΔS: Subsurface runoff rate and changes in storage, mm/year

The hydrologic equation says that the precipitation is equal to the surface runoff, evapotranspiration and subsurface runoff. The subsurface runoff includes also changes in the storage of groundwater. Thus the hydrological water balance is needed to calculate how much water is stored in the underground and how much water runs off at the surface. This is important to assess the saturation of a landslide. Furthermore, with a hydrogeological water balance of a landslide it can be calculated, if more water is flowing in or out of the landslide. This is important for the investigation of the groundwater origin in a landslide. The hydrological catchment is not necessarily the same as the hydrogeological catchment. If the total runoff is larger than the net precipitation (precipitation minus evapotranspiration) then groundwater is flowing into the system through the bedrock. This is for example the case at the Triesenberg landslide (François et al., 2007).

Advantages of the method: A hydrological water balance quantifies the hydrology of a landslide. This is helpful for the calculation of the saturation of a landslide and the evaluation, if groundwater from the bedrock is infiltrating into the landslide mass.

Disadvantages of the method: Often uncertainties exist about the parameters rainfall, run-off, infiltration, storage and evapotranspiration (Uhlenbrook et al., 1999). With precise in-situ pluviometer and weirs, the rainfall and the run-off can be monitored relatively precisely, whereas the evapotranspiration and the storage are much more difficult to assess.

Application of the method in the present study: On the Pont Bourquin landslide, the precipitation was measured with tipping bucket rain gauges. The evapotranspiration was measured with a meteorological station. A weir was installed and equipped with water pressure sensors for measuring the flux of the spring. The flux of several creeks was measured manually. Based on this data, a rough hydrological water balance was calculated for different parts of the Pont Bourquin landslide. For the Rüdlingen experiment, the hydrological water balance was estimated with monitoring of the rain intensity, overland flow and soil saturation. The surface runoff was collected with a trench that was connected with a weir.

4.11   Hydrogeochemical analyses

To understand the cause of the slope instabilities, it is important to not only evaluate the influence of water on the moving mass but also to investigate the origin of groundwater (Bonnard et al., 1987). In most cases it is difficult to trace the origin of groundwater (Ronchetti et al., 2009). Due to heterogeneities, the hydrochemical characterization of landslides may be very complex. Natural chemical and isotopic tracers are used to 1) trace the origin of the groundwater, 2) obtain information about the location and connectivity of water flow paths, 3) obtain

information about the velocity of water flow in landslides (De Montety et al., 2007; Bogaard et al., 2007) and 4) to obtain information about the subsurface architecture and composition of different aquifers in a landslide (Guglielmi et al., 2002). Additionally, chemical analysis may provide information about the physical material properties because the pore fluid composition may influence the soil strength (Bogaard et al., 2007).

To check the reliability of the chemical water analysis, a balance between the anions and cations is made. The balance is calculated with the following formula (concentrations in meq/l):

$$Balance = \frac{\Sigma_{anions} - \Sigma_{cantions}}{\Sigma_{anions} + \Sigma_{cantions}} 100 \qquad (4.7)$$

The equivalent (symbol: eq or Eq) is a unit of amount of substance which will supply one mole of electrons in a redox reaction. To obtain meq/l, the concentration in mg/l has to be divided by the molar mass and multiplied by the valence of the ion (1 mmol/l = 1 mEq/l). For freshwaters, the analysis is consideret as reliable if the balance is $<5\%$. The analysis should be rejected if the balance is $>8\%$.

Advantage of the method: Water samples are easy to take. No special field equipment is needed.

Disadvantage of the method: Laboratory infrastructure is needed for the chemical analysis. If the geology is complex (for example due to tectonics) or if all samples show a similar hydrogeochemical signature, it is difficult to define different groundwater types.

Application of the method in the present study: Hydrochemical analyses were performed of groundwater from piezometers, springs and creeks in all case studies. The aim was to define different groundwater types. From observation wells, the water samples were extracted with hand sampling tools. The water samples were filled in 500 ml bottles. The electric conductivity and temperature was measured for all samples in the field with WTW[3] sensors. The samples were analysed in the *Laboratory of engineering and environmental geology, EPFL*. The anions (F^-, Cl^-, NO_3^-, SO_4^{2-}) and the cations (Na^+, K^+, Mg^{2+} and Ca^{2+}) were detected by liquid chromatography with a Dionex DX-120 device. HCO_3^- was analysed by acid-base titration. Trace element analyses (Si^{4+} and Sr^{2+}) were performed with the Inductively Coupled Plasma Sector Field Mass spectrometer Finnigan^{TM} Element2 High Performance High Resolution ICP-MS.

4.12 Tracer experiments

Tracer experiments are made to trace the flow path of groundwater and to determine the flow velocity. The chemical composition of water depends on the regional lithology. If the lithologies in the catchment do not show different geochemical signatures, artificial tracers like fluorescent dyes (Fluorescein/Uranine and Rhodamine) and halides (chloride, bromide and iodide) can be used (Lutz et al., 1987; Bonnard et al., 1987). Tracers, which are preferentially chemically conservative, are injected at a distinct location (for example in observation wells). Downwards from the injection point, groundwater will be sampled for example in springs, creeks or observation wells in certain time intervals in order to trace the arrival and through-flow of the tracer (Hoelting and Coldewey, 2009). If only the time of arrival is of interest, fluocapteur like active coal can be placed at the sampling point. Different application fields of tracer tests and details about the procedure can be found in Schudel et al. (2002).

---

[3] *Wissenschaftlich Technische Werkstätten* (WTW) is a company that develops and makes articles for water analysis.

Advantage of the method: Tracer experiments provide information about the flow path and flow velocity of groundwater. They are among the most important methods in the applied hydrology and hydrogeology.

Disadvantage of the method: Tracer experiments need exact planning and enrolment. The risk for environmental pollution has to be taken into account by performing tracer tests (Schudel et al., 2002). The interpretation of tracer tests may give unclear results. For example it may be known, which aquifers are not connected. But it may remain unknown, which aquifers are connected.

Application of tracer tests in the present study: A small scale tracer test was performed on the Rüdlingen test site. The aim of this test was to estimate the flow velocity and hydraulic conductivity of the underground. For this purpose, 100g of uranine was injected in auger hole Piezo1 (see Figure 5.5) and rinsed with 100 litres of water. Three active coal samples were placed in Piezo3. The three bags were then removed after 1, 11 and 15 days, respectively. To extract the fluorescein, the active coal was rinsed in ammoniac and methanol. The dilution was analysed in a HPLC DAD UV. Estimates could be made for the hydraulic conductivity in the unsaturated soil based on the time t until the tracer arrived in Piezo3. The distance L between the piezometer divided by the time gives the average interstitial velocity $\mathbf{v}_i$. This velocity has to be multiplied with the effective porosity n_{eff} in order to obtain the apparent velocity $\mathbf{v}$ (= Darcy-velocity or hydraulic flux $\mathbf{q}$). The hydraulic gradient $\mathbf{i}$ was assumed to be parallel to slope inclination. The maximum total porosity of 0.45 of was determined by laboratory analyses (Casini et al., 2010) and the minimum effective porosity was estimated to be 0.05. This low value was chosen because the experiment was not carried out in the saturated zone and thus the tracer could only spread in the saturated pore. The hydraulic conductivity was calculated with the following equation:

$$k = -\frac{v_i n_{eff}}{i} \tag{4.8}$$

k: Hydraulic conductivity [m/s]
v_i: Average interstitial velocity $v_i = L/t$ [m/s]
n_{eff}: Effective porosity [-]
$\mathbf{i}$: hydraulic gradient, $\mathbf{i} = L/dh$ [-]

4.13 Sulphur isotope analysis

Similar to the chemical composition of water, the isotopic signature may give information about the origin of groundwater and water transit time (Guglielmi et al., 2002; Mikos et al., 2004; Bogaard et al., 2007). Isotopes are atoms whose nuclei contain the same number of protons but a different number of neutrons. Different chemical, physical and biological processes are responsible for the partitioning of isotopes between two substances (isotope fractionation). The two main stable isotopes of sulphate are ^{34}S and ^{32}S with 94.93 % and 4.29%, respectively. Sulphur isotope composition of minerals gives information about the origin and diagenesis of sulphur compounds. The isotopic composition is expressed in terms of δ-value.

$$\delta^{34} S \, in_{VCTD} = \frac{R_{Sample} - R_{Standard}}{R_{Standard}} 1000 \tag{4.9}$$

R_{Sample} is the measured isotope ratio ^{34}S/^{32}S and $R_{Standard}$ is the standard value from the Vienna-Canyon Diablo Triolite (V-CDT). δ^{34}S can range from -40 to +50 ‰(Hoefs, 2009).

^{34}S/^{32}S gives information about the origin of groundwater because sulphur from pyrite has a lower δ ^{34}S than sulphate from evaporites. The following table gives some δ^{34}S values.

Location, mineral, geological formation	δ^{34}S value	Reference
Mean ocean water today:	21 ‰	(Hoefs, 2009)
Gypsum:	10 - 30 ‰	(Hoefs, 2009)
Triassic and Jurassic carbonates:	15 - 25 ‰	(Hoefs, 2009)
Pyrite, Animas River, Co, USA:	-7 to 2.5 ‰	Nordstrom et al. (2005)
Gypsum/anhydrit, Animas River, Co, USA:	15 to 18 ‰	Nordstrom et al. (2005)
Upper Triassic sediments, worldwide:	13.5 - 18.5 ‰	Boschetti et al. (2011)
Gypskeuper, Jura mountains, Switzerland:	14.6 -16.5 ‰	Boschetti et al. (2011)
Pyrite, Austria:	-8 - 9.3 ‰	Spötl et al. (1998)
Pyrite, Binntal, Switzerland:	-25 - 3 ‰	Hofmann and Knill (1996)

Table 4.2:

Advantages of the method: In landslide investigations, analysis of sulphur isotopes may give information about the origin of the groundwater.

Disadvantages of the method: Good laboratory infrastructure is needed for the analysis. Otherwise, the costs for external analyses are high.

Application of the method in the present study: Sulphur samples were prepared at the *Laboratory of engineering and environmental geology, EPFL*. They were precipitated as BaSO$_4$. The δ^{34} from filtered and dried bariumsulphate was analysed with an *Element Analyser (EA) Isotope Ratio Mass Spectrometer (IRMS) L δ^{34}S* at the *Institute of Mineralogy and Geochemistry, University of Lausanne*.

4.14 Extensometer measurements

An extensometer is an instrument to measure variations of the distance between two points. This can be done for example with laser, cameras or a wire. On landslides, extensometers are placed at scarps or fractures. It is important to use a fix-point located outside of the moving mass.

Advantages of the method: The manual measurements between two points is a simple and cheap methode to obtain data about the local movement and acceleration of a landslide.

Disadvantages of the method: It is not always evident to choose a fix-point that is not moving. It may be time consuming to make frequent manual measurements. If the measurements are not made frequently, it is possible that an acceleration of the movement is not detected. With this method, only the local movement between two points is measured which could be just superficial. More sophisticated methods are expensive.

Application of the method in the present study: On the Pont Bourquin landslide, the distance between two rods was measured manually with a measuring tape.

4.15 Time-domain reflectometer (TDR)

With Time-domain reflectometers, the volumetric water content of the soil is measured (Topp et al., 1980). The technique is based on determining the dielectric constant in the soil. For this

purpose, the travel time of an electric pulse that travels through two coaxial transmission rods into the soil and back ia measured. The electric conductivity of the soil matrix and thus the travel time increases with increasing soil saturation.

Advantages of the method: TDRs are a relatively cheap method to measure variations of the soil saturation at different depth.

Disadvantages of the method: During the installation of TDRs, the soil is disturbed. Thus it may be difficult to measure under completely natural conditions. TDRs give rather a relative than an absolute value of the soil saturation because of limited resolution and noises. A good calibration of the sensors is important.

Application of the method in the present study: TDRs were installed at several soil depth on the Rüdlingen test site to measure the soil saturation during the triggering experiment.

4.16 Tensiometer

Tensiometers are used to continuously measure the suction (0 to -850 hPa) in unconsolidated sediment. The measurement is made with a ceramic-cell filled with water and isolated from air placed in the unconsolidated soil. The maximum pore diameter of the cell is 1 μm. The water level in the cell is controlled from the surface with a plastic tube. Depending on the saturation of the unconsolidated sediment around the cell, an under pressure is produced in the cell to establish an equilibrium with the pore water in the environment. With sensors, the suction is measured.

Advantages of the method: This is a relatively simple method to measure the soils suction. The measurement is independent of the soil type, temperature and other parameters.

Disadvantages of the method: By the installation of tensiometers, the permeability of the unconsolidated sediment may be disturbed. The suction can vary spatially but the measurement is made at a single point. The water in the tensiometers has to be controlled and by temperatures below the freezing point, polyethylenglykol (PEG) or similar has to be added to avoid freezing.

Application of the method in the present study: Tensiometers were installed at several soil depth on the Rüdlingen test site to measure the suction during the triggering experiment.

4.17 Remote sensing

Remote sensing is important to investigate the shape of landslides and to monitor their movement. It covers a broad spectrum of acquisition methods to record information about the earth surface by reflected electromagnetic radiation. The signals can be emitted and received from satellites, aircraft or ground-based devices like radar interferometry and terrestrial laser scanning (TLS):

- Light Detection and Ranging (LIDAR): The distance to the target is measured with light (often with laser).

- Radio Detection and Ranging (RADAR): The target is localised with electromagnetic waves.

- Photogrammetry: The properties of an object are determined from photographs.

- Total station measurements: Electronic theodolite.

- Digital Global Positioning System (DGPS).

Advantages of the method: The advantage of these techniques is that high-resolution images (mm-scale) of the earth surface can be obtained rapidly over large areas and landslide displacements are detected over the entire landslide area.

Disadvantages of the method: A disadvantage is that the techniques are very expensive.

Application of the method in the present study: On the Pont Bourquin landslide, DGPS and LIDAR measurements were performed. On the Rüdlingen test site, total station measurements were made and during the triggering experiment, photogrammetry was performed.

Chapter 5

Landslide triggering experiment, Rüdlingen (SH)

5.1 Introduction

How can the triggering of a real-scale rapid landslide be studied? The triggering is a temporally and spatially very limited process. How can we know where and when a rapid landslide will occur? A promising but not evident option is the artificial triggering of a landslide. The infrastructure for such an experiment is enormous and to find an accessible location where the provoked damage will be limited is a challenge. Additionally, a location with a significant landslide history is preferable.

In the framework of the *Triggering of Rapid Mass Movements in Steep Terrain* (TRAMM) project, a landslide triggering experiment was carried out on a forested hillslope in Rüdlingen, Canton Schaffhausen. TRAMM was financed by the *Competence Centre Environment and Sustainability* (CCES). During several months of field work, the experiment was prepared. First the slope was geologically and geotechnically investigated and a 10 x 30 m large test field was chosen. The depth to bedrock was investigated with penetration tests. 1 - 2 m deep test pits were digged to extract samples from unconsolidated sediment and to make hydrological tests. Several short drill holes were made to perform infiltration tests and to install piezometers. A 23 m-deep drill hole was constructed at the top of the slope. Trees on the test site have been cut. A net barrier at the toe of the slope, floodlight and cameras were installed. The test field was equipped with sprinklers and numerous sensors to measure hydrological and geotechnical parameters during the experiment. A first sprinkling experiment was carried out during five days in October 2008. The slope remained stable. To prepare a second experiment, the sprinklers were rearranged to be more efficient in the upper part of the slope. Roots around the test site were cut with a spade shovel to a depth of 0.5 m. During the second experiment in March 2009, the slope failed after 15 h of sprinkling. This unique experiment reveals an interesting picture about hydrological and geomechanical processes before and during the landslide triggering.

In the following, the focus will be put on the hydrological and hydrogeological interaction between bedrock, weathered bedrock and unconsolidated sediment. Of special interest are groundwater flow paths in the slope, saturation patterns, and the triggering mechanism. A hydrogeological conceptual model of the slope was made based on data from:

- Bedrock surface;

- Lithological profiles of drill holes;

- Infiltration tests performed before the experiment;

- Measurements of the hydraulic parameters during the experiment (with pluviometer, water pressure sensors, TDR, tensiometer, ERT, overland flow trench);

- Photographs taken after the triggering.

This model will be discussed by applying the hydrogeological landslide classification presented in Chapter 3. In the following, the experiment location and setting are described.

5.1.1 Location

Rüdlingen is an enclave of Canton Schaffhausen at the bank of the River Rhine. In May 2002, several landslides were triggered on the steep slopes along the River Rhine after a strong rainfall event of 100 mm in 40 minutes (Thielen, 2007). The location of the landslides, the villages Rüdlingen and Buchberg and the test site are shown on the shaded relief on Figure 5.1. The slopes between the village Buchberg and the River Rhine are locally over 50° steep and are subject to continuous creeping and retrogressive erosion, especially in the gullies seen on Figure 5.1.

5.1.2 Geology

Rüdlingen is located in the distal part of the Swiss Molasse basin. Figure 5.2 shows a geological map (including hydrological features) of the area around the experiment. Figure 5.3 shows a profile along the slope. Outcrops of Molasse Sediments have been mapped as well as springs, wet zones, and ancient landslide deposits. The Molasse sediment in the area is horizontally layered. The test site lies in the Lower Freshwater Molasse (LFM, Aquatanian). The LFM is composed of grey medium- to fine-grained sandstone that intersects with a coloured reddish-orange marlstone deposited in a typical fluvio-terrestrial environment. The upper part of the test site lies in sandstone which is partly very poorly lithified and the lower part consists of marlstone. Above the test site gray variously banked (1 cm - 10 cm thick layers) sandstone from the Upper Marine Molasse (UMM, Burdigalian) is outcropping. Further upslope follows the Upper Freshwater Molasse (UFM, Tortonian) (Matter et al., 1988; Keller et al., 1990; Hantke, 1967). Quaternary sediment along the slope consist mainly of colluvium as a result of former mass movements.

5.1.3 Hydrogeology

Each geological unit has different hydrogeological characteristics which influence the stability of the slope. Numerous small springs are present in the Upper Marine Molasse which can be observed especially in winter when ice layers form along permeable layers and above low permeable sandstone layers (see Figure 5.4 A). These springs indicate the presence of groundwater in more permeable layers of the UMM. In areas where the springs are covered by colluvium and soil, the water can build up porewater pressure from below and favour the triggering of shallow landslides (as described in Chapter 2, see Figure 2.16). Below the spring horizons, humid zones are formed which could additionally favour the landslide triggering especially during heavy or long-term rainfall or snowmelt. On the contrary, the sandstone of the LFM is characterized by large vertical joints which are parallel to the River Rhine and have a spacing up to several tens of cm (see Figure 5.4, B). These joints can act as efficient drainage paths for the groundwater.
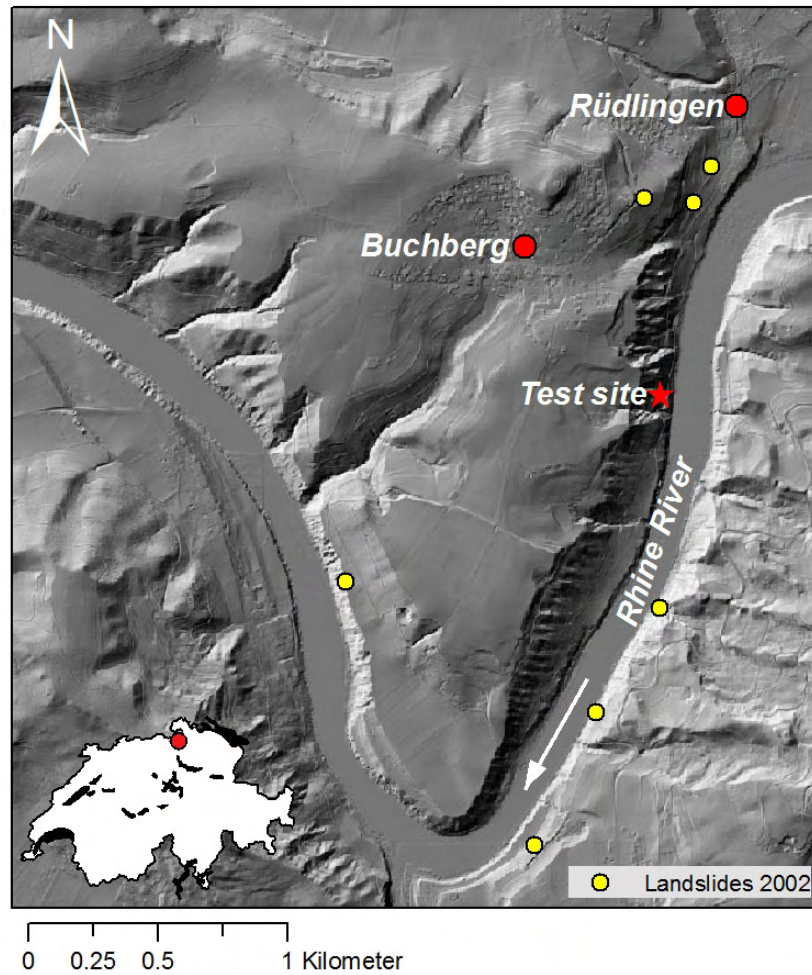
Figure 5.1: *Locations of the test site and six landslides triggered in Rüdlingen vicinity in May 2002. Gullies affected by retrogressive erosion can be seen on both boards of River Rhine, especially in the area of the test site (shaded relief from GIS of Canton Schaffhausen, http://www.gis.sh.ch).*
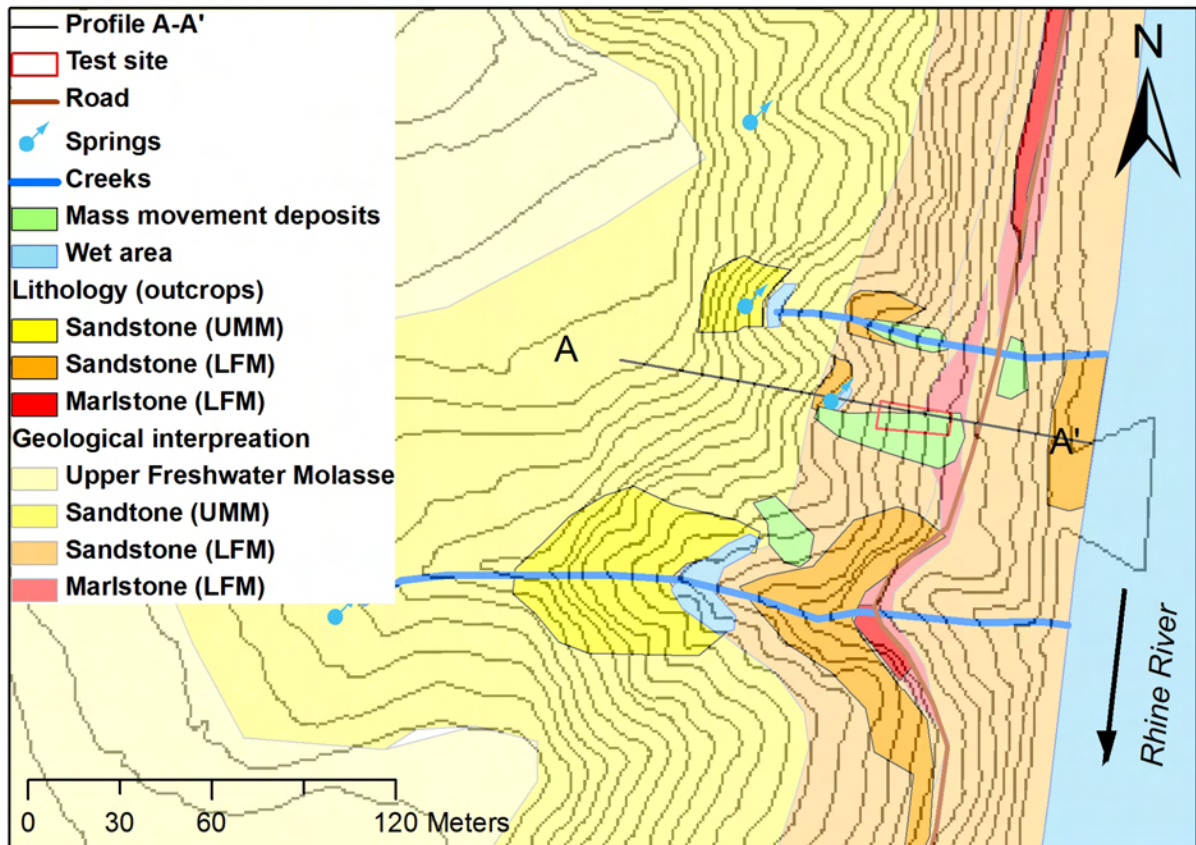
Figure 5.2: *Geological and hydrological map of the area around the triggering experiment (contour lines from GIS of Canton Schaffhausen, http://www.gis.sh.ch). The profile A-A' is shown on Figure 5.3.*
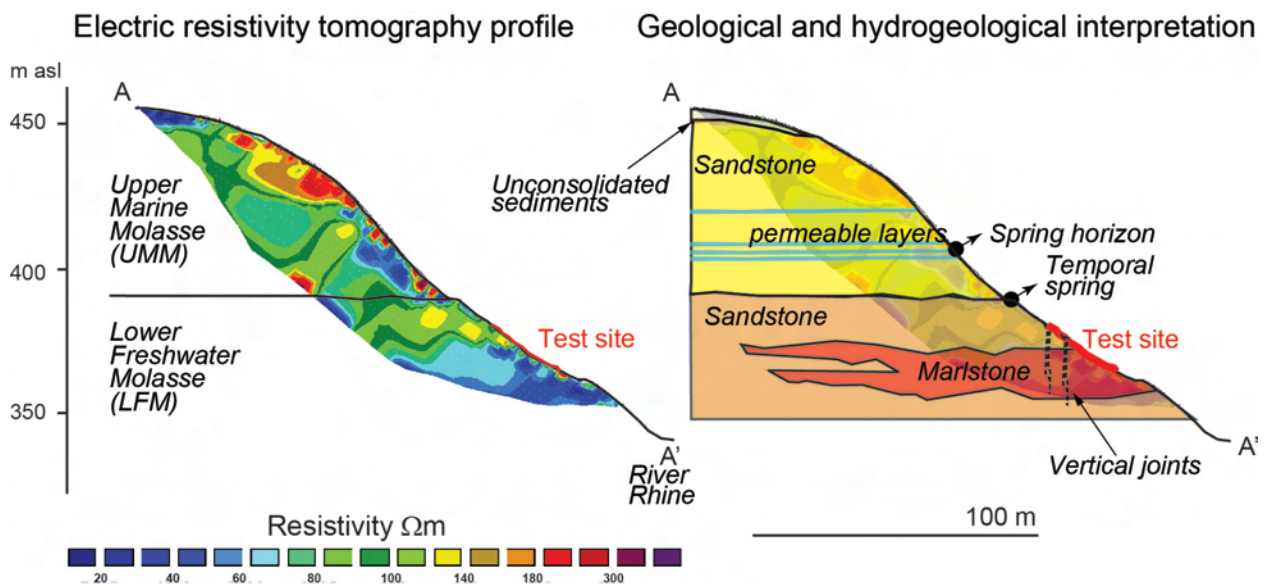
Figure 5.3: *Geological profile of the slope from Buchberg to the River Rhine. The lithological boundary between the marlstone and the sandstone of the LFM and hydrological features are visible on the ERT profile recorded along the slope (Gambazzi and Suski, 2009). Marlstone and saturated layers are low resistive (40-70 Ohm.m) and unsaturated sandstone is higher resistive (100-150 Ohm.m).*
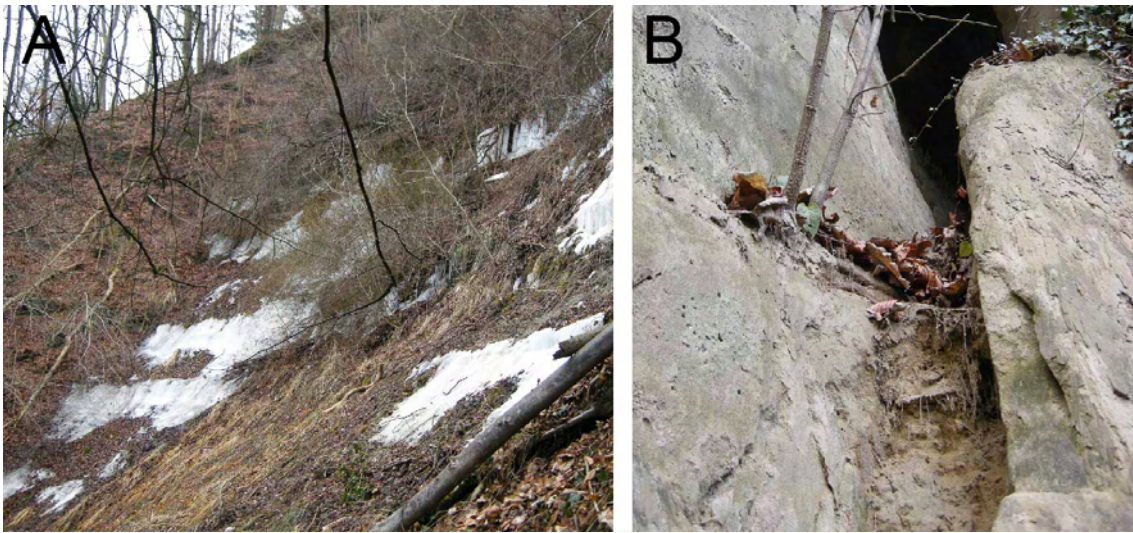
Figure 5.4: *A) Photograph showing ice layers along spring horizons in the Upper Marine Molasse during winter. B) Photograph showing a large joint in the Lower Freshwater Molasse. Aperture of the joint is 25-50 cm.*

5.2 Test site description

The test site is located on a forested slope. It is 9 m wide and 23 m long, has a mean slope angle of 38°, and is up to 42° steep (see Figure 5.5). The test site is possibly located on a former thalweg which is now covered by silty and sandy colluvium of about 1 to 5 m thickness containing stones and wood fragments. These deposits result either from on-going retrogressive mass movement processes on the steep slopes along the River Rhine or from a larger landslide event. Small deposits of fresh mass movements were observed behind trees in the slope. This gave evidence of continuous erosion processes.

Before the triggering experiment, the bedrock surface and soil thickness has been surveyed, lithologies and soil properties have been characterized, and infiltration tests have been performed. In the following, the results of these investigations are shown.

5.2.1 Bedrock topography and soil thickness

The depth of the unconsolidated sediment has been measured by Amin Askarinejad from *Institute for Geotechnical Engineering*, ETH Zürich (Springman et al., 2009) with Dynamic Probing Light DPL all around and across the test field (see Section 4.7 for description of the method). Figure 5.6 shows the topography, depth of the bedrock and thickness of the unconsolidated sediment. The mean thickness of the soil is about 2 m. The bedrock on the northern side of the experiment field is shallower than on the southern side. On the southern side, the bedrock shows a depression in the middle part of the slope. In the lower part, a ride strikes along the slope. This is consistent with the findings from the ERT data (see next section and Figure 5.13).

5.2.2 ERT profiles

Before the experiment, two ERT profiles were recorded longitudinally along the test site (Figure 5.7). Electrode spacing was 0.5 m (see Section 4.3 for a description of the method).

The ERT data show mainly three zones: the bedrock in the lower part of the slope with a resistivity of 20-60 Ωm, the bedrock in the upper part of the slope with resistivity between
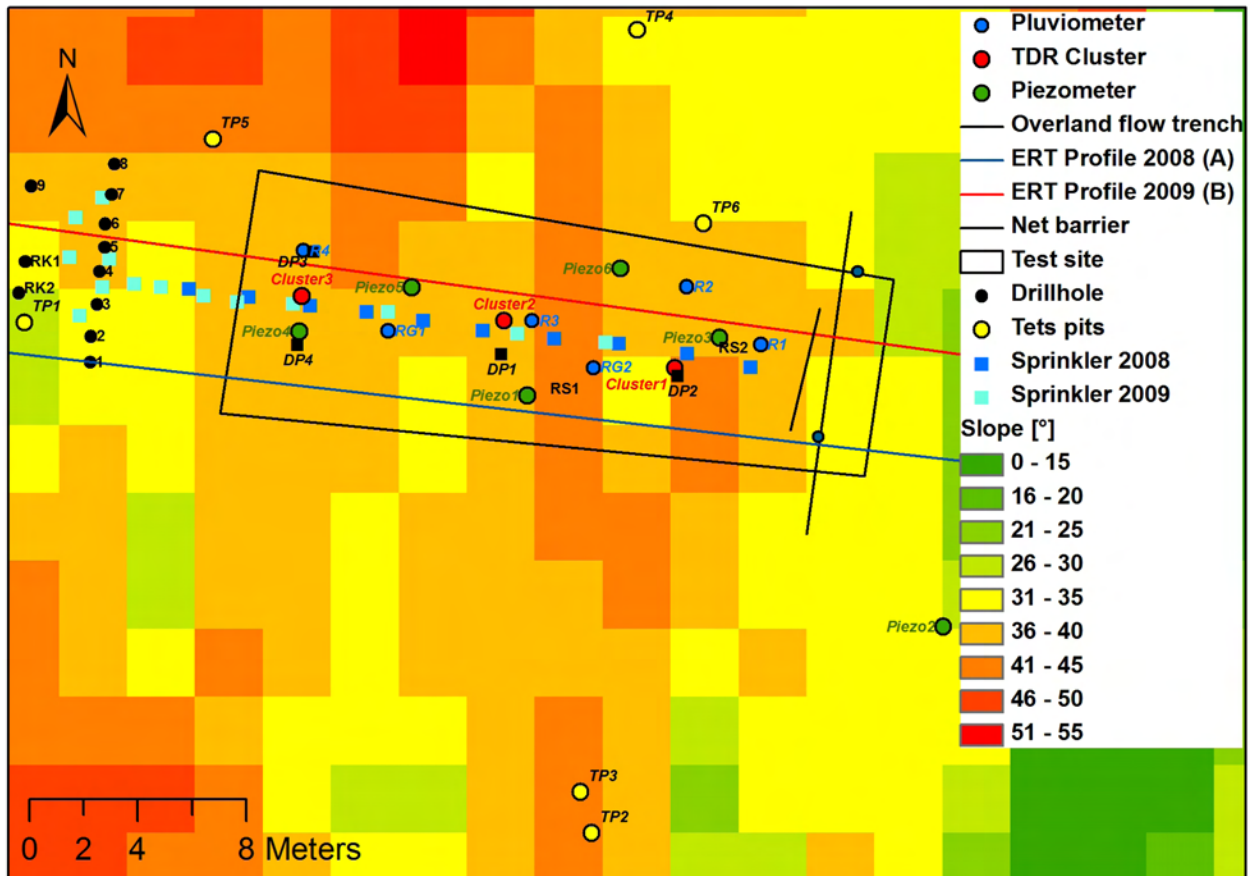
Figure 5.5: *Map showing slope inclination, perimeter of the test site and the triggered landslide, and installations. Slope inclination was calculated with a 2.5 m-DEM provided by the Swiss Federal Institute for Forest, Snow and Landscape Research (WSL). TDR are instruments to measure the soil water content.*
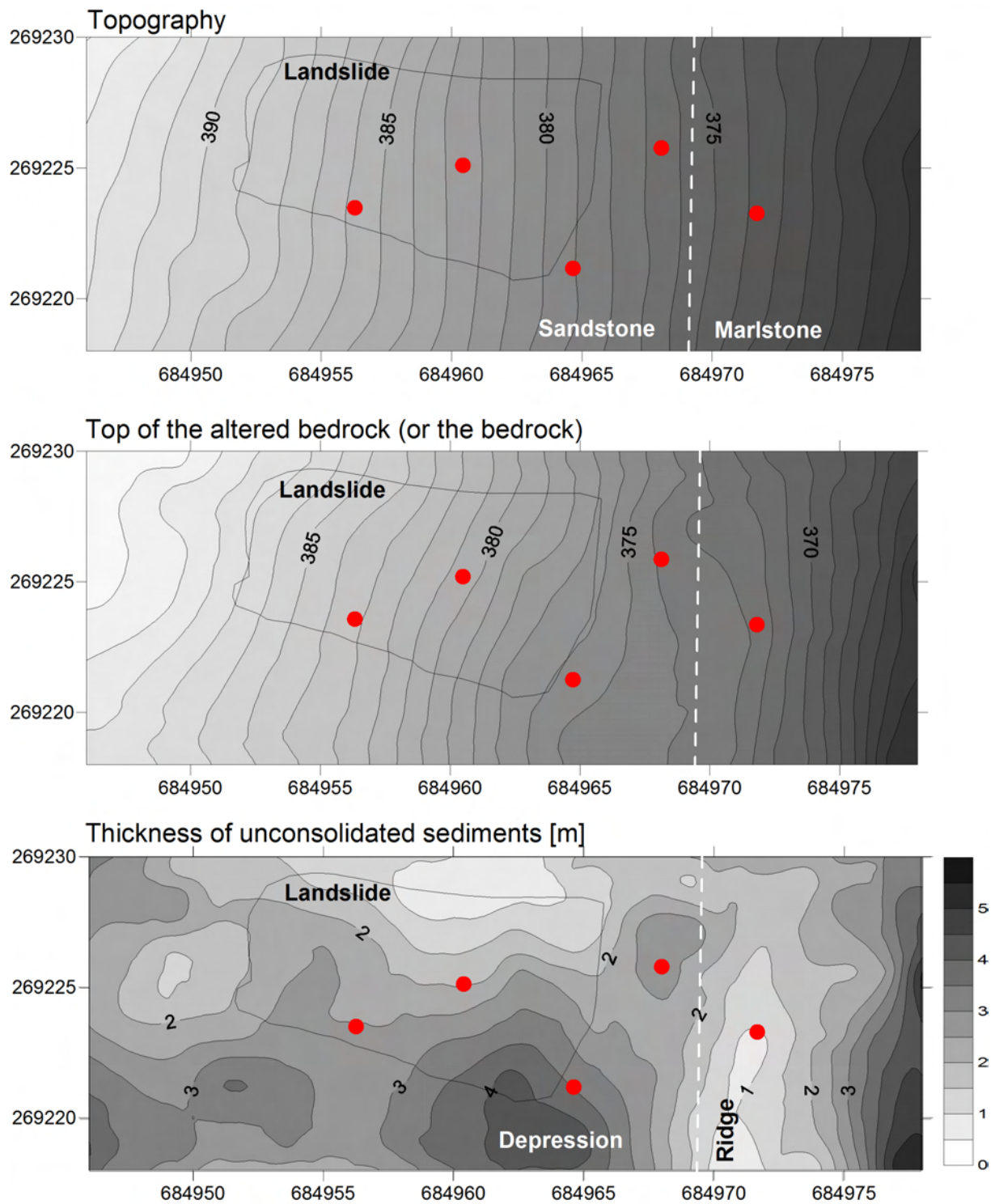
Figure 5.6: *Maps showing the topography (top), the depth of the bedrock surface (middle) and the thickness of the unconsolidated sediment (bottom) in the area of the test site. The triggered landslide is indicated. Red dots are the locations of the installed piezometers. The dashed white line indicates the boundary between the marlstone and the sandstone.*

100 and 250 Ωm and the unconsolidated sediment with resistivity between 40 and 250 Ωm. Interesting features indicated on Figure 5.7 are:

- Low resistive layer parallel to the bedrock surface in the left (upwards view) upper part of the slope between the bedrock and the unconsolidated sediments.

- Low resistive horizontal layer in the upper part of the slope.

- High resistive horizontal layer in the lower part of the slope.

The upper high resistivity part is interpreted as sandstone and the lower low resistive part is interpreted as silt and marlstone, both covered with unconsolidated sediments with variable resistivity depending on the clay content and the degree saturation. The high resistive layer in Figure 5.7 is interpreted as competent sandstone layer. The low resistive layer indicated on Figure 5.7A could be the weathered bedrock which is either finer grained or more saturated than the overlaying unconsolidated sediment. The low resistivity layer indicated on Figure 5.7B is interpreted as a layer of less cemented sandstone.

5.2.3   23 m-deep lithological profile

A 23 m-deep borehole (RK1, see Figure 5.5 for location) has been drilled above the test site in order to obtain a complete lithological profile from the bedrock of the test site. Four water pressure sensors were installed in the borehole (see Section 4.6 for descriptions of the method). The aim was to measure groundwater fluctuations in different sediment layers. The lithological profile is shown on Figure 5.8 and supplementary hydrological and geological descriptions can be found on Figures A.1 and A.2 in Appendix A. The lithological profile recorded from the drill hole cores confirms the stratigraphic boundary in the middle of the slope found by ERT. In the following, the different lithologies are described.

Unconsolidated sediments

The top meter is composed of silty sand-sandy silt containing gravel of sandstone with a diameter < 3 cm and fragments of wood and roots. This lithology is interpreted as ancient mass movement deposit.

Laboratory analyses of the unconsolidated sediment (0 - 2 m depth) from test pit 1 (TP1) located next to RK1 (see Figure 5.5) has been performed by *Institute for Geotechnical Engineering* (IGT), ETH Zürich (Casini et al., 2010). Grain size analyses showed irregular gravel content of 1 - 12 %. With increasing depth, the clay and silt fraction increased from 4 to 10 % and from 25 to 32 %, respectively. The sand fraction decreased from 67 to 56 % with depth. The analysed parameters are shown in Table 5.1.

Weathered bedrock

Between 2 and 2.5 m depth is the transition to weathered bedrock that is classified as silty sand with stones and blocks of sandstones. Depending on the initial bedrock strength and the degree of cementation, the layer of weathered bedrock is more than a meter thick. At the location of the drill hole the thickness is about 0.5 m.

Sandstone

Between 2.5 and 19 m depth, sandstone from the Lower Freshwater Molasse was found. It is grey-brown, rather homogeneous, medium-grained and horizontally layered. Some layers are
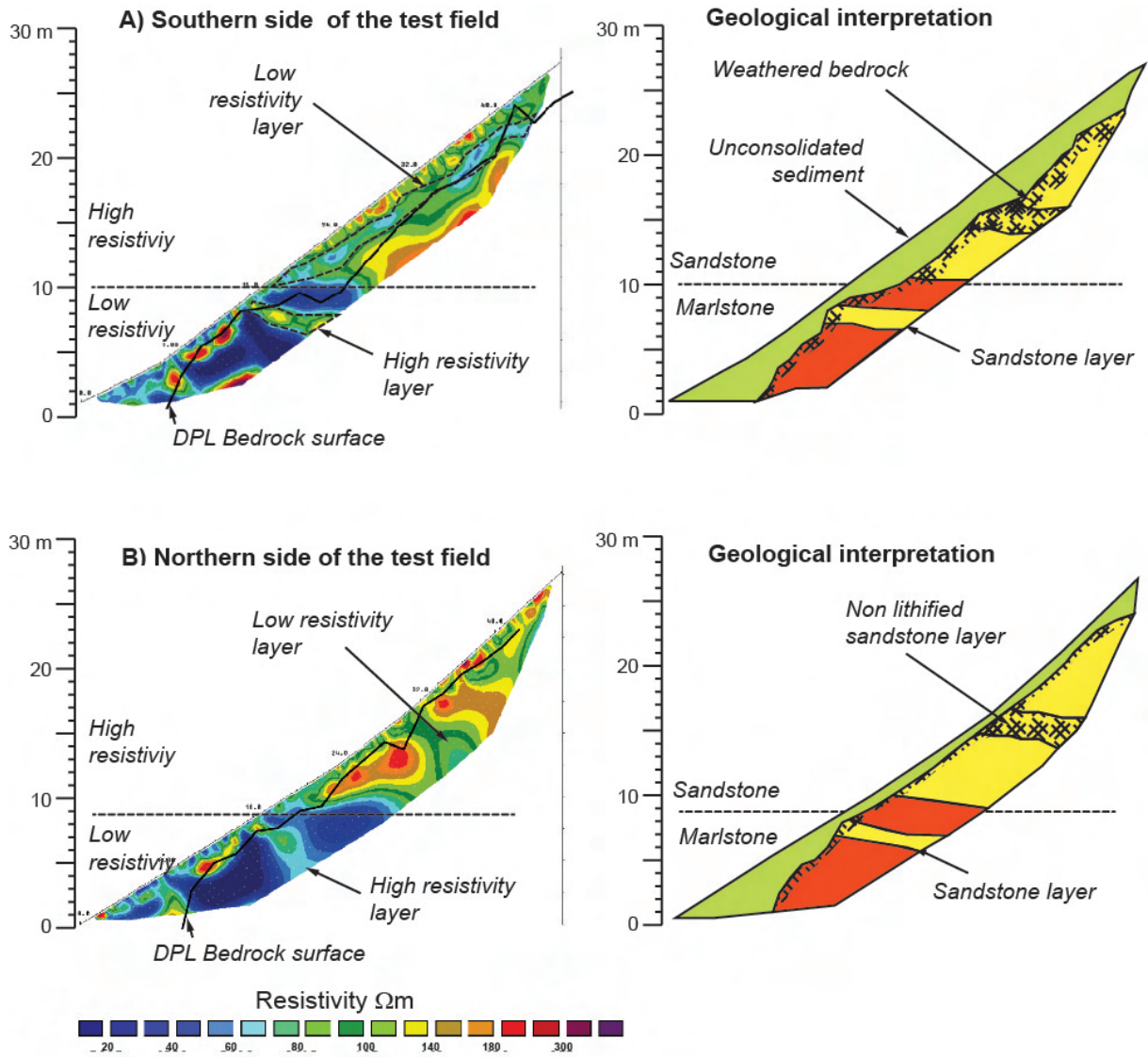
Figure 5.7: *ERT profiles recorded before sprinkling along the test site (Gambazzi and Suski, 2009). The data of the bedrock surface recorded by DPL investigation consist well with the ERT profiles. For location of profile A and B see Figure 5.5.*

Gravimetric water content w:	20-24 %
Plastic limit w_p:	20-24 %
Liquid limit w_l:	24-36 %
Plasticity index I_p:	6-12%
Activity index I_A:	1.25 - 0.75
Unit weight of the saturated soil $\gamma_s at$:	16.7 kN/m^3
Unit weight of the solid soil γ_s:	25.8 kN/m^3
Porosity:	0.45
Saturation:	60.6 %

Table 5.1: *Mean soil parameters from unconsolidated sediment samples from TP1 (0-2 m depth, see Figure 5.5 for location, Casini et al. (2010)). All parameters w, w_p, w_l and I_p decreased with depth. The soil was classified as a medium to low plasticity silty sand with a decreasing activity I_A of >1.25 in the upper part and 0.75 below 1 m depth. The activity I_A was derived from chloritic-smectitic clay fraction (Colombo, 2009).*

little or no-lithified and therefore very weak (can be crumbled by hand). Only in 3.5, 7.5 and 18 m depth the sandstone was completely cemented and strong (did not collapse after ten blows with a geological hammer).

Marlstone

The bedrock between 19 and 23 m depth is composed of grey fine-grained sandstone and ochre-orange siltstone. Around 19 and 21.5 m depth the siltstone is plastic and weak. Otherwise it is rather brittle.

5.2.4   Hydrogeology in the drillhole

Even though no springs were observed on the test field, it is possible that groundwater is circulating in the Molasse bedrock below the test field. Seven weathered and coloured horizons observed in the drill hole gave evidence for water circulation. These horizons were found at 2 m, 5.5 m, 7.5 m, 10.5 m, 18.5 m, 19.5 m and 21.5 m depth. A second important hydrogeological feature observed in the drill hole were vertical joints found at 4 m and 8.5 m depth. During the coring, hundreds of litres of drilling water drained rapidly into the bedrock at a depth of 4 m, 8.5 m, 18 m and 21 m. Thus it is likely that joints are present in those depths. On the contrary, just below 18 m and 21 m water was ponding after drilling, most likely because of impeding layers.

Based on these observations, four water pressure sensors were installed at 2.3 m, 6.8 m, 18.7 m and 21.3 m depth (see Figure 5.8, left side) in order to test the hypothesis of groundwater circulating in more permeable layers in the Molasse sediments. The difficulty for the installations was to take into account the draining joints: Is it better to install a sensor in the vicinity of a joint because during high intensity rainfall, the joint will be filled with water? Or should the sensors be installed away from the joints because they are draining the bedrock and a sensor would never record anything? The main arguments to choose the depth of the sensors were the altered horizons (because these horizons gave evidence of water circulation) and the water that was ponding during drilling (because it was assumed that at locations where water was ponding, no draining fractures are crossing the drill hole).

The data records from the four pressure sensors are discussed in Section A.2. A water pressure of 1 m was measured at the interface between the sandstone and the marlstone at 18.7 m depth. But no correlation between groundwater fluctuations and precipitation events could be made. It is concluded that water flows through permeable layers and fractures in the bedrock. But in the area of the experiment, large joints are draining the bedrock. No groundwater table builds up close to the surface.

5.2.5   Hydraulic conductivity

The hydraulic conductivity is the determining parameter for the groundwater flow, as discussed in Chapter 2. It controls the rate of water infiltration. The hydraulic conductivity can vary strongly depending on the scale and saturation. For a real scale experiment it is therefore important to measure the field hydraulic conductivity with in-situ infiltration tests. This was done in several drill holes along the test site (RK2, RS1, RS2, HA1, HA3, HA8 and HA9, see Figure 5.5 for locations) using the Inversed Auger Method for data interpretation (Oosterbaan and Nijland, 1994). RK2 was drilled with a TerrBohr Bohranlage MC 400 device, RS1 and RS2 were drilled by engine auger and HA1, HA3, HA8 and HA9 were drilled by hand auger. The aim of these tests was to measure an approximate hydraulic conductivity at different locations in the
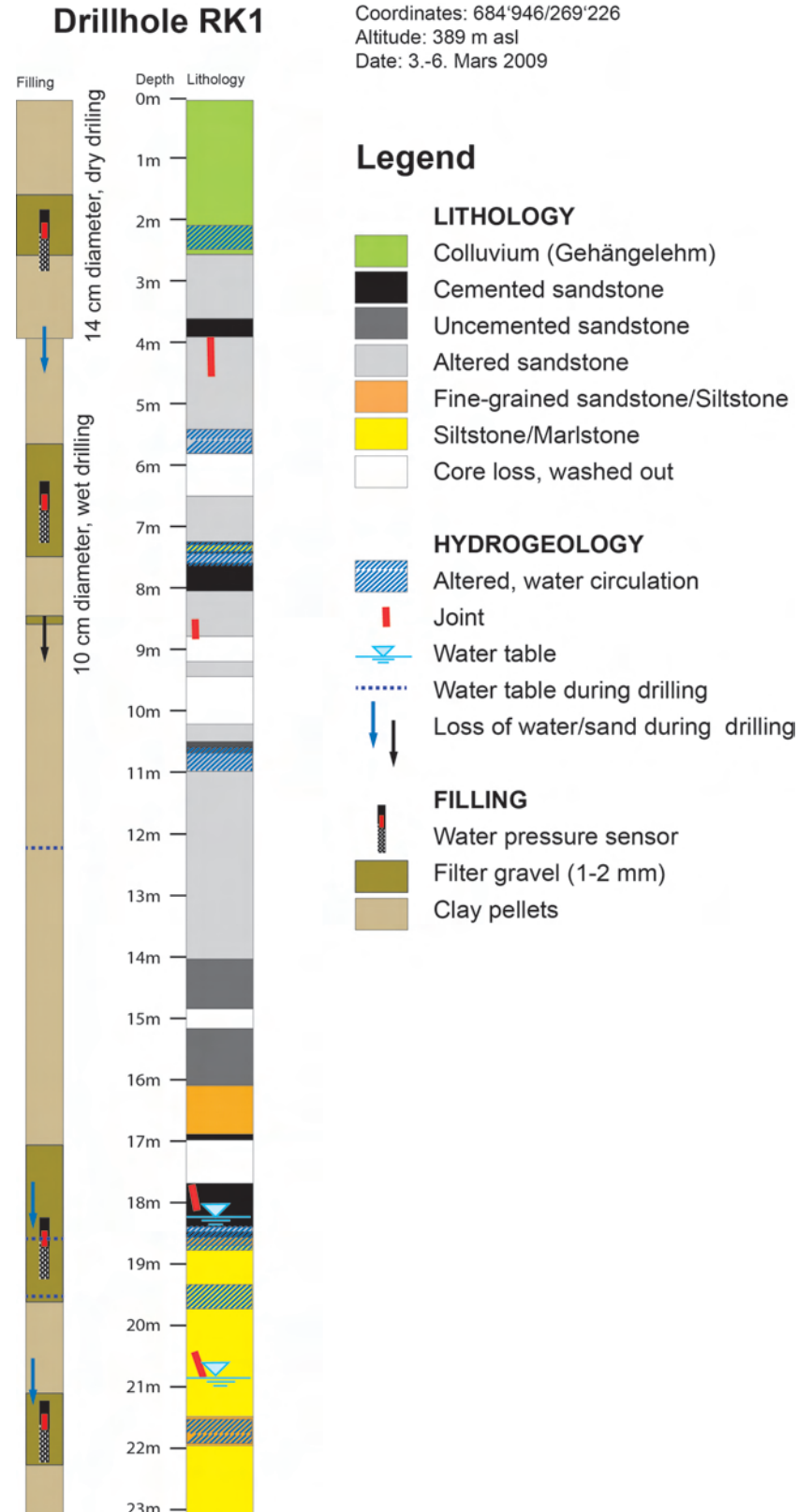
Figure 5.8: *Lithological profile of the 23 m deep borehole drilled above the test site.*

unconsolidated sediment and the altered bedrock.

Table 5.2 shows the depth of all holes and the calculated hydraulic conductivity (see Section 4.9 for the method). The hydraulic conductivity of the weathered sandstone averages 10^{-4} m/s. The silty and sandy colluvium has hydraulic conductivity values between 10^{-6} and 10^{-7} m/s. The calculated k-value in RS1 and RS2 is 0.001 - 0.01 m/s or higher. 0.01 m/s was the limit of manual water infiltration (100 litres water in 5 minutes). It is possible that more water would have infiltrated if it were possible to add more water. Thus it is likely that the infiltration rate exceeds 0.01 m/s. Due to compaction of the unconsolidated sediment during drilling, the values for the hydraulic conductivity may be rather too small, especially if the unconsolidated sediment was plastic and contained clay minerals.

Hole	Depth [m]	Date	Lithology	Hydraulic conductivity [m/s]	Drilling method
Piezo1 (RS1)	4.5	9.10.2008	silty clayey fine sand 3-3.9 m: very weathered bedrock 3.9-4 m: sandstone	10^{-2} - 10^{-3}	Engine auger
Piezo3 (RS3)	3.3	9.10.2008	0.4-1.1 m: silty clayey fine sand, very weathered bedrock 1.1-3.5 m silty clay, red-yellow, stiff, weathered bedrock	10^{-2} - 10^{-3}	Engine auger
RK2	3.2	10.3.2009	altered bedrock, sandstone	10^{-4}	MC 400 Rig TerrBohr AG
HA1	0.67	3.3.2009	silty sand, colluvium/altered bedrock	10^{-5}	Hand auger
HA3	2.3	3.3.2009	sandy silt, colluvium/ altered bedrock	10^{-7}	Hand auger
HA8	1.66	3.3.2009	sandy silt, colluvium/ altered bedrock	10^{-7}	Hand auger
HA9	2.88	3.3.2009	silty sand, colluvium/ altered bedrock	10^{-6}	Hand auger

Table 5.2: *Values for the saturated hydraulic conductivity k measured in different drill holes along the test site.*

Infiltration characteristics

The infiltration characteristics of the unconsolidated sediment were tested by Peter Kienzler from IGT ETHZ (Springman et al., 2009; Casini et al., 2010) performing a small scale sprinkling and dye tracer experiment at TP3, TP4 and TP5 (see Figure 5.5 for locations). An area of 1 m^2 was sprinkled for 2-5 h with an intensity of 60 mm/h. Brilliant blue food dye (4 g/l) was added to the water in order to see the infiltration flow path in sections of 1.2 m depth which were excavated the day after sprinkling.

During these experiments, no overland flow but a high infiltration capacity of > 60 mm/h of the soil was observed. Springman et al. (2009) described very homogeneous infiltration and little preferential flow in the unconsolidated sediment (see Figure 5.9). At the transition between subsoil and weathered bedrock, at 1 - 1.2 m depth at TP4 and TP5, the infiltration was limited.

Staining parallel to bedrock surface was observed which indicated lateral flow. In TP4 staining was also observed along fractures in the bedrock (see Figure 5.9).
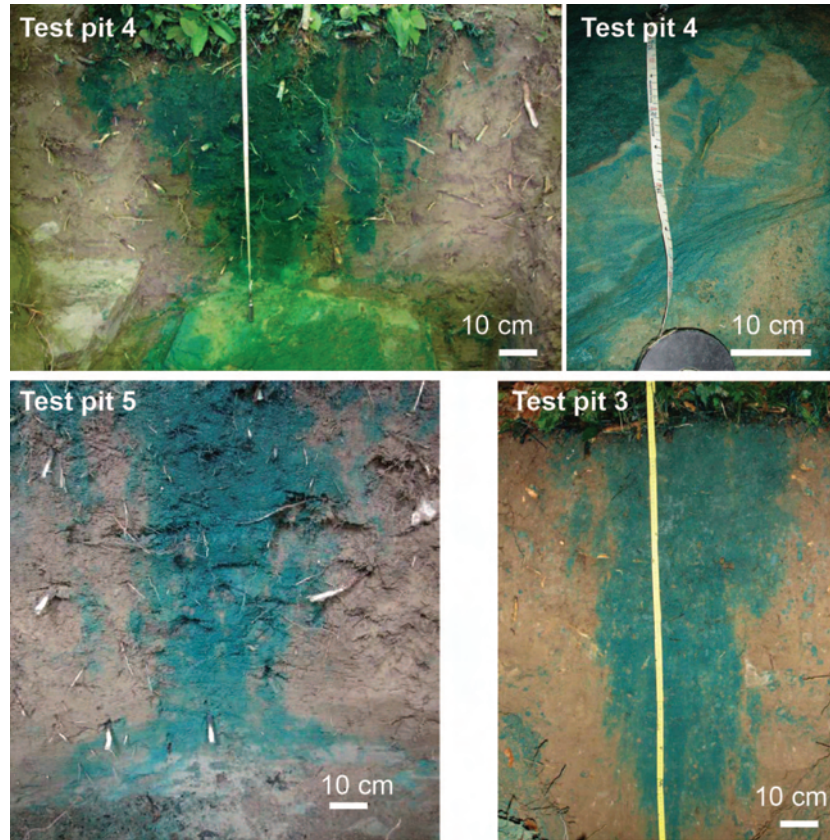
Figure 5.9: *Photographs of the sections excavated in test pit 3, 4 and 5 the day after the small sprinkling experiment. Homogeneous flow in TP3 and lateral flow at the bedrock surface at TP 5 occurred (Springman et al., 2009; Casini et al., 2010).*

Tracer test

Values for the hydraulic conductivity were estimated with the aid of a tracer test. The test was conducted on the test field between auger holes Piezo1 and Piezo3 (see Figure 5.5 for location). The method is described in Section 4.12. The distance L between the two piezometers was 7.5 m and the Δh was 5.5 m which gives a hydraulic gradient **i** of 0.7 if it is assume that the whole paths was totally saturated. The tracer was injected on 9 October 2008. Three fluocapter were analysed:

Date of injection:	9 October 2008
Fluocapter sampled 10 October 2008:	negative
Fluocapter sampled 20 October 2008:	negative
Fluocapter sampled 24 October 2008:	positive

Table 5.3: *Results of the fluocapters analyses.*

This gives a minimum travel time t of 12 days and a maximum travel time t of 15 days. Taking into account the range of porosity (0.05 - 0.4) and travel time, the maximum hydraulic conductivity is $2 \cdot 10^{-6}$ m/s and the minimum hydraulic conductivity is $4 \cdot 10^{-7}$ m/s.

Uncertainties about the flow path, heterogeneities, porosity and the saturation exist especially because the test was conducted in the unsaturated zone. The hydraulic gradient had to be estimated as well as the effective pore volume. Nevertheless, this test can be used in combination with infiltration tests to estimate an approximate value for the hydraulic conductivity. The order of magnitude of k-values is the same like the one calculated with infiltration tests.

5.3   Setup for the triggering experiment

The test site was densely equipped with different instruments. In three clusters, sensors were installed in 0.15 - 1.50 m depth. During the experiment, the logging interval was 5 min. Figure 5.5 shows the locations of the following installations (Askarinejad et al., 2010b):

- Sprinklers: For the first experiment, 10 sprinklers were regularly distributed along a central line which led to a higher sprinkling intensity in the lower part of the test site due to higher hydrostatic pressure. For the second experiment, 14 sprinklers were used and they were rearranged towards the upper part of the test site.

- 6 Water pressure sensors: The sensors were installed in 6 piezometers in order to measure the groundwater level in 2-4 m depth.

- Time Domain Reflectometers (TDR): To measure the volumetric water content in the soil, TDR were installed at each cluster in 60, 90, 120 and 150 cm depth.

- Jetfill tensiometer: To measure the soil suction, tensiometer were installed at each cluster in 15, 30, 60, 90, 120 and 150 cm depth.

- Pluviometer: 6 pluviometers were placed on the test site to measure the rain intensity.

- Photogrammetry cameras: To analyse the movements at the surface, 4 photogrammetry cameras were installed on trees at the toe of the test slope.

- Deformation probes: 4 flexible probes were equipped with strain gauges in order to monitor the movements in the underground (Askarinejad, 2009b).

- Electrical resistivity tomography (ERT): ERT profiles were recorded hourly during the experiment in order to analyse preferential water flow paths and saturation patterns in space and time.

- Trench to measure the overland flow: At the toe of the experiment site, a 20 cm deep trench was dug and equipped with plastic tubes in order to collect the overland flow. The water was conducted in plastic tubes to a weir to monitor the flux.

Additional sensors which will not be discussed in more detail were: Decagons, soil temperature sensors, earth pressure cells, acoustic sensors and an instrument to manually measure root reinforcement.

5.4   First experiment, October 2008

5.4.1   Sprinkling intensity and overland flow

A total amount of 1600 mm water was sprinkled from 28 October - 1 November 2008. The sprinkling intensity was higher in the lower part of the test site because all the sprinklers were feed from the same tank above the experiment site. Therefore the hydraulic head was higher in

the lower part. A first rain impulse lasted 3 h and reached mean intensities of 20 and 40 mm/h at pluviometer 1 and 2 (see Figure 5.5 for location), respectively (average 35 mm/h), followed by a drying period of 20 h. Then the intensity was 10 and 20 mm/h (average 17 mm/h) for 1.5 day before it was shortly increased up to an average of 45 mm/h. Then the average intensity was 30 mm/h for 1.5 days (first 15/45 mm/h for half a day and then 25/45 mm/h for another day).

The increase in the sprinkling intensity was also observed in the overland flow (Kienzler, 2008): A higher sprinkling intensity led to a higher overland flow and only to a slight increase of infiltration.

5.4.2 Soil saturation and groundwater table

Figure 5.10 shows the volumetric water content, the suction and piezometric level at the three clusters during the first experiment. In the following, the data is described and the time lag of the response to the rain in the different depths is compared.

In all three clusters, the sensors located at 60 cm depth responded in less than one hour after the start of sprinkling. The deeper sensors reacted later but indicated a higher saturation than the shallower ones, except for the TDRs located at 1.2 m depth. They reacted at the same time as the upper sensors or even faster. The sensors at 1.5 m depth responded with a time lag higher than 24 hours and showed the highest soil water tension. Also subsequent rain intensity changes are reflected in the water content and suction data, especially the restart of sprinkling at 14:00 on 28 of October.

The amount of water stored in the soil was calculated by subtracting the initial volumetric water content from the final water content in each depth (see Figure 5.11). About 400 mm water was stored in the unconsolidated sediment between 0 - 1.5 m depth.

Figure 5.12 shows the time lag of three events in all clusters. The first event (black) represents the start of the sprinkling in the first experiment. The second event (grey) is the re-start of sprinkling in the first experiment after the break of 20 h. The third event (red) corresponds to the start of sprinkling during the second experiment in March 2009. This will be discussed in the next section. The sensors respond much faster to the second event than to the first, especially in soil depth >60 cm. This shows how the hydraulic conductivity of the unconsolidated sediment increases with increasing soil saturation. If it is assumed that the water flow has only a vertical downwards component (hydraulic gradient =1) the hydraulic conductivity can be estimated by dividing the sensor depth by the time lag. At 0 - 60 cm depth, a k-value of 10^{-3} to 10^{-4} m/s and in 60-150 cm depth a k-value of 10^{-4} to 10^{-5} m/s was calculated. These k-values are higher than the ones obtained by infiltration tests, most likely because of preferential flow paths. At about 120 cm depth, the flow velocity was increased because the TDR in this depth reacted faster than the shallower ones. The wetting front of the second event arrived about two times faster than for the first one. This indicates that the hydraulic conductivity was increased for about 200% for the second wetting front.

After 2.5 days of sprinkling, a groundwater table of 10 cm and 20 cm was measured first at the bottom of the slope in Piezometer 3 (in 3 m depth) and then in the middle part of the slope in Piezometer 1 (in 4 m depth), respectively. A third piezometer located outside of the sprinkling area (see Figure 5.5 for location) remained dry during the entire experiment.

The increasing saturation of the unconsolidated sediments was also monitored with ERT (Figure 5.13.2 - 5.13.4). Decreasing resistivity indicates increasing saturation. The electrical resistivity

Figure 5.10: *Soil water content, soil tension, groundwater level measured at the three clusters and the mean rain intensity during the first experiment in October 2008. Data from Amin Askarinejad, Institute for Geotechnical Engineering, ETHZ.*
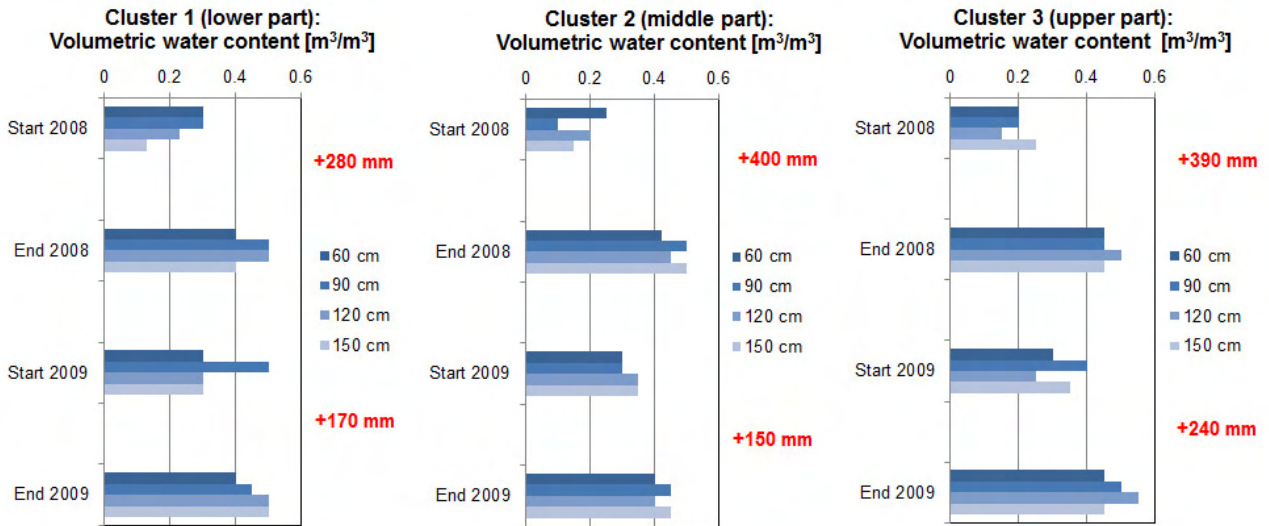
Figure 5.11: *To calculated the water that was stored in the upper 1.5 m of soil, the difference of volumetric water content in the soil before and after the experiment was multiplied by the thickness of the respective soil section: 0-60 cm, 60-90 cm , 90-120 cm and 120-150 cm depth. Data from Amin Askarinejad, Institute for Geotechnical Engineering, ETHZ.*

Figure 5.12: *Plots showing the arrival of the wetting front in all clusters for three events: black is the start of sprinkling in October 2008, grey is the re-start of sprinkling after a break of 12 h and red is the start of sprinkling in March 2009. Data from Amin Askarinejad, Institute of Geotechnical Engineering, ETHZ.*

decreased especially in the top layer in the upper part of the slope, where bedrock consists of sandstone (Figure 5.13.2). This indicates increasing saturation in the weathered bedrock and the unconsolidated sediment. It is possible that preferential lateral flow occurred in this layer. Also in the bedrock the saturation increased locally in more permeable sandstone layers (Figure 5.13.3). It is possible that those layers were fractured and less cemented and that they drained the unconsolidated sediment.

5.5 Second experiment, March 2009

In this section, the data from the second experiment are described, interpreted and compared to the data from the first experiment.

5.5.1 Sprinkling intensity

Total rain input for the second experiment was 150 mm in 15 hours.The mean rain intensity during the second experiment was 15, 12 and 8 mm/h in the upper, middle and lower cluster, respectively. Above the test site, where the upper six sprinklers were rearranged close to each other (see Figure 5.5), an intensity between 20 and 40 mm/h was estimated. The experiment started with a sprinkling duration of 2.5 h followed by a 40 min-sprinkling break. After 12 more hours of sprinkling, the slope failed. Overland flow was observed only in the upper part of the slope which reinfiltrated in the lower part. Therefore no overland flow could be measured in the trench located at the toe of the slope.

At the three clusters, the rain intensity never reached the maximum of 45 mm/h from the first experiment, but the intensity in the upper part was considerably higher compared to the first experiment due to the rearrangement of the sprinklers.

5.5.2 Groundwater

Figure 5.14 shows the measured soil saturation, suction and groundwater table in the three clusters. In general, the sensors react similarly to the first experiment. This means that the shallower sensors react first but the deeper sensors react more pronounced. A difference concerning the first experiment is the time lag which is shorter for all sensors in the upper cluster (see Figure 5.12). That means that the wetting front arrived faster in the second experiment. On the contrary, the lowest cluster responds later than in October 2008 due to the smaller sprinkling intensity in the lower part of the slope. The time lag for the sensors at 60 - 150 cm depth in the lower cluster is about 6 h whereas in the first experiment, the time lag was clearly higher for the deeper sensors. This could be because during the second experiment, the wetting front arrived at the lower cluster by lateral subsurface stormflow. Lateral flow occurred probably along the weathered sandstone.

The higher initial saturation of the soil in March 2009 can also be seen in the ERT data (Figure 5.13). Thus in March 2009, less water could be stored in the soil. In the upper part of the slope, where the sprinkling intensity was smaller during the first experiment, 240 mm water could be stored. This is more than in the lower part of the slope, where only 150 mm was stored. It is likely that the same amount of water like in the first experiment (400 mm) could be stored above the uppermost cluster (then in this area, the sprinklers were rearranged more densely for the second experiment). Thus an average value for the amount of stored water during the second experiment is assumed to be 300 mm.
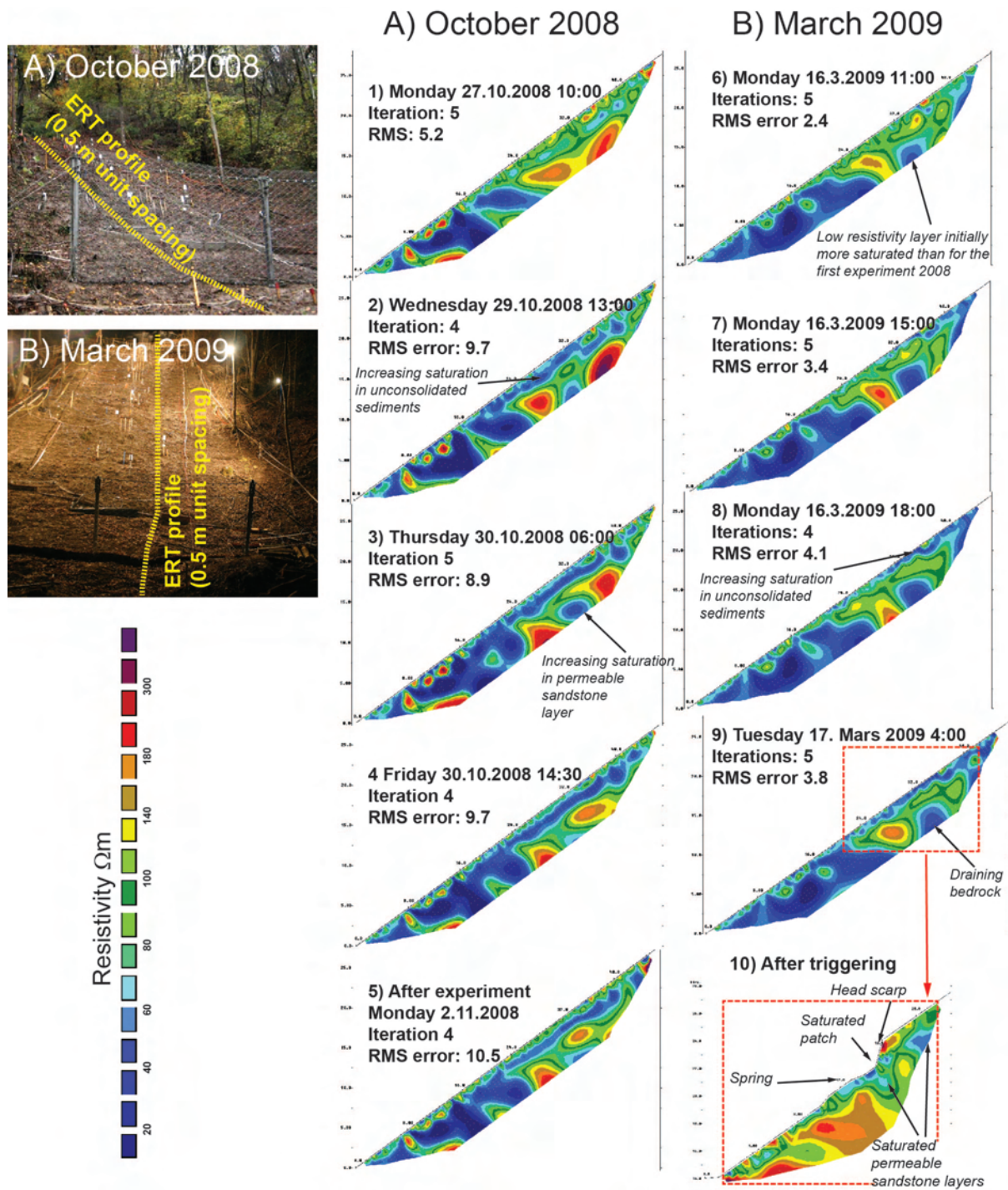
Figure 5.13: *ERT profiles recorded before and during the first experiment in October 2008 and the second experiment in March 2009 (Gambazzi and Suski, 2009).*
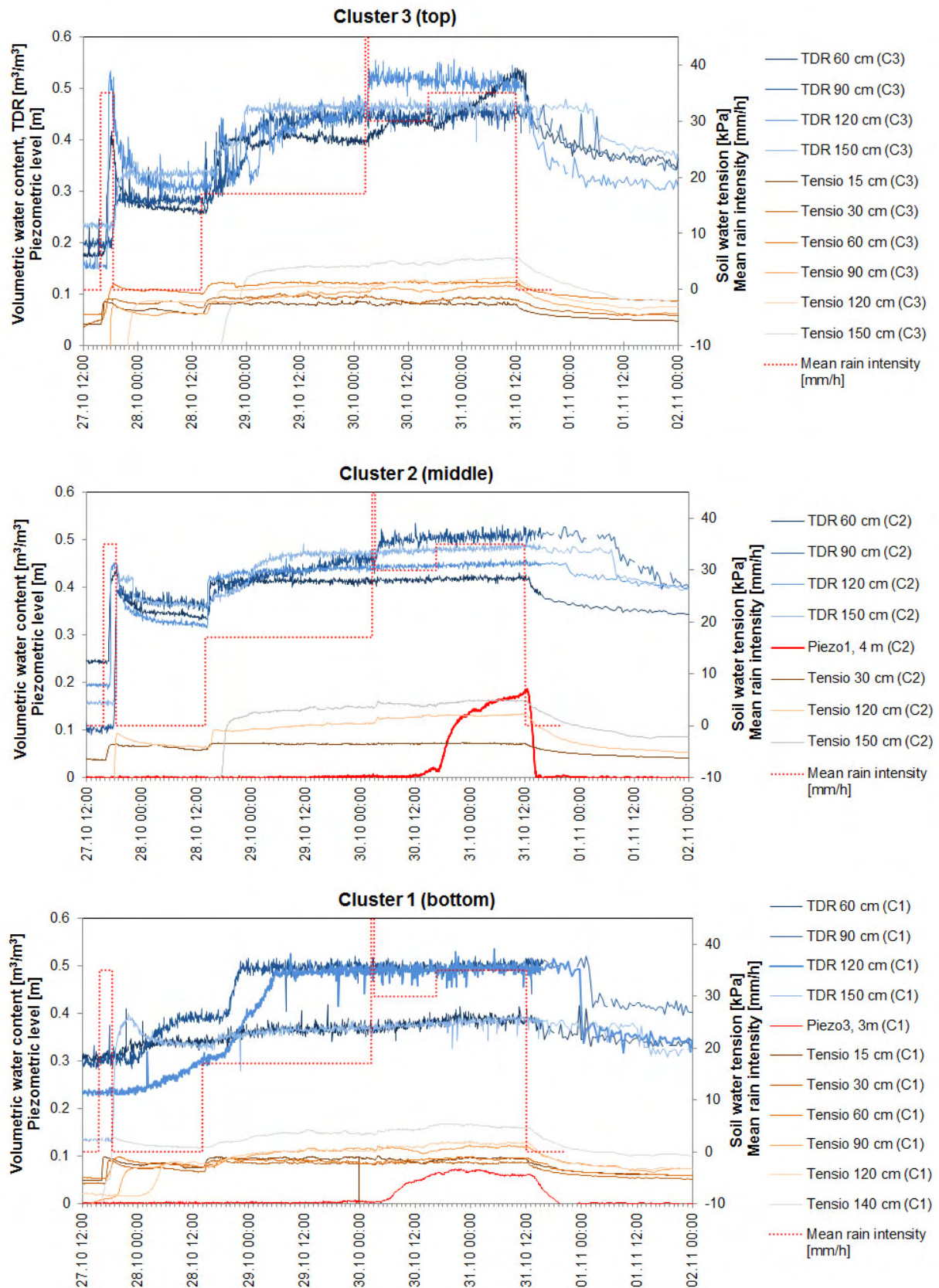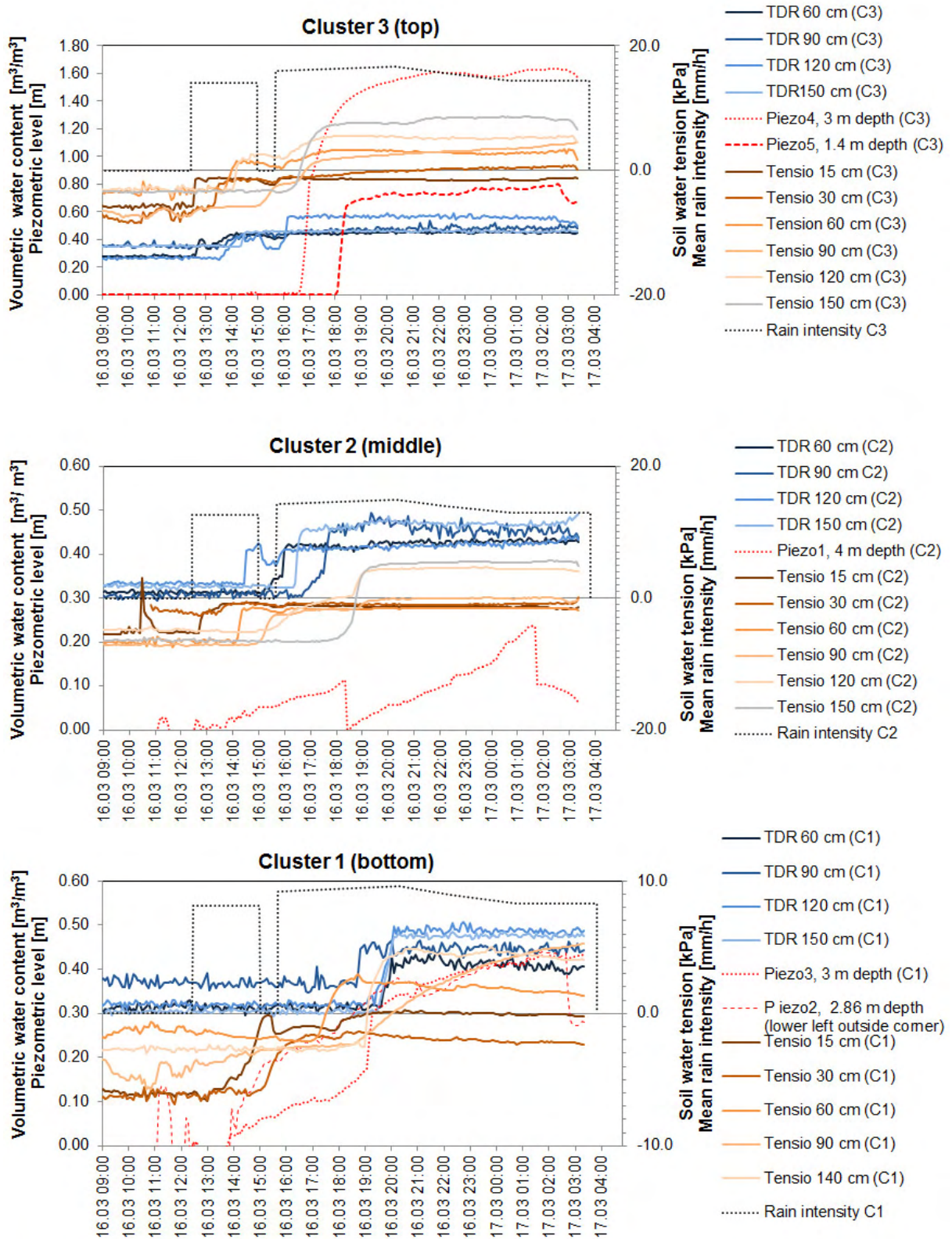
Figure 5.14: *Soil water content, soil tension and groundwater level measured at the three clusters and rain intensity during the second experiment in March 2009. Data from Amin Askarinejad, Institute for Geotechnical Engineering, ETHZ.*

Piezometers 4 and 5 in the upper cluster showed a groundwater table of 0.6 and 1.6 m after 6 h of sprinkling. The high level of the groundwater led to the assumption that these piezometers react rather as wells and do not show the real groundwater table. After 3 h of sprinkling, piezometer 1 in the middle part, piezometer 3 in the lower part of the slope and piezometer 2 located outside of the sprinkling started to react. A groundwater table of 10-25 cm built up in four hours. At 18.25 h, piezometer 1 drained suddenly and the groundwater table in piezometer 3 rose for 20 cm. Then all three piezometer show an increasing water table up to 20 and 40 cm in the middle and lower part, respectively. 2 hours before failure, piezometer 1 drained again immediately for 15 cm and piezometers 2 and 5 drained suddenly 1 hour before failure for 15 cm even the sprinkling rate remained constant. In the piezometers installed in the 23 m-deep drill hole, no response to the sprinkling could be measured.

The reaction of piezometer 2 which is located outside of the sprinkling area is very interesting. During the first experiment, this piezometer remained dry but during the second experiment, it reacted after 2 hours of sprinkling. This leads to the interpretation that an important groundwater flow occurred through permeable subsurface hydraulic connections. This could be either lateral flow along the bedrock surface like observed in the dye infiltration tests, or flow in fractures and joints and along permeable layers in the bedrock. The fact that all three piezometer started reacting at the same time leads to the assumption that they are hydrologically connected by permeable layers or joints. The sudden drop in piezometer 1 could be due to movements in the slope or even the bedrock which opened new draining paths. The sudden rise in piezometer 3 around 18:00 h could be related to the draining of piezometer 1 or to the re-start of sprinkling. The sudden drops of the groundwater level in piezometer 1, 2 and 5 around 2:00 h in the morning could be related with the failure, indicating pre-failure movements and subsequent opening of draining flow paths in the soil and bedrock. The reaction in piezometer 2 is surprising because it is located about 30 m away from the triggered landslide.

The piezometric data shows that lateral groundwater flow occurs probably at 3 - 4 m depth or deeper in a continuous perched aquifer. The faster and the more distinct reaction of the piezometers in contrast to the first experiment lead to the interpretation that the bedrock was probably nearly saturated at the beginning of the second experiment. It is to say that in October 2008, hundred litres of water have been put in piezometer 1 and 3 and drained immediately. Even though the sprinklers were shifted towards the top of the test site, piezometer 2 and 3 at the toe of the slope reacted after 2 hours of sprinkling. The bedrock depression on the left side of the slope (as seen in ERT profiles and DPL, see Figure 5.6) probably favoured the formation of a groundwater table at this part of the slope.

Another observation which supports the assumption of groundwater flow through the bedrock was water that started flowing out of large joins located below the test site (see photograph on Figure 5.4) a few hours before the triggering. This joints are at the same level as Piezometer 3, but they are located 100 m to the South of the test site. This water flow continued for a few hours after the experiment.

A higher initial saturation of the bedrock in March 2009 is also observed in the ERT data (see Figure 5.13.6).

A few hours after the triggering, an additional ERT profile was recorded along the landslide slip surface (see Figure 5.13.10). Two layers with lower resistivity are indicated. These layers are interpreted as more permeable bedrock where the water probably infiltrated during the experiment.

A photograph that was taken a few seconds after the triggering showed accumulated water in the upper part of the landslide before failure occurred along the slip surface (see Figure 5.15). Water exfiltrating from a water patch in the upper left corner of the landslide and a spring in the middle part of the landslide was flowing down slope. This two accumulations of groundwater could be related with the layers of low electrical resistivity indicated on the ERT profile Figure 5.13.10. Water that had infiltrated during the experiment in high permeable weathered bedrock and permeable sandstone layers exfiltrated after the triggering. This permeable sandstone layers were also observed in the drill hole.
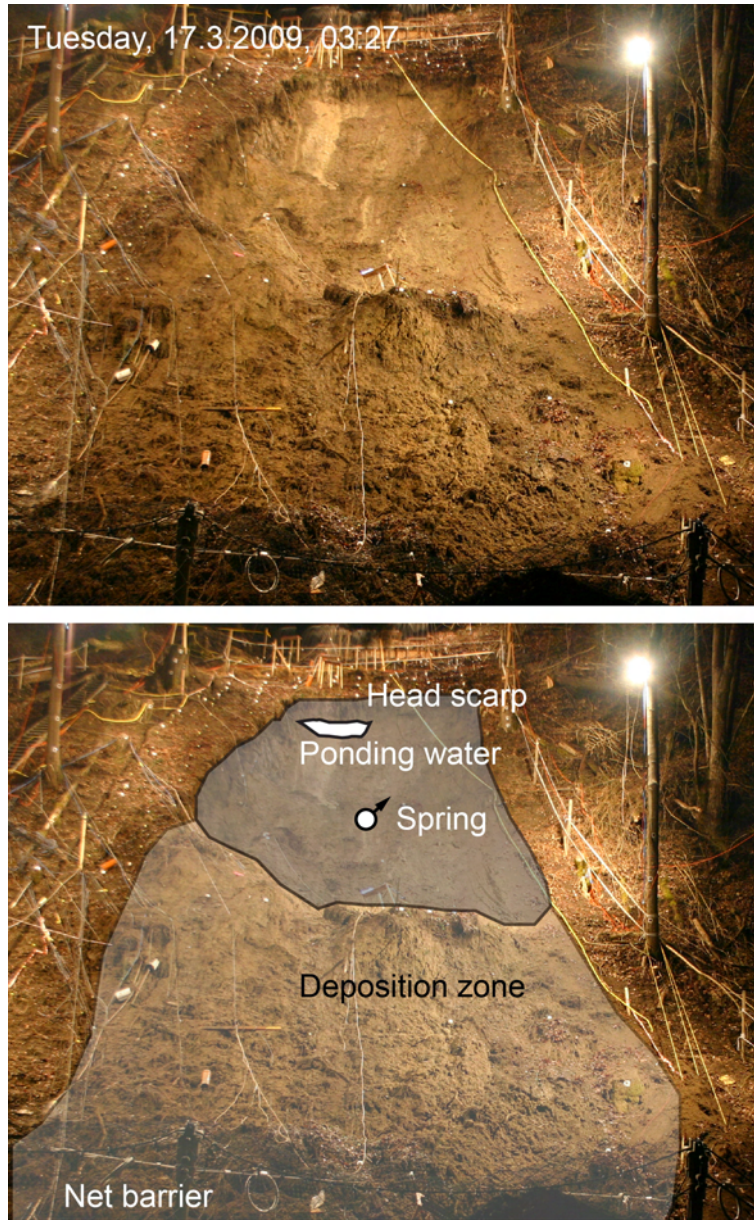
Figure 5.15: *Photograph of the test site taken a few seconds after the landslide triggering. Water that accumulated in the upper left corner of the landslide just below the head scarp is flowing down after the triggering. The spring marked in the bottom photograph continued to flow for several hours after the triggering. Photographs taken by Amin Askarinejad, Institute for Geotechnical Engineering, ETHZ.*

5.6   Hydrogeological conceptual model

Figure 5.16 summarises the results from drill holes, bedrock surface survey, ERT profiles, and hydrological monitoring. The permeability of the bedrock in the area of the experiment is very heterogeneous: The cemented sandstone layers and the marlstone are low-permeable if not fractured and a perched groundwater table can be built up above the bedrock. But the uncemented sandstone layers are permeable and water can either infiltrate into or exfiltrate from these layers. Additionally, large vertical joints that are crossing the bedrock act as drains for the unconsolidated sediment and the bedrock. The importance of these joints became obvious during infiltration tests, when water infiltrated immediately. The refilling of the 23 m deep drill hole with sand also showed the importance of the joints because 60 kg of sand just disappeared. An other important observation was made during and after the second experiment: Water was flowing out of joints (seen on Figure 5.4) located about 100 m to the south of the test site. Thus bedrock infiltration was a dominant process during both experiments. Little bedrock exfiltration could be observed after the landslide triggering in the upper part of the test slope, where a spring continued flowing for hours after the experiment. A positive pore water pressure in the unconsolidated sediment could only be built up when either the joints were saturated (bottom up saturation) or when the rain intensity and infiltration exceeded the draining capacity (perched groundwater, top down saturation). It is assumed that locally both processes occurred. The questions arise why the slope did not fail the first time. What was the difference between the first and the second experiment?

Based on data of the rain intensity, overland flow and soil saturation, the hydrological water balance was calculated. During the first experiment, total water input was 1650 mm, measured overland flow was 500 mm, and the soil between 0 and 150 cm depth stored 400 mm of water. Thus a volume of 750 mm was lateral subsurface stormflow and vertical loss into the fractures. This is about 44% of the total input. The volume of the joints in the vicinity of the test site must be several cubic meters. During the first experiment, these joints were efficiently draining the overlaying soil. The sprinkling intensity in the upper part of the slope was probably too low to build up positive pore water pressure and a perched groundwater table was formed only in the bedrock depression in the lower left part of the slope.

For the second experiment, the hydrologic balance is different. Total input was only 150 mm. This is about 10 times less than during the first experiment. No overland flow was recorded at the toe of the slope during the second experiment thus all the water infiltrated. It is assumed that the soil could have retained more than 150 mm. Thus lateral and vertical drainage along and into the bedrock occurred most likely only locally along preferential paths, nevertheless the slope failed. This could be due to several reasons:

- Initial saturation: The initial saturation of the bedrock and the soil was higher in March 2009 than in October 2008. The second experiment took place after and during snow melt. Additionally, it is possible that in March the saturation of the soil was still affected by the first experiment and by the drilling campaign conducted at the top of the slope a few days before the second experiment. On the contrary, in October 2008, the soil was drier and evapotranspiration reduced additionally the water content in the soil. Thus during the second experiment, less water was necessary to establish positive pore water pressure.

- Infiltration capacity: Because of the larger initial saturation of the soil in March 2009, the infiltration capacity was higher from the beginning. The upper sprinklers, where the sprinkling intensity was maximal during the second experiment, were in a less steep part of the slope, so that the water could probably infiltrate easier due to local ponding.
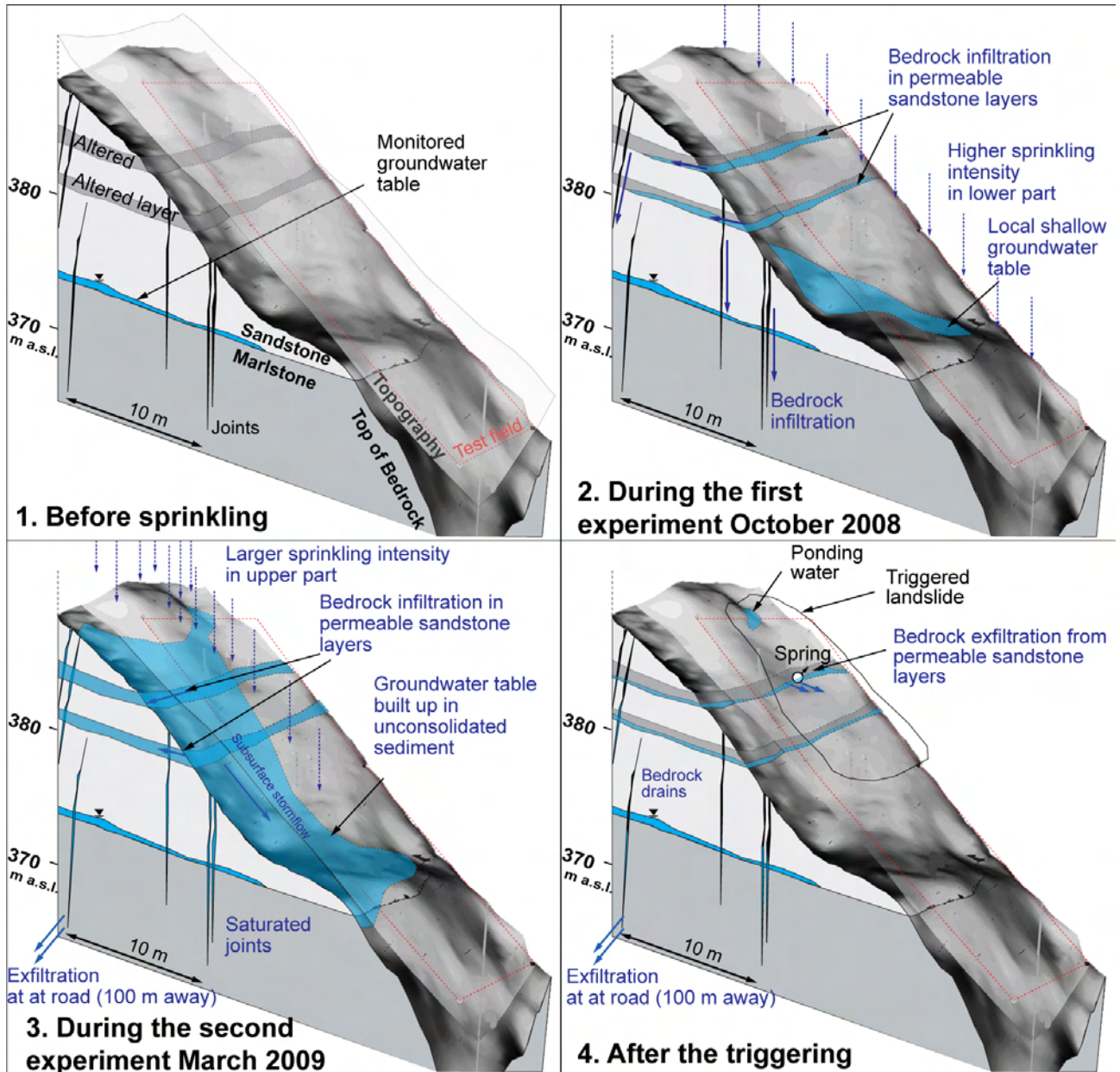
Figure 5.16: *Conceptual hydrogeological model of the Rüdlingen landslide triggering experiment.*

- Sprinkling intensity in the upper part: In March 2009, the sprinkling intensity in the upper part of the slope was large enough to establish perched groundwater.

- Tree roots: The strength of the tree roots was more important for the first experiment because trees located on the test site were cut only a few weeks before the first experiment. Thus the effect of the roots was more pronounced during the first experiment. Additionally, before the second experiment roots around the test site were cut with a motor saw up to 0.5 m depth.

This experiment showed the complexity of different hydrogeological processes. Phenomena like bedrock infiltration and exfiltration are very local. Therefore it is not possible to extrapolate the results of the experiment on the entire slope between Buchberg and the River Rhine. Nevertheless, it is possible to define hydrogeological processes that should be taken into account by analysing the landslide susceptibility and slope stability in the area:

- The bedrock and unconsolidated sediment are locally drained by large vertical joints. Bedrock infiltration is the dominant process in the area of the sprinkling experiment.

- Well cemented sandstone layers and marlstone act as impeding layers if there are no vertical joints. Thus, locally positive pore water pressure can be formed in the unconsolidated sediment above the low permeable bedrock.

- Uncemented sandstone layers are permeable. At locations where no vertical joints are draining those layers, aquifers can be formed in those permeable layers. Spring horizons, for example observed in the Upper Marine Molasse above the test site, indicate the location of such permeable sandstone layers.

5.7 Triggering mechanisms

Two different situations have to be distinguished to classify the case of Rüdlingen. These are natural shallow landslides and the triggering experiment with artificial rainfall (see Figure 5.17).
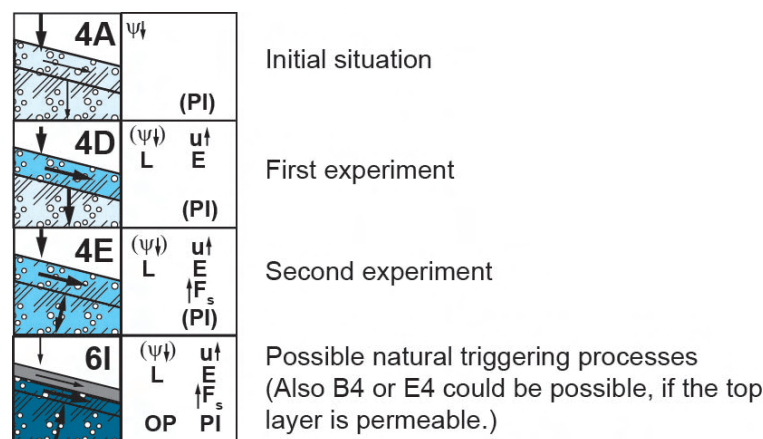
Figure 5.17: *The hydrogeological classification applied for natural landslides and the artificially triggered landslide in Rüdlingen. The unconsolidated sediment and the bedrock are permeable. Both were initially unsaturated. During the first experiment, saturation was reached only in the unconsolidated sediment. During the second experiment the bedrock was most likely also saturated.*

Potential triggering mechanisms for the artificial landslide are (according to the hydrogeological classification):

- Rise in pore water pressure: During the second experiment, positive pore water pressure was build up rapidly in the unconsolidated sediment. This decreased the shear strength of the material and led to seepage. Positive pore water pressure was probably not the most dominant triggering mechanism, because prior to the failure, the pore water pressure decreased abruptly. Porewater pressure fall prior to landslide movement (especially rapid landslides) is interpreted to occur due to draining fissures that opened prior to the failure (Harp et al., 1990). Another explanation for the drop in the porewater pressure prior to failure is dilation of the soil (and subsequent increase of the pore volume) at the shear zone (Askarinejad et al., 2010a).

- Seepage forces: Slope parallel seepage occurred along the bedrock surface. Local exfiltration from permeable bedrock layers (as observed below the head scarp) most likely caused horizontal or even upward oriented seepage, which influenced the triggering.

- Seepage erosion: Seepage erosion was most likely an important triggering mechanism. This was also observed in triggering experiments in different permeable sandy soils performed by Harp et al. (1990). They described that the pore water pressure dropped 5 - 50 min previously to failure. This drop in pore water pressure occurred before visible cracks formed, like in Rüdlingen. Harp et al. (1990) observed water flow rates at cut slope faces. They found out that flow through fractures and macropores was predominant and that the water flow path and permeability were changing. And as the slope failed, water poured out of the slope along the failure surface, like it was the case in the upper left corner in the Rüdlingen experiment. The flow of this muddy water shows that water could accumulated locally in fractures. Thus preferential flow and seepage erosion played an important role for the triggering. When fine grained soil fraction is removed along a potential slip surface, the apparent cohesion of the soil is reduced which decreases the shear strength.

- Upward seepage and liquefaction: No liquefaction was observed during the triggering. After the landslide was triggered, very small slips and flows of saturated soil was observed in the head scarp area.

- Effect of water on clay minerals: The plasticity index of the unconsolidated sediment in Rüdlingen is 6-12% which is rather low. Even though little swelling of the soil could be observed, it is assumed that the clay minerals played a minor role by the triggering.

For the natural landslide triggering in the area of the distal Molasse, it is possible that local confined aquifers may play an important role. The springs and spring horizons observed above the test site give evidence for the occurrence of groundwater in more permeable sandstone layers. This would additionally lead to exfiltration and overpressure from below the landslide.

The example of the Rüdlingen triggering experiment shows how different triggering mechanisms may play together. Like it can be seen on Figure 8.9 in Chapter 8, the case of the experiment and the natural landslides are both in the "high criticality" zone.

Chapter 6

Active earth flow-debris slide Pont Bourquin (VD)

6.1 Introduction

Complex geology, several small springs, heterogeneous groundwater flow, ponding water and swampy zones on the low permeable moraine, clayey landslide material, and numerous small debris slides-earth flows triggered by rainfall are characteristics of the continuously flowing Pont Bourquin landslide (see Figure 6.1). To find out more about the comportment of this 250 m long and 30-50 m wide landslide, detailed investigation and monitoring were carry out since summer 2009. Main interests of the present study were:
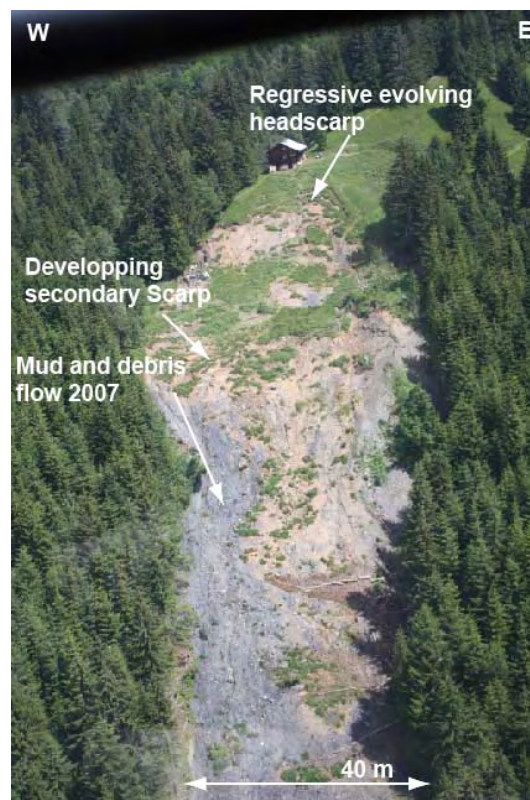
Figure 6.1: *The upper and middle parts of the Pont Bourquin landslide in July 2009 (Photo: M. Jaboyedoff).*

- Geological, geomorphological and hydrogeological mapping and description of surface processes in order to have a detailed map of the landslide surface.

- Drill holes and geophysical investigation (seismic refraction and electric resistivity tomography) in order to make a 3D geological model of the landslide including the slip surface and lithological boundaries in the subsurface.

- Trace the origin of the groundwater and water flow path in the landslide in order to create a conceptual hydrogeological model. For this purpose, the following investigations were performed:

  * Measurements of precipitation and flux of springs and creeks in order estimate the water input and output on the landslide.

  * Monitoring the groundwater level in observation wells.

  * Measurements of the hydraulic conductivity of the landslide material with infiltration and pumping tests.

  * Hydrochemical analyses of major elements and isotopic analyses of sulphur from water samples (from springs, creeks and observation wells) in order to obtain information about the origin of the groundwater.

  * Additionally, ERT gave evidence for the existence of groundwater.

- Evaluate the effect of the groundwater on the triggering.

The geophysical investigations have been carried out in collaboration and under the supervision of Institute of Earth Science ISTerra, University J. Fourier, Grenoble (F), with the support of Institute of Geophysics IG, University of Lausanne. In addition, this project was initiated by a summer school organized by Foundation Qunaterra and Institute of Geomatics and Risk Analyses IGAR, University of Lausanne within the European project Mountain Risks. Several test and two boreholes were performed during this school in summer 2009.

6.2 Regional context and landslide history

The Pont Bourquin landslide is located in the Western Prealps of Switzerland between the village Les Diablerets and the Pillon Pass at an altitude between 1340 and 1440 m above sea level. The average annual precipitation in Les Diablerets is 1500 mm (values from 2000-2009 from the MeteoSchweiz station DIB 7940 located 2 km west of Pont Bourquin landslide at 1162 m a.s.l., see Figure 6.24). A continuous snow cover is usually found from December to April. Snowmelt usually occurs in April.

The landslide lies in a tectonically complex zone between Helvetic and Ultrahelvetic nappes (see Figure 6.2). Three major thrust faults dipping approximately 35° towards the North are crossing the landslide. The following four nappes from top (North) to bottom (South) are found on the landslide (Badoux et al., 1990): Meilleret nappe (cellular dolomite and heterogeneous Flysch composed of carbonatic sand- and siltstone), Arveyes nappe (black shale, typically Aalenian age), Plaine Morte Flysch and Bex nappe (cellular dolomite and gypsum).

Large landslides cover the slopes around the village of Les Diablerets (Figure 6.3). The activity of this large slope instabilities initiated most likely after the last glaciation period due to the retirement of large glaciers (Noverraz et al., 1998). The Parchets landslide, which is located to the North of the Pont Bourquin landslide, had important crises around 2000 y BP. Today it is moving
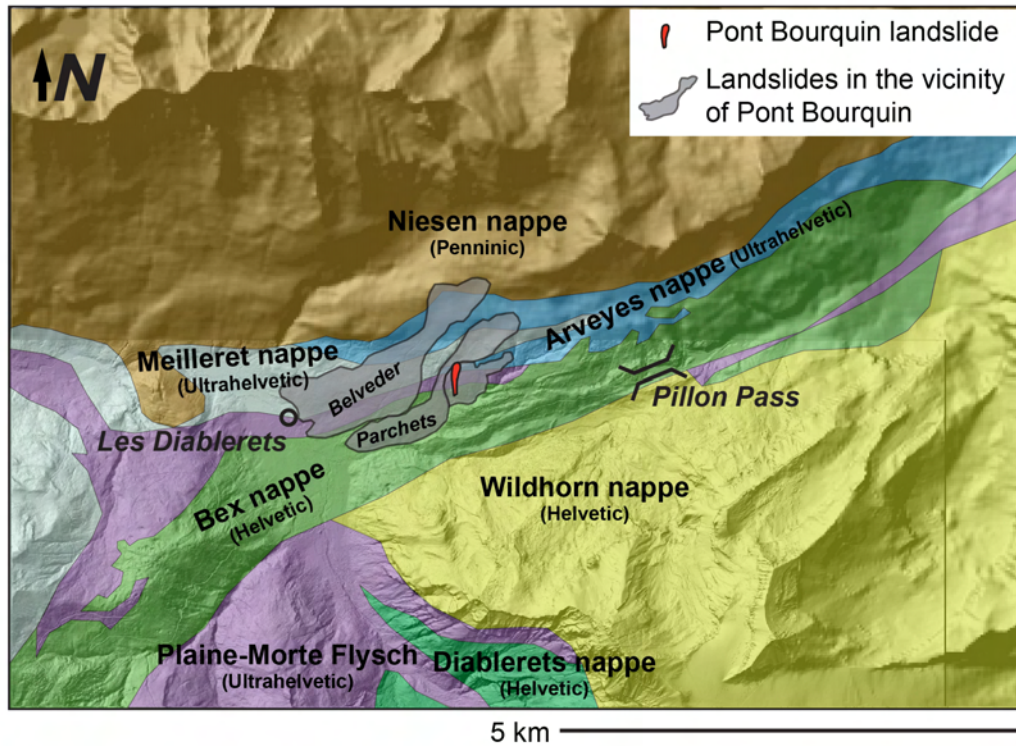
Figure 6.2: *Tectonic map of the region around the Pont Bourquin landslide (after Badoux et al. (1990), shaded relief from ©2004 Swisstopo). The Pont Bourquin landslide lays in a zone largely affected by landslides between the village Les Diablerets and the Pillon Pass.*

2-10 cm per year (Schoeneich et al. (1996), GIS of Canton Vaud, http://www.geoplanet.vd.ch). The Pont Bourquin landslide is considered as a local reactivation of a more regional slow creeping zone (see Figure 6.3). The mean slope angle of the Pont Bourquin landslide is 25° (22° in the upper part, 27° in the middle and lower part of the landslide). The Pont Bourquin landslide initiated in the Aalenian black shale lithology in a zone where the slope was more than 50° steep and showed a rather convex topography.

Figure 6.4 shows aerial photographs from 1998, 2004 and 2008 where the initiation of the Pont Bourquin landslide can be followed. The important reactivation of the Pont Bourquin landslide started in 2004, probably favoured by exceptional snow melt in spring and heavy rainfalls in August of the same year. Three years later, on the 5 July 2007 (see Figure 6.24), heavy rainfall triggered a rapid earth flow with a volume of 11'000 m^3 which cut the road between Les Diablerets and Gstaad (Jaboyedoff et al., 2009). A precipitation rich period preceded the triggering of this earth flow (130 mm in 4 days, 306 mm in 1 month). In summer 2010, superficial displacements of 20 m in three month have been measured with LIDAR and total station (see Section remotesensing) by the *Institute of Geomatics and Risk Analyses*. In July 2010, rain storms triggered an earth flow with a volume of several cubic meters which reached again the edge of the road. In August 2010, a debris slide with an estimated volume of more than 1'000 m^3 reached the creek at the toe of the landslide. After August 2010, remediation work was conducted on the landslide. Superficial drains were installed and the toe was stabilised with a wood-construction. Since then, debris flows-earth slides in the order of cubic meters are periodically triggered.
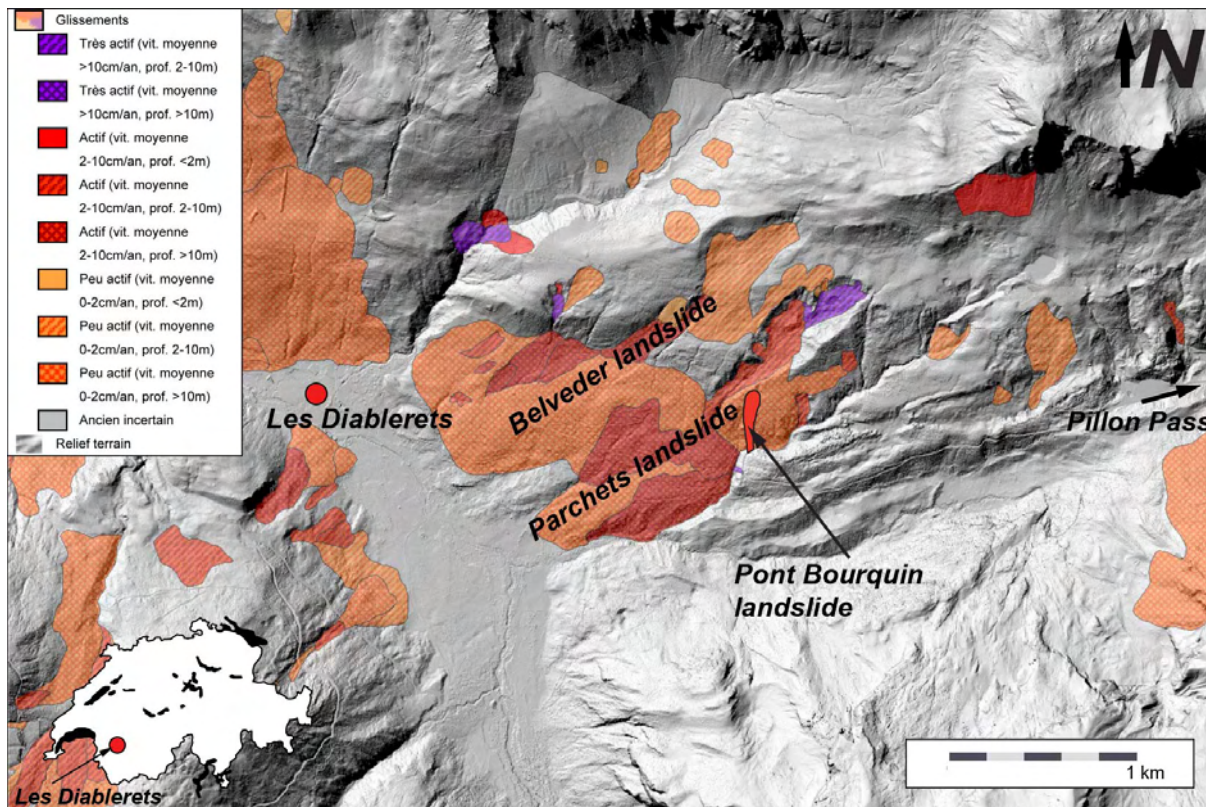
Figure 6.3: *Map with the landslide phenomena around the village of Les Diablerets indicating different landslide depth and activities (landslide data from GIS of Canton Vaud, http://www.geoplanet.vd.ch) and shaded relief based on ALS-DEM from ©2001 Swisstopo).*
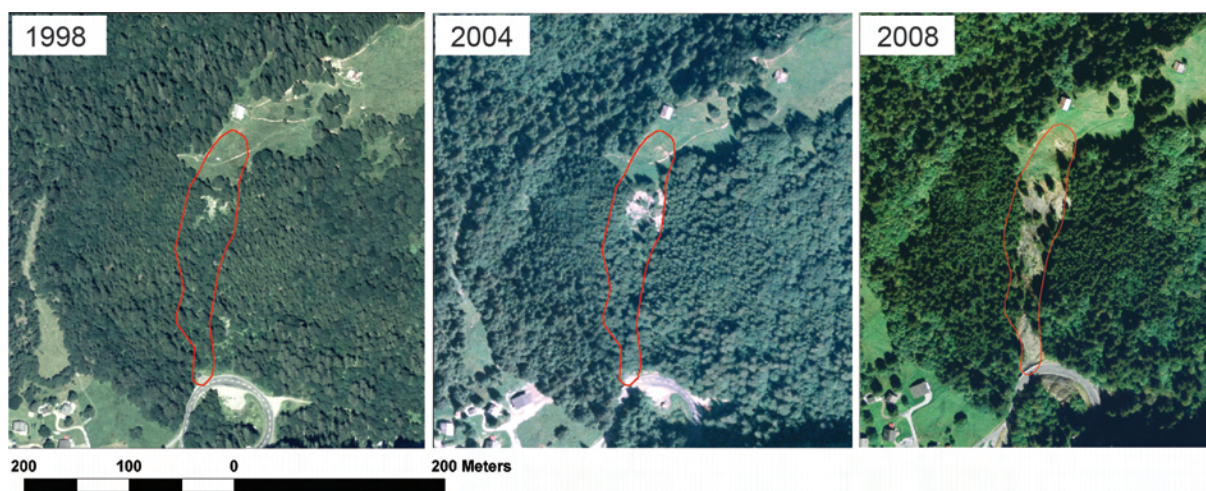
Figure 6.4: *Orthophotos from 1998, 2004 and 2008 showing the initiation of the Pont Bourquin landslide (data from SWISSIMAGE ©2008 Swisstopo (DV012716).*

6.3 Geological characterisation

Lithological map

- ↥ Tectonic boundary
- ☐ Pont Bourquin landslide

Outcrops
- ■ Black shales
- ■ Grey shists
- ■ Cornieule
- ■ Gypsum
- ■ Light siltstone-sandstone
- ■ Graded Sandstone

Geological interpretation
- ☐ Cornieule with gypsum
- ☐ Sandstone - siltstone
- ☐ Black and grey shales

40 20 0   40 Meters
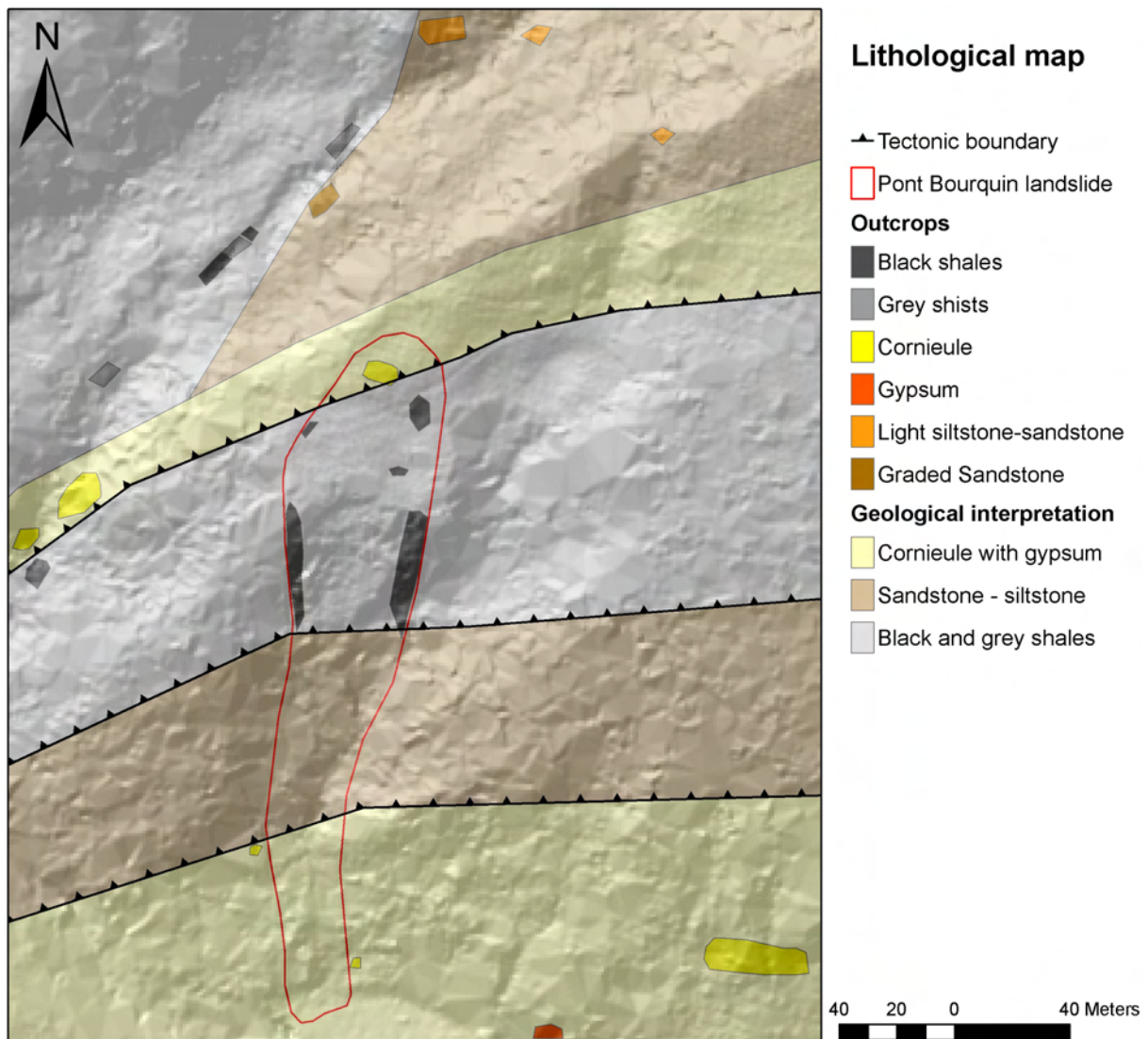
Figure 6.5: *Lithological map of the area around the Pont Bourquin landslide underlain by a shaded relief based on ALS-DEM from ©2001 Swisstopo. Three tectonic faults separate the different geological units of the landslide (modified after (Badoux et al., 1990)). Intense colours: Mapped outcrops mainly on the landslide and in the nearby stream. Light colours: Interpretation of the lithological formations. Quaternary sediments are shown on Figure 6.7.*

Figure 6.5 shows a geological map of the Pont Bourquin landslide. In the head scarp area, Triassic **cellular dolomite**[1] is outcropping. This lithology is very heterogeneous, partly massive and partly porous with cells in mm- and cm-scale. Main component is carbonate (Dolomite: $CaMg[CO_3]_2$) and the colour is ochre-beige. Cornieule is associated with gypsum ($Ca[SO_4]2H_2O$). The pores result from the dissolution of the gypsum. Cellular dolomite associated with gypsum is also found at the toe of the landslide.

Below the head scarp area is the boundary between cellular dolomite and **black shale**. The black shale has Aalenian age (early Dogger) and is silver grey to dark grey and locally orange coloured. It contains calcite and quartz layers, clay minerals and pyrite (FeS_2, from microscopic

---

[1]Also named cornieule or cargneule.

up to cm-scale). Orange discolouring indicates the oxidation of the pyrite. The black shale is foliated in mm-scale and breaks easily along the foliation planes (see photo on Figure 6.6). The black shale is heavily fractured due to tectonic faults and landslide activity. Due to the landslide movement the black shale is exposed to weathering and erosion. This clayey lithology was the initiation zone of the landslide. The landslide mass is mainly composed of black shale debris.
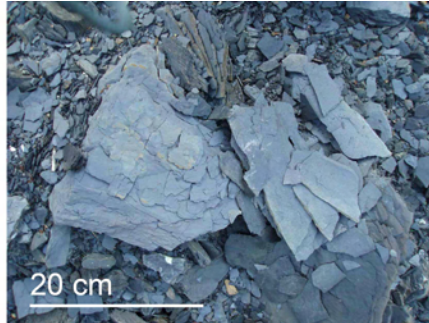
Figure 6.6: *Photograph showing the fractured black shale lithology.*

Along a little creek located to the West of the Pont Bourquin landslide, black shale is associated with **grey shale**, a clay-siltstone which contains nodules of fine grained sandstone. This lithology is interpreted as a variation of the black shale lithology. Above the landslide, heterogeneous Flysch from the Meilleret Nappe is locally outcropping. This is a grey-greenish **light siltstone-fine grained sandstone** that contains chlorite and nodules of calcite and a carbonate grey-brown **sandstone-schist** that contains graded sandstone layers.

Between the black shale and the cellular dolomite at the toe of the landslide, Flysch lithology is expected. In 2007, outcrops of this lithology were described (Jaboyedoff et al., 2009) which are now covered by landslide debris. This is a sandstone-siltstone composed of a succession of thin bedded turbidites.

Except in the bed of the little creek and on the landslide, the bedrock is mostly covered by quaternary sediments, basically moraine and colluvium. Above the landslide, the rock is covered by several meters of **moraine**. The Pont Bourquin landslide is partly composed of moraine. The moraine is beige and clayey silt with little sand and large boulders and rocks of cellular dolomite, sand- and siltstone (found in drill holes in depth <10 m). The moraine has a high plasticity index of 14 - 39%. Results from grain size and plasticity analyses are summarized in Table 6.1 (Feissli, 2010). The moraine is very low permeable (see Section 6.9) and shows generally a high water content which results in a pasty texture/consistence. Calcite is probably washed out. This moraine is classified as ground moraine from the last glaciation period.

Above the landslide and in swampy areas below the main scarp, the moraine is often covered by **gley**. Gley is oxidised (brown-reddish) and reduced (grey) soil. This soil has a high plasticity, but the cohesion is smaller than the cohesion of the moraine (less sticky).

The main unconsolidated sediment cover in the area of the Pont Bourquin landslide is moraine and colluvium. This includes deposits from ancient landslides (for example talus from the Parchets landslide) and products from soil erosion and weathering. The talus contains a mixture of moraine material and black shale, silty clay and clayey silt with sand, gravel and stones found at the surface and in drill holes on the landslide. Plasticity analyses of a colluvium sample, which

Sample name	P61	P54	P45	P36
Fraction > 0.2 mm [%] (Coarse-grained sand)	16	0	14	8
Fraction 0.06 - 0.2 mm [%] (Fine-grained sand)	20	0	9	17
Fraction <0.06 mm [%] (Silt and clay)	64	100	77	75
Plasticity Index I_p [%]	19	14	39	18
Specific surface S_s [m^2/g]	31	17	151	29

Table 6.1: *Results from grain size and plasticity analyses of four samples from the Pont Bourquin landslide. P61, P54 and P45 are samples from moraine and P36 is a colluvium sample from black shale (Feissli, 2010). The samples were taken along the geophysical profiles ERT5 shown on Figure 6.11 and are numerated according to the posts of the geophysical profile.*

was composed mainly of black shale, had a plasticity index I_p of 18% (see Table 6.1, sample P36).

Quaternary sediments are shown on the geomorphological map Figure 6.7 in the next Section.

6.4 Geomorphological characterisation

The geomorphological map of the Pont Bourquin landslide (Figure 6.7) shows the following features:

- **Scarps:** Three retrogressively eroding scarps can be observed on the Pont Bourquin landslide: The **headscarp**, an upper and a lower **secondary scarp**. The lower secondary scarp was formed during summer 2010. Figure 6.8 shows photographs of the three scarps and also from a large **side scarp**, where the landslide mass is retained by tree roots.

- **Cracks:** Zones with pronounced cracks were mapped. Important areas where cracks are forming are above the secondary scarps. This is due to the retrogressive erosion of the scarps.

- **Perennial and ephemeral springs:** Springs are mainly observed in the upper part of the landslide and below the scarps. An exception is spring 32 in the middle part of the landslide which showed the highest flux of all springs (see Figure 6.10).

- **Swampy areas:** Swampy areas are observed mainly in the upper part of the Pont Bourquin landslide and towards Northeast at an altitude of 1400-1440 m above sea level. In the upper part of the Pont Bourquin landslide, hydrophilic plants indicate the swampy areas (see Figure 6.10).

- **Creeks:** Two creeks were mapped outside of the Pont Bourquin landslide: a small stream to the West of the landslide and an ephemeral creek, which is infiltrating at an altitude of about 1420 m a.s.l., to the East. The ephemeral creeks on the landslide are continuously adapting to the changing topography. A main creek was flowing down on the western side of the landslide and a second main creek was flowing downwards from spring 32. They were draining the landslide below the lower second scarp towards the little stream to the West.

- **Bodies of moraine and black shale debris:** In the middle part of the Pont Bourquin landslide, large unstable bodies of moraine and black shale debris are sliding downwards.
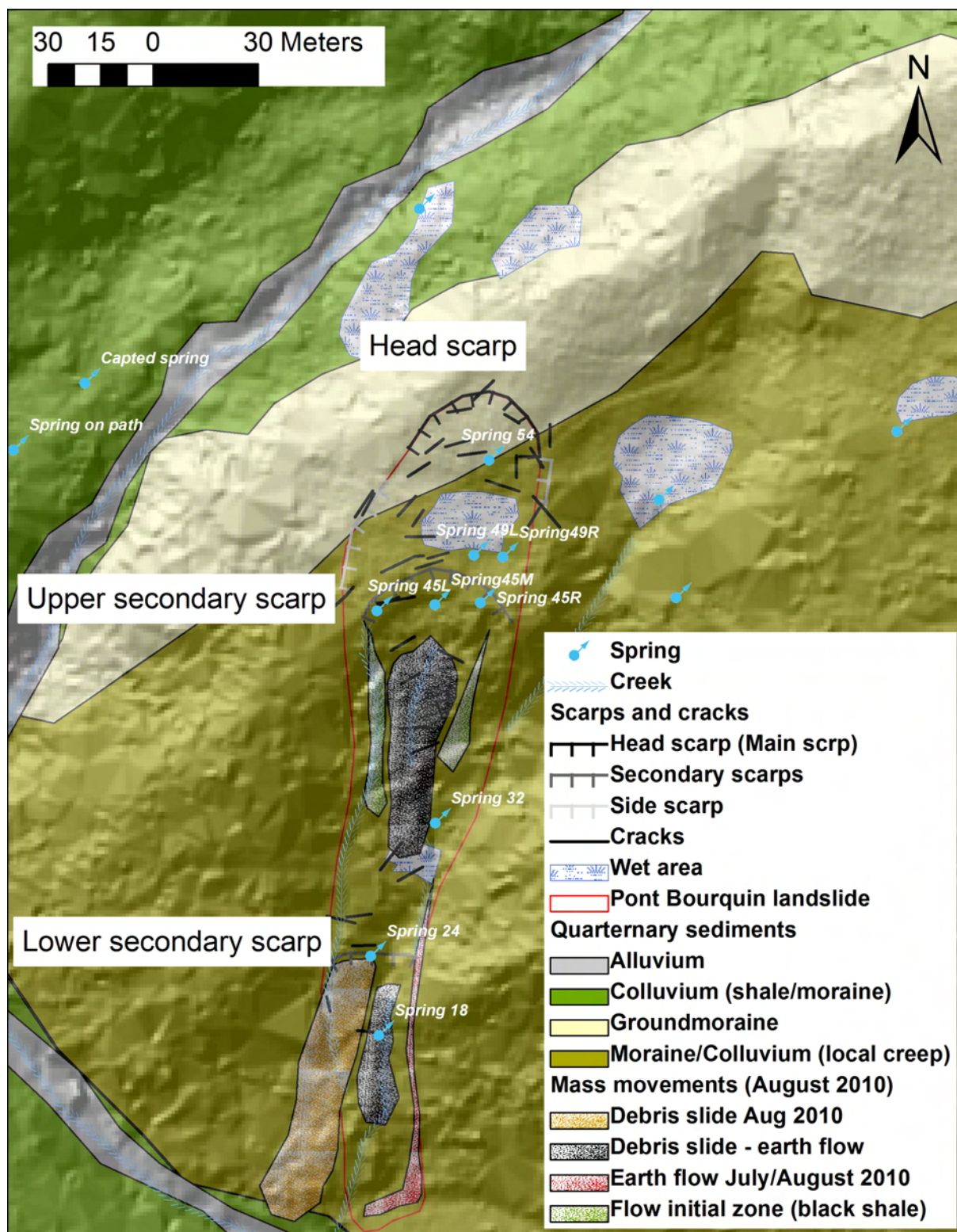
Figure 6.7: *Geomorphological-hydrogeological map of the Pont Bourquin landslide and the surrounding area, including quaternary sediment (August 2010, before remediation work was conducted, shaded relief based on ALS-DEM from ©2001 Swisstopo).*

These masses of material have also been mapped. Especially, two major events from summer 2010 which reached the edge of the road have been mapped: a **mudflow from July 2010** and a **debris slide from August 2010** (see photographs on Figure 6.9).

Headscarp,
19 August 2010

Secondary scarp (middle part),
19 August 2010

Secondary scarp (lower part),
19 August 2010

Crack in black shale debris
(midle part), 12 May 2010

Crack in moraine
(upper part), 28 Sept 2010

Sidesacarp (upper part),
12 May 2010
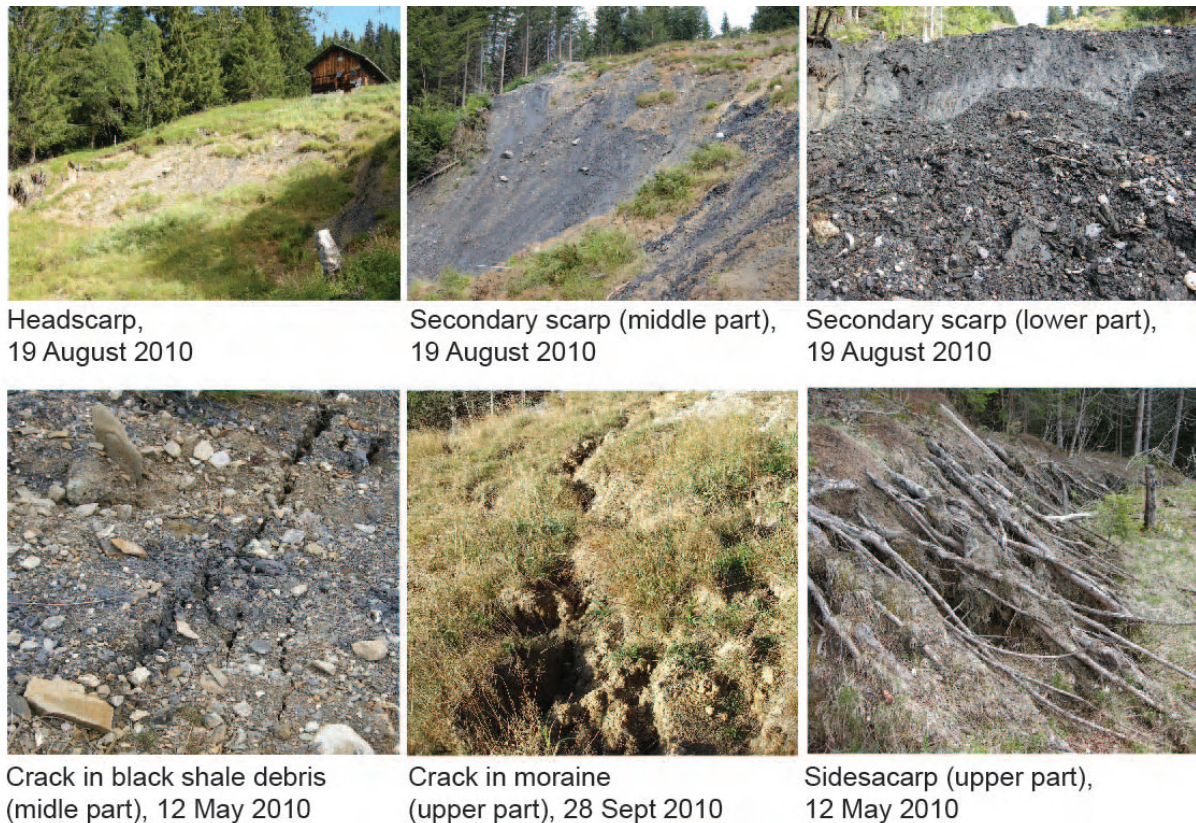
Figure 6.8: *Photographs showing the scarps and some cracks of the Pont Bourquin landslide.*

The landslide can be divided into the following three main parts which are limited by the two secondary scarps:

- The upper part extends from the main scarp to the upper secondary scarp and is less steep than the lower parts of the landslide. Below the main scarp, the bedrock is exposed and consists of cellular dolomite. The plateau below the outcrop represents a swampy zone where water accumulates on the low permeable moraine. Large extension-cracks parallel to head and side scarps form retrogressively.
  Rapidly evolving cracks perpendicular to the slide movement and regressive erosion of head and side scarps indicate the activity of this part. Overall the upper part shows less activity than the lower parts of the landslide. It is creeping a few cm per month and shows a rotational-translational movement.

- The middle part is over-steepened and extends from the upper secondary scarp the lower secondary scarp. Below the upper secondary scarp, the bedrock is exposed and consists of black shale.
  This is the most active part of the landslide. Along the rapidly regressive eroding upper secondary scarp, material is continuously mobilized and slides downwards. Movements of one meter per month were measured (see Figure B.1 in Appendix B). Exposed Aalenian rock and moraine bodies are in disequilibrium. They represent the initiation zone of numerous earth slides and debris flows which can reach the edge of the road. Superficial translational

Earthflow July 2010
(photographs from 28 July 2010)

Debris slide August 2010
(photograph from 19 August 2010)

Figure 6.9: *In July 2010, a thunderstorm triggered a mudflow in the lower left part of the Pont Bourquin landslide. This flow with a volume of several m^3 reached the edge of the road. In August 2010, a medium size debris slide was triggered during a thunderstorm and formed the lower secondary scarp. This slide had a volume of several 10 m^3.*

Weir of spring 32, middle part of Pont Bourquin landslide, 28 June 2010

Spring 54 (upper part), typical red discolouring in the black shale, 9 July 2009

Spring in the forest E of the Pont Bourquin landslide, 19 August 2010
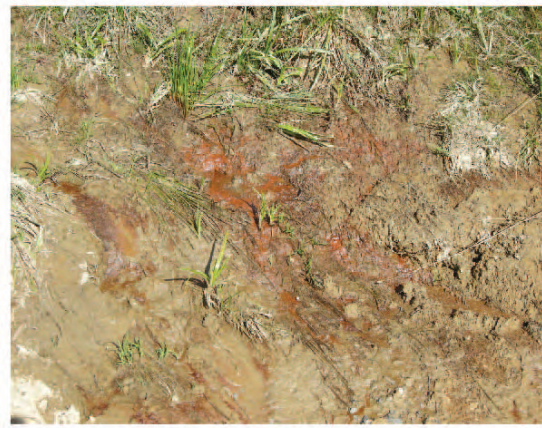
Spring 49 R (upper part of the Pont Bourquin landslide), red mud: iron(III) oxide-hydroxide, 23 September 2010

Swampy area in the upper part of the Pont Bourquin landslide, 22 June 2009

Swampy areas above the Pont Bourquin landslide, 9 July 2009

Figure 6.10: Photographs with different springs and wet areas on and beside the Pont Bourquin landslide. Spring 32 has been trapped in June 2010 in order to measure the flux.

slides and flows show displacement of up to 20 m in 3 month in summer 2010. Small flows of several m^3 are triggered during strong rainfall events and create several levee-channel structures. Sheared inclinometer tubes indicate movements along different internal shear planes.

- The lower part represents the accumulation zone of the landslide and extends from the lower secondary scarp, which was formed in August 2010, to the toe of the landslide. It consists of several meters thick accumulations of debris composed of black shale fragments, moraine material and cornieule boulders. It overlies a brownish sandy unit at about 10 m depth.
  Cracks are forming continually especially above the lower secondary scarp. Masses of debris are sliding towards the creek and the road. Levees and channels evolve continuously. In August 2010, a debris slide with an estimated volume of >1'000 m^3 reached the creek at the toe of the landslide and the lower secondary scarp was formed.

6.5 Seismic refraction

Two short and one long seismic refraction profiles were conducted with 24 and 72 4.5-Hz geophones, respectively (see Table 6.2 for profile details and Figure 6.11 for profile locations). For the short profiles, the seismic signal was obtained with a sledge hammer and for the long profile with explosives in 0.5 - 1 m deep hand auger holes. The location of the blasts is listed in Table B.1 in Appendix B. The travel-time diagrams were first analysed and then seismic tomography was performed. Travel time diagrams help to discover horizontal layering and to create an initial velocity-model for the tomography. For details about the method, see Section 4.4.

Profil name	Number of geophones	Spacing, m	Horizontal length, m	Orientation	Nr. of shots	Geophones (Hz)	Date
P1	24	3	65	W-E	9	4.5	8 July 2009
P3	24	3	60	N-S	9	4.5	8 July 2009
P4	72	5	342	N-S	25	4.5	29 Sept 2009

Table 6.2: *Details of the seismic refraction profiles performed on the Pont Bourquin landslide.*

6.5.1 Travel-time diagram analyses

Figure 6.12 shows the travel-time curves of 11 shots along the longitudinal profile P4: At geophones GP 2 and GP 3 at the toe of the slope, at GP 9 and GP 11 at the toe of the landslide, at GP 33, GP 36 and GP 39 located in the black shale lithology in the middle part of the landslide, at GP 54 and GP 57 in the head scarp area of the landslide and at GP 69 and GP 72 at the top of the slope. Three main observations are made:

- In the upper part of the slope, one velocity change and thus two layers are observed.

- In the lower part of the slope, two velocity changes and thus three layers are observed.

- The first layer is thicker in the lower part than in the upper part (indicated with black arrows).

- The curves are steeper in the lower part of the landslide and thus indicated lower p-wave velocities than in the upper part. Pronounced lateral changes in the velocity values were observed at GP 14, GP 33 and GP 50. Most likely the lithology changes laterally at those locations.
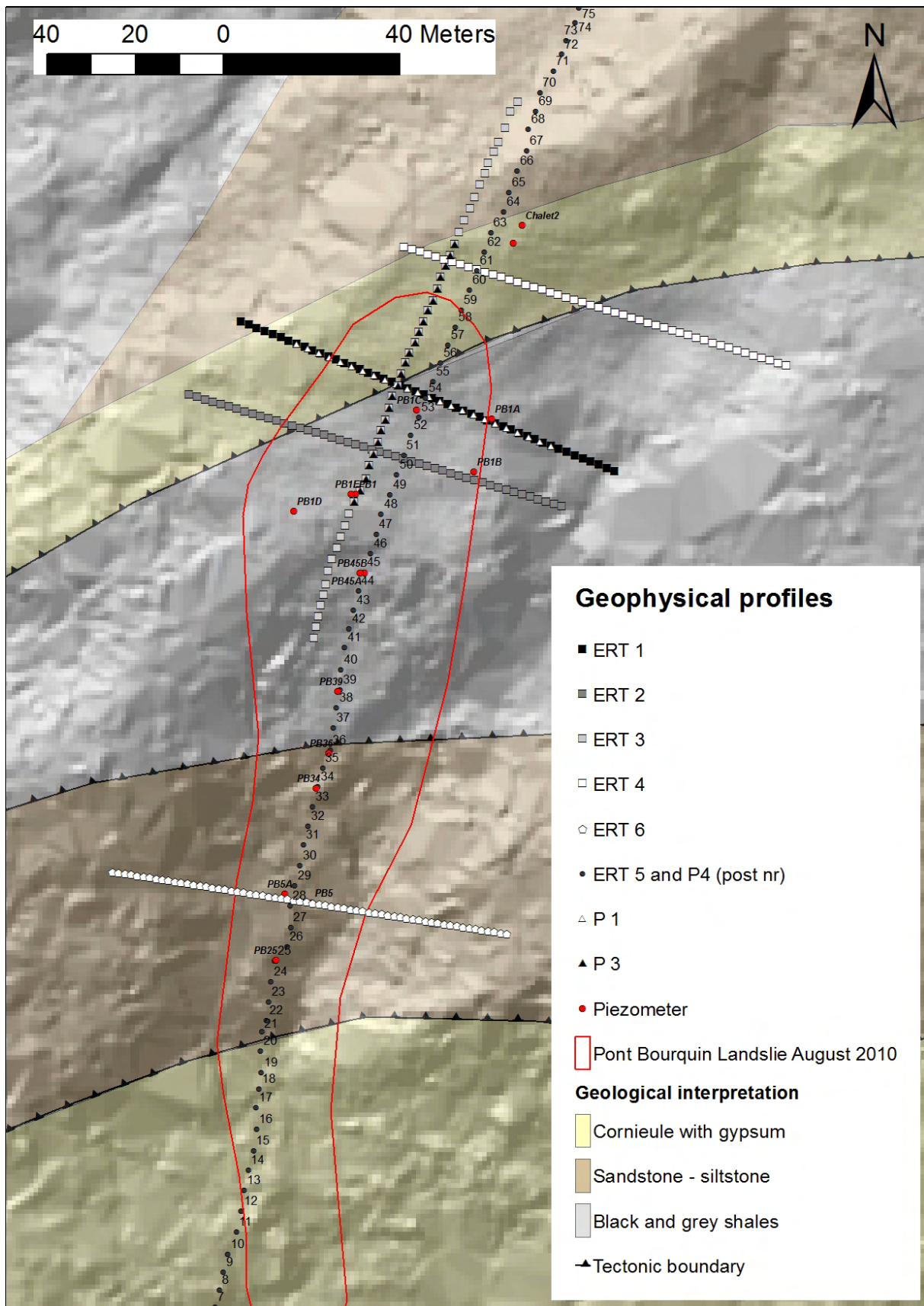
Figure 6.11: *Location of 3 seismic and 5 ERT profiles along and across the Pont Bourquin landslide. Post nr. 4 correspond to geophone and electrode nr. 1 and post nr. 75 correspond to geophone and electrode nr. 72.*

- Small undulations are repeated in all travel-time curves (red shaded in Figure 6.12) and are therefore interpreted as irregularities either in the layer thickness or layer property. "Hills" could for example represent depressions in the slip surface of the landslide (Magnin and Bertrand, 2005).
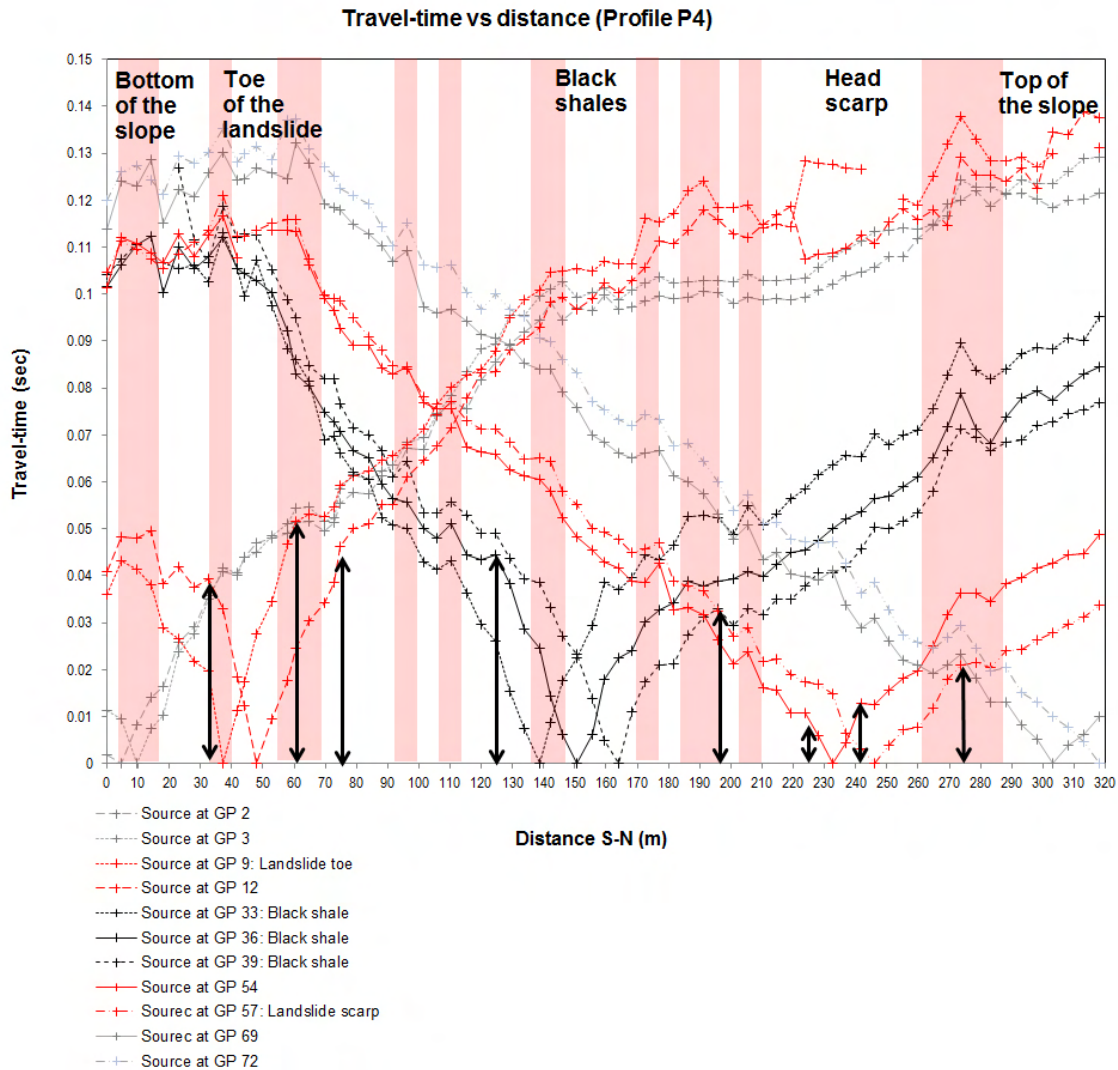
Figure 6.12: *Graph showing the p-wave travel-time versus profile length of P4. The bottom of the slope (geophone 1) is on the left side. Travel-time curves from 11 explosives were chosen to represent the structure at 5 locations of the slope: at the bottom of the slope (left side), at the toe of the landslide, in the middle part of the landslide, at the head scarp and at the top of the slope (right side). The change in the slope of the curves indicates different p-wave velocities. Undulations (orange shaded) are the same for the different travel-time curves. Therefore we can assume that the irregularities result from an irregular surface which is most likely the slip surface.*

Travel-time curves from the short profile P3 (shots at geophones 1 and 7) travel-time curves from the long profile P4 (shots at geophones 57 and 60) are compared in Figure 6.13. The geophones from the two profiles were approximately at the same locations. The p-wave velocity of the top layer in the small profile is about half the velocity from the long profile. This could be due to the limited resolution of the long profile. The resolution of the long profile is not good enough to display the uppermost thin layer which represents the landslide.
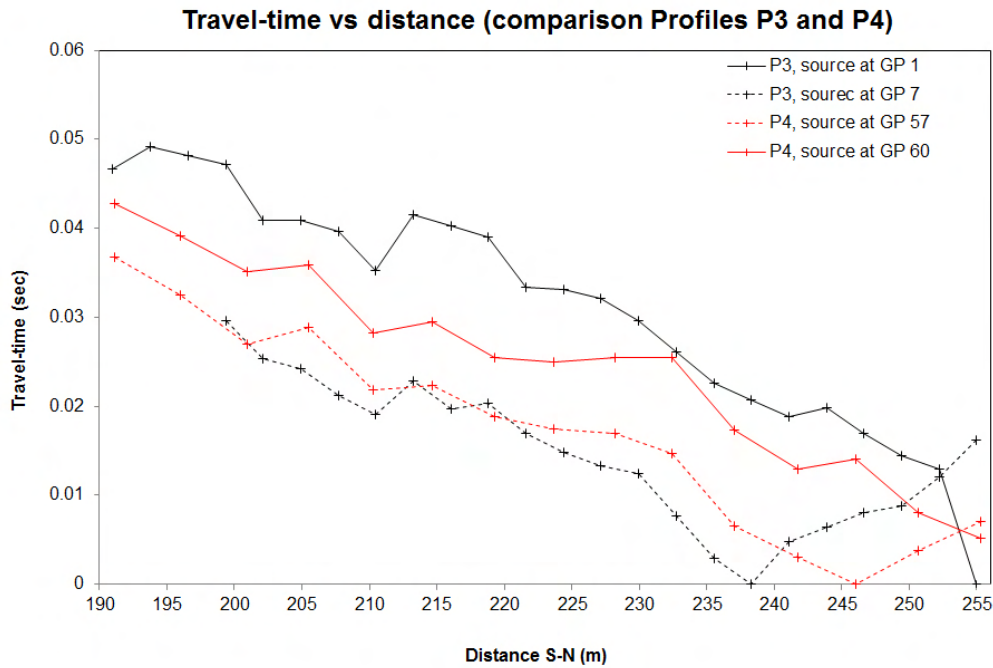
Figure 6.13: *Graph showing the p-wave travel-time versus profile-length of P3 comparing with the travel-time curves of P4 in this section. Small scale irregularities correlate in the two profiles P3 and P4. Nevertheless, the resolution of P4 was not good enough to also record the first low velocity layer.*

6.5.2   Seismic refraction tomography

All inversion models of P1, P3 and P4 were carried out twice: First with a homogeneous model with a p-wave velocity of 4000 m/s and then with a simplified 3-layer initial model without lateral changes. Three layers were chosen because in the middle part of the landslide, three layers were observed in the travel time diagram. To obtain best results with the software Sardine, the initial model should always contain bigger velocities than observed in reality. Table 6.3 shows the velocities for different layers used in the initial model:

	Depth (m)	P-wave velocity (m/s)
Layer 1	0-2	700
Layer 2	2-10	2500
Layer 3	>10	4000

Table 6.3: *Initial 3-layer model used for the seismic refraction tomography.*

More complex initial models could have been tested. For example a model where the upper most layer (velocity of 600 m/s) becomes thinner further up-slope. Or a model where the velocity of the second layer changes laterally: 1250 m/s in the lower part (0 - 130 m, Gypsum) and 2500 m/s in the upper part of the slope (130 - 320 m). But a homogeneous initial model showed the best results (see next paragraph), therefore no complex initial models are chosen.

Figure 6.14 shows the inversion results of the short profiles P1 and P3. In the substratum of the Pont Bourquin landslide, no velocities bigger than 3000 m/s were observed. Therefore all velocities bigger than 3000 m/s (red on the profiles) should be neglected. The two P1 models (C and
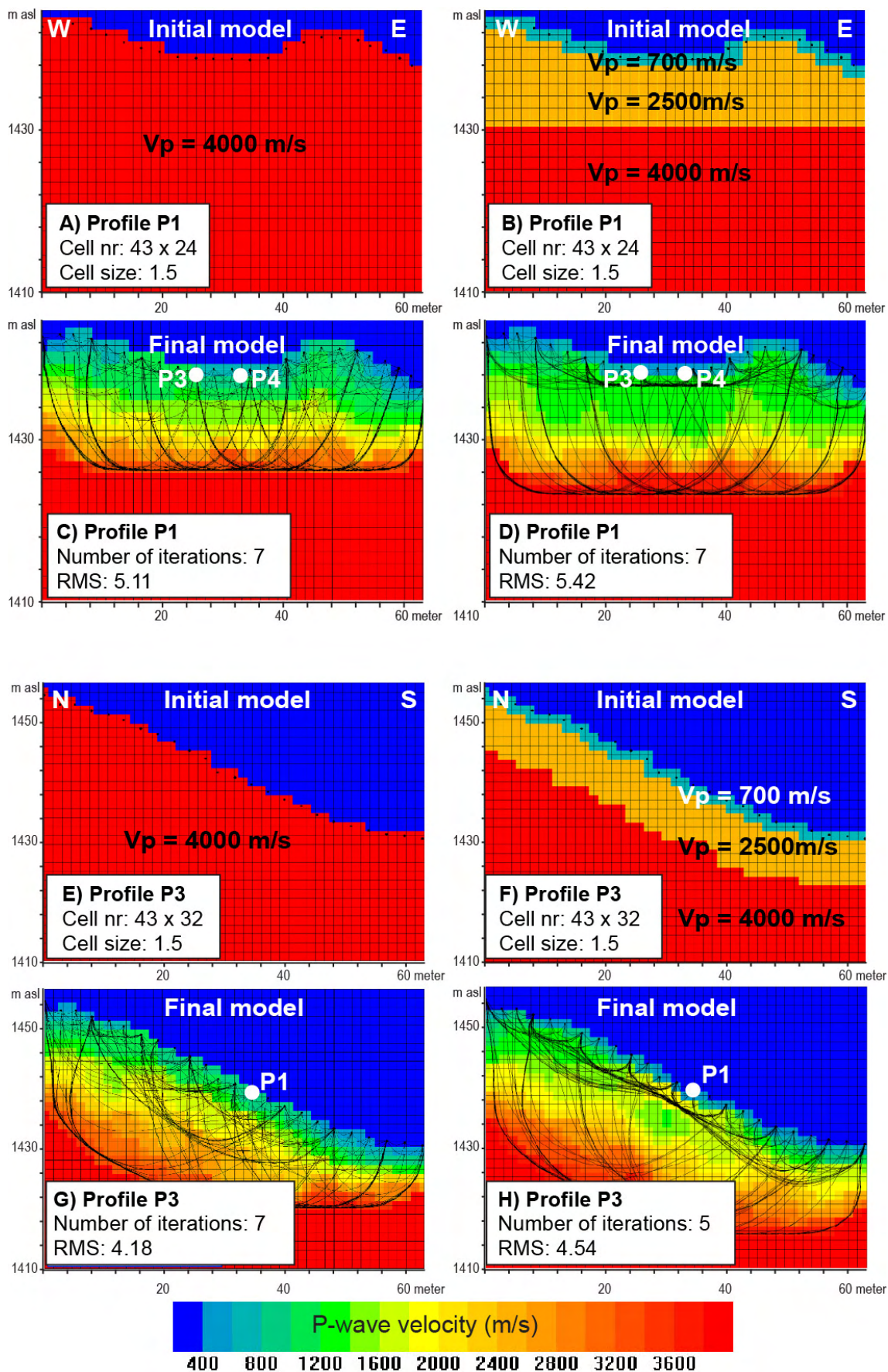
Figure 6.14: *Initial models (A, B and E, F) of short profiles P1 and P3 and the corresponding final seismic refraction tomography models (C, D and G, H). Velocities bigger than 2000 m/s are due to the initial model and are beyond the penetration depth and should therefore be neglected.*

D) are similar, but the RMS error[2] after 7 iterations is slightly better by using the homogeneous initial model (C). A pronounced shallow refractor observed in D) follows the layer boundary from the initial model at about 3 m depth, whereas C) shows a less pronounced first refractor at 3 - 5 m depth. In D) the first layer with velocities <1200 m/s does not change laterally, whereas in C) it gets slightly thinner towards the sides of the profile. The total penetration depth is about 13 m and 16 m in C) and D), respectively.

For the profile P3, the RMS is also smaller by using a homogeneous initial model (F). The 3-layer model was stopped after 5 iterations because the internal structure started to become heterogeneous and the RMS stopped to decrease whereas for the homogeneous initial model, 7 iterations were performed. Like in P1, the first refractor observed in P3 is more pronounced by using the three layer initial model in a depth of 3 to 5 m (F and H). With the homogeneous model, less distinct refractors are observed at about 5 and 10 m depth. The penetration depth for the homogeneous initial model is 24 m and for the 3-layer initial model it is 28 m. In both models it can be seen that the top low velocity layer <1200 m/s becomes thinner towards the middle of the slope.
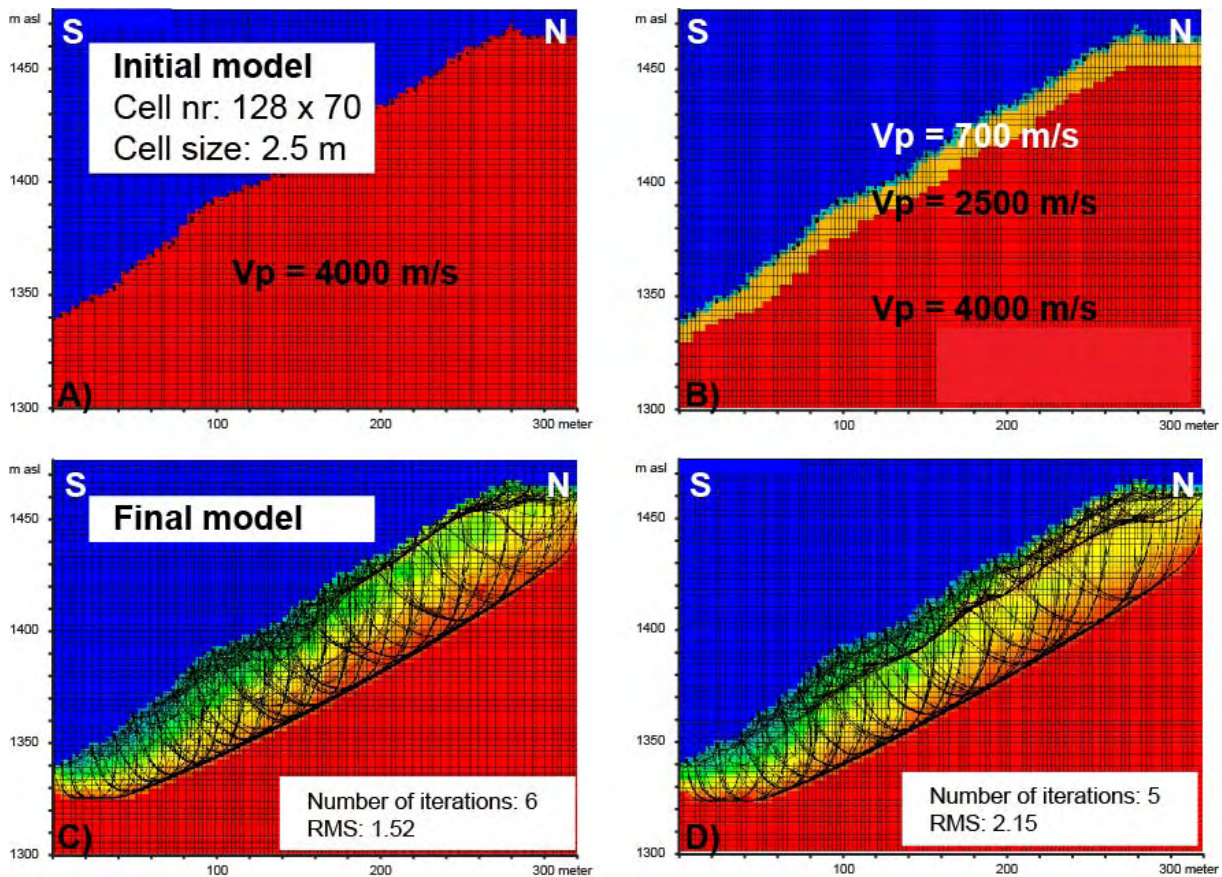
Figure 6.15: *Initial and final seismic refraction tomography model of the long profile P4. Velocities bigger than 3000 m/s are due to the initial model and are beyond the penetration depth and should therefore be neglected.*

Figures 6.15 and 6.16 shows four different inversed models of the long profile P4 each obtained by a homogeneous (A) and a 3-layer (B) initial model:

---

[2]The root mean square error (RMS) is a measure of precision for the model. It is the differences between values predicted by the model and the observed values.
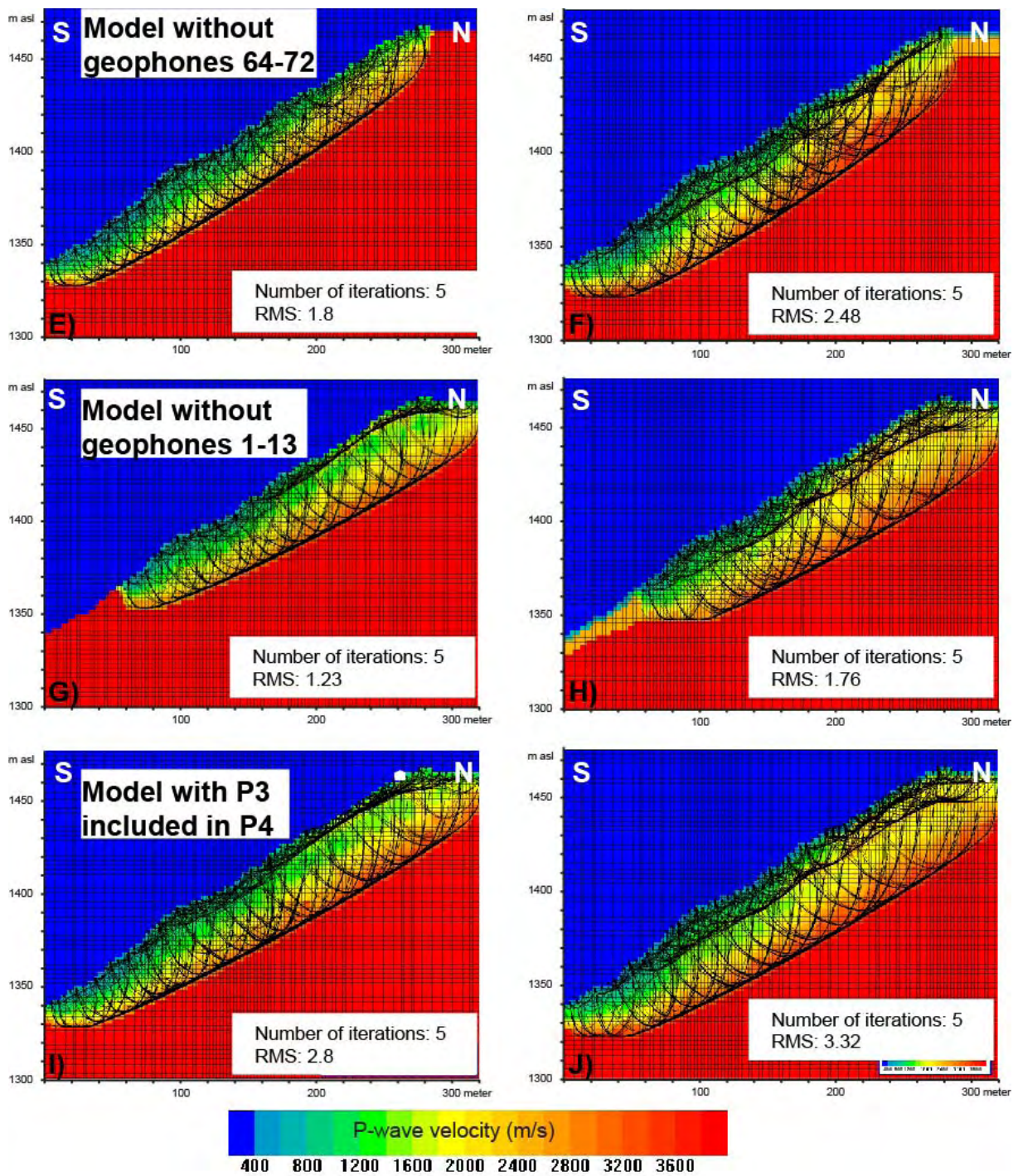
Figure 6.16: *Final seismic refraction tomography models of the long profile P4. Top: Model without geophones 64-72 because of inverse topography. Middle: Model without geophones 1-13 because of velocity decrease in the travel-time versus distance diagram. Velocities bigger than 3000 m/s are due to the initial model and are beyond the penetration depth and should therefore be neglected.*

- C and D:L The data of all geophones of P4 were used.

- E and F: At geophones GP 65 - GP 72 of the long profile P4, the topography is inversed. Therefore, these last 8 geophones were neglected for a second inversion model, to test the effect of the inversed topography.

- G and H: The travel-time diagrams of P4 show a negative velocity recorded at geophones GP 1 - GP 13. This is not realistic if it is assumed that the velocity decreases with depth (see Figure 6.12). These geophones were therefore neglected for a third model.

- I and J: A last model was made where the database from profile P3 was included in the database of P4 .

The penetration depth using the homogeneous initial model (C) is about 50 m. Using the 3-layer initial model (D) it is slightly more. For the models where geophones were neglected, it is less. The refractors of the 3-layer models are clearly influenced by the initial model and therefore probably less meaningful than in the case of the homogeneous initial model. The homogeneous models C, E, G and I show a first refractor which is similar for all profiles. This refractor is located deeper in the lower part of the landslide than in the upper part. At an altitude of 1450 m it is less than 3 m deep. In profile E, where the 8 uppermost geophones are neglected, this shallow reflector is absent. Nevertheless, on all other profiles it can be observed. The top refractor can be seen best on models C and I.

In C and I, the first layer with a velocity smaller 1000 m/s is very thin or absent in the upper part of the landslide and becomes up to 14 m thick towards the toe of the landslide. The resolution of P4 was probably not good enough to record this low velocity layer also in the upper part of the profile (see previous section). In the short profiles P1 and P3, we can observe the thin low velocity layer also in the upper part of the landslide. The first refractor is interpreted as bedrock and main landslide slip surface. In the upper part of the landslide, the bedrock is only a few meters below the surface, most likely because the cover of unconsolidated sediment has already slid downwards. In the lower part of the landslide, the bedrock surface is deeper. This section is interpreted as accumulation zone of the landslide and of ancient mass movements.

6.5.3 Summary seismic refraction

- The seismic refraction tomography shows distinct refractors which are interpreted as the surface of the bedrock. Most likely, this surface corresponds to the main slip surface of the landslide. Using a homogeneous initial model of 4000 m/s, this first layer is thicker in the lower part of the landslide.

- The final velocity model depends on the initial model. The refractors are strongly linked to the velocity-boundaries which are implied by the initial model. The RMS is always better for the homogeneous initial model.

- It is difficult to make a realistic initial model, because the geology in the area of the Pont Bourquin landslide is not only heterogeneous with depth, but also laterally. Therefore, most reliable results are obtained with the homogeneous initial model, which confirms the observations made by Demanet (2000).

- The travel-time diagrams show variations along the slope which reflects lateral changes in the lithology.

- If we compare the short profiles P1 and P3 with the long profile P4, we can see that on the one hand the resolution of the long profile is not good enough to represent the topmost thin low velocity layer. On the other hand, the penetration depth of the short profiles is not deep enough to reach bedrock with high velocities of 4000 m/s.

6.6   Electric resistivity tomography (ERT)

On the Pont Bourquin landslide, five short and one long ERT profiles were recorded with a Syscal R1 Plus device, using 48 and 72 electrodes respectively (see Table 6.4 for profile details and Figure 6.11 for profile locations). Electrode spacing was 1.5 and 2 m for the transversal short profiles, 3 m for the longitudinal short profile and 5 m for the 355 m longitudinal long profile. The Wenner-Schlumberger and the Schlumberger-VES method were chosen for the long and the short profiles, respectively. See Section 4.3 for descriptions of the methods.

Profil name	Number of electrodes	Spacing, m	Horizontal length, m	Orientation	Electrode configuration (Array)
E1	48	2	92	W-E	Sch-VES
E2	48	2	92	W-E	Sch-VES
E3	48	3	131	W-E	Sch-VES
E4	48	2	92	W-E	Sch-VES
E5	72	5	324	S-N	W-Sch
E6	64	1.5		W-E	W-Sch

Table 6.4: *Characteristics of the performed ERT profiles. Sch-VES: Schlumberger-Vertical electrical sounding, W-Sch: Wenner-Schlumberger.*

On Figure 6.17, the longitudinal ERT profile E5 is displayed. The absolute error of the profile after 11 iterations is 1.4. A low resistivity top layer with < 100 Ωm which is up to 10 m deep and gets thinner towards the top of the slope is observed. Below this layer, several units which are dipping into the slope are distinguished. These are from bottom to top: A unit of 500 Ωm with a high resistivity block of >3000 Ωm close to the top, a unit of 2500 Ωm, a unit of 500 Ωm, a unit of very low resistivity around 100 Ωm, and again a unit of 500 Ωm.

The 5 short profiles are displayed on Figure 6.18. 6 to 9 iterations were performed and absolute error between 1.4 and 2.1 was obtained. Higher resistivity around 500 Ωm are observed in the western part of the transversal profiles from the head scarp area E1, E2 and E4, in the the upper part of E3, and in the lower part of E6. Two different surface layers can be distinguished: a low resistivity layer (10 - 80 Ωm) and an irregular high resistivity layer (200 - up to several 1000 Ωm). Further, a deep low resistivity unit (70-100 Ωm) can be observed in the middle/eastern part of E1 and E2 and in the lower part of E3. An intermediate low resistivity layer in less than 5 m depth is seen in the eastern part of profile E1 and E4.

The low resistivity top layer observed in all profiles except E4 is interpreted as the landslide. It becomes thinner toward the top of the slope and disappears below the chalet. The bedrock below the landslide can be divided in different lithologies (see Figure 6.19). The high resistivity block at the bottom of the profile is interpreted as cellular dolomite associated with gypsum. The middle part with resistivity between 400 and 2000 Ωm could be Flysch or again cellular dolomite associated with gypsum. The low resistivity area in the upper part of the landslide is interpreted as shale lithology, overlaid by high resistive cellular dolomite. The lithological boundaries dip steep into the slope with about 45°. The high resistivity areas in the western part of E1, E2 and
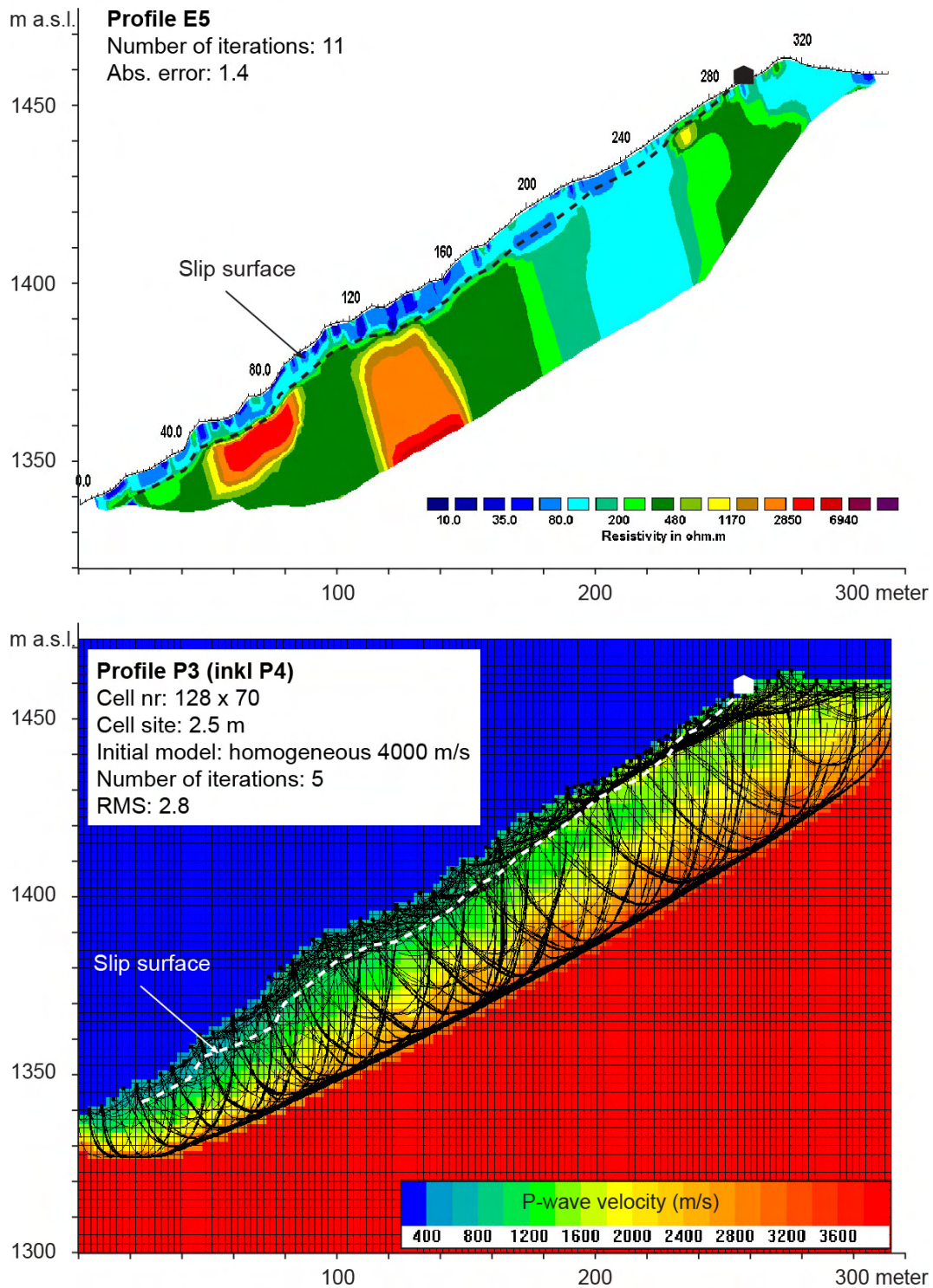
Figure 6.17: *ERT profile E5 recorded along the Pont Bourquin landslide compared with seimic reraction profile P4 from the same location. The slip surface observed in both profiles coincides well.*
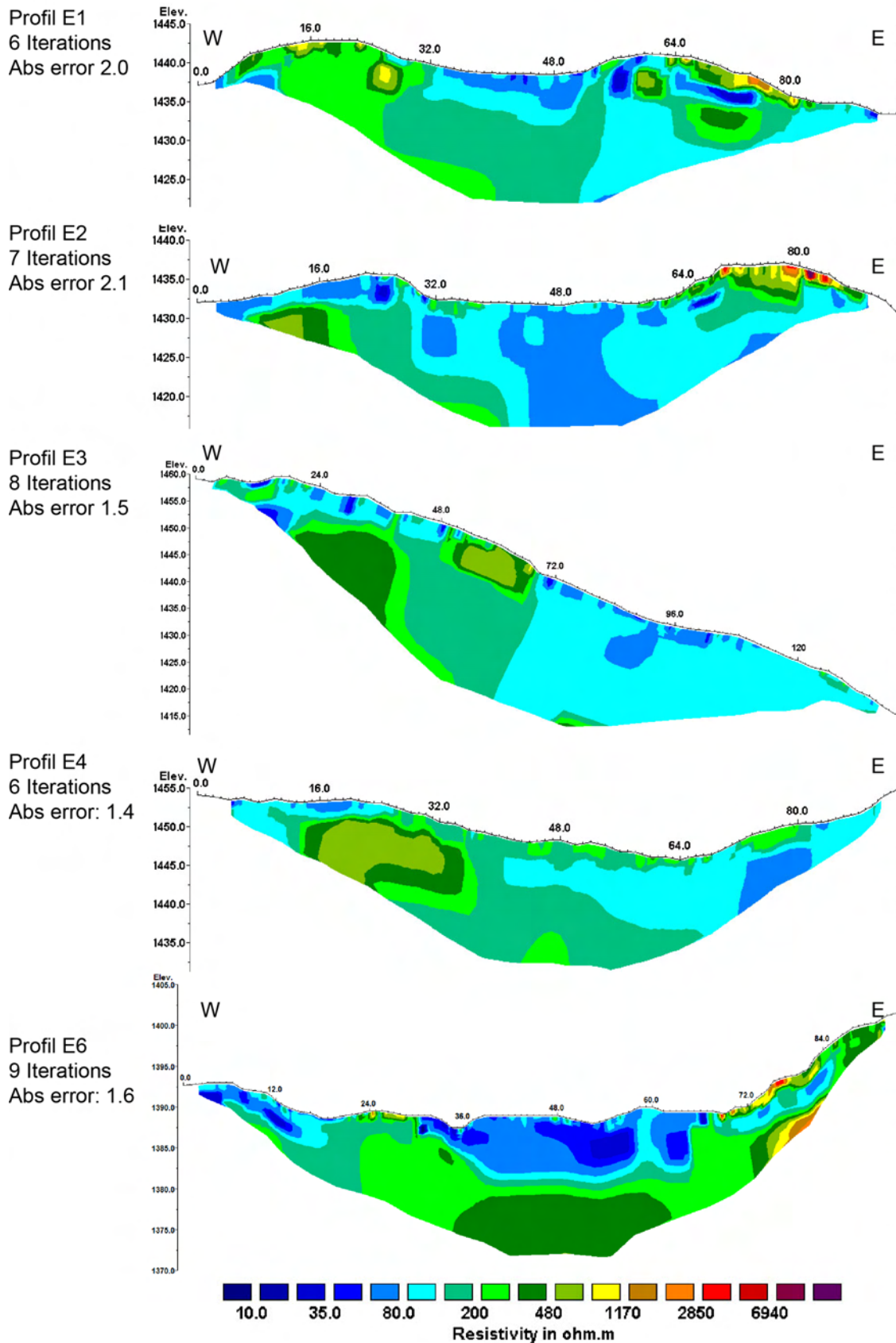
Figure 6.18: *Short ERT profiles across (E1, E2, E4, E5) and along (E3) the Pont Bourquin landslide.*

E4 most likely are cellular dolomite overlaid by saturated moraine. In the middle part of E1 and E2 black shale is overlaid by the landslide. In the western part it is overlaid by moraine. The boundary between black shale and cornieule can also be seen in the middle on profile E3. Profile E6 shows the landslide mass in the middle overlaying Flysch or cellular dolomite rock. In this area, the landslide is much thicker due to the accumulation of debris.
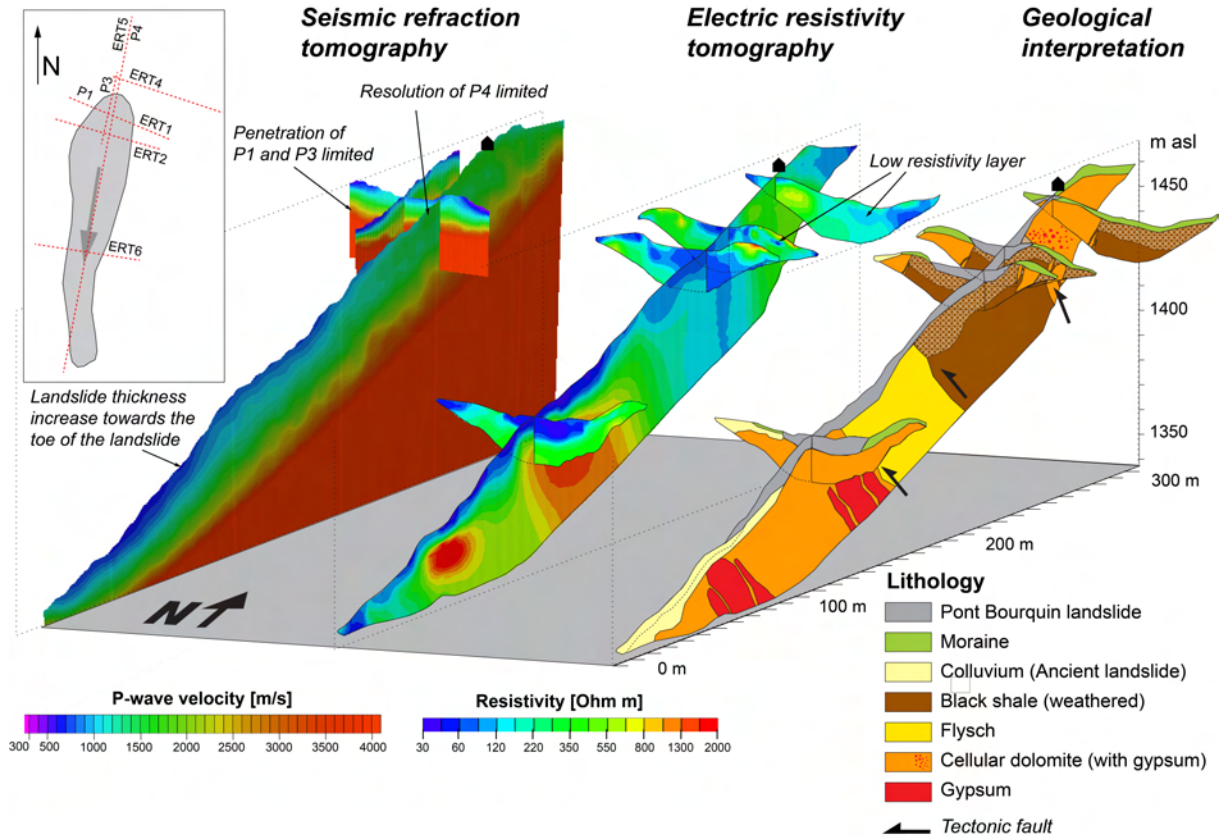
Figure 6.19: *Geological interpretation of the geophysical profiles.*

6.6.1   Summary ERT and comparison with seismic tomography

The best results were obtained with the robust inversion method. With the ERT profiles three important information about the Pont Bourquin landslide were obtained:

- The low resistivity top layer most likely represents the landslide (see Figure 6.19). It is up to 14 m deep, the average depth is less than 10 m and it becomes thinner towards the top of the slope. The slip surface detected in the seismic refraction and ERT are consistent.

- The bedrock below the landslide is divided in different lithologies: The high resistivity areas in the lower part of the landslide and at the top west of the landslide is interpreted as cellular dolomite (associated with gypsum), the low resistivity area in the upper and eastern part is the black shale formation and the high resistivity area in the middle could correspond to Flysch.

- A last feature are the intermediate low resistivity layers in the east of the landslide. The low resistivity of these layers could indicate saturation of either moraine or fractured black shale bedrock. The second explanation seems more likely because of the depth of these layers (see Figure 6.19).

- The combination of the two methods was very useful. It confirmed the observation of the slip surface. In the upper part of the landslide, where the bedrock has the same resistivity as the landslide, the seismic profile was very useful to trace the slip surface. In contrast to the seismic profiles, the resistivity profiles show more details, vertical structures and variations in the bedrock lithologies.

6.7 Observation wells

In June 2009, three observation wells (PB1, PB5, 1D) were drilled on the Pont Bourquin landslide with a Tripod Hammer rig and a Geotool GTR crawler drilling rig. A depth between 5 and 9 meters was reached. Additionally, 13 wells with a diameter of 5 - 7 cm and depth between 1 and 2.2 m were drilled by hand auger. All observation wells and their depth are listed in Table 6.5. The profiles are shown on Figure 6.20 and the location is shown on Figures 6.25.

PVC tubes, slotted for 0.5 - 1 m at the bottom, were installed in all bore holes. Disturbed samples were described in MR1D and MR5. Beside the drill holes Ch1/Ch2, 1A, 1B, 1C and 5A, five dynamic penetration test were performed (see Section 4.7 for the method). Cone diameters of 2 and 4 cm were used. The groundwater level was measured periodically in all observation wells from June 2009 - August 2011. Schlumberger water pressure sensors with acquisition interval of 30 min were installed in four piezometers for continuous monitoring (see Table 6.5). Barometric sensors were installed in borehole PB5 and Ch2 in order to correct the piezometric measurements for air pressure.

Name	Depth	Pressure sensor
Chalet2 (Ch2)	1.13	x
Chalet1 (Ch1)	1.22	
PB1A	1.45	
PB1B	2.23	
PB1C	1.84	x
PB1D	2.09	
PB1E	1.73	x
PB5A	1.2	
PB1 (Inclinometer)	4.65	
PB5 (Inclinometer)	4.1 (9.1)	x
PB25	1	
PB34	1	
PB36	1.6	
PB39	1	
PB45A	2	
PB45B	1	

***Table 6.5:** List of piezometers on the Pont Bourquin landslide with depth and installed pore water pressure sensors.*

6.7.1 Core descriptions

Core PB1D

In the upper 0.5 m of the drilled core 1D, silty clay with organic material was found, followed by nearly saturated grey clay with fragments of black schist. From 2.5 to 5 m, schist with calcite
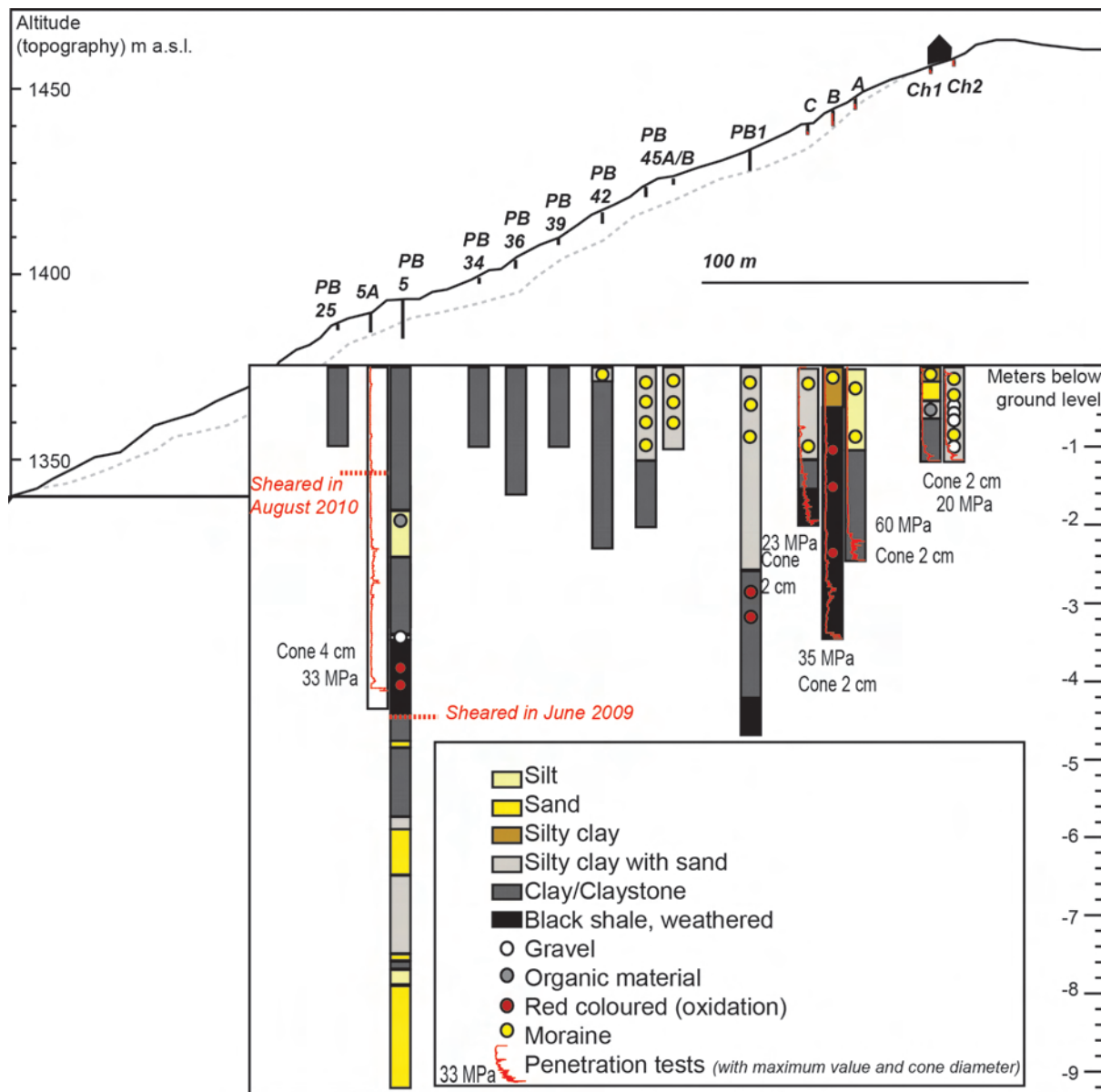
Figure 6.20: *Profile with the lithological data from drill holes and 5 penetration tests performed in the framework of the Mountain Risks summer school 2009. The vertical scale for the drill hole depth is 1:20 referred to the topography.*

lenses and orange coloured oxidized layers were found.

This material was interpreted as weathered and heavily fractured black shale bedrock from the Aalenian formation that was incorporated in the landslide.

Core PB5

In core PB5, no soil layer was found. The upper 2 meters were fine grained schist with downwards increasing water content. At 2 m depth, a 20 cm thick brownish silt layer that contained organic material was found. From 2 to 3.5 m silty clay with rock fragments and fractured shale was found. This layer was partly saturated. Below, a coarse-grained more competent layer followed which contained fragments of grey shale. This section was unsaturated but reddish colouring from oxidation gave sign of water circulation. At 4.5 - 8 m depth, less competent grey clay with little fragments of shale was found, interbedded with reddish sandy layers at 4.7, 6 and 7.5 m depth. In 8 - 9 m depth, reddish to brown partly saturated sand with fragments of calcite was found. During drilling, artesian water was observed.

This profile can be interpreted as a succession of moraine material (clay matrix, sandy layers, fragments of shale) and sections of weathered black shale rock (e.g. from 3.5 to 4.5 m depth), representing the mass movement deposits. Several internal slip surfaces were observed. The PVC tube was sheared after 4 days of installation in a depth of 4.1 m. Piezometer 5A, which is located next to PB5, was sheared in August 2010 at a depth of 1 m.

6.7.2 Results of penetration tests

Penetration tests Ch1/Ch2 showed a more competent layer at about 1.3 m depth and penetration test 1A at about 2 m depth. 1B and 5A showed an increasing resistance (20 MPa) in 2.5 to 3 m depth followed by a softer layer, before a very competent layer was reached at 3.5 and 4.5 m depth, respectively. Profile 1C showed a rather continuous increase in resistance with depth.

The higher resistive sections in profile 1B and 5A could represent boulders of weathered shale in the clayey moraine matrix. The lower limit of the profiles (20-30 MPa) at depth between 1 to 4.5 m could either represent large boulders in the moraine or the transition to the weathered bedrock.

6.7.3 Groundwater level monitoring

Figure 6.21 shows the observation wells installed on the Pont Bourquin landslide with high and low groundwater level and the locations of the pressure sensors. Figure 6.22 shows the data of all pressure sensors installed in the piezometers corrected for barometric pressure. The 4 of July 2010, the water was removed of the wells to take samples and to perform pumping tests (see Section 4.9 for the method). Figure 6.23 shows the groundwater level fluctuations, temperature and electric water conductivity values measured in PB5 for the period February 2010 - August 2011. The following observations and interpretations were made:

- The measured mean annual groundwater table in the upper part of the landslide was about 1 m and in the lower part about 2 m below ground surface. These are local perched water levels which form due to heterogeneities in the permeability of the landslide mass.

- Piezometer 5A, 1B, 1D, PB45B and PB36 were always dry when measured manually. This could be because the piezometers were not installed correctly and they clogged after installing or because the groundwater level is below the piezometer.

Figure 6.21: *Profile with the piezometers installed on the Pont Bourquin landslide. High and low stand groundwater level is displayed for each drill hole. Piezometers 1B, 1D, 5A and PB36 remained always dry. The depth of the piezometers is exaggerated 1:20. Piezometer A and B are located outside of the landslide. See Figure 6.25 for the location of the piezometer.*
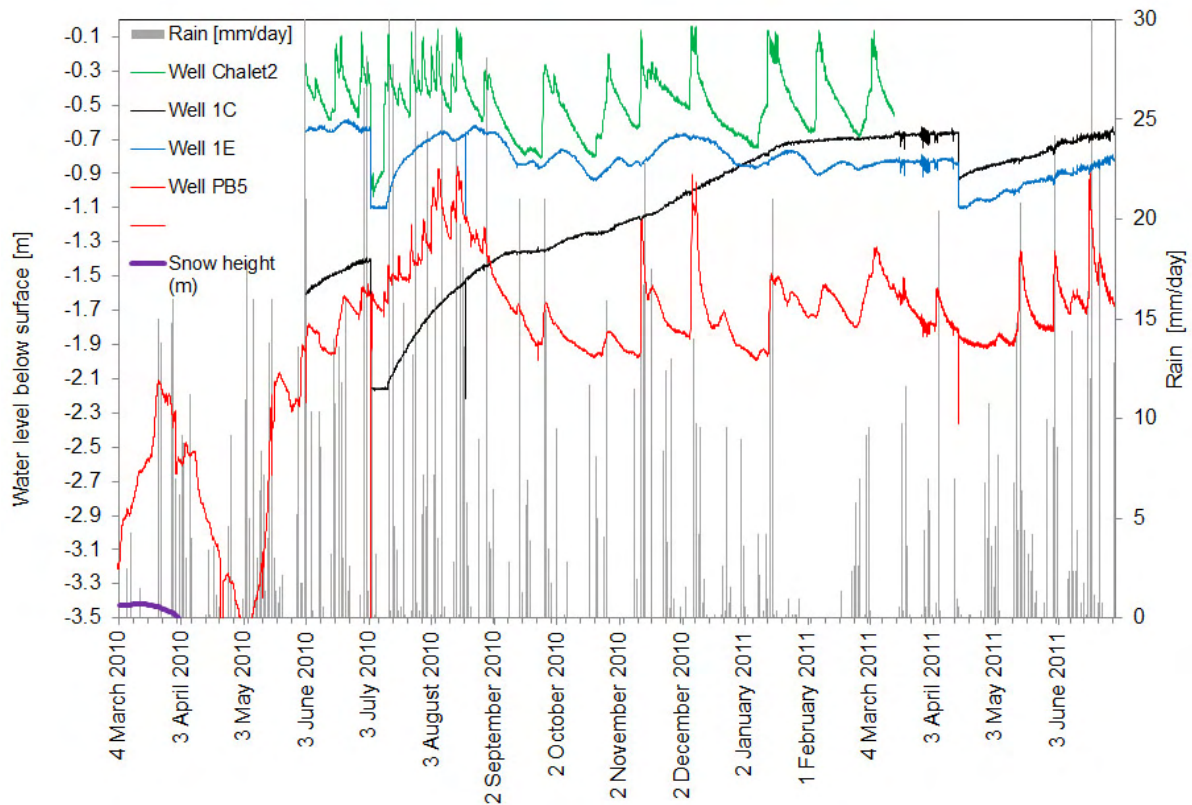
Figure 6.22: *Precipitation data and groundwater level measured in the observation wells Ch2, 1E, 1C and PB5.*

- The water level in piezometer Ch2 rose immediately after rainfall events. This is because by-pass occurred along the piezometric tube. The falling limb of the groundwater level curve was used to calculate the permeability of the moraine (see next section).

- Piezometer C showed a smoothed reaction to rainfall events. After pumping, the water table only established very slowly. This indicates the low permeability of the moraine.

- The groundwater level in piezometer E was constantly rising except two drops due to pumping. The rain events cannot be seen in this groundwater curve. In winter 2011, a constant level of 0.8 m below ground surface was reached. The slow filling of piezometer E shows the low permeability of the moraine.

- The reaction time of the groundwater table to rainfall events in PB5 changed over time. During rainy weeks around 1 and 16 June the signal arrived with a delay of several days, whereas after 29 June 2010, a sudden groundwater level rise of several cm was recorded during rain events. During the summer and autumn 2010, piezometer PB5 showed a similar behaviour like Ch1: rapid rise after rainfall followed by slowly dropping. During winter 2011, the reaction of the water pressure after rainfall was again smoothed. These variations of the reaction time are related to changes in the permeability caused by the movement of the landslide. In the proximity of PB5, numerous extension cracks were observed which could be responsible for by-pass during summer and autumn 2010.

- The value of the electrical water conductivity measured in PB5 decreased during rain events. With a delay of 2-3 days it rose 100 - 300μS/cm (see Figure 6.23). The initial decrease is interpreted as dilution with rapid infiltrating meteoric water through fractures.

The delayed increase is interpreted as arrival of pre-event water by piston flow mechanism. Such a dual porosity was also observed on the La Clapière (Guglielmi et al., 2002) and the Super-Sauze landslide (De Montety et al., 2007).
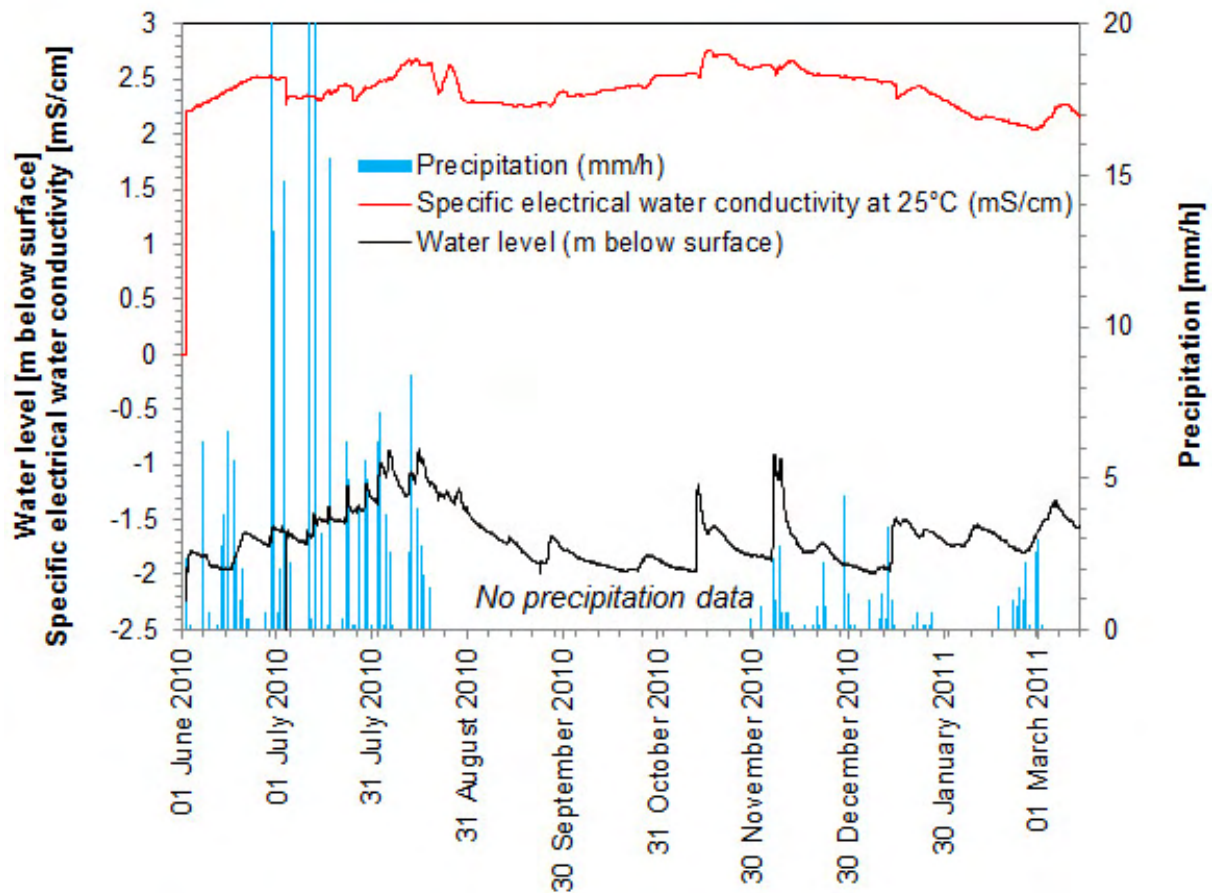
Figure 6.23: *Precipitation data and groundwater level, temperature, and electrical conductivity measured in observation well PB5.*

An inverse correlation between the water pressure and the air pressure, which would indicate perched water tables, could not been observed. To summarise the observations made in the wells on the Pont Bourquin landslide it can be said that a dual porosity was observed: the morainic landslide material has a very small permeability, but due to fractures and extension cracks, meteoric water can infiltrate rapidly. In the following, some measured values for the hydraulic conductivity at different locations are shown.

6.7.4 Hydraulic conductivity

Saturated infiltration tests (Guelph Penetrometer and the Inverse Auger hole tests) were carried out at wells Ch1, 1A, 1B, 1C, 5A. The Guelph test was carried out in the upper half meter of the soil profile in boreholes of 5 - 7 cm of diameter. The inverse-auger hole tests were performed in holes less than 0.5 m deep with a diameter of 5 cm.

Additionally, the curves of the rising water table after pumping in piezometer 1C, 1E, Ch1 and PB5 and the falling head curve after rainfall events in piezometer Ch1 and PB5 were analysed with the Lefranc and inveres-auger hole method, respectively (see Section 4.9 for the method).

Piezometer	Date	Depth, m	Method	k-value (m/s)
Ch2	2.6.2009	0 - 0.5	Inverse-auger hole, K-O	$7 \cdot 10^{-8}$
Ch2	2.6.2009	0.2 - 1.1	Guelph, H=5cm	$5 \cdot 10^{-10}$
Ch2	4.7.2010	0.8 - 1.1	Lefranc (slug test)	$5 \cdot 10^{-8}$
Ch2	6.8.2010	0.3 - 1.1	Natural Inverse-auger hole, K-O	$3 \cdot 10^{-8}$
1A	2.6.2009	0 - 0.5	Inverse-auger hole, K-O	$2 \cdot 10^{-6}$
1A	2.6.2009	0.2 - 1.5	Guelph, H=5cm	$3 \cdot 10^{-7}$
1B	2.6.2009	0.2 - 2.2	Guelph, H=5cm	$1 \cdot 10^{-10}$
1B	2.6.2009	0.2 - 2.2	Guelph, H=5cm	drained immediately
1C	2.6.2009	0 - 0.5	Inverse-auger hole, K-O	$1 \cdot 10^{-6}$
1C	2.6.2009	0.2 - 1.8	Guelph, H=5cm	$1 \cdot 10^{-9}$
1C	2.6.2009	0.2 - 1.8	Guelph, H=10cm	$7 \cdot 10^{-8}$
1C	4.7.2010	1.4 - 1.8	Lefranc (slug test)	$1 \cdot 10^{-9}$
1E	4.7.2010	0.7 - 1.7	Lefranc (slug test)	$7 \cdot 10^{-9}$
5A	2.6.2009	0 - 0.5	Inverse-auger hole, K-O	$4 \cdot 10^{-5}$
5A	2.6.2009	0 - 0.5	Inverse-auger hole, K-O	drained immediately
5A	2.6.2009	0.2 - 1.2	Guelph, H=5cm	$3 \cdot 10^{-8}$
5A	2.6.2009	0.2 - 1.2	Guelph, H=10cm	$5 \cdot 10^{-7}$
PB5	2.6.2010	1.8 - 4.1	Lefranc (slug test)	$8 \cdot 10^{-8}$
PB5	4.7.2010	1.6 - 4.1	Lefranc (slug test)	$1 \cdot 10^{-7}$
PB5	24.7.2010	1.4 - 4.1	Natural Inverse-auger hole, K-O	$1 \cdot 10^{-7}$
PB5	6.8.2010	1.1 - 4.1	Natural Inverse-auger hole, K-O	$1 \cdot 10^{-8}$

Table 6.6: *Table with the calculated values for saturated hydraulic conductivity (K-O = Kessler-Oosterbaan).*

Table 6.6 shows the calculated hydraulic conductivity values.

The calculated saturated permeability values range between 10^{-6} and 10^{-10} m/s. The upper soil is higher permeable than the moraine and weathered black shale (clayey silt and silty clay) in 1 - 4 m depth. The low permeability of the landslide material explains the pounding water on the landslide.

At location B1 and 5A, the water drained immediately. This high permeability was explained by extensional cracks in the landslide mass which quickly drained the water.

6.8 Precipitation

From November to December 2010 an electric tipping-bucket pluviometer and from April 2010 until today a *Davis Pro* meteorological station were installed a few meters above the head scarp of the landslide (see Figure 6.25 for the location). During the missing measuring periods, the daily precipitation recorded from the MeteoSchweiz station in les Diablerets village (Swiss coordinates 577990/133590, 1162 m a.s.l.) was used (uncorrected for difference in altitude). Figure 6.24 shows the precipitation data measured in the year 2010 compared with data from 2000-2009.

Mean annual precipitation was 1500 mm. A mean annual evapotranspiration of 500 mm was measured with the Davis Pro meteorological station. This coincides with the values from the Atlas of Switzerland 2.0 (©2004 Swisstopo).
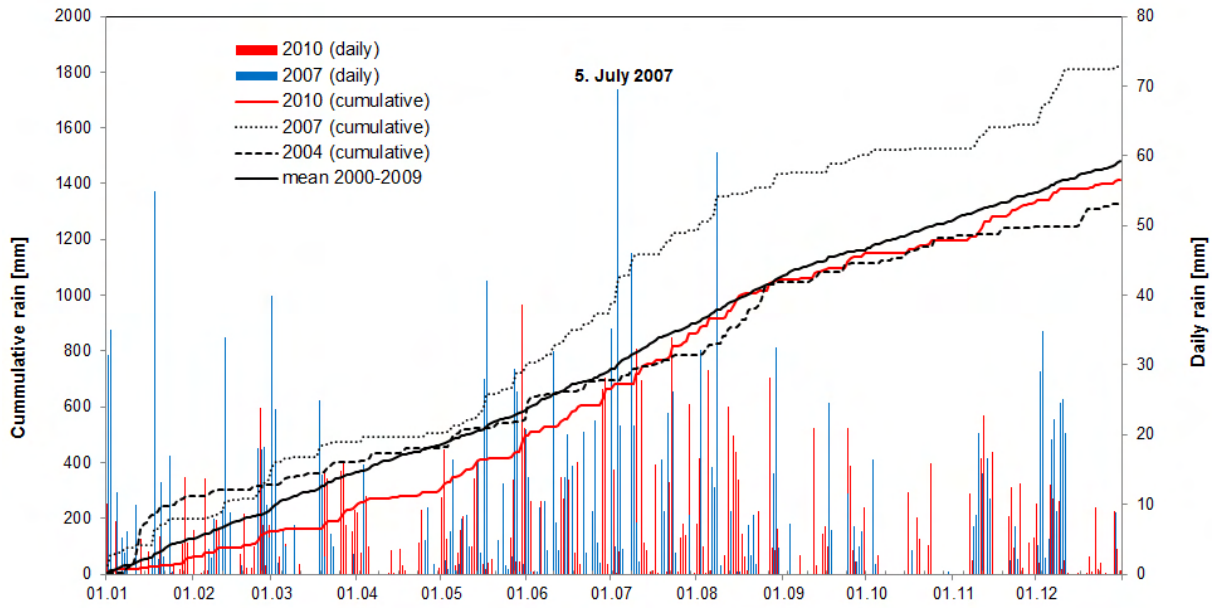
Figure 6.24: *Cumulative and daily precipitation at Les Diablerets. The mean value between 2000 and 2100 was calculated from the MeteoSchweiz station DIB 7940. On 5 July 2007, an earth flow was triggered on the Pont Bourquin landslide.*

6.9 Springs

Several springs were observed on the Pont Bourquin landslide (see Figure 6.26). They were named according to their position along the geophysical profiles ERT5 and P4 (Figure 6.11). Their flux Q was measured and estimated during two years from summer 2009 to summer 2011. The values for the flux reported on Figure 6.26 are mean annual estimates. Based on these fluxes, the infiltration rate and the infiltration coefficient were calculated with Equations 6.1 and 6.2 (derived from the hydrological equation 4.6, see Section 4.10).

$$I = (P - ET) - R \tag{6.1}$$

$$C_i = \frac{Output}{Input} = \frac{Qt}{(P - ET)A} \tag{6.2}$$

I: Infiltration rate [mm/year]
P: Precipitation, 1500 mm/year
ET: Evapotranspiration, 500 mm/year
R: Run-off rate (flux measured at springs at the outlet of each catchment) [mm/year]
C_i: Infiltration coefficient
Q: Flux measured at springs at the outlet of each catchment [l/min]
t: time, 1 year
A: Surface of the catchment

The aim of those calculations was to estimate the loss of water into the underground or additional water exfiltrating from the underground into the landslide. This was made for three topographic catchments in order to compare different zones of the landslide (the catchments are shown on Figure 6.25). The three catchments are:
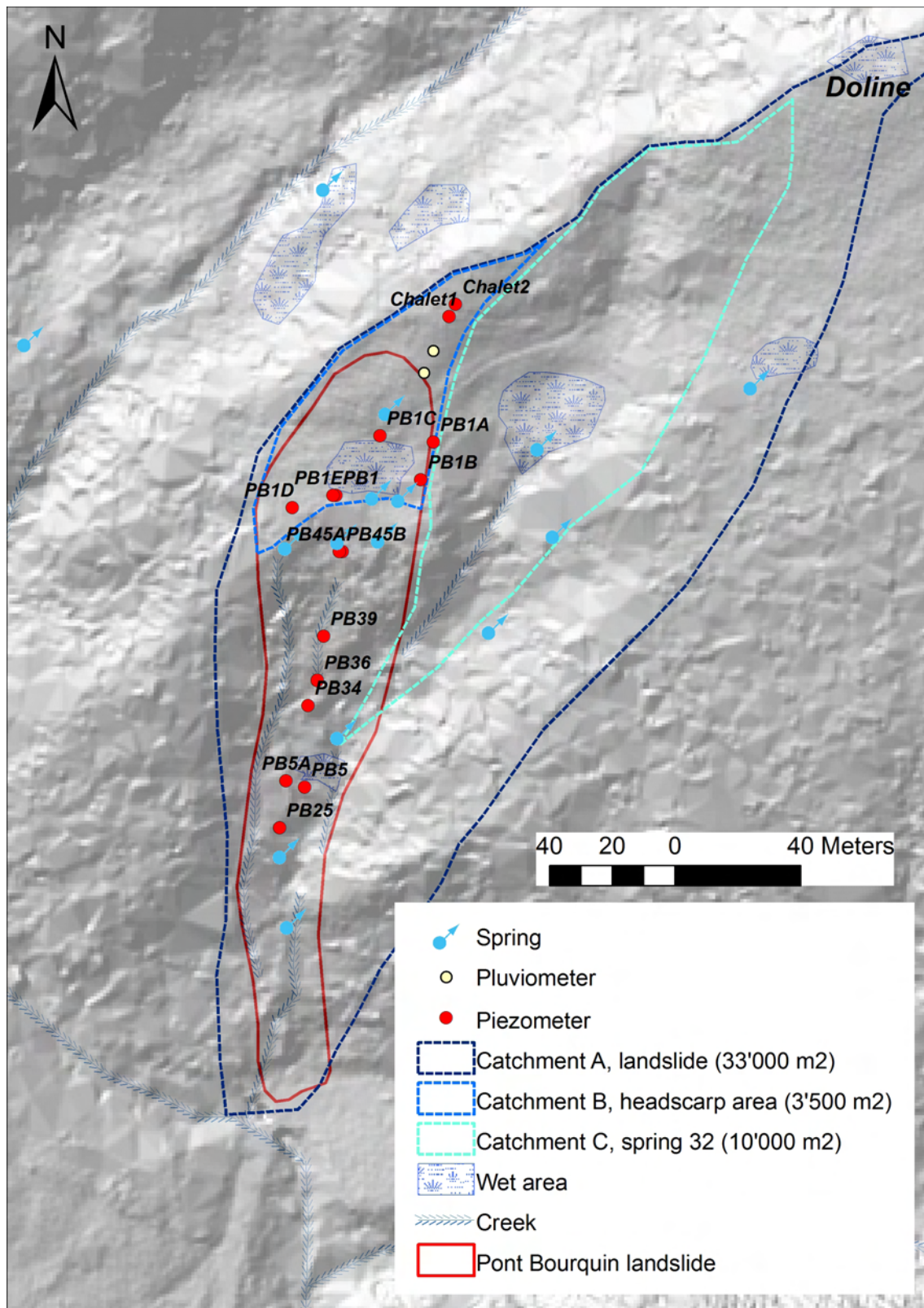
Figure 6.25: *Hydrological map of the Pont Bourquin landslide and the surrounding area. Springs, creeks, wet zones and piezometers are shown as well as the locations of the installed meteorological station and the pluviometer, the catchment for the landslide (A) and two sub catchments of the head scarp area (B) and of Spring 32 (C).*
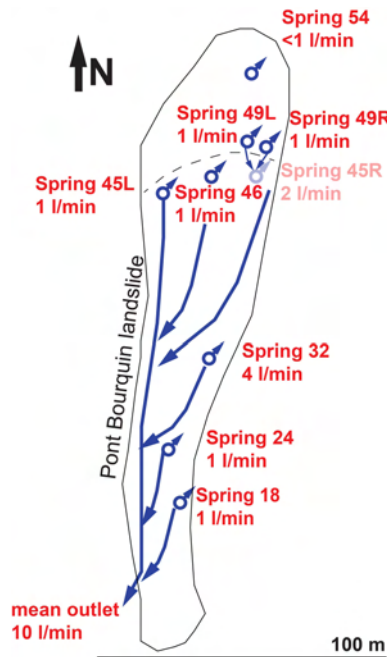
Figure 6.26: *Map showing the springs on the Pont Bourquin landslide and the mean flux. The flux of spring 45R is composed of the flux from springs 49L and 49R that infiltrates and re-exfiltrates and is therefore not taken into account for the balance.*

- Catchment of the Pont Bourquin landslide (A): During dry periods, a flux of 3-10 l/min was measured at the outlet of the catchment, whereas during rain events, it was estimated to be higher than 10 l/min. As a mean annual value, 10 l/min were estimated.

- Catchment of the swampy head scarp area where several springs were observed (B): A mean flux of 2-4 l/min has been measured at springs at the edge of the head scarp area. Thus almost half of the water running of the Pont Bourquin landslide originates in this rather small area.

- Catchment of spring 32 (C): The flux of spring 32 was measured with a weir. In summer 2010, a flux between 3 and 8 l/min was measured during dry and wet periods. A mean annual value of 4 l/min was estimated.

Table 6.7 shows the calculated values for the infiltration rate and the infiltration coefficient.

Catchment	A, m^2	Q, l/min	R, m/y	I, m/y	$Q\,t$, m^3	$(P\text{-}ET)\,A$, m^3	C_i
A	33'000	10	0.16	0.84	5'256	33'000	0.16
B	3'500	4	0.60	0.40	2'102	3'500	0.60
C	10'000	4	0.21	0.79	2'102	10'000	0.21

Table 6.7: *Table showing the infiltration rate I and the infiltration coefficient C_i for the three topographic catchments A, B and C. P-ET was assumed to be 1 m/year.*

The infiltration and infiltration coefficient give information, if

- groundwater is flowing into the system, for example from an aquifer in the hydrogeological catchment that is larger than the hydrological catchment. If I is small or negative and C_i is about 1 or larger, then groundwater is flowing into the system (in addition to precipitation).

- water is flowing out of the system, for example infiltrates into the bedrock.

An infiltration rate of about 0.8 m^3/(m^{2}a) has been calculated for the catchments A and C of the Pont Bourquin landslide as well as Spring 32, whereas the calculated infiltration rate for the head scarp area B is about half of that. This could be because in this area, the top soil is less permeable and less water infiltrates. It is also possible that comparing to catchment A, area B has an additional input. It is possible that groundwater is flowing into the head scarp area of the Pont Bourquin landslide through the underground from a hydrogeological catchment which is larger than the surface catchment. If it is assumed that the infiltration in catchment B is equal to A and C, then the rate of the additional input would be 0.4 m/y. It is possible that the run-off was underestimated for all three catchments.

6.9.1 Hydrograph of spring 32

The spring 32 has been trapped in a weir during two periods: 28 July - 14 August 2010 and since 15 Mars 2011. The spring was caught in a tube which conducted the water into a 1 m x 0.5 m x 0.5 m large box equipped with a *Schlumberger CDT diver* to measure the electric conductivity (EC) and water temperature and a *Schlumberger micro diver sensor* to measure the water pressure. The flux of the spring was calculated based on the water pressure and manual point measurements of the flux. The weir had to be completely rebuilt because it was destroyed in August 2010. Figures 6.27 and 6.28 show the curves of the rain intensity, specific EC (T$_{ref}$ 25°C) and calculated flux.
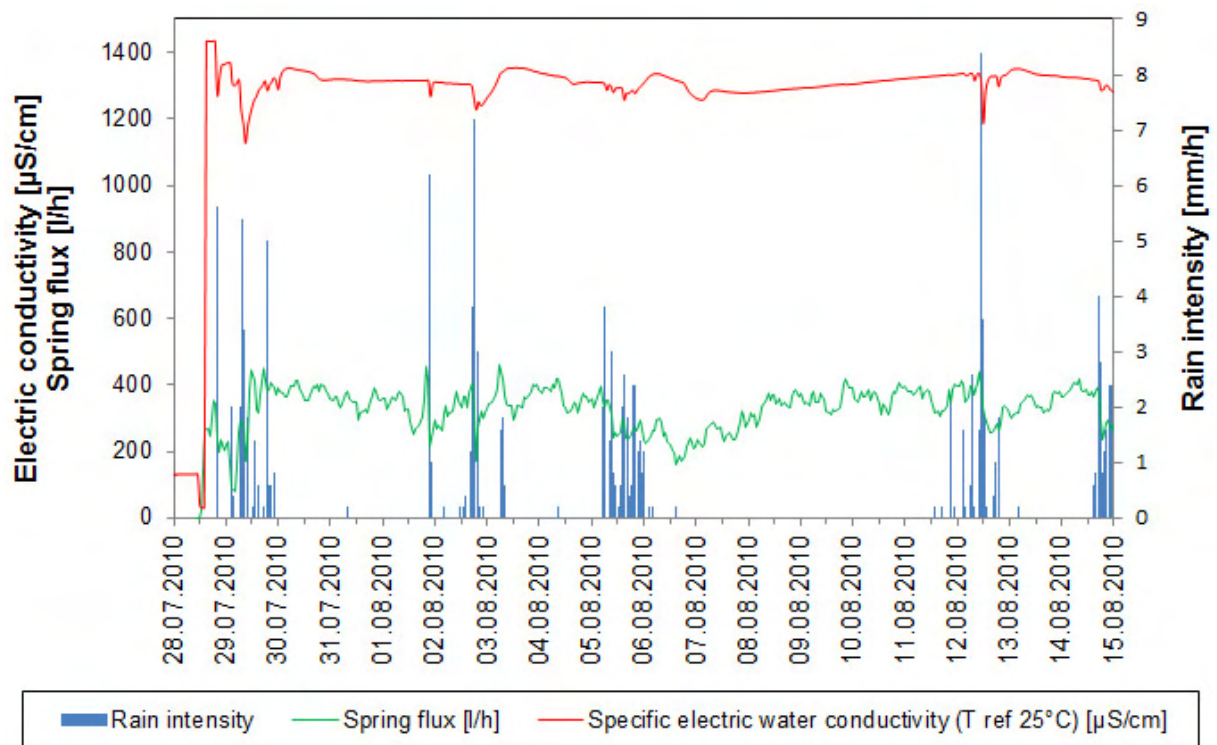
Figure 6.27: Rain intensity, EC and calculated flux from spring 32 measured in summer 2010.

Different features which are observed in the two curves are described and interpreted in the following:

- In summer 2010, the EC was around 1.3 mS/cm and in 2011 it was about 1.7 mS/cm.
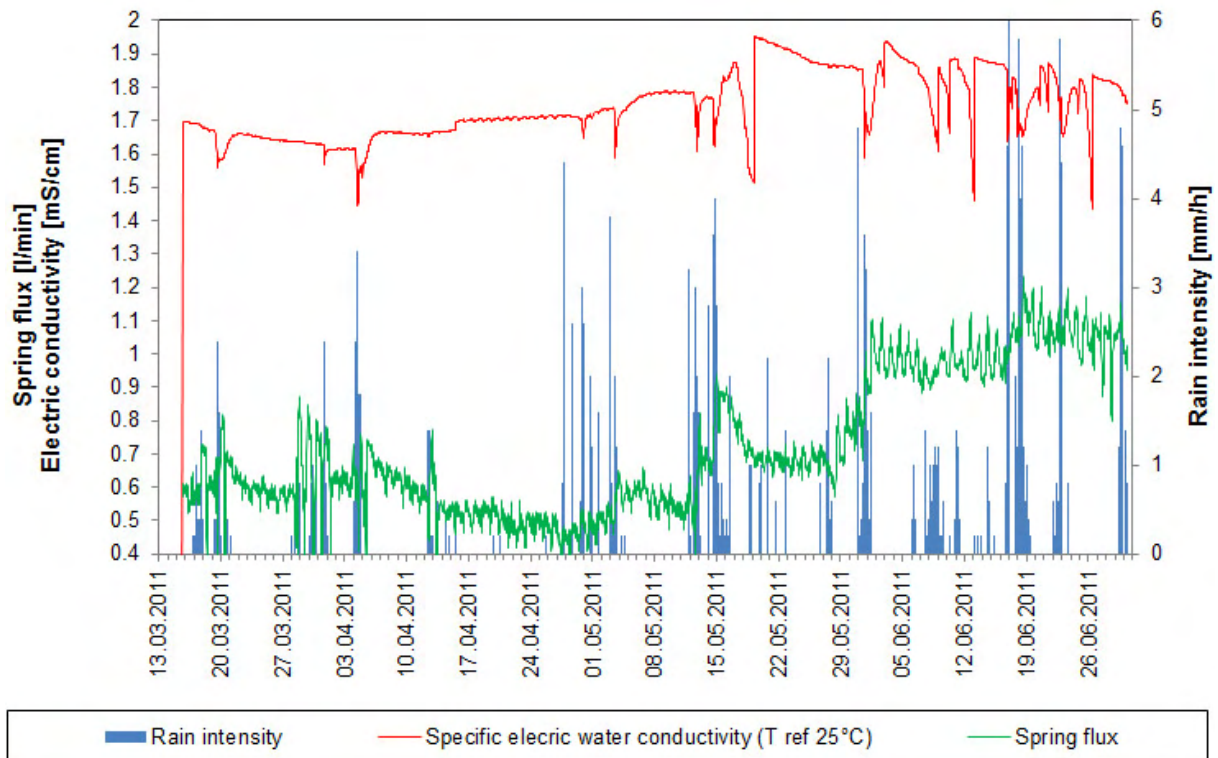
Figure 6.28: *Rain intensity, EC and calculated flux from spring 32 measured in spring and summer 2011.*

These are values for rather high mineralised water. The variations are more meaningful than the absolute values.

- In both periods, a rapid fall in EC can be observed at the begin of rainfall with an intensity > 5 mm/h in 2010 and > 2 mm/h in 2011. This shows the dilution with meteoric water as it was also observed in PB5.

- With a delay of 1-3 days, after the initiation of strong rain, the EC rose up for several 100 μS higher than the initial value. This indicates delayed piston flow like it was also observed in PB5. Mineralized groundwater was "pushed" by the infiltrating rain water and arrived a few days after the rain event at the spring. This could be water that was flowing in fractures of the landslide. On 19 May 2011, the EC was rising for 0.45 mS/cm to a value of nearly 2 mS/cm. This was extraordinary high. A hypothesis is that the aperture of fractures due to landslide activity released water which was more mineralized than usually.

- The flux in 2010 varies between 3 and 8 litres and in 2011 it varies between 0.5 and 1 litre. This is because the weir 2011 was built after superficial drainages were built by the canton of Vaud and it was not possible to trap the entire spring any more.

- The water flux shows daily fluctuations which are more pronounced during the summer months. These fluctuations could be related to evapotranspiration.

- After rain events, the flux in 2010 raised 4 l/min to a value of 8 l/min. But after the rain events 5, 12 and 15 August 2010, the measured flux seems to decrease. This could be artefacts due to tilting of the weir. In 2011, the flux was rising for 0.5 l/min after rain events, which is about 50%. The event from 15 May 2011 shows that after the flux had

reached the maximum value of 2 l/min, it was decreasing during 3 - 4 days. The piston flow arrived with a delay of 4 days after the flux had established a mean value of 0.7 l/min.

Spring 32 is perennial and shows a high mineralisation. Like in PB5, a dual porosity was observed. The fraction of rainwater can roughly be calculated with a "mixing model" with equations 6.3 and 6.4.

$$x_1 EC_{rain} + x_2 EC_{spring} = (x_1 + x_2) EC_{mix} \qquad (6.3)$$

$$x_1 = \frac{EC_{spring} - EC_{mix}}{EC_{spring} - EC_{rain}} \qquad (6.4)$$

x_1 = fraction rainwater
x_2 = fraction average spring water = 1 - x_1
$x_1 + x_2 = 1$
EC_{rain} = Electric conductivity of rain, $\approx 10 \mu S/cm$
EC_{spring} = Average electric conductivity of the spring water $[\mu S/cm]$
EC_{mix} = Electric conductivity measured during precipitation

If we assume that the rainwater has a EC of 10 $\mu S/cm$, then it contributes with an average flux of 8 - 9 % to the total measured discharge. Table 6.8 shows the calculated values.

Year	EC_{spring}, $\mu S/cm$	EC_{mix}, $\mu S/cm$	x_1, fraction rainwater
2010	1300	1200	0.08
2011	1700	1550	0.09

Table 6.8: *Table showing the mean values for the calculation of the fraction of rainwater in the spring water during precipitation events.*

To summarise, it can be said that the water from Spring 32 has two origins: Water that is rapidly flowing in fractures close to the surface and deeper groundwater which is strongly mineralized and arrives with a delay of a few days after a rain event.

6.10 Hydrogeochemistry

Water samples were taken from observation wells, springs and ephemeral creeks on and close to the Pont Bourquin landslide from summer 2009 until spring 2011. Water temperature and electrical conductivity (EC) of the water were measured in the field. For some samples, also the pH and the redox potential Eh were measured. The pH and Eh values shout be taken with caution because the sensors were not very stable. The concentration of major cations (Na^+, K^+, Mg^{2+} and Ca^{2+}) and major anions (F^-, Cl^-, $NO_3{}^-$, $SO_4{}^{2-}$ and $HCO_3{}^-$) from each sample and additionally the elements Si and Sr from selected samples were analysed at *Geolep, EPFL*. $\delta^{34}S$ isotopes were analysed at *Institute of Mineralogy and Geochemistry, University of Lausanne*. The results are listed in Tables B.2 and B.3 in Annexe B. The location of the samples are shown on Figure 6.29. For the description of the methods see Section 4.11 and 4.13.

6.10.1 Major ions

The balance between the anions and cations was 0.6% in average with a maximum of 3.6% at piezometer 1A. Thus, no analyses had to be rejected (see Section 4.11 for the method). The
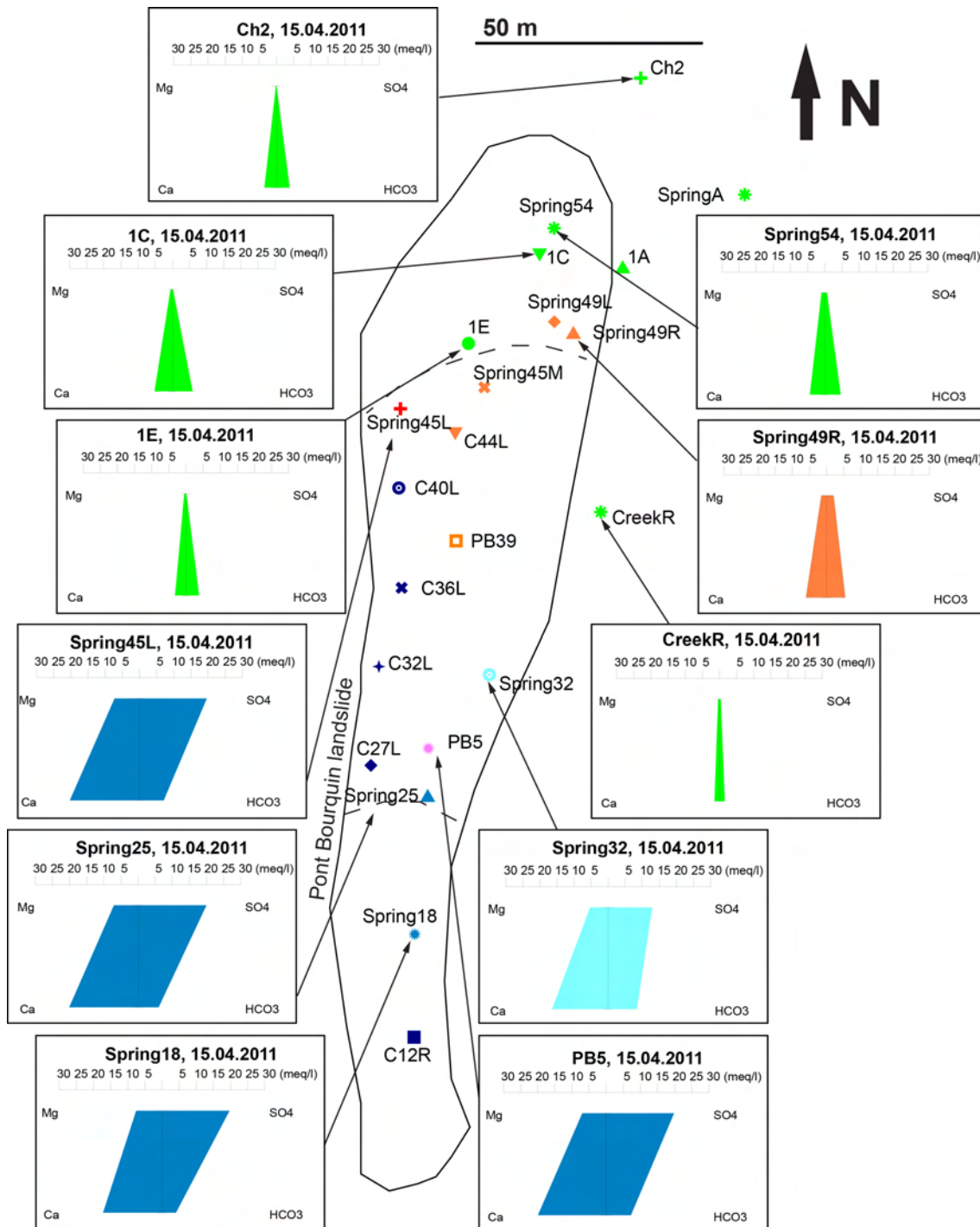
Figure 6.29: *Map showing the locations of water samples from creeks (C), observation wells and springs. The symbols for the sampling locations are used in the scatter plots on the following figures. Stiff diagrams are plotted for eleven water samples from 15. April 2011.*

groundwater of the Pont Bourquin landslide is composed to 98.5 % of the cations Mg^{2+} and Ca^{2+} and the anions SO_4^{2-} and HCO_3^{-}. Figure 6.29 shows Stiff diagrams with these four ions for eleven water samples taken on 15. April 2011. In Figure 6.30.A, the cations Mg^{2+} and Ca^{2+} are plotted versus the anions SO_4^{2-} and HCO_3^{-}.

Highest Ca^{2+} and Mg^{2+} concentrations of 25 meq/l and 10 meq/l, respectively, were measured in PB5 whereas in the water samples from the moraine the Ca^{2+} and Mg^{2+} concentrations were less than 6 and 1 meq/l, respectively. The mean ratio Ca^{2+}:Mg^{2+} in all samples is about 3:1 (see Figure 6.30.B).
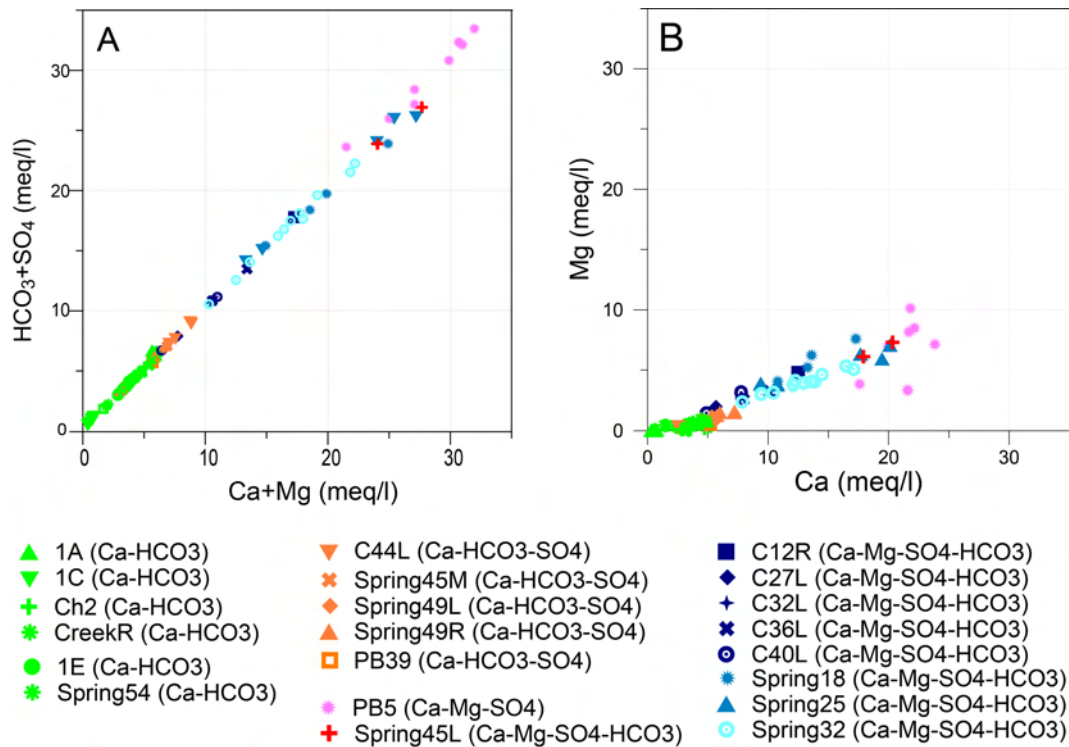
Figure 6.30: *Scatter plot showing the principle cations Mg^{2+} and Ca^{2+} versus the principle anions SO_4^{2-} and HCO_3^{-}.*

The concentration of SO_4^{2-} ranges from 1.5 to 30 meq/l. A few samples from the moraine in the upper part of the landslide (1A, SpA, CreekR, Ch2 and 1C) have not really been in contact with SO_4^{2-}. The SO_4^{2-} concentration is highest in PB5 and the springs in the lower part of the landslide and in spring 45L below the upper secondary scarp. HCO_3^{-} ranges from 0.5 to 7 meq/l with a mean value of 3.9 meq/l. The samples from the moraine at the top and to the East of the landslide (1A, SpA, CreekR) show the lowest and the springs in the lower part of the landslide (Spring 32, Spring 25 and Spring 18), observation well PB5 and Spring 49 in the upper part of the landslide show the highest HCO_3^{-} concentrations.

Temporal variations

On Figure 6.30 it can be seen that there is a large temporal variation in the water chemistry especially for the Spring 32 and observation well PB5. The dates of the samples are shown on Figure 6.31. The groundwater in observation well PB5 (Figure 6.31.A) is higher mineralised during the winter months. For spring 32 no seasonal trend is observed (Figure 6.31.B). In (Figure

6.31.C) the temperature measured for each sample is plotted versus the conductivity values. The temperature variation is larger in the piezometers in the moraine (2 - 17°C) than in observation well PB5 and spring 32 (5- 13°C). The variation in mineralisation is smaller in the samples from the upper part of the landslide than for PB5 and Spring 32.

The temporal variations at single locations may reflect long-term seasonal changes or short-term dissolution during and after rain events.
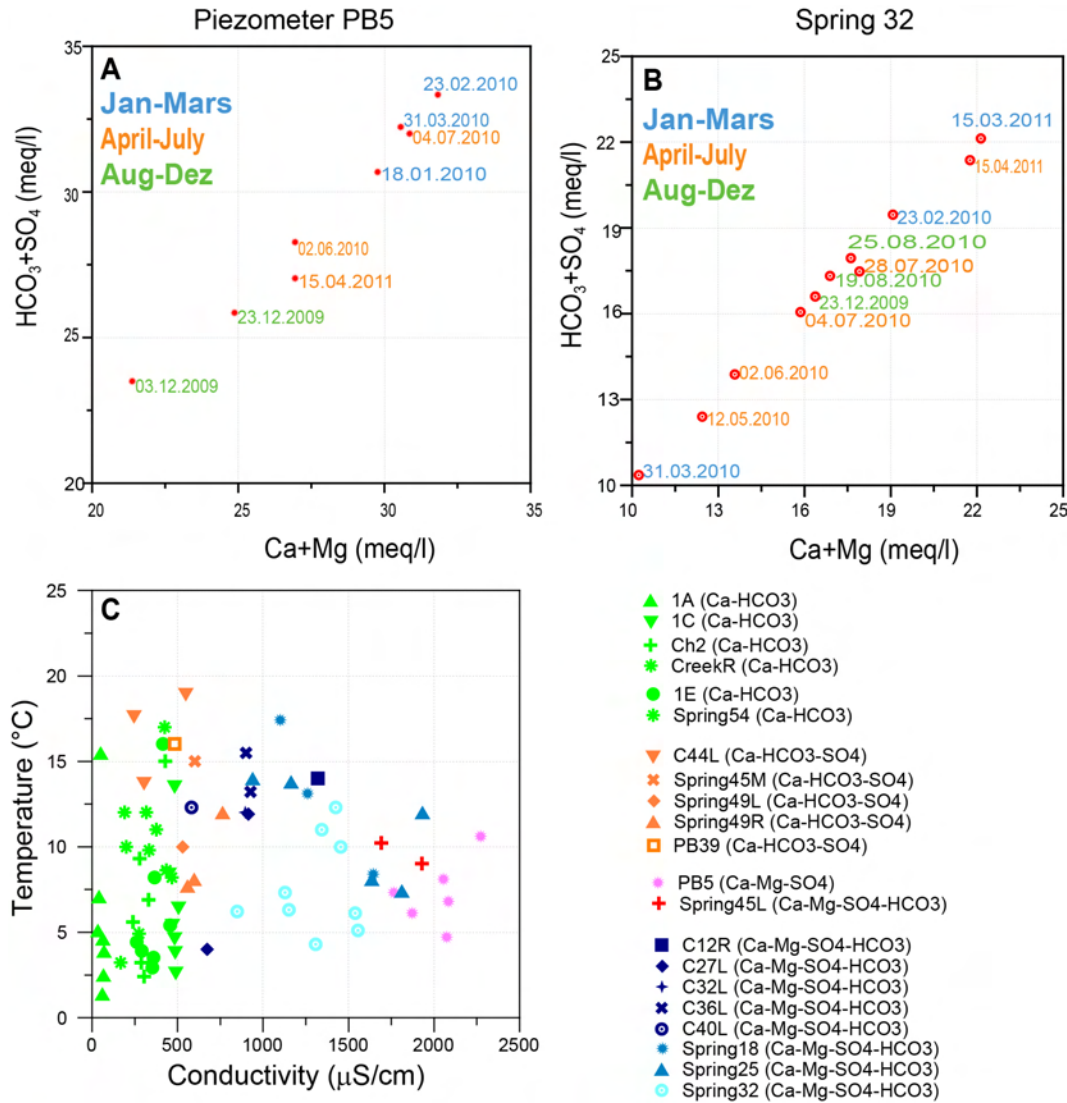
Figure 6.31: *A and B: Temporal variations of the concentrations of Mg^{2+}, Ca^{2+}, SO_4^{2-} and HCO_3^- in observation well PB5 and Spring 32. C: Temperature plotted against the electric water conductivity of the samples illustrates temporal variations.*

Origin of the major elements

Mg^{2+}, Ca^{2+}, SO_4^{2-} and HCO_3^- are typical major ions in water that was in contact with evaporitic and carbonate rocks. This can be seen in Figure 6.30.A because the slope is 1:1. Ca^{2+} and Mg^{2+} comes most likely to large parts from the dissolution of calcium carbonate $CaCO_3$, dolomite $CaMg[CO_3]_2$, and evaporites gypsum $Ca[SO_4]2H_2O$, anhydrite $Ca(CO_3)$ and magnesium sulphate $Mg(SO_4)$. The HCO_3^- comes most likely to large parts from calcium carbonate

$CaCO_3$ and dolomite $CaMg(CO_3)_2$ that reacted with H_2CO_3. The SO_4^{2-} could originate from evaporites gypsum $Ca[SO_4]2H_2O$, anhydrite $Ca(SO_4)$ and magnesium sulphate $Mg(SO_4)$ associated with the cellular dolomite. Furthermore it could originate from pyrite FeS_2 present in the black shale. The concentration of Sr^{2+} and the $\delta^{34}S$ can give important information about the origin of SO_4^{2-}.

6.10.2 Strontium

Strontium analyses were carried out in order to test the evaporitic impact upon the water chemistry. High strontium concentration is explained by the dissolution of celestite $Sr(SO_4)$ which is associated with evaporites. The highest Sr^{2+} concentration was measured in PB5 (1.5 g/l) and springs 32 and 25 (0.8 mg/l) (see Figure 6.32).

These are rather low values compared to evaporitic springs in the Western Swiss Alps, where strontium concentrations between 1 and 15 mg/l (mean 7.9 mg/l) were described (Mandia, 1991). The ratio Sr^{2+}/Ca^{2+} in PB5 and Spring32 is 0.0014 and 0.0011, respectively. A ratio Sr^{2+}/Ca^{2+} > 0.001 (expressed in meq/l) is typical for evaporitic water (De Montety et al., 2007). In Super-Sauze landslide, a ratio between 0.0012 and 0.0078 meq/l has been measured (De Montety et al., 2007). Thus the evaporitic origin of SO_4^{2-} in the groundwater of the Pont Bourquin landslide is not very pronounced compared with other locations.
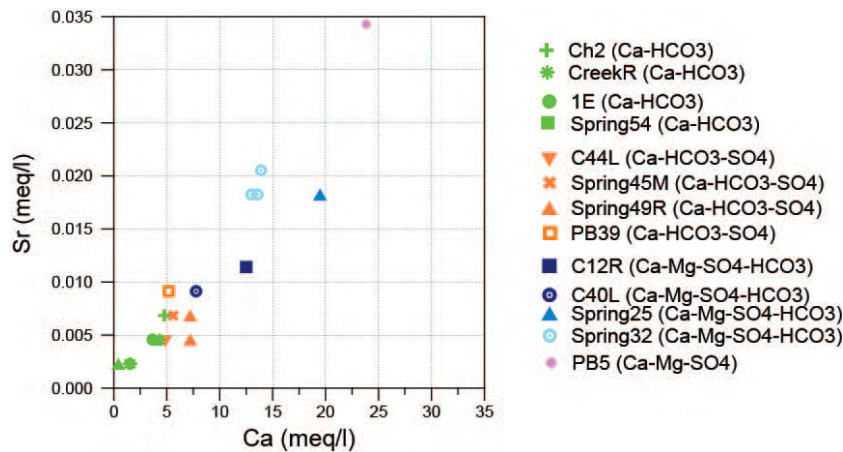
Figure 6.32: *Strontium versus Calcium concentration.*

6.10.3 Sulphur isotopes

Sulphur isotopes from six groundwater samples were analysed to obtain information about the origin of SO_4^{2-} from the dissolution of evaporites or from pyrite. The results are shown on Figure 6.33 and in Table B.3 in Annexe B. The measured $\delta^{34}S_{VCTD}$ values range between 3.8 and 10.8 ‰. The lowest value is observed in Spring 49R in the upper right part of the landslide. This spring originates in black shale (see Figure 6.10, middle right). Generally, the $\delta^{34}S_{VCTD}$ values are increasing towards the toe of the landslide.

This $\delta^{34}S_{VCTD}$ values are interpreted as a mixture of SO_4^{2-} from the dissolution of pyrite and evaporites. Typical $\delta^{34}S_{VCTD}$ values for pyrite and Triassic gypsum/anhydrite are -25 to 2.5 and 15 to 17 ‰, respectively (see Section 4.13). The lower values observed in the upper part of the landslide indicate a larger contribution from pyrite dissolution. This led to the assumption that

the water observed at Spring 49R was flowing through fractured black shale. In the lower part of the landslide, the $\delta^{34}S_{VCTD}$ values are higher. This could be because water that was in contact with gypsum bedrock underlying the landslide in at the location of Spring 32 and observation well PB5.

6.10.4 Groundwater types

Based on the hydrochemical and isotopic analyses, five different groundwater types observed on the landslide were defined. Scatter plots of anions ($SO_4{}^{2-}$ and $HCO_3{}^{-}$) versus cations (Mg^{2+}, Ca^{2+}) helped to visualise the different types (see Figure 6.34). The five groundwater types found on the Pont Bourquin landslide are (see Figures 6.29 and 6.33):

- Type 1, $HCO_3{}^{-}$-Ca^{2+}: This type of groundwater is found in shallow piezometers, springs and creeks in the moraine above and in the upper part of the landslide. The electrical conductivity (EC) is 50 - 500 μS/cm. It is interpreted as groundwater from the moraine that was not or only little in contact with sulphate. The ratio Ca^{2+}:$HCO_3{}^{-}$is about 1:1 and $SO_4{}^{2-}$ and Mg^{2+} concentrations are small. This can be seen on the Stiff diagrams on Figure 6.29.

- Type 2, $HCO_3{}^{-}$-$SO_4{}^{2-}$-Ca^{2+}: This groundwater type was found in springs above and below the upper secondary scarp where black shale are outcropping. It has an increased content of SO_4 and increased EC of 300 - 700 μS/cm compared to Type 1 (see Stiff diagrams on Figure 6.29). The ratio Sr^{2+}/Ca^{2+} is < 0.001 and the $\delta^{34}S$ is the smallest in this groundwater. Thus it is interpreted as a mixture of groundwater from the moraine and groundwater that was flowing through fractures in the black shale.

- Type 3, $HCO_3{}^{-}$-$SO_4{}^{2-}$-Ca^{2+}-Mg^{2+}: This water shows high EC, high concentration of $SO_4{}^{2-}$ and the $\delta^{34}S$ is slightly higher than in Type 2. It is interpreted as groundwater that was flowing through the fractures of black shale. Spring 45L shows a higher $\delta^{34}S$ value than Spring 49R and is probably a mixture of groundwater which was flowing through black shale and evaporites.

- Type 4, $HCO_3{}^{-}$-$SO_4{}^{2-}$-Ca^{2+}-(Mg^{2+}): This groundwater is only found at spring 32. It also shows high EC and is very rich in $SO_4{}^{2-}$. It shows higher concentrations of Ca^{2+}-$HCO_3{}^{-}$ than Type 3. The $\delta^{34}S$ and the ratio Sr^{2+}/Ca^{2+} is slightly higher compared to Type 2 and 3. Therefore this water was most likely in contact with gypsum. Spring 32 is located at the exit of CreekR which has Type 1. This explains the higher concentration of Ca^{2+} and $HCO_3{}^{-}$ in Spring 32. Thus, Type 4 is interpreted as a mixture of Type 1 and Type 3 waters, thus with a signature from all main lithologies: black shale, gypsum and moraine.

- Type 5, $SO_4{}^{2-}$-Ca^{2+}-Mg^{2+}: Groundwater Type 5 is the most mineralized and has a high EC of 2 mS/cm. Like Type 4, the values for $\delta^{34}S$ and the ratio Sr^{2+}/Ca^{2+} are slightly higher compared to Type 2 and 3. This groundwater is interpreted as Type 3 water that was flowing through the black shale debris of the landslide mixed with groundwater that was in contact with gypsum. If the $\delta^{34}S$ for a water sample from piezometer PB5 would not be so different from the $\delta^{34}S$ of Spring 49R (Type 3), this two types could be put together. Looking at the Stiff diagrams (Figure 6.29) Type 3 and Type 5 are identical.

6.11 Conceptual hydrogeological model

Based on groundwater level measurements, spring flux measurements, permeability data, and hydrogeochemical analyses, a conceptual hydrogeological model of the Pont Bourquin landslide
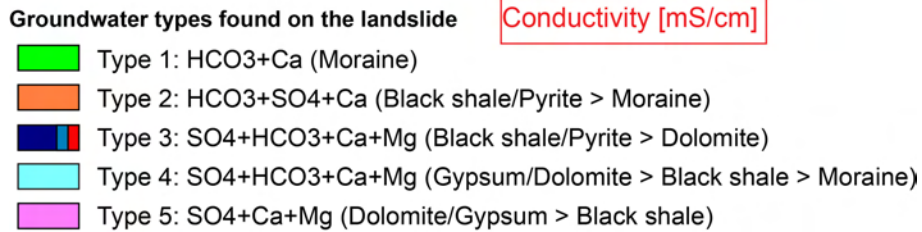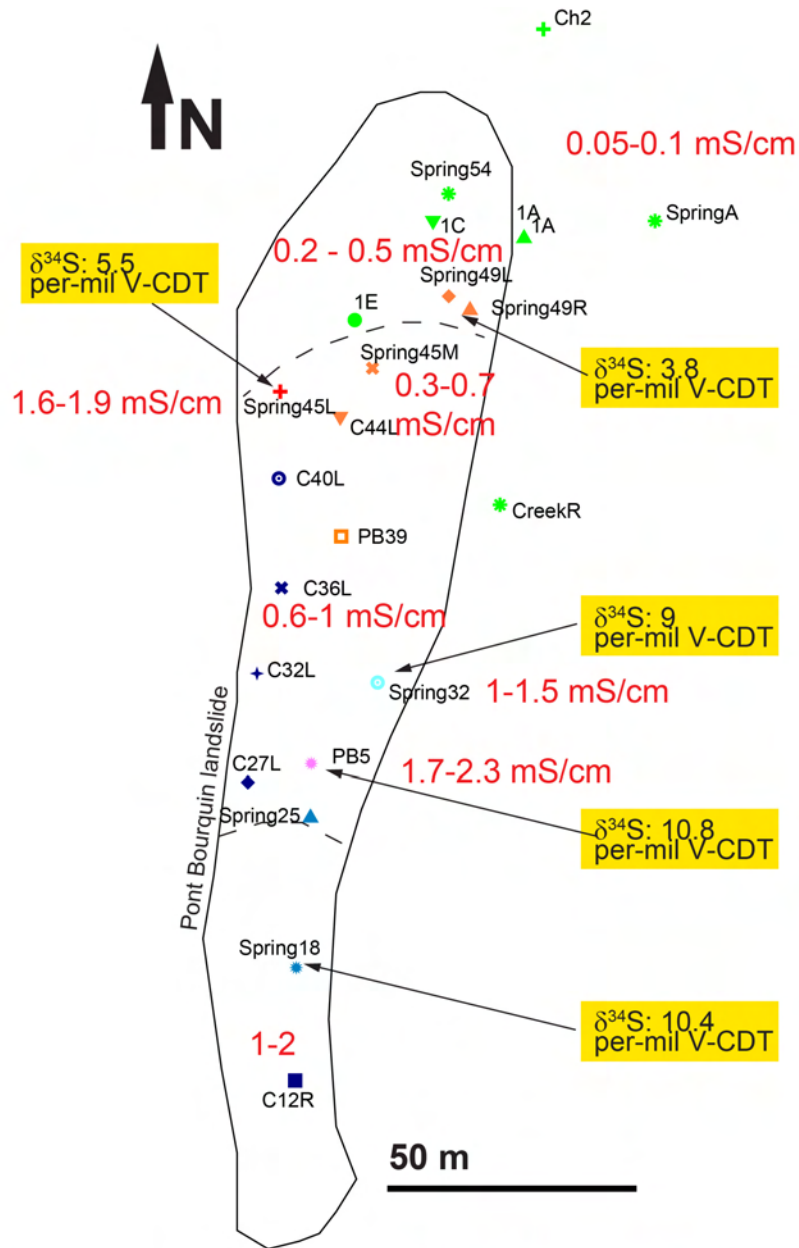
Figure 6.33: *Map with locations of water samples, the average electric water conductivity (red coloured) and the results from six sulphur isotope analyses $\delta^{34}S$.*
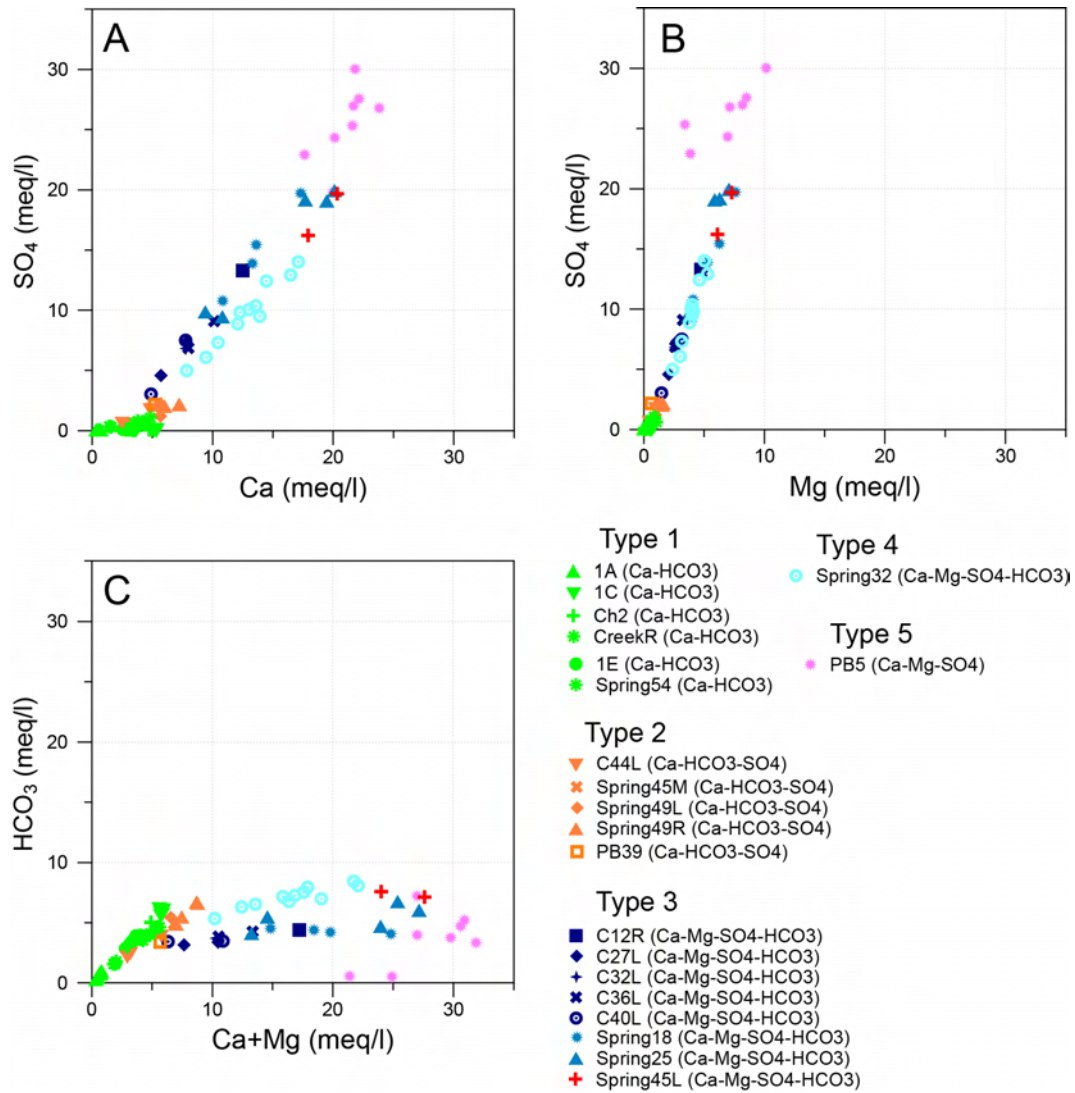
Figure 6.34: *Plotting the anions ($SO_4{}^{2-}$ and $HCO_3{}^{-}$) versus cations (Mg^{2+}, Ca^{2+}) helps to distinguish differenet groundwater types. For further explanation see text.*

was made which showed the groundwater flow paths in the landslide. The five groundwater types defined in the previous section originate most likely from three major hydrogeological units (see Figure6.35):

- Moraine: Moraine is found above the landslide and in the upper part of the landslide.

- Fractured black shale containing pyrite: Shale is generally low permeable. But it is assumed that due to tectonics, toppling and landslide activity, the black shale unit is locally permeable due to fractures. Groundwater in this lithology was also found at a depth between 20 and 70 m in two deep drill holes located 600 and 800 m to the West of the Pont Bourquin landslide (data from the Geological Cadastre of Canton Vaud, http://www.geocad1.vd.ch/index.php?mode=display&view=carte).

- Cellular dolomite associated with evaporites: This unit is found in the upper and the lower part of the landslide. Cellular dolomite is associated with gypsum, especially at the toe of the landslide. Gypsum could represent a fourth hydrogeological unit.

In terms of groundwater flow, three different parts were distinguished on the Pont Bourquin landslide. The upper part includes the zone below the head scarp. In this part, cellular dolomite underlays low permeable moraine. It is assumed that due to dissolution of gypsum, the dolomite is permeable. Additionally, wet hollows (most likely dolines) were observed further upslope. In these zones, water may infiltrate into the cellular dolomite. Most likely, the dolomite is an aquifer which is drained towards the little stream to the West of the Pont Bourquin landslide. A part of the groundwater present in the cellular dolomite may infiltrate into the fractured black shale located below the dolomite. The groundwater in the dolomite could not be measured directly (for this purpose, deeper drill holes would be necessary). But the chemistry of the groundwater below the head scarp gives evidence that it was flowing through this unit (Groundwater Type 3, rich in SO_4^{2-}, Ca^{2+} and Mg^{2+}). The question arise, if during snowmelt and heavy precipitation, the water level in the dolomite rises and builds up hydraulic pressure below the low permeable moraine. The groundwater level in the moraine (Groundwater Type 1, rich in HCO_3 and Ca^{2+}, found in observation wells 1A and Ch1, Spring A and CreekR) is locally less than one meter below the ground surface (perched groundwater) and several "slope springs" exfiltrate from the moraine. These springs feed the swampy area below the head scarp. The formation of this swampy zone was favoured by the topography (less steep). Due to the low permeability of the moraine, water is ponding at the surface and in cracks. At Spring 49R and 49L, which are located in the eastern part of the swampy area, groundwater that was flowing through the fractures in the black shale unit exfiltrates.

The middle part extends from the transition of cellular dolomite to black shale (above the upper secondary scarp) to the dolomite formation in the lower part of the landslide. In this part, an intermediate permeable layer of weathered and fractured black shale (and Flysch) lies between the low permeable bedrock and the low permeable landslide mass. It is assumed that black shale bedrock becomes permeable when it is fractured due to tectonics, landslide movements and toppling. Groundwater from the moraine and the cellular dolomite located above the black shale may infiltrate in those fractures and forms Type 2 and Type 3 groundwater, respectively. The water flowing through the black shale gets rich in SO4 with low $\delta^{34}S$ that comes from the dissolution of pyrite. Some of the springs show red "iron mud" which could be Iron(III)oxyde-hydroxyde, a dissolution product from pyrite in the black shale (see Figure 6.10). This water exfiltrates partly at springs along the upper secondary scarp (Spring 45 and 49), flows partly in the fractures of the weathered black shale incorporated in the landslide mass, exfiltrates partly at springs in the lower part of the landslide (Spring 18 and 25), and most likely infiltrates into the
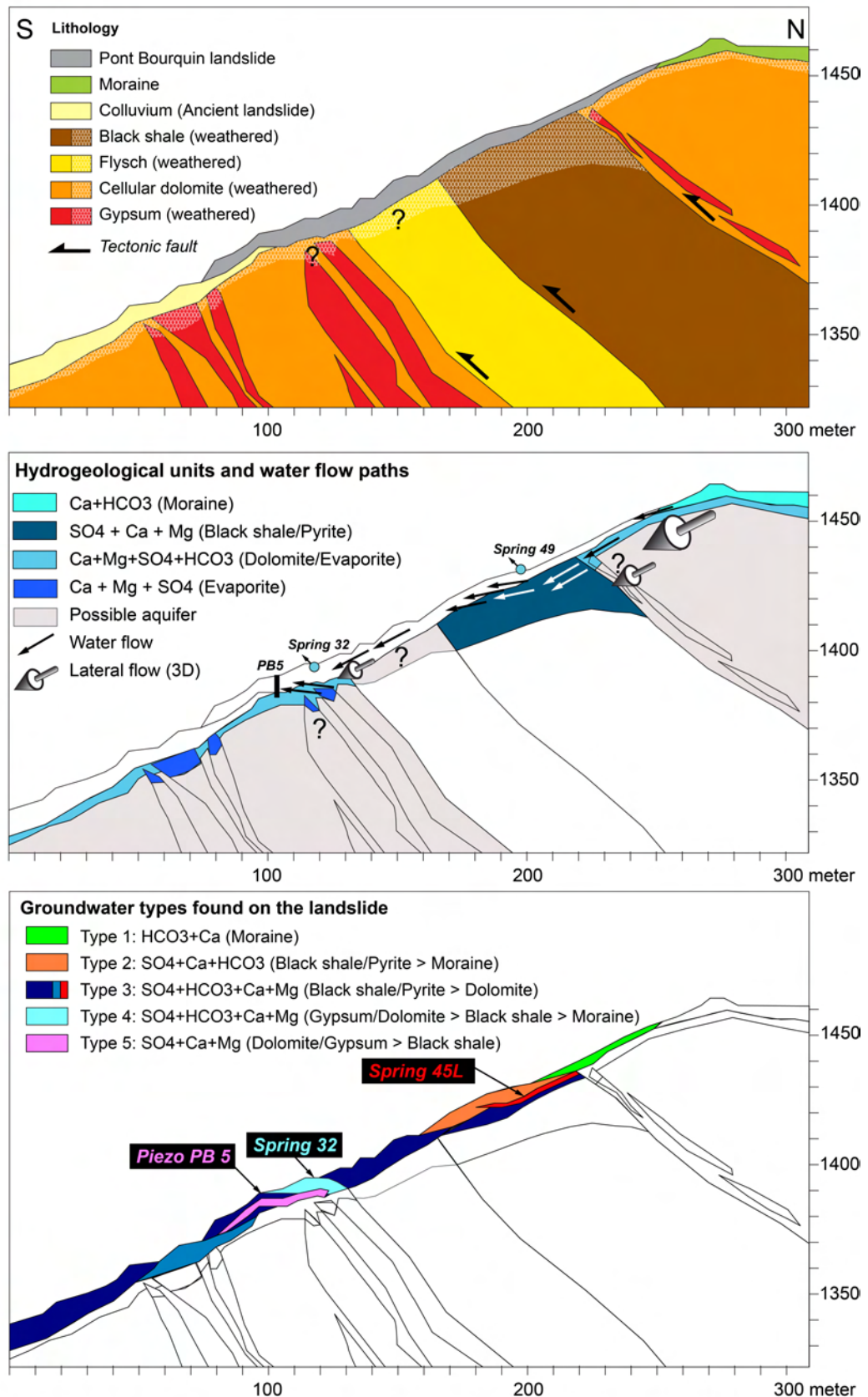
Figure 6.35: *Conceptual geological and hydrogeological model of the Pont Bourquin landslide: Based on ERT profiles, the geological model of the landslide and the substratum was made (top). This was the base for the hydrogeological model, which shows the hydrogeological units and water flow paths (middle) and the mixture of groundwater found in the landslide (bottom).*

permeable cellular dolomite at the toe of the landslide. The groundwater in the black shale circulates most likely only along preferential flow paths, because several piezometers in this lithology (PB1, D, 5A, PB36, PB45A nd B) always remained dry. It is possible that the Flysch has a similar weathered layer like the black shale. The hydrogeological role of the Flysch lithology is unknown as no outcrops and no drill holes are available.

In the lower part of the landslide, permeable cellular dolomite and evaporites underlie low permeable landslide deposits. Most likely, this formation is draining the landslide towards the creek to the West. But after heavy precipitation or snow melt, water rich in SO_4^{2-} may exfiltrates from these lithology and mixes with Type 3 to form Type 5 groundwater (rich in SO_4^{2-} from dissolution of gypsum) which was found in PB5. The observation in PB5 and Spring 32 of more mineralised water that arrives a few days after heavy rainfall events (piston flow) supports this hypothesis. It is also possible that the groundwater in the landslide gets this additional signature of gypsum by lenses of gypsum which are incorporated in the landslide mass. To test if the cellular dolomite and gypsum are aquifers, deeper observation wells would be necessary. Spring 32 (Type 4 groundwater) is located in the transition from the middle part to the lower part of the landslide. As PB5, it has a signature of additional gypsum dissolution. This spring showed a mixture of Type 3 water and morainic groundwater that exfiltrated at SpringA and re-infiltrated along CreekR into the fractures of the black shale. The water temperature of Spring 32 rose in summer up to 12° C and sunk in winter to 4 °C. This temperatures are similar to the ones measured in observation well PB5 next to Spring 32. This indicates that the origin of the spring is probably a few meters below the surface. Furthermore, even during dry periods, this spring was continuously flowing, which may indicate that it is feed by deeper groundwater.

6.12 Triggering mechanisms and landslide causes

The potential hydrogeological triggering mechanisms in the case of the Pont Bourquin landslide are complex. According to the hydrogeological landslide classification, the Pont Bourquin landslide can be divided in three different parts (see Figure 6.36). The middle part is the most critical part. Local confined groundwater may build up in the fractured black shale. Increasing pore water pressure, seepage forces and overpressure may lead to a loss of the shear strength and liquefaction. Additionally, the high plasticity of the landslide material favours the occurring of landslides. Inner erosion is not expected due to rather small grain size of the land slide mass. Intense rainfall may trigger rather superficial slides and flows whereas snow melt and long-term wet periods are determinant for the acceleration of the deeper creeping. In the upper and lower part, the gypsum and cellular dolomite may act as sink for the groundwater. In these parts, the temporal rise of the groundwater table in the bedrock below the landslide should be verified with drill holes. The Pont Bourquin landslide is an example, how three dimensional groundwater flow (water possibly infiltrates into dolines further upslope) may be reduced to two dimension for applying the classification. The criticality of the Pont Bourquin landslide is shown in Figure 8.9 in Chapter 8.

6.13 Summary

The Pont Bourquin landslide initiated over ten years ago in the black shale lithology. The bedding of this tectonically weakened lithology is dipping about 30° into the slope and thus favours toppling processes. In 2007, flexural toppling was also observed in the Flysch unit below the black shale which is now covered by debris of black shale (Jaboyedoff et al., 2009). Erosion processes
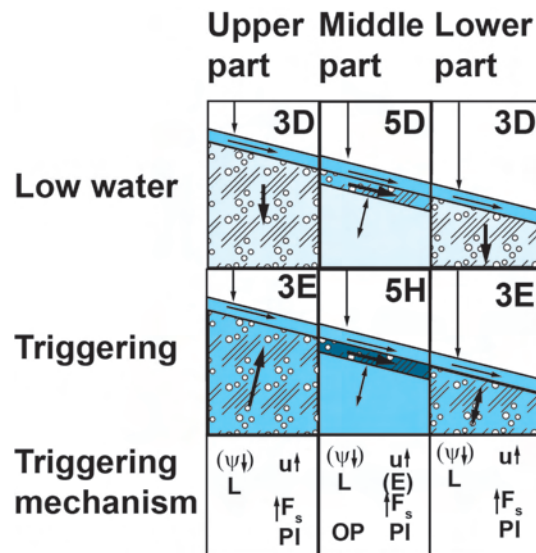
Figure 6.36: *The hydrogeological landslide triggering classification applied for the case of the Pont Bourquin landslide.*

were accelerated because of the growing outcrops of fissured black shale (below the current upper secondary scarp) and the progressively vanishing vegetation. This provided material for the continuously occurring superficial debris and earth flows and slides. Due to unloading and toppling, more fractures developed in the weathered black shale and additional water infiltrated (most likely from the overlaying cellular dolomite). Due to exposure and weathering, the strength of the clayey soil and rock is reduced which supplementary favoured the destabilisation of the slope. Extension cracks formed continuously at the top and the sides of the landslide and on the landslide itself which favoured the infiltration of meteoric water. It is possible that the dissolution of gypsum in the lower part of the landslide additionally destabilises the slope (Jaboyedoff et al., 2009). Nevertheless, at the toe of the landslide the bedrock may drain the landslide towards the creek to the West. This seems to rather stabilize the slope. No displacements of the road could be observed. But material from both the superficial debris and earth flows and slides and the deeper creeping of the approximately 10 m thick Pont Bourquin landslide is accumulating at the edge of the cantonal road. This accumulations form a steep bulge with a thickness >10 m which may fail in near future.

Comparing the map of present landslides (from GIS of Canton Vaud, http://www.geoplanet.vd.ch), the geological map and the slope angle, it can be seen that in the region between the Pillon pass and the village Les Diablerets, landslides often initiate in steep terrain (> 20°) located in Aalenian black shale lithology. Generally the slope along this weak Aalenian lithology has been smoothed in the past by erosion processes and landsliding. Nevertheless, some over-steepened Aalenian slopes (> 20° steep) exist. Black Aalenian shale favours the occurrence of landslides because of the disposition to weathering and forming plastic clay (Bianchetti and Crestin, 2004) with unfavourable strength properties (see Section 2.5.7). Also the Les Parchets landslide located NW of the Pont Bourquin landslide initiated in argillaceous schist of the Arveyes nappe and the sliding mass is mainly composed of debris of black shale (Schoeneich et al., 1996).

The example of the Pont Bourquin landslide showed how complex the interaction between groundwater and different geological lithologies may be. Without drill holes that reach into the bedrock, it may be impossible to know the origin of the groundwater in the landslide, because fragments of bedrock may be incorporated into the sliding mass. Groundwater that was

flowing through the landslide may have a similar hydrogeological signature like water that originates from the bedrock. The following drilling locations could be of special interest: Around post 57 (to investigate, if the cellular dolomite in the upper part of the landslide is an aquifer) and, more important, above Spring 32 (to investigate the location of the gypsum and to investigate, if the bedrock is an aquifer). Due to lithological heterogeneities, it would be important to install water pressure sensors at different depths.

This case study has shown, how the classification can be applied to construct a conceptual model of different landslide parts. For the Pont Bourquin landslide, the middle zone underlain by black shale is the most susceptible part for landsliding. Local confined aquifers, liquefaction and mechanisms related to high plasticity are important for the landslide triggering.

Investigations of the Pont Bourquin landslide are ongoing. In the area of the lower secondary scarp of the landslide, continuous seismic sensors were installed during spring and summer 2010 for monitoring with the "ambient seismic noise correlation technique" (see Section 4.5 for the description of the method). The seismic velocity of the sliding material, measured from daily noise correlograms, displayed a continuous and rapid drop several days before the catastrophic event in August 2010 (Mainsant et al., 2011). Ambient seismic noise correlation is a promising method for the prediction of the triggering of landslides. These investigations as well as monitoring by several remote sensing techniques (LIDAR, photogrammetry, total station, see Section 4.17) will continue on the Pont Bourquin landslide.

Chapter 7

Hydrogeological monitoring of a slope prone to landslides, Rufiberg (SZ)

7.1 Introduction

"Water that was under pressure, extruded fountain like from the Rufiberg slope", remembers district forester Sigi Weber referring to the heavy rainfall event from August 2005 that triggered numerous landslides on the Rufiberg (see Figure 7.1). This was not the first time that this area was subject to landslides: "Rufi" means shallow landslide in Swiss dialect. Why is the Rufiberg susceptible for landsliding? Where did the described "fountain like" water come from? What are the hydrogeological landslide triggering mechanisms in the area of the Rufiberg? To answer these questions, a test site on the Rufiberg was chosen in the framework of the TRAMM project to carry out hydrological, hydrogeological, geophysical and geotechnical investigations. In the following, the findings of these studies are presented with focus on the hydrogeology of the slope.
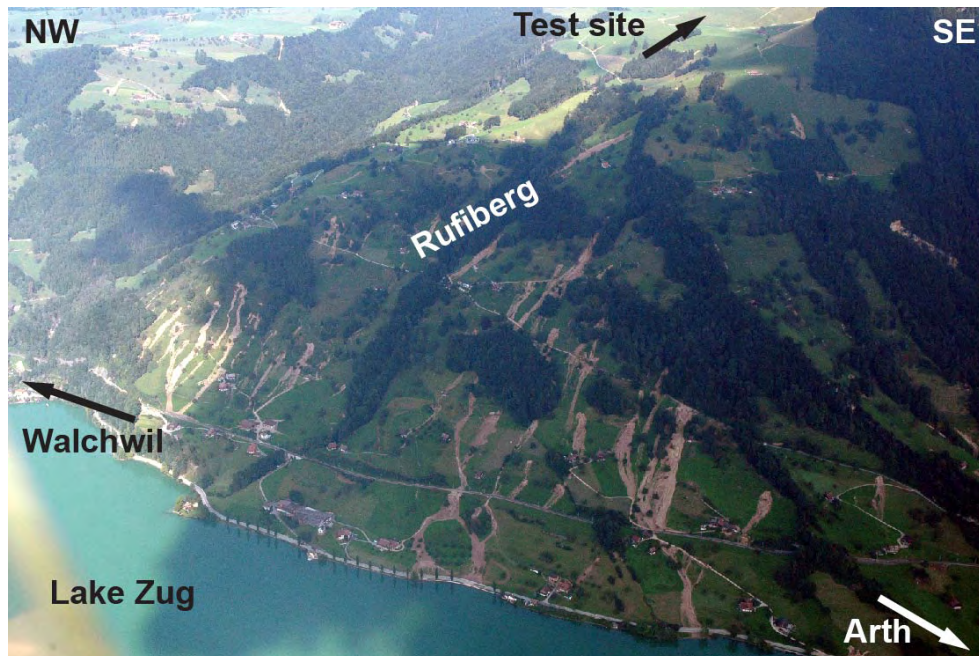
Figure 7.1: *Aerial photograph of the Rufiberg taken on the 5th of September 2005 after heavy rainfall events that triggered numerous shallow landslides on the 22 August 2005 (Photo: Louis Ingenieurgeologie GmbH, Weggis).*
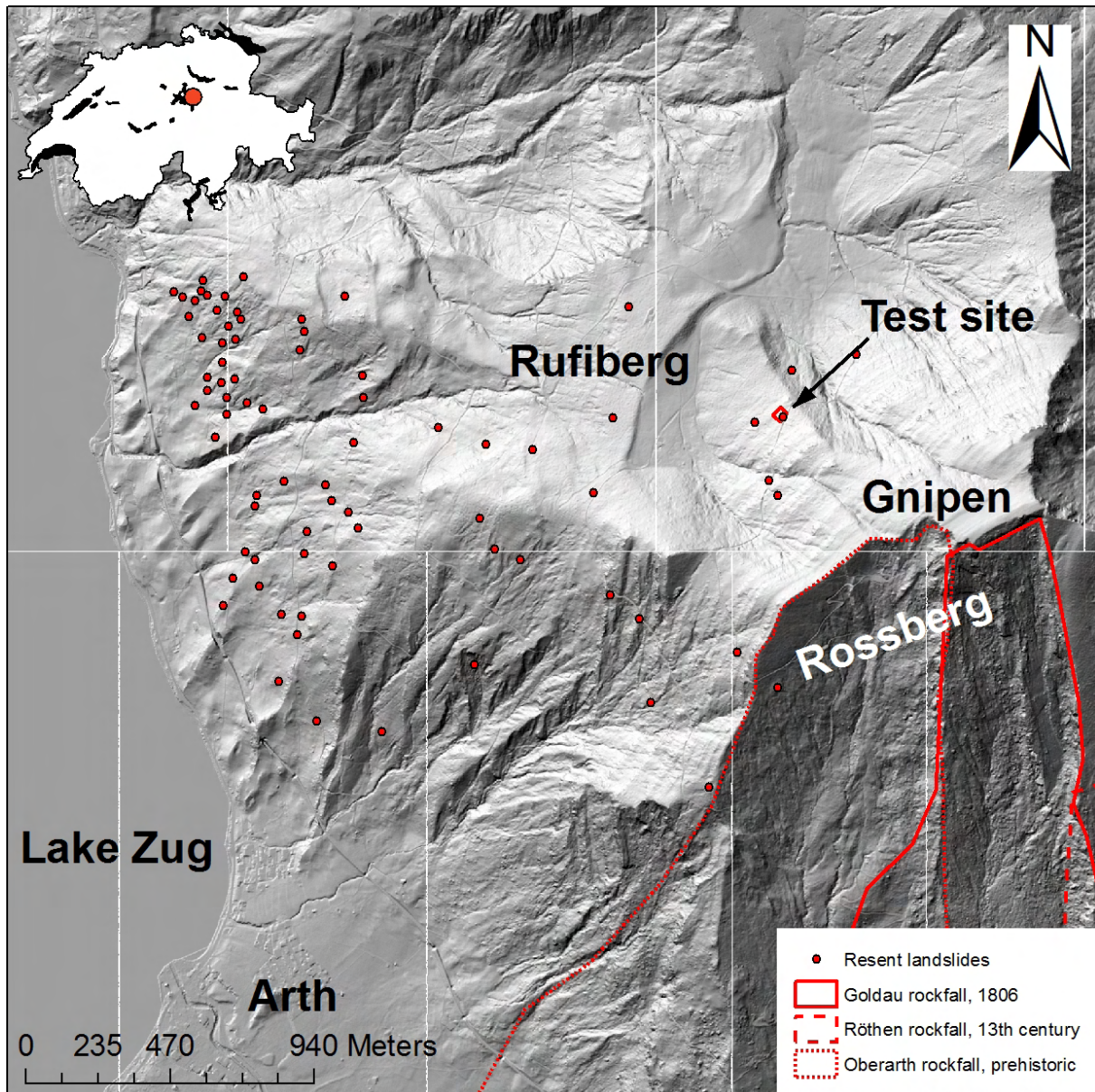
Figure 7.2: *Shaded relief of the Rufiberg. Red dots indicate head scarps of recent landslides. Most of them were shallow landslides triggered by a heavy rainstorm event in August 2005. 2m-digital elevation model reprinted with permission of the Environment Department of Canton Schwyz. Locations of landslides based on field observations, aerial photographs, orthophotographs from http://map.geo.admin.ch, and SormMe landslide database of Canton Schwyz.*

7.2 Regional context

The Rufiberg is located above the village Arth in Canton Schwyz (see Figure 7.2) at the opposite hill side of the famous rockfall from Goldau that was triggered in 1806 by heavy rainfalls. This event was preceded by a rainy summer, very late snow melt and a snow rich winter (Thuro et al., 2006). This rockfall with a volume of 35-40 Mio m^3 was not unique at the Rossberg. Already in prehistoric times (rockfall from Oberarth) and in the 13th century (Röthener rock fall) large masses were released, and this processes continue until today (recent rock slide on the Gnipen with a volume of 5'000 m^2 in 2002).
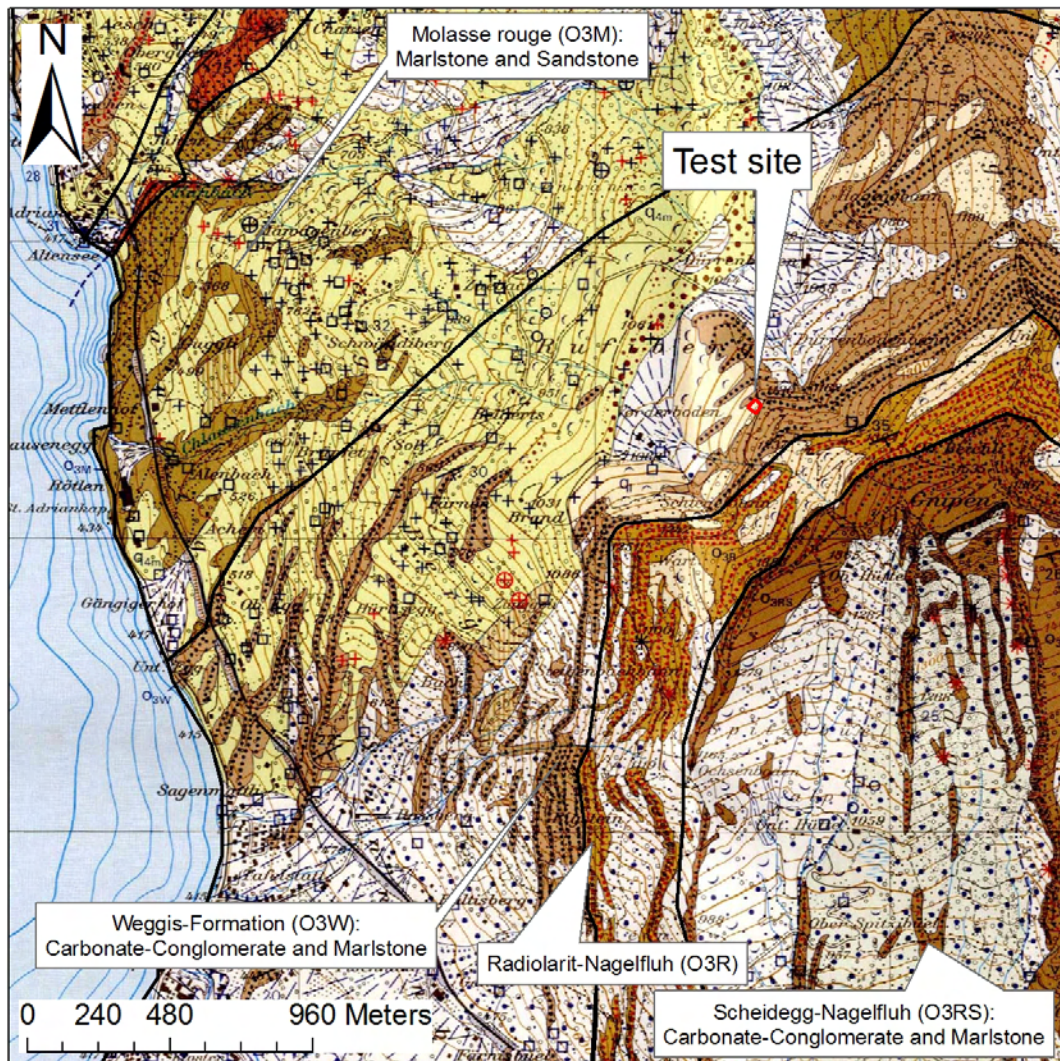
Figure 7.3: *Geological map 1:25'000 (Hantke, 2006). Different units of the Lower Freshwater Molasse are indicated.*

The geology of the Rossberg favours the occurrence of slope instabilities. The Rossberg and the Rufiberg belong to the Rigi-Rossberg nappe located in the subalpine Molasse (Oligocene). This nappe dips 20-30° towards SSE because it was thrusted towards NNW over more distal Molasse sediment deposits. Figure 7.3 shows a the geological map 1:25'000 (Hantke, 2006). The sediments are a succession of thick conglomerate banks interbedded by marlstone and sandstone from the Lower Freshwater Molasse (LFM). On Figure 7.3 the different formations that build up the LFM are indicated. Figure 7.4 shows photographs from the three lithologies. On the
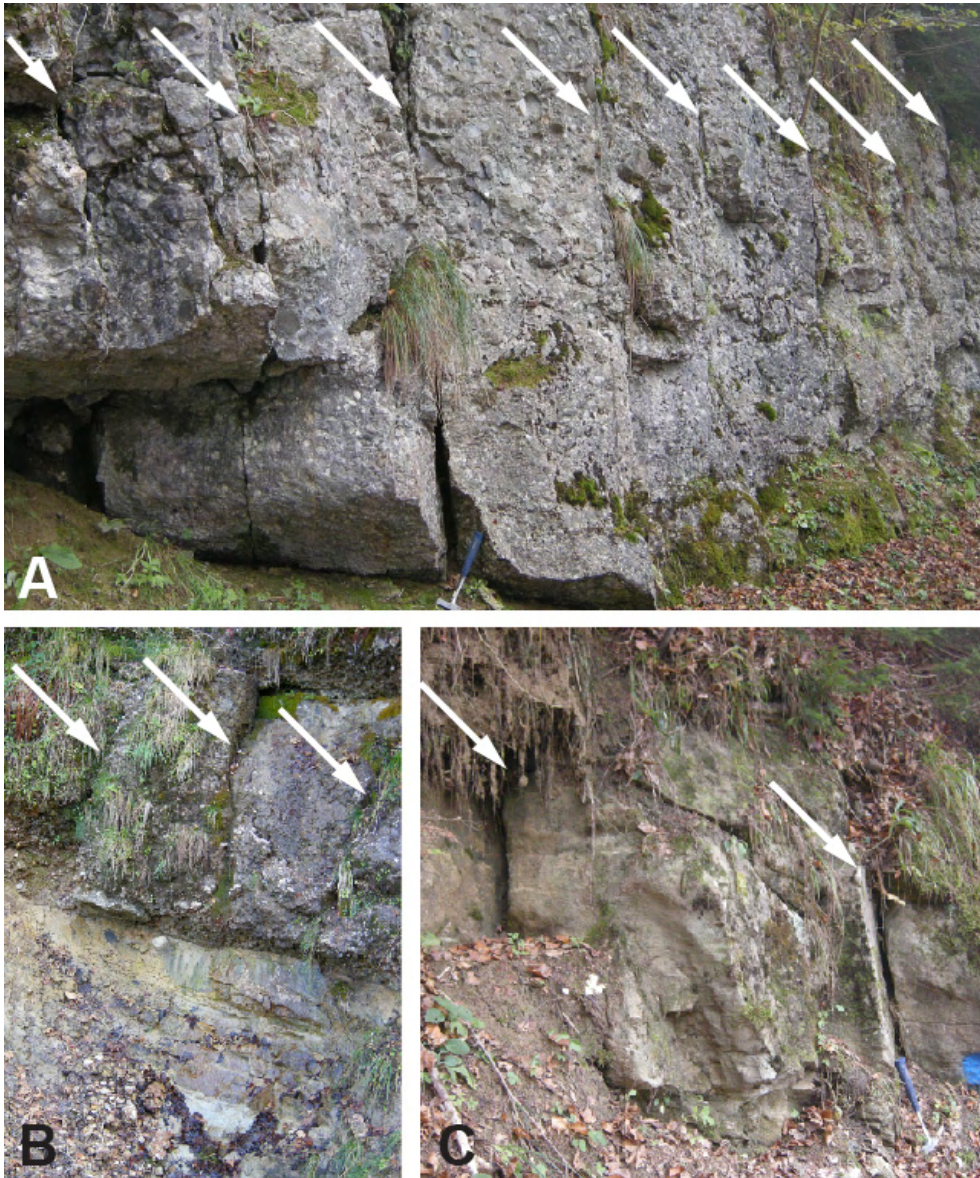
Figure 7.4: *Photographs of the three main lithologies found at the Rufiberg. Joints are indicated with arrows. A: Conglomerate, orientation of joints 235/90, the spacing of joints is up to 20 cm. B: Coloured marlstone underlying fractured conglomerate. Water was seeping out of joints in the conglomerate. C: Sandstone, medium-grained, homogeneous, orientation of the joints 244/88.*

Rossberg side, the sediment layering runs approximately slope parallel whereas on the Rufiberg side, it dips into the slope. On the shaded relief of the area (Figure 7.2) and the slope map (Figure 7.5), the sediment layering can be seen because the competent conglomerate bands form steps and vertical rock walls in the landscape. On the Rossberg side, the marlstone beds act as excellent slip surface, especially when they are weathered (Berner, 2004a). Several vertical joint groups are crossing the mountain. These cut the conglomerate banks in large cubes. Figure 7.6 shows a map with the strike and dip of measured joints. Main orientations of the joints are NW-SE, N-S and W-E with sub vertical dipping.

After snowmelt and strong rain, high pore water pressure can build up in the joints. This pore water pressure was described as main triggering mechanism of the Goldauer rockfall (Berner, 2004a). It is assumed that on the Rufiberg side, water that flows through joints and fractures in the conglomerate and sandstone formations also affects the triggering of landslides.
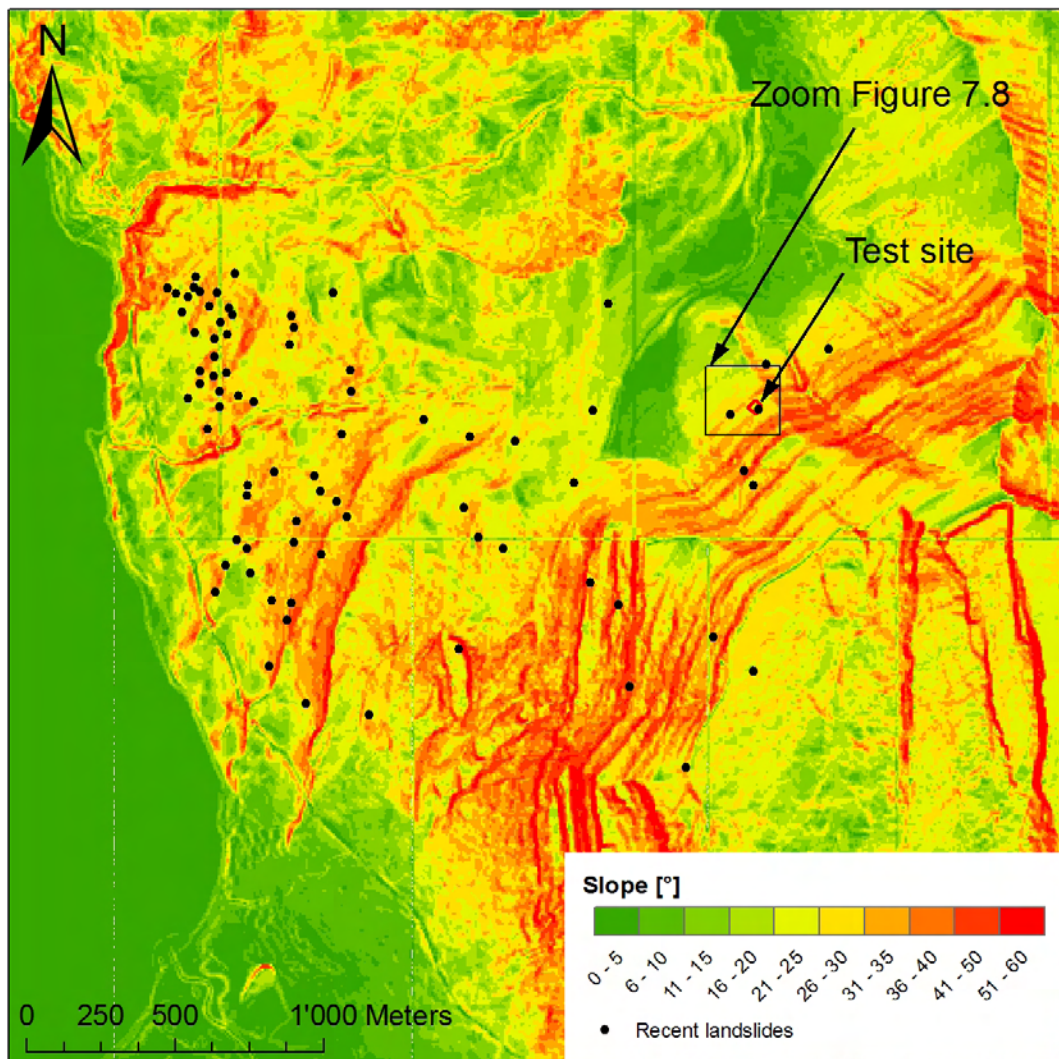
Figure 7.5: *Map of the slope. The geological layering is visible because the competent conglomerate bands form steep rock walls whereas the less competent marlstone layers show a flatter topography. Red dots indicate head scarps of recent landslides. 2m-digital elevation model used with permission of the Environment Department of Canton Schwyz.*
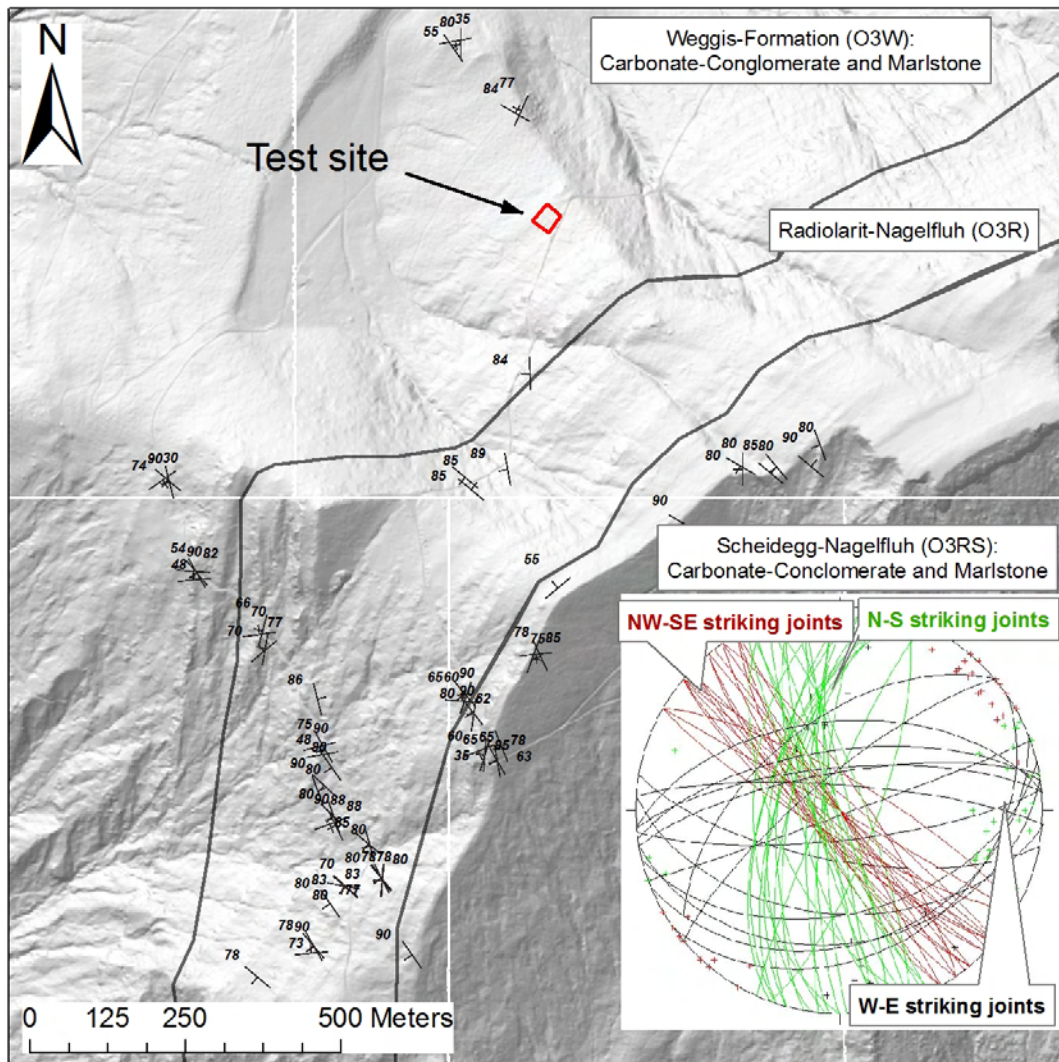
Figure 7.6: *Shaded relief with the strike and dip of measured joints. Main orientations are NW-SE, N-S and W-E with sub vertical dipping. The red square indicates the test site. 2m-digital elevation model used with permission of the Environment Department of Canton Schwyz.*

7.3 Test site

To test the hypothesis about groundwater flow in fractured bedrock and subsequent overpressure below the potential landslide, ERT profiles and 2-9 m deep drill holes were performed on a test site on the Rufiberg in the framework of this study. The approximately 1000 m^2 large test site is located between 1165 and 1180 m above sea level (Swiss coordinates: 684'535/215'450) and the mean slope angle is 25° (see Figures 7.7 and 7.8). Geologically, it lies in the *Weggis-Formation* that is composed of alternating carbonate conglomerate, sandstone and marlstone layers. It is assumed that the geology is similar on the entire Rufiberg and therefore the test site is representative for this area.

The test site belongs to a meadow used for pasturing and it is accessible from a forest road passing above it. This site has been allocated for research from the *Unterallmeid-Korporation Arth*. The hydrogeology of the unconsolidated sediment was studied by Seraina Kauer (Kauer, 2010) from the *Geographical Institute, University of Zürich* and geotechnical soil parameters were investigated by Linda Seward and Georgiana Maries (Maries, 2011) from *Institute for Geotechnical Engineering, ETH Zürich* (IGT). Geophysical investigations were performed in collaboration with the *Swiss Federal Institute for Forest, Snow and Landscape Research (WSL), Birmensdorf.*
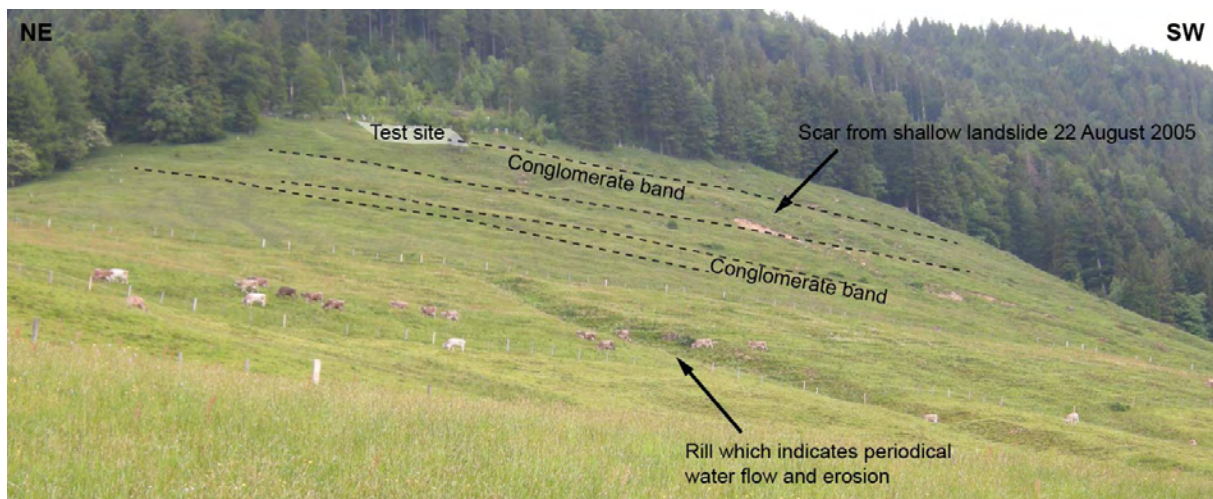
Figure 7.7: *Photograph of the investigated slope on the Rufiberg. The test site is indicated at the top left of the slope.*

7.4 Electrical resistivity tomography

Two electrical resistivity tomography (ERT) profiles were recorded, each with 48 electrodes, along the test site (see Figure 7.8 for location): A short profile to obtain information about rather shallow lithologies and their saturation pattern and a long profile to investigate the deeper lithologies and saturation patterns in the bedrock (see Table 7.1 for details about the profiles). The profiles were made three times in order to study variations of the saturation in the underground:

- 19 Mars 2010 before snow melt.

- 5 May 2010 after snow melt.

- 19 may 2010 during light rain fall.
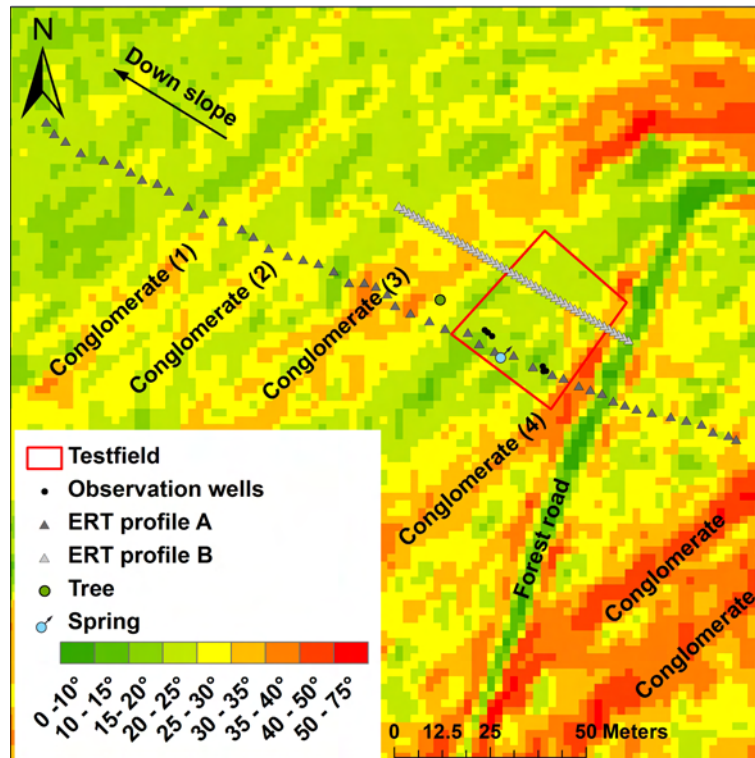
Figure 7.8: *Slope map of the test site. Locations of observation wells and ERT profiles are indicated. For location of this zoom see Figure 7.5.*

Figure 7.9 shows the inverted profiles A and B recorded on 19 March, 5 May and 19 May 2010. The inversion was performed with the software Res2Dinv. The robust constraint method was used because sharp boundaries between conglomerate and marlstone were expected (with robust data constraint cut-off factor = 0.05 and robust model constraint cut-off factor = 0.005). Because large resistivity variations appeared near the surface, a model with cell width half the unit electrode spacing was used. Iterations were performed until the difference between two iterations was smaller than 5%. Between five and ten iterations were performed. The absolute error was the most acceptable for the first profiles from 19 Mars and it was poor for the profiles recorded in May.

The electrical resistivity varies between 10 and approximately 1000 Ωm. Abrupt sub vertical and slope parallel changes can be observed. Three horizontal layers are distinguished: 0 - 1 m depth (can be seen better in the short profiles), about 1 - 10 m depth and > 10 m depth. The vertical structures from bottom to top are: A low resistivity area followed by two high resistivity layers, a low resistive zone, a rather high resistivity block and a low resistivity block at the top. This electrical resistivity pattern could be well interpreted because the geology in the area is well known.

The top horizontal layer was interpreted as unconsolidated sediment. Between this layer and the bedrock, a rather thick stratum of weathered and fractured bedrock is present. The sub vertical higher resistive structures coincide well with the steep bands observed on Figures 7.8 and 7.7 and are therefore interpreted as conglomerate and sandstone beds (numbered 1 - 4 from bottom to top). The low resistivity deep areas are interpreted as marlstone. On the bottom of Figure 7.9 the geological interpretation is shown.
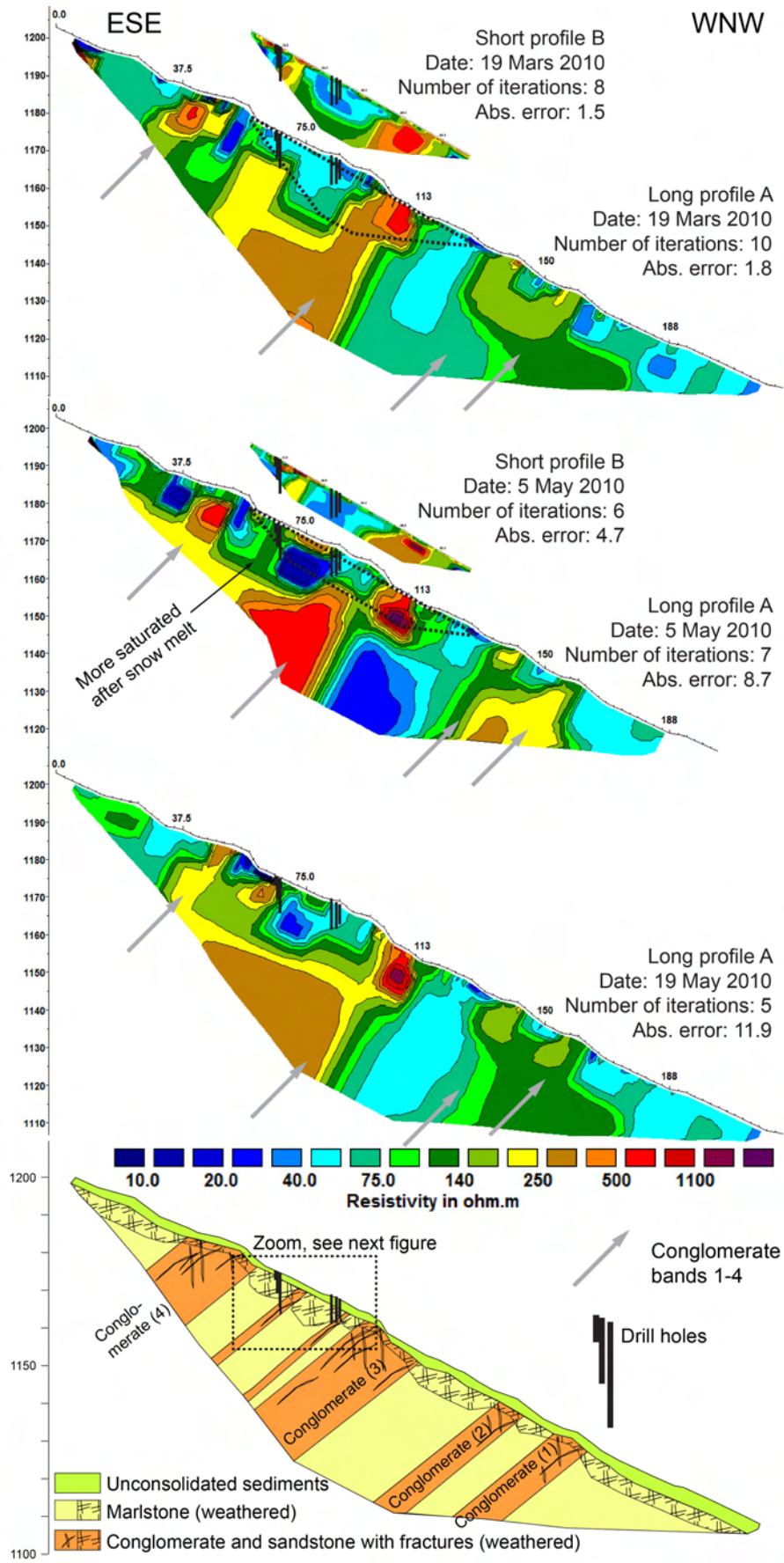
Figure 7.9: *Inverted long and short profiles recorded in March and May 2010 with the geological interpretation. Resistivity changes in time can be observed mainly in the area of conglomerate band 4. This could be due to changing saturation in the bedrock.*

Profile name	Nr. of electrodes	Spacing, m	Length, m	Electrode configuration	Date 2010
A	48	5	200	M	19 Mars
B	48	1.5	70	M	19 Mars
A	48	5	200	M	5 May
B	48	1.5	70	W-VES	5 May
A	48	5	200	M	19 May
A	48	5	200	W-VES	19 May
A	48	5	200	Sch-VES	19 May

Table 7.1: *Characteristics of the performed ERT profiles (A: long profile, B: short profile). M: Mixed Wenner-Schlumberger, Sch-VES: Schlumberger-Vertical electrical sounding, W-VES: Wenner-Vertical electrical sounding.*

The lower part of the profile (conglomerate bands 1 - 3) coincides well on all three long profiles whereas in the upper part (conglomerate band 4), resistivity changes in time can be observed. The weathered bedrock in the upper part of the profile shows lower resistivity after snowmelt on 5 of May 2010 (indicated on Figure 7.9). This could be because the absolute error is not the same for the three profiles or because the bedrock was more saturated after snow melt.

The two short profiles coincide well with the long profiles. They are particularly useful to detect the top layer because their resolution is higher than for the long profiles. The boundary between the weathered bedrock and the fresh bedrock can also be seen on the short profile from 19 Mars 2010. This interface is at the lower border of the profile where the accuracy is smaller. Therefore the long profiles are more useful to define this boundary.

The long profile A was recorded three times on 19 May 2010 in order to test different electrode configurations (see Figure 7.10). The general structures described above can be observed in all three profiles. The thin top layer is clearer visible with the mixed and the Wenner method. The intermediate layer is clearer detected with the Wenner method whereas the Schlumberger configuration displays the vertical layers more pronounced. The generally used mixed method was well adapted for the case of Rufiberg as it displays well the vertical and horizontal structures. The structures are poorly identified with the Schlumberger array.

A rough image of the underground could be made with the aid of the ERT sections. But thin sediment layers cannot be detected with ERT. To verify and refine the geological interpretation of the ERT profiles and to obtain more information about the groundwater, several drill holes were made and observation wells were installed (next section).

7.5 Geology and hydrogeology in drill holes

In November 2010, six drill holes with depth between 2 and 9 meters were performed on the Rufiberg test site with a flexible 1.5-tonne drilling rig operated by *Gasser Felstechnik AG*, Lungern OW. Through the unconsolidated sediment, it was drilled destructively without water but with air pressure of several bar to eject the cored material to the surface trough the drilling rods. The advantage of this method was that the presence of groundwater could be identified easily when humid and muddy material was ejected. In the bedrock, it was partly cored (not a destructive drilling method) with a diamond drilling head using water for cooling. If the rock was too soft, it was washed out by the water what leaded to clogging of the drilling head. An advantage of coring with water was that the draining effect of the bedrock could be observed during drilling
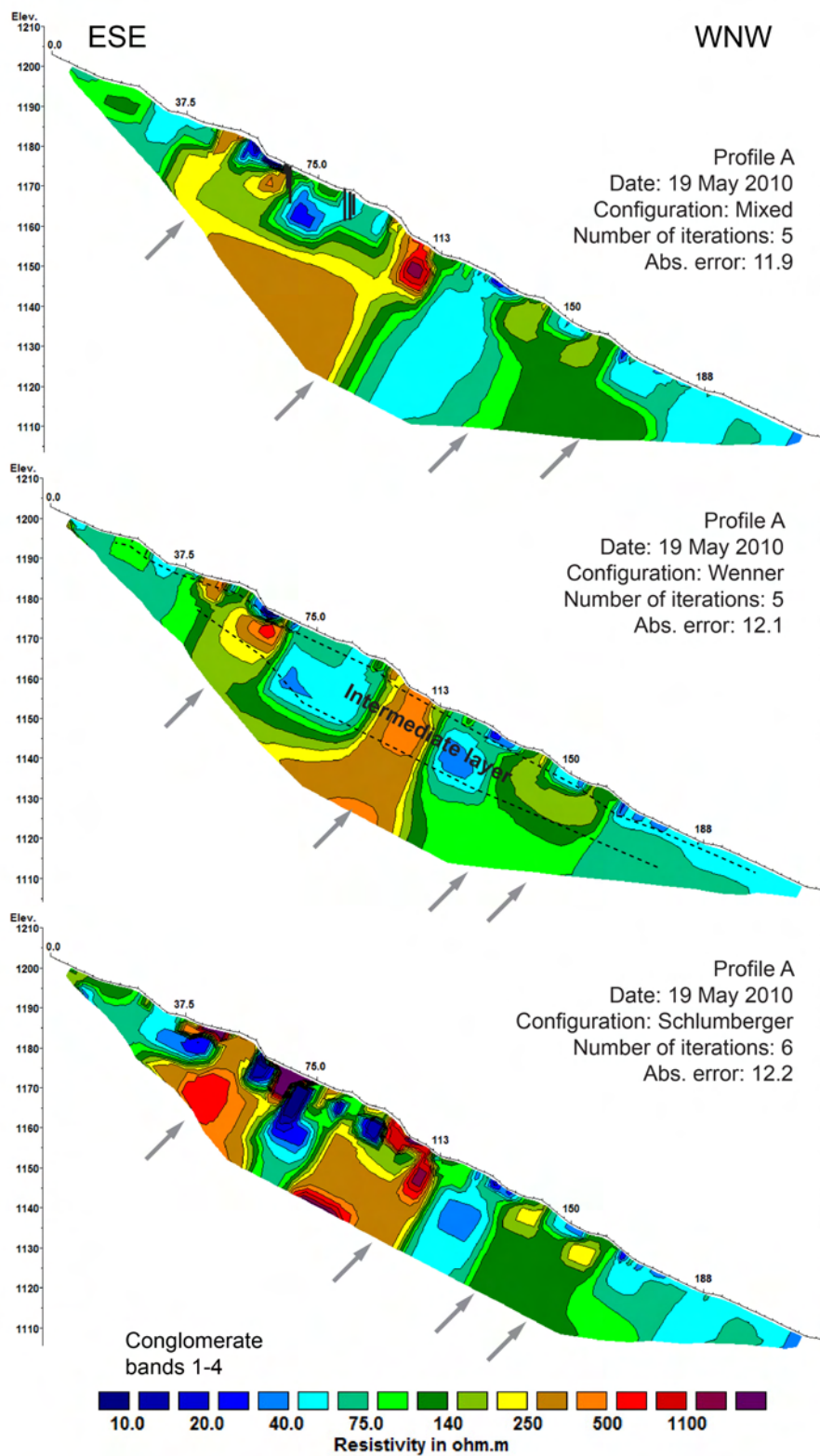
Figure 7.10: *Profile A recorded on 19 May 2010 with three different array methods: Top: mixed method, middle: Wenner, bottom: Schlumberger.*

when water was lost in the drill hole.
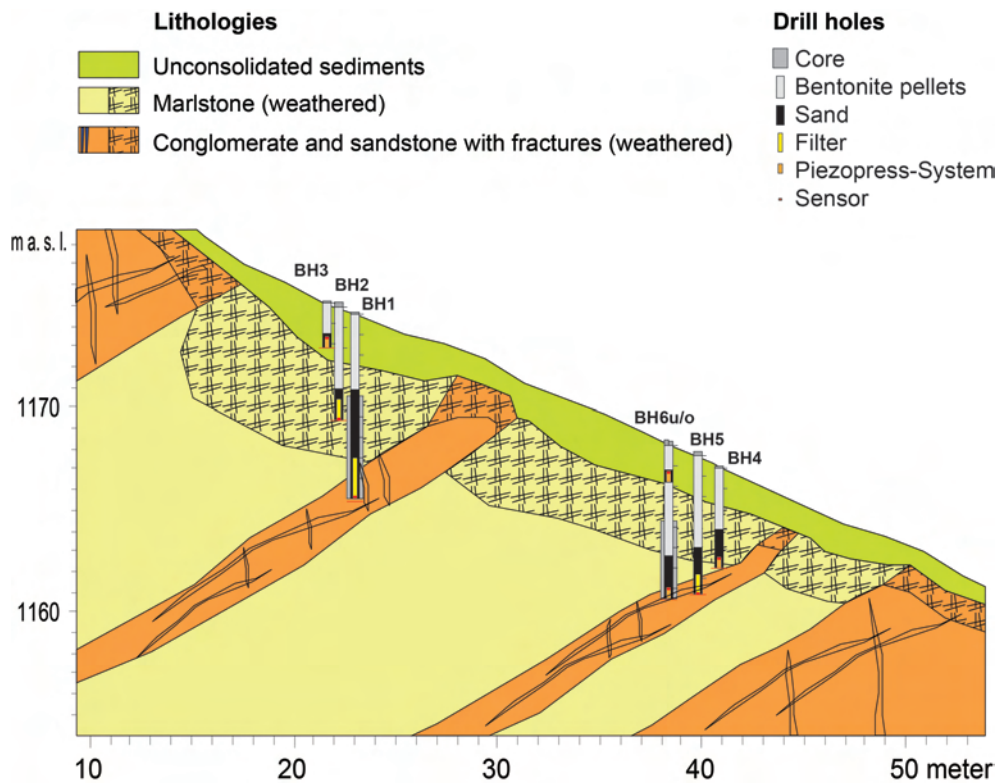
Figure 7.11: *Profile along the Rufiberg slope showing the six drill holes. The type of refilling material, observation well and sections where a rock core was evacuated are indicated. The bottom of the wells was refilled with sand for at least one meter. The rest of the bore hole was sealed with compactonit pellets to avoid bypass.*

It was expected to find groundwater rather in joints in the conglomerate and sandstone formations than in marlstone. Based on the ERT profiles and observations in the field, three drilling locations were initially planned in the vicinity of the long ERT profile: on the road to catch an aquifer in the thick conglomerate bed number 4, (see Figure 7.9), below this conglomerate layer where a thin layer of competent rock was expected, and above the second thick conglomerate bed below the test site. At each location, three observation wells were planned, one in the unconsolidated sediment, one in the weathered bedrock layer and one in the fresh but fractured bedrock. It was planned first to core the deepest drill hole in order to know the lithological profile and then to drill destructively the two other shallower drill holes just beside the first one. An option was to install two piezometric tubes into the same drill hole depending on the depth of the sensors (minimum 5 m spacing between two sensors in order to prevent by-pass of groundwater).

Because of the complicate manoeuvre of the drilling rig and the unfavourable soil and rock material, the drilling had to be adapted successively. The rig could only be moved in the axis of the slope as it was mounted with a cable and it was only possible to drill at less steep places in the slope. Additionally, it turned out that the soft weathered bedrock and the very hard sandstone and conglomerate rock was difficult to core. Even with the destructive method it was not possible to pass a certain depth. Finally, it was feasible to drill each three holes at two locations which are 20 m apart. The locations of the two clusters are shown on Figure 7.8. Photographs on Figure C.1 in Appendix C show the clusters and Figure 7.11 shows a geological profile with the six drill holes and installations. Table 7.2 gives an overview of depth and

drilling method (destructive or coring) for each drill hole. Boreholes BH1, BH5 and BH6 had to be stopped because the drilling rig could not pass the hard conglomerate or sandstone bedrock.

Two different systems were used to equip the boreholes: Open water piezometer to measure the peizometric level and the sealed PiezoPress system to measure the water pressure (see Section 4.8). At the bottom of each borehole a sensor was placed. In BH6, two observation wells equipped with sensors were installed. It was planned to use 2"-tubes for the open water piezometers to be able to take water samples for chemical analyses. But it turned out that it was very difficult to fill the boreholes with sand and compactonite (bentonite-clay pellets) when a 2"-tube was installed, because the drilling diameter of 7 cm was too small. Therefore, in the second cluster, also for the open water table piezometer 1"-tubes were used. The length of the slotted filter and the sand refilling was between 0.5 and 2 m.

Location/	Name	Depth	Method	Sensors	Diameter
Cluster1	BH1	9.15 m	4 to 3.1 m core	Pressure sensor in 9 m	2"
Cluster1	BH2	5.5 m	destructive	Pressure sensor in 5.5 m	2"
Cluster1	BH3	2.2 m	destructive	PiezoPress in 2.2 m	1"
Cluster2	BH4	4.9 m	destructive	PiezoPress in 4.9 m	1"
Cluster2	BH5	6.8 m	destructive	Pressure sensor in 6.8 m	1"
Cluster2	BH6o	7.5 m	3.7 to 7.5 m core	PiezoPress in 7.5 m	1"
	BH6u			PiezoPress in 1.8 m	1"

Table 7.2: *Table with the realised drill holes, equipment of the observation well, and the installed sensors.*

7.5.1 Description of the lithologies

Unconsolidated sediment

In BH1, clayey silt - silty clay with little sand and few poorly rounded gravel was found in 0 - 2 m depth. This sediment was plastic and the colour was brown-ochre with orange and blue-grey-greenish mottles. Orange coloured rusty mottles were formed during dry phases under aerobic conditions due to the oxidation of iron. Blue-grey-greenish colours indicate reduction of iron during saturated anaerobic conditions. The conjoint appearance of oxidised and reduced parts indicates a regular fluctuation of slope water. In depth of 0.5 - 1 m, the material was reduced. This lithology is a typical gley and it is interpreted as a weathering product from the underlying bedrock (eluvium) and deposits from ancient small mass movements (colluvium). A more detailed profile from 0 - 1.66 m depth locaded 10 m to the North of drill hole cluster 1 was described by Linda Seward from *Institute for Geotechnical Engineering(IGT)*, ETH Zürich. The transition to weathered bedrock was observed in 1 - 2 m depth. Table 7.3 shows the analysed mean soil parameter for this profile and Figure 7.12 shows the mineralogy, grain-size and plasticity indices of samples from different depth of the profile. The carbonate boundary was found in 1 m depth indicating the zone which is permanently saturated. The amount of illite and smectite, which are typical clay minerals for Molasse rocks (Bilgot, 2011) increases with depth up to 40 wt%. The sand fraction decreases and silt and clay fraction increases with depth. The plasticity index shows a loose downwards trend towards higher plasticity values in 2 m depth from 15 to 26%. The deepest sample at 1.66 m depth has a slightly lower PI of 23% than the sample above. The plasticity values are moderate to high. The soil is classified as medium plastic clay (CM) according to the USCS and SN 670 008 classification. The permeability was calculated with infiltration and pumping tests. k-values of 10^{-8} m/s were calculated with the Lefranc method (see next section). It is possible that locally the permeability in the unconsolidated sediments

is larger due extension cracks, bioactivity and blocks of conglomerate from ancient rockfalls. It is also possible that due to the compaction of the sediment during drilling, the hydraulic permeability around the drill hole decreased.

Total porosity	33%
Density	2.6 g/cm^3
Liquid limit:	43%
Plastic limit:	22%
Plasticity Index:	21%
Activity:	1

Table 7.3: *Mean parameters determined from soil samples between 0 - 1.66 m depth excavated 10 m to the North of drill hole cluster 1. Analyses were performed by Linda Seward from Institute for Geotechnical Engineering (IGT), ETH Zürich.*

Figure 7.12: *Mineralogical composition, grain size and plasticity values of the unconsolidated sediment from soil samples (0 - 1.66 m depth) excavated in a trench located 10 m to the North of drill hole cluster 1. Analyses were performed by Linda Seward from Institute for Geotechnical Engineering (IGT), ETH Zürich.*

Marlstone and fine-grained sandstone

Marlstone interbedded by fine-grained sandstone was found in 2 - 7.5 m depth in BH1 and in 2 - 7 m depth in BH6. This ochre-grey coloured lithology is strongly weathered and fractured. Close to the surface, 2-5 fractures were counted per 10 cm core depth. The fractures are mainly vertical or dipping 30-60°, which favours that the rock breaks into small cubes. The fracture surfaces are red, orange, dark-grey discoloured which indicates that water is circulating in those fractures. The marlstone is very weak and can be broken by hand whereas some interbedded fine-grained sandstone layers are very strong. Some joints are partly refilled with calcite. The volume of the fractures with an aperture > 0.3 mm was calculated by segmentation, a method based on X-ray Computed Tomography For this purpose, the pores > 0.3 mm in a 3D image of a fractured core sample were extracted by image treatment (Grondin et al., 2011). The maximum calculated aperture of the fractures was 0.4 mm and the volume of fractures with an aperture >

0.3 mm was 0.15 %.

Photographs on Figure 7.13 show the different joints and fractures in BH1. The most dominant fracture in the Marlstone was observed in 5.5 m depth. In about 5 m depth, the fractured marlstone started to drain rapidly the drilling water.

Coarse-grained sandstone and conglomerate

In the lowest meter of BH1, very strong conglomerate interbedded with coarse-grained to medium-grained sandstone was cored. The colour of this lithology is light grey, it shows stratifications, is well cemented and without small scale fractures. No alterations caused by water circulations could be observed. Three large sub horizontal fractures could be observed in the conglomerate, but it is probable that they were produced during the drilling. At the end of the drilling in BH1, the water table remained almost constant at the level of a possible fracture at a depth of about 8.5 m (see Figure 7.13, E).

The lowest half meter of BH6 was very strong rock and the core could not be evacuated. The drilling was very similar like in BH1, therefore most likely in BH6 coarse-grained sandstone and conglomerate was also drilled at the bottom.

7.5.2   Groundwater monitoring

The main aim of the drilling was to measure groundwater fluctuations in the bedrock during precipitation and snowmelt. It was expected that the occurrence of groundwater in the bedrock depends strongly on the joints and fractures and thus can vary rapidly in space and time. Due to this heterogeneity, it was not sure if with a few drill holes such a water flow path will be crossed. During destructive drilling, it could be observed if groundwater was reached. In cluster 1, no signs of groundwater were found. In BH4 at 4.9 m depth, humid weak marly material was ejected to the surface, even though the drilling took place in a rather dry period. Therefore it was assumed to have hit an aquifer and the drilling was stopped in this depth. In BH5 which is situated next to BH4, in a depth of 6.5 m several centimetres of water pressure were measured during drilling. Therefore the drilling was stopped at 6 m depth.

Water pressure and temperature in the observation wells were monitored with a 30 min interval from November 2010 until August 2011. These data records and hourly precipitation data from the SwissMetNet climate station Cham/ZG (Swiss coordinates: 677825/226880, 440m a.s.l.) are shown in Figure 7.14. 21 precipitation events were defined (named on Figure 7.14, blow ups of the events are shown on Figures 7.15 and 7.16). 18 of them showed a reaction of the water pressure in the observation wells. Event 4, 7 and 10 showed no reaction in the observation wells. Event 4 was probably snow fall and Events 7 and 10 occurred in a generally very dry period and were not strong enough to saturate the bedrock up to the level of the sensors.

The time span from the beginning of precipitation to the rise in water level in cluster 2 is between 5 and 14 hours. No clear correlation could be made between the recorded water pressure in the drill holes and the cumulative rainfall, beginning, duration, and intensity of rainfall. This could be because Cham is located 12 km to the NNW of the Rufiberg. The long-term annual precipitation in Cham is about 1000 mm, whereas at the meteorological station Zugerberg/ZG (Swiss coordinates: 682975/222000, 920 m a.s.l.) 1500 mm/year are measured. It is assumed that a correlation between the cumulative rain or rain intensity and the maximum water level
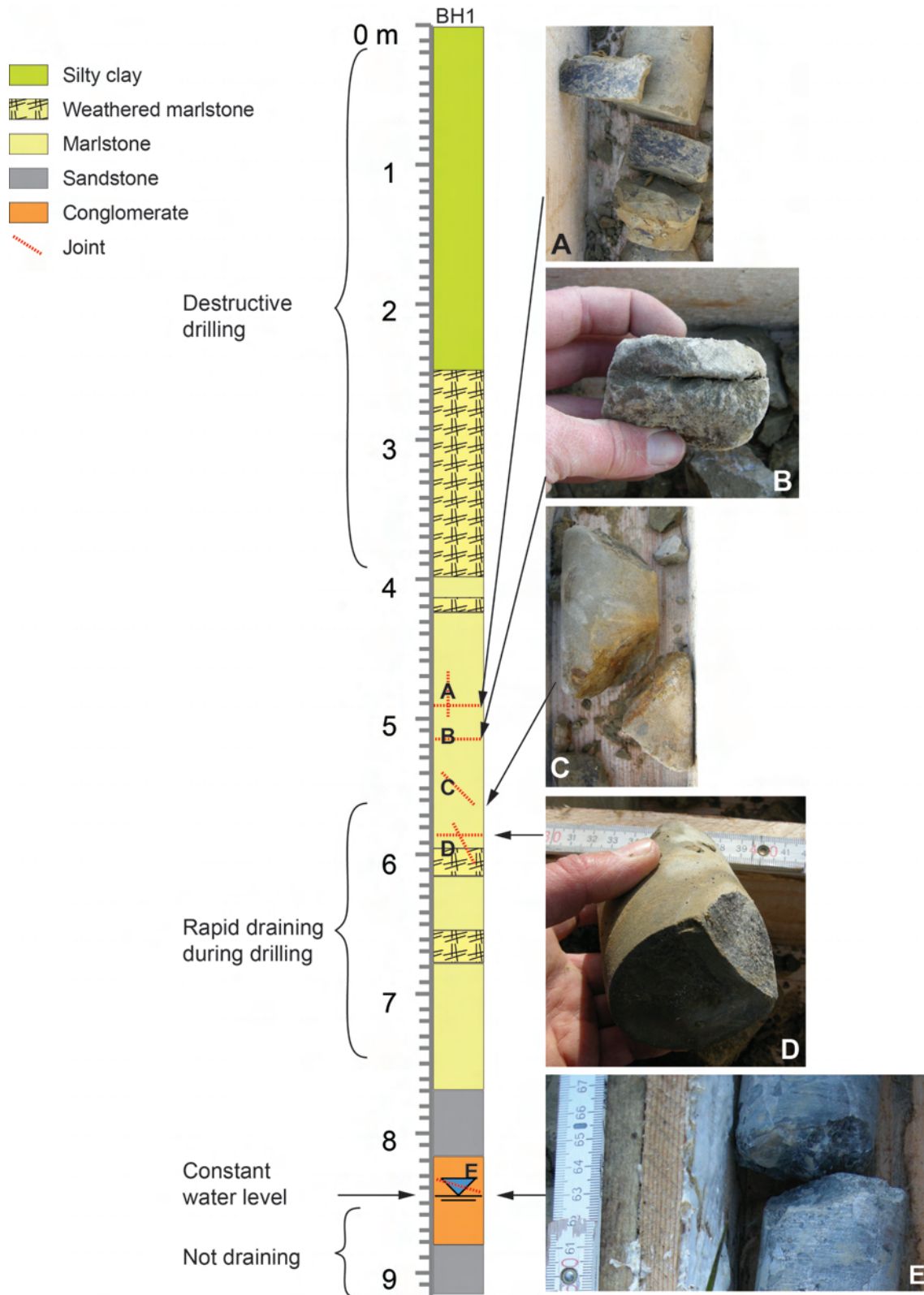
Figure 7.13: *The 9.1 m long core of borehole BH1 (cored 4-9.1 m). The altered bedrock starts at about 2 m depth. The Marlstone is an alteration between very weak and more competent layers and is generally strongly fractured. Hard bedrock (conglomerate and sandstone) starts at about 7.5 m depth. Photographs show different fractures.*
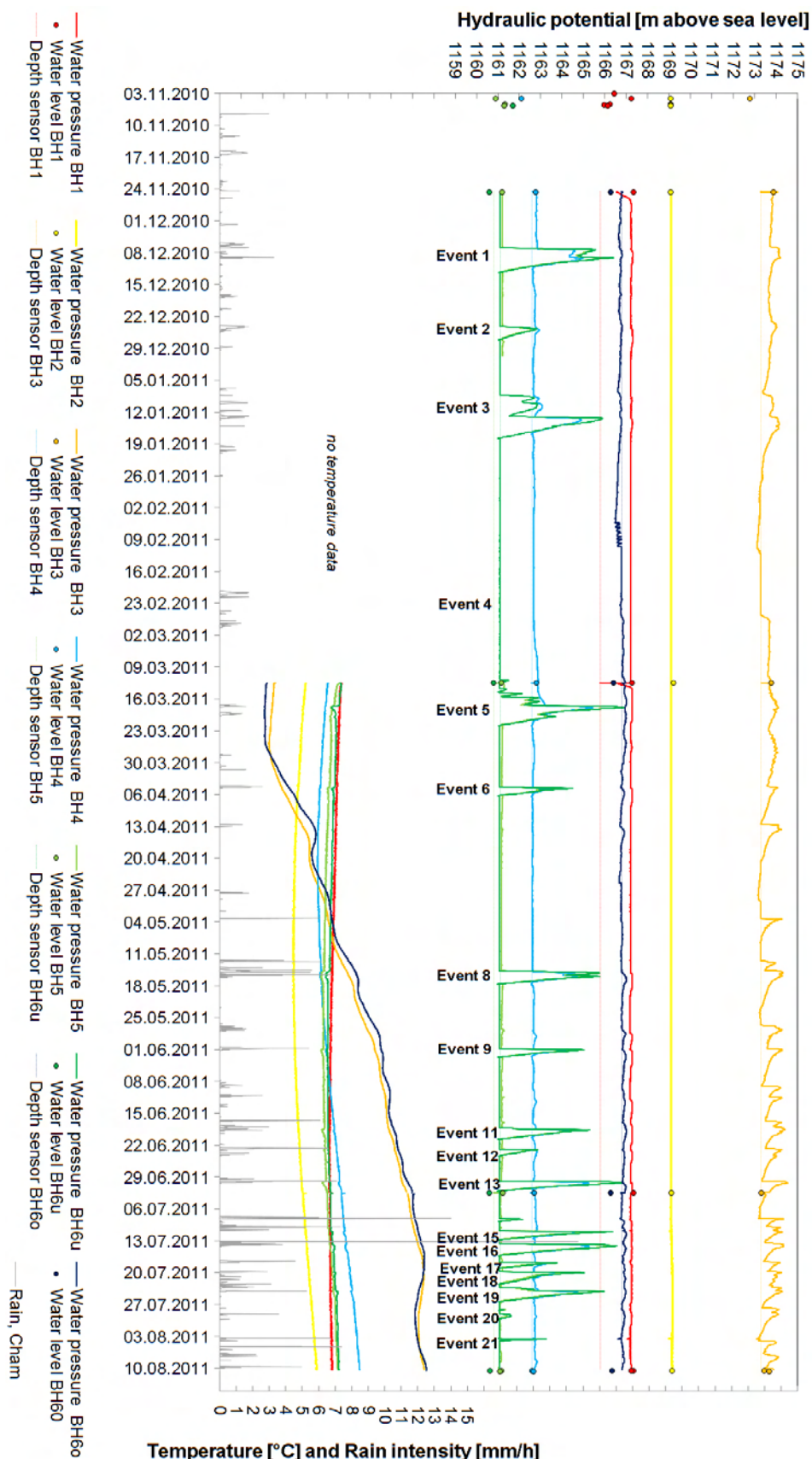
Figure 7.14: *WHydraulic potential in meters above sea level (upper part of the plot) and temperature (lower part of the plot) measured in the 7 observation wells and rain intensity. Additionally, several hand measured water levels are plotted. The resolution of the water pressure sensors is between 2 mm and 1 cm and the accuracy of the height above sea level is 10 cm (measured with a digital GPS). The hourly precipitation record is from the nearby SwissMetNet climate station in Cham/ZG.*
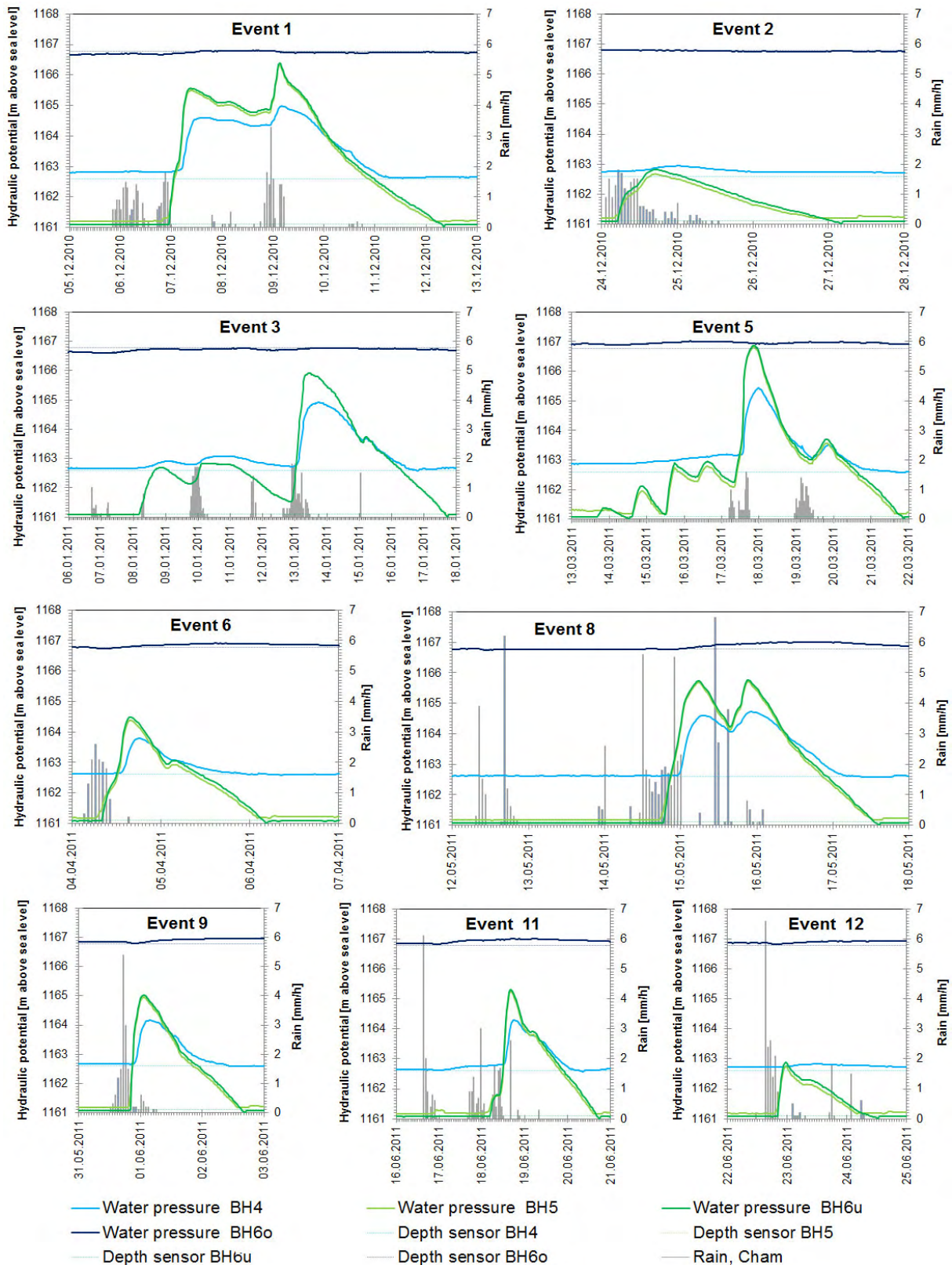
Figure 7.15: *Water level and temperature measured during precipitation events 1 - 12 observed in cluster 2.*
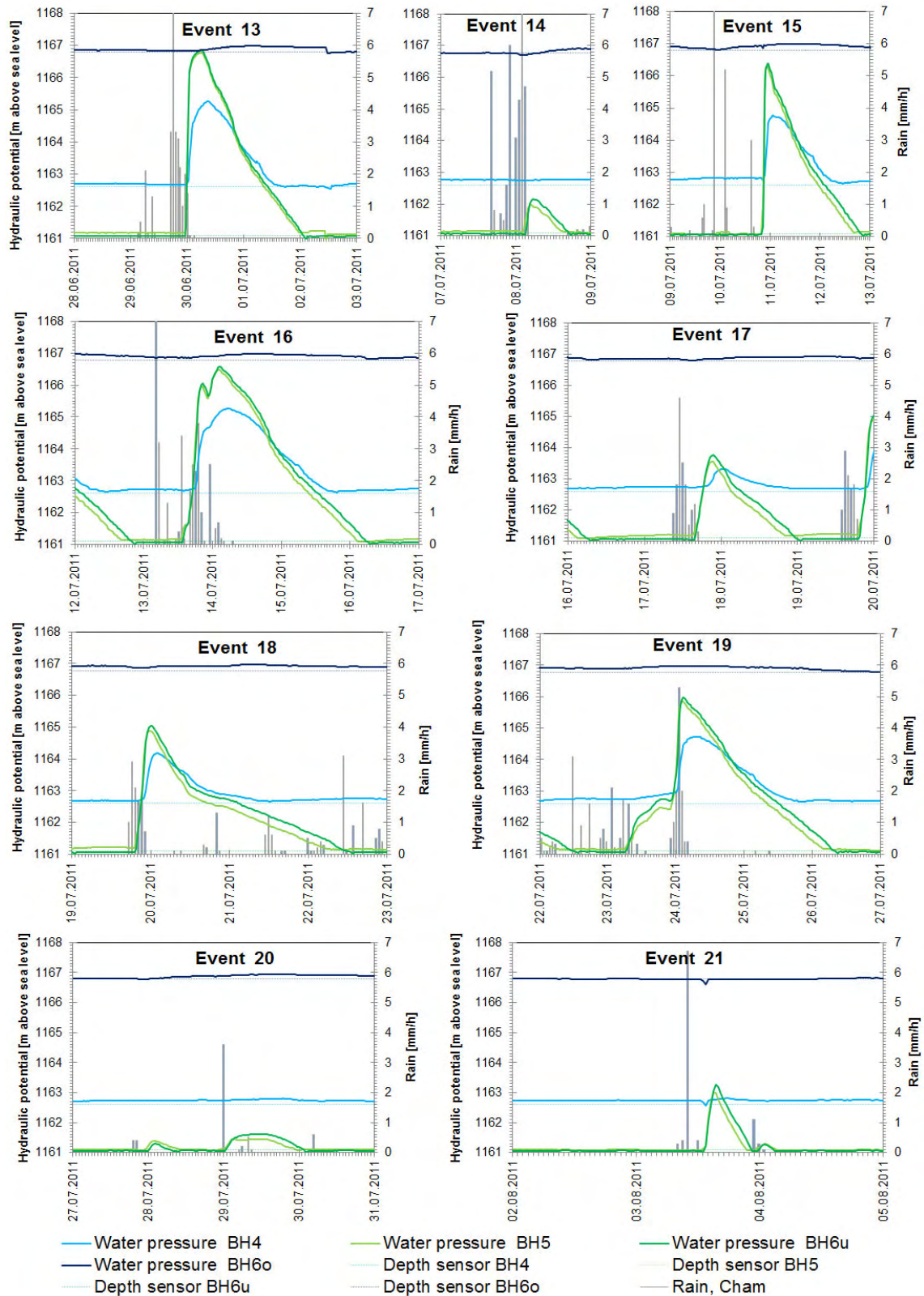
Figure 7.16: *Water level and temperature measured during precipitation events 13 - 21 observed in cluster 2.*

exists. In the following, the data records of each sensor will be described and interpreted.

Sensor in BH1

Description: At the bottom of BH1 at 9 m depth in fresh conglomerate bedrock, a constant groundwater level between 1.4 m and 1.5 m above the sensor was measured. Also the water temperature shows no variations. On 2 July 2011, 3 litres of water were put in the observation well to conduct a small infiltration test. But the water drained immediately. On 24 November 2010 and 16 Mars 2011, small pumping experiments were performed. The water level established slowly in two days and a hydraulic conductivity in the range of 10^{-8} m/s was calculated.

Interpretation: It is likely that at the constant level of the groundwater table, a fracture is draining the drill hole (see Figure 7.13). Below this fracture, water is "trapped" in the observation well. It can not be excluded that water seeps out from the unconsolidated sediment and refilled the bottom of the well after the pumping tests.

Sensor in BH2

Description: Sensor 2 is located at 5.5 m depth in the weathered and fractured marlstone. Only after a rainy period in July 2011, a little pressure of 6 cm was measured, otherwise the well remained dry.

Interpretation: The measured water could have seeped out from the overlaying unconsolidated sediments. Most likely, during the monitored period, the fractures around sensor 2 were draining the bedrock.

Sensor in BH3

Description: This sensor is installed 1.7 m below the ground surface. Generally it responds simultaneously with rainfall and the groundwater rises up to 0.47 m below surface. The falling limbs of the groundwater level curve for those events were used to calculate the hydraulic permeability. With the Lefranc method, k-values of 10^{-8} m/s were calculated. In March 2011, daily fluctuations of about 10 cm with a maximum shortly before midnight were observed. The long-term temperature variations are about 10 °C.

Interpretation: The rapid response after rainfall is lost likely due to bypass along the piezometric tube. The groundwater fluctuations observed in March 2011 of 10 cm in 10 h are most likely due to snowmelt. Temperature variations reflect the ambient temperature because the sensor is close to the surface.

Sensor in BH4

Description: Sensor 4 was installed in wet weathered marlstone at 5 m depth. In this observation well, two types of groundwater variations can be observed:

1. Fluctuations of several tens of cm, which can not be observed in BH5 and BH6u. These variations are best observed at the beginning of Event 5.

2. Sharp peaks similar to those observed in BH5 and BH6u. The maximal rise of those peaks is 2.8 m which corresponds to a level of 1.5 m below ground surface (Events 5 and 13). The groundwater level in BH4 starts rising rapidly when the level in BH5 and BH6u is
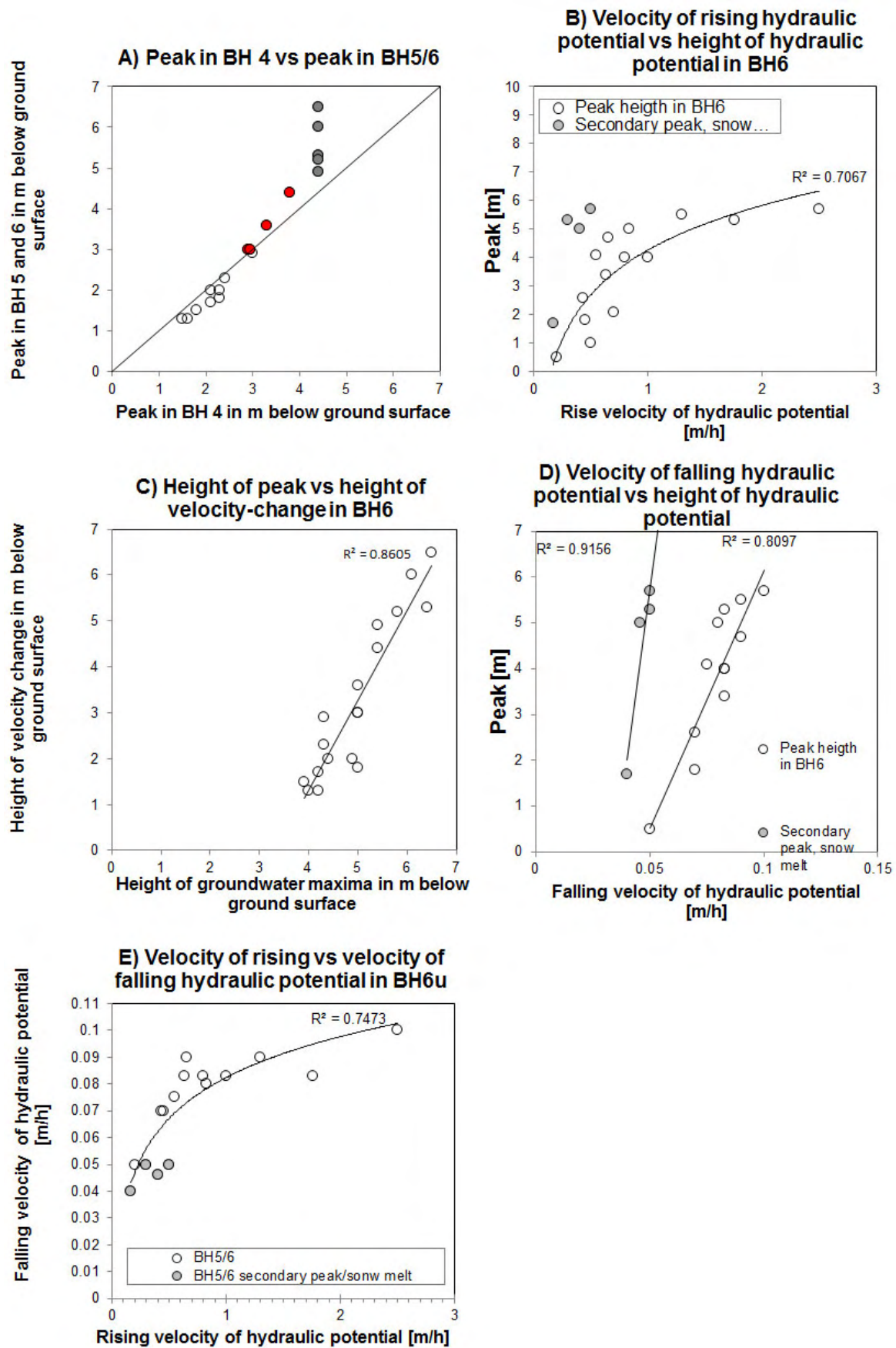
Figure 7.17: *Scatter plots showing the relationship between the velocity of water level increase, water level decrease and maximum water level in cluster2.*

higher than 5 m below ground surface (see Figure 7.17, A, red dots). When the hydraulic potential is shallower than 3 m below ground surface in BH4, BH5 and BH6u, the level in BH5 and BH6u "overtakes" the level in BH4 (see Figure 7.17, A, transparent circles). The groundwater in BH4 is rising with an average velocity of 0.6 m/h, like also in BH5 and BH6u, but the peak is reached with a delay of about 2 h compared to BH5 and BH6u (see for example Event 6). The falling limb of the peaks in BH4 is less steep than the rising limb and also than the falling limbs in BH5 and BH6u. The temperature in BH4 is falling for about 0.1 °C instantaneously with the rapid rising of the water pressure, which is less than in BH5 and BH6u.

After pumping on 12 March and 2 July 2011, water flowed slowly back into the observation well and established at the initial level. A k-value of $6 \cdot 10^{-8}$ was calculated with the Lefranc method.

Interpretation: The two types of groundwater fluctuations show that the water pressure in BH4 is influenced by two different aquifers. The first shallower aquifer can only be observed in BH4. It is probably feed by lateral downhill flow through the fractures in the weathered marlstone after snow melt and strong precipitation. The existence of this aquifer was also seen with the result of the pumping test. The second aquifer originates most likely deeper in the bedrock and is only temporal. Bypass from BH5 and BH6u towards BH4 cannot be excluded because the rapid rise in BH4 is little smoothed compare to BH5 and BH6u and the groundwater level peak is reached about 2 h delayed. The interaction between the two aquifers can be seen on Figure 7.17, A: only when a hydraulic head of 5 m below ground surface is reached in BH5 and BH6u, the second aquifer reaches also BH4. The small reaction in the temperature shows that the water in the drill hole is mixed with fresh water.
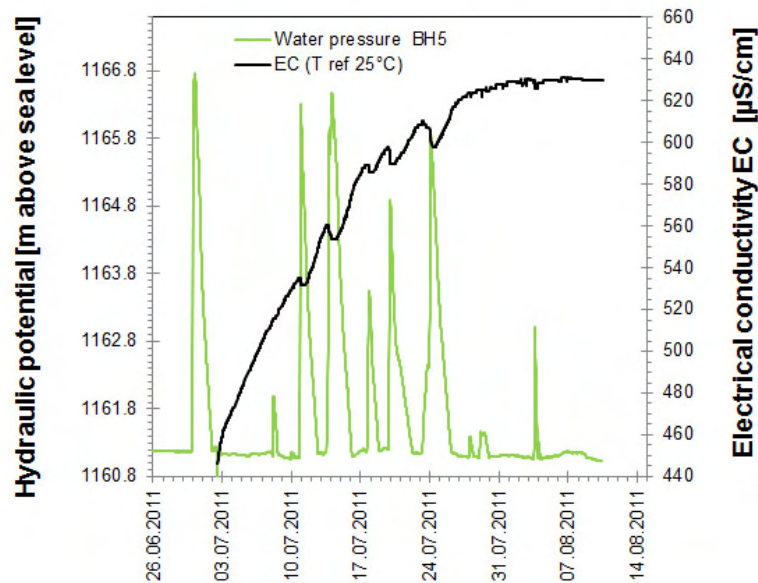
Figure 7.18: *Electrical water conductivity measured in BH5 in July and August 2011. The progressive increase of the EC is most likely due to the settlement of mud at the bottom of the observation well and should be neglected.*

Sensors in BH5 and BH6u

Description: These two sensors react almost identically and are therefore discussed together. They are installed in very hard rock approximately 1 m apart from each other. The two drill

holes have approximately the same depth, but sensor 6 was installed in a sealed Piezo Press system and sensor 5 was installed in an open water piezometer and is therefore 40 cm deeper (see Section 4.8). During drilling, several cm of water were observed at the bottom of BH5. In BH5, a permanent water pressure which is fluctuating between 0.4 and 0.5 m above the ground of the piezometer is measured. After pumping, this water level establishes in few hours. The sensor in BH6u remains dry between the rain events. With the Lefranc method, a k-value of $2 \cdot 10^{-8}$ m/s was calculated based on the rising water table after pumping in BH5. For some events (for example Events 2, 14, 17 and 18), the pressure in BH5 is a few cm lower than in BH6u. Only in the Event 20.1, the pressure was higher in BH5 than in BH6u. Rare fluctuations in the range of 10 cm can be observed in BH5 whereas BH6u remains dry (for example on 16 June 2011 around midnight). The maximal rise in BH5 is BH6u m to a level of 0.8 m below ground surface (Event 5 and 13). Maximal rise in BH6u is 5.8 m to a level of 1.2 m below ground surface.

The velocity of water level rise varies between 0.2 and 2.5 m/h with a mean value of 0.6 m/h. This is also observed in BH4. This velocity of the rising water table correlates logarithmically with the maximum water level (see Figure 7.17, B). This means the faster it rises the higher it rises. After snowmelt (Event 5) or after a first rain pulse (Events 1, 3 and 8), a higher peak is reached (grey circles on Figure 7.17, B). The groundwater level in BH5 and BH6u falls with a bigger velocity than in BH4 and an abrupt change of the velocity can be observed in most events, for example in Event 18 on 20 July 2011 at 12:00 o'clock. First the water table decreases for an average of 0.16 m/h and then it decreases with about half this velocity with an average of 0.08 m/s. The higher the maximum water level, the earlier this velocity change occurs (Figure 7.17, C). The first falling velocity does not correlate with the maximum water level whereas the second falling velocity is linear and seems to correlate with the peak water level (Figure 7.17, D) and the rising velocity (Figure 7.17, E): The faster the level rises and the higher the maximum water level, the faster the level decreases. If the bedrock was initially saturated due to a precedent precipitation event or snow melt, the level rises and falls slower but it reacts immediately and reaches a higher maximum water level (grey circles). The temperature reacts immediately when the hydraulic potential starts to rise (Figure 7.14). In the winter month, the temperature decreases for 0.5 - 0.1 °C and in the summer months it rises less than 0.2 °C. The electric water conductivity EC has been measured in BH5 in July and August 2011 (see Figure 7.18). It rises progressively from 440 to 630 μS/cm and decreases for maximal 15 μS/cm simultaneously with the increase of the hydraulic potential.

The following interpretations of these data were made:

- Rapid rise of the hydraulic potential in BH5 and BH6u a few hours after precipitation events: It takes only a few hours (at least 5 hours) to fill the aquifer in the bedrock up to the level of the sensors (1161 m a.s.l.) after a precipitation event.

- First velocity of water level decrease: This velocity is probably related to the length and intensity of precipitation/snow melt event. It reflects if the end of the rain event was progressively or immediately. If the rain stopped progressively, the hydraulic potential drops slower than if the rain stopped suddenly.

- Second velocity of water level decrease: This velocity is linear and depends on the maximum hydraulic potential. It reflects most likely the draining capacity of the massive. But it is not clear, why this capacity should be larger after reaching a higher hydraulic potential. Data of more precipitation events are necessary to make significant statistics. This velocity reflects probably the draining velocity of the massive in a larger scale, whereas the first velocity reflects the local drainage of the fractures.

- Water level increase in BH5 but not in BH6u, constant water level between 0.4 and 0.5 m in BH5 and pumping test in BH5: It is possible that BH6u remains dry after small rain events whereas BH5 reacts slightly because BH5 is 40 cm deeper than BH6u. Or it is possible that bypass exists between BH5 and the weathered bedrock. The facts that a permanent water table exists in BH5 that the water level established after pumping and that during drilling, a water level of several centimetres was measured, leads to the assumption that the bottom of BH5 touches an aquifer. It is possible that like in BH1, a fracture is draining BH5 at a level between 0.4 and 0.5 m above the bottom.

- Simultaneous decrease in temperature and EC with increase of hydraulic potential: The decrease in temperature and EC is interpreted as mixture with rainwater. Because it is assumed that the water in the observation well is not well mixed with the fresh water, it is not possible to exactly calculate the fraction of fresh water. Using Equation 6.4 and by assuming a rain temperature of 1.5°C for the Event 5 and a rain EC of 50 μS/cm for Event 18, the portion of fresh water would only be 3-7%. But it can be concluded that the water that arrives at BH5 is rather fresh rain water than old piston flow water. No increase of EC can be observed which would indicate piston flow. The progressive rise of EC in Figure 7.18 is most likely due to muddy water that accumulates at the bottom of the observation well and should be neglected. The manually measured water conductivity in BH 5 ranges between 450 and 490 μS/cm. In the two shallow piezometers Bh3 and BH6u, no sudden temperature change can be observed, most likely because the temperature in those observation wells is equal to the rain temperature.

- The fact that the water level in BH5 and BH6u reacts at the same time let to assume that locally the permeability in the bedrock is very large due to joints.

Sensor in BH6o

Description: This sensor is the shallowest one and installed in unconsolidated sediment in a depth of 1.3 m below the ground surface. BH6 was always dry when measured manually (see Figure 7.14). Nevertheless, the pressure record shows a rise in pressure of maximal 24 cm to a level of 1.06 m below ground surface during rain events. The temperature shows a seasonal long-term trend and short-term smoothed fluctuations.

Interpretation: It is not clear if the measured fluctuations are representative because no groundwater table was manually measured in BH6.

Event 5: Snowmelt

Event 5 shows four pore water pressure peaks in BH5 and BH6u on the 13, 14, 15 and 16 March 2011 and also a slight increase of the water pressure in BH3 and BH4 even though no precipitation was recorded. The water level in BH4 rose progressively for about 20 cm and in BH3, groundwater fluctuations of 10 cm in 10 h are observed. The maximum water level in BH5 and BH6u was always reached in the evening between 16:0 and 21:00 o'clock. A very small decrease in the water temperature of less than 0.1 °C could be observed simultaneously with the rise in pore water pressure.

This variations in the water pressure are interpreted as snow melt. In March, maximal snow melt is expected to occur between 13:00 and 15:00 in the afternoon. Thus the water level rose in only a few hours. In Event 5 it can be seen that if the water level was already high due to snow melt (or a precedent rain event), a further small pulse of rain leads to an instantaneous rise of the water table in cluster 2.

7.5.3   Hydrogeochemistry

The major ions of water samples from a creek located 150 m to the NE of the test site, from a spring located between the two ERT posts 17 and 18, and from BH1, BH4 and BH5 were analysed. The main objective of these analyses was to compare the different groundwater and to see if they originate from the same aquifer. The results of the analyses are shown in Table C.1 in Annex C. In all samples, the main ions were HCO_3^- and Ca^{2+} with concentrations of 50-100 mg/l and 100-400 mg/l, respectively. In the samples from the observation wells, additionally small concentrations of Mg^{2+} and SO_4^{2-} were measured.

The difference in the water chemistry was best observed by plotting the concentration of Mg^{2+} versus the concentration of SO_4^{2-} (see Figure 7.19). The water from the spring and the colluvium was not in contact with sulphate. The origin of the spring is probably the unconsolidated sediment and not the bedrock. The groundwater in the three observation wells shows a slightly different signature in sulphate and magnesium. This shows that the aquifers of the three wells are probably separated from each other by low permeable layers. This is consistent with the interpretations based on the pore water pressure measurements: The water in BH1 may be trapped in the low permeable conglomerate bedrock. The groundwater in BH4 represents a local small aquifer in the weathered marlstone and in BH5 a local aquifer which is 2 m deeper is measured. During high water, the water level in the bedrock rises and BH4 and BH5 become most likely connected.
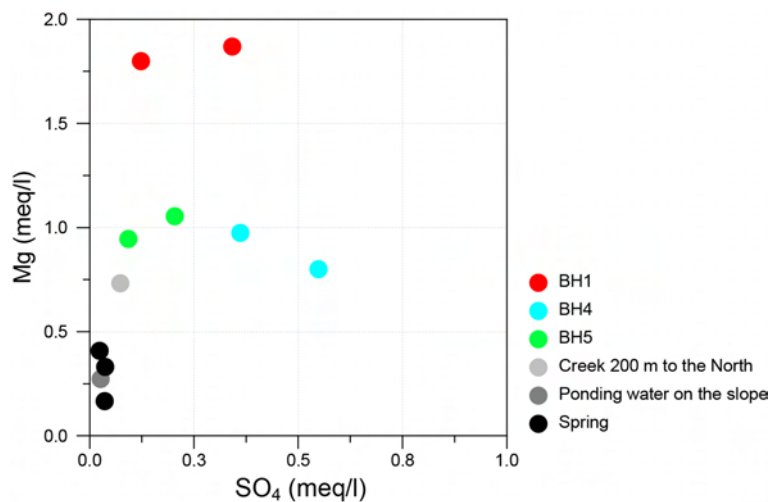
Figure 7.19: *Mg^{2+} vs SO_4^{2+} concentrations of groundwater from the drill holes compared with spring and creek water.*

7.6   Hydrogeological conceptual model

Figure 7.20 summarises the hydrogeological observations and measurements made in the drill holes on the Rufiberg test slope. Swampy areas and hydrophilic plants give evidence that a lot of water is present in the slope of the Rufiberg. The unconsolidated sediment remains always partly saturated due to the small permeability and high water retention. It is likely that the weathered bedrock below the unconsolidated sediment is more permeable due to numerous fractures and joints. Therefore, a capillary barrier may form along the interface between unconsolidated sediments and weathered bedrock. On the one hand, the weathered bedrock may be locally saturated where it is underlain by low permeable fresh marlstone. On the other hand, where it is underlain
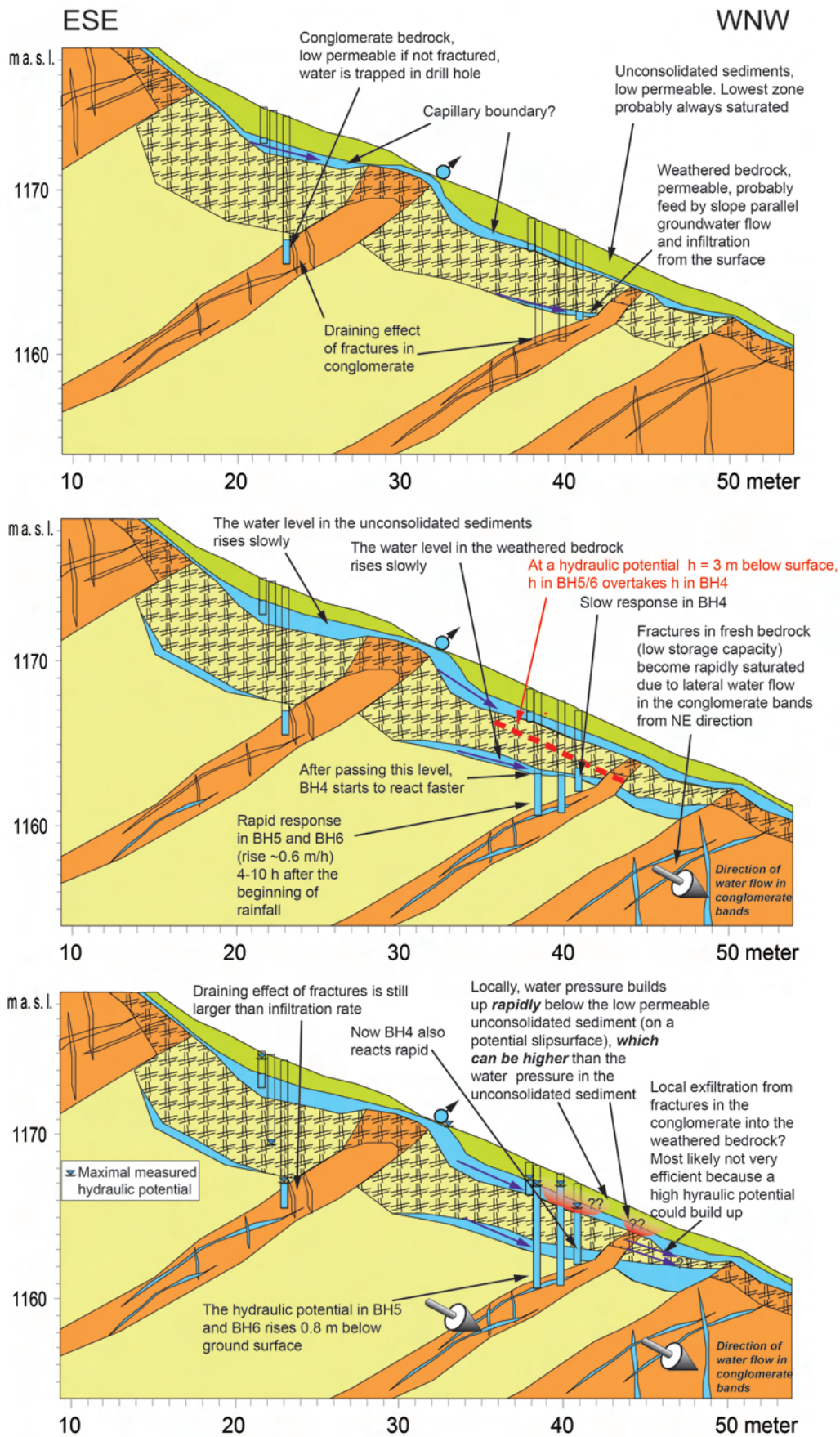
Figure 7.20: *Conceptual hydrogeological model of the Rufiberg for dry periods (top), after a small rainfall event (middle) and after a strong rainfall or snowmelt together with rainfall (bottom).*

by conglomerate and sandstone beds, large joints and fractures may drain it during dry periods. Thus, the bedrock is locally an aquiclude (marlstone, unfractured conglomerate and sandstone) and locally an aquifer (weathered bedrock and fractures in the conglomerate and sandstone).

A few hours after the start of a rain event, the groundwater starts rising slowly in the aquifers in the unconsolidated sediment and the weathered bedrock, whereas it starts rising rapidly in the fractures of the conglomerate and sandstone bands in cluster 2. The decreasing temperature and hydraulic conductivity that coincides with the rising water pressure in the drill holes in cluster 2 let assume that young precipitation water fills rapidly the fractures in the bedrock. The water level in the bedrock starts to rise as soon as the infiltration (related to the rain intensity) exceeds the draining capacity of the fractures. It is like a bathtub with a small outlet: The water level in the bathtub starts rising if more water flows in than can flow out. The volume of the fractures and thus the storage capacity of the bedrock is most likely small then also after small rain events, the water pressure increases rapidly.

The permeability of the unconsolidated sediment is too small as that the rapid raising hydraulic potential in 7 m depth could be explained by in-situ infiltration from the surface. Not even an irrigation experiment (Maries, 2011) which was conducted on the test site did not give any signal in the observation wells. Most likely, the water infiltrates further upslope where fractured conglomerate bands are outcropping and flows along this lithology in a SW direction. Thus it is important to look at the system in three dimensions. When the hydraulic potential in BH5 and BH6u reaches a level of 5 m below ground surface, also the level in BH4 starts to rise rapidly. When a level of 3 m below ground surface is reached, the groundwater level in BH5 and BH6u "overtakes" the level in BH4. This leads to the assumptions that two aquifers exists: one in the fractured bedrock (BH4) and one in the joints in the deeper bedrock (BH5 and BH6u). The two aquifers are only connected, when the water level rises high enough.

In all three boreholes of cluster 2, the hydraulic potential may rise higher than the saturated zone in the unconsolidated sediment. This provokes an additional pore water pressure (overpressure, see Section 2.5.6) from below the potential landslide. The fact that the pore water pressure rises more or less constantly during one event (thus the rising did not change when reaching the weathered bedrock) leads to the assumption that the draining effect of the weathered bedrock layer can be neglected. Otherwise the hydraulic potential would probably rise slower when the groundwater level reaches the weathered bedrock. The water storage ("fractured pore space") is assumed to be larger in the conglomerate than in the weathered marlstone.

If the fractures in the bedrock are saturated from a precedent precipitation event or snow melt, the pore water pressure rises immediately when it starts raining. This leads to the assumption that the rain water infiltrates close to the drill holes, approximately 10 - 100 m. It is difficult to assume the travel time of the water from the infiltration location to the drill holes because the size of the aquifer that has to be filled with water is not known. Most likely, the pore water pressure in the drill holes starts to rise because the water table in the slope rises and not, because the wetting front through the fractures arrives at the sensors. A rough estimation is made by assuming a flow path of 100 m and a reaction time of 10 h which results in a flow velocity of 10 m/h which corresponds to a k-value of in the range of 10^{-3} m/s. Berner (2004b) conducted a tracer experiment in the year 2003 between the Rufiberg road (Swiss coordinates: 682930/215810, 700 m a.s.l.) and a spring at Guggli on the Rufiberg (Swiss coordinates: 682580/215640, 400 m a.s.l.). He measured a main flow velocity of 10^{-5} m/s and a less distinct velocity of 10^{-3} m/s. He assumed that rapid flow occurs trough joints in the sandstone layers and along the interface

with the low permeable marlstone layers.

Two important conclusions can be made:

- The pore water pressure in the bedrock in 7-5 m below the ground surface can rise rapidly up to at least one meter below the ground surface in a few hours after a normal rain event started.

- If a precipitation event coincides with snow melt or occurs after precedent precipitations, the water level rises immediately and reaches a higher value.

Important questions are:

- Is this raise in hydraulic potential just a very local phenomenon in small fractures in the bedrock or does the pore water pressure increase in a larger area along a potential slip surface?

- How high must the hydraulic potential below a potential landslide rise for triggering?

- What rain intensity and duration is necessary to reach such a pore water pressure?

The fact than in all three drill holes of cluster 2 a rise in porewater pressure was measured leads to the assumption that this phenomenon can occur at least in an area in the range of square meters. The effect of this groundwater overpressure is discussed in the next section. For further analyses of rain intensities, data from an in-situ rain gauge and a longer monitoring period would be necessary.

7.7 Hydrogeological triggering mechanisms

Figure 7.21 shows the application of the hydrogeological classification for the case of the Rufiberg slope. In the area of the test site, the Rufiberg can be divided in three layers: A top layer of very low permeable unconsolidated sediment with a thickness of 1 - 2 m, an intermediate layer of weathered bedrock and a bottom layer of fresh bedrock. If joints cross the bedrock, which is the case in the sandstone and conglomerate formations, it is permeable, whereas the fresh marlstone is assumed to be impermeable. Additionally, the changing saturation of the underground in time 7.20 is displayed: For the conglomerate the saturation changes from 3D $\rightarrow$ 6D ($\rightarrow$ 6E) $\rightarrow$ 6I and for the marlstone bedrock 3D $\rightarrow$ 5D $\rightarrow$ 5G. The criticality of the Rufiberg slope to landslides is shown on Figure 8.9 in Chapter 8. It may be not clear why a type 3 can change to a type 5 or 6. This is, because three-layer cases like Rufiberg are reduced to two layer-cases if only the upper two layers are concerned (see Section 3.3.4).

In all cases shown on Figure 7.21, the increasing porewater pressure and seepage force in the unconsolidated sediment and a high plasticity index may favour slope instabilities. Inner erosion can rather be neglected due to the small grain size of the material. A more critical situation establishes when the saturation in the bedrock reaches the potential slip surface. Then also upward seepage and the build-up of overpressure should be taken into account as potential triggering mechanisms. The importance of groundwater flow through the weathered marls for the triggering of landslides has also been discussed by Eberhardt et al. (2005). Additionally, Berner (2004b) mentioned the small sediment thickness as unfavourable for the triggering. Thus the dominant type for the triggering at Rufiberg is 6I. The other types mentioned in Figure 7.21 may just help to make a simple conceptual model of the slope. In the previous section it was mentioned that the hydrogeology in the Rufiberg slope should be viewed in three dimensions because the
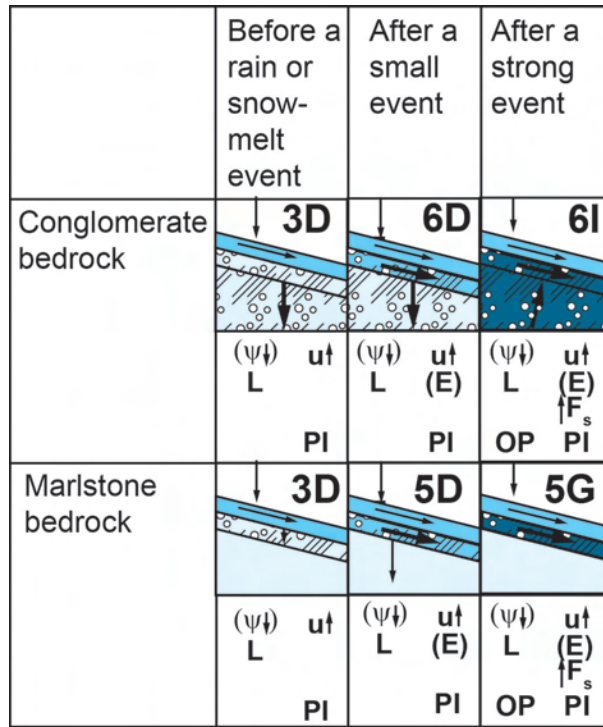
Figure 7.21: *The hydrogeological classification applied for the case of the Rufiberg: It can be distinguished if the bedrock consists of conglomerate/sandstone or marlstone. Furthermore, the different saturation phases are displayed.*

groundwater flows laterally in the conglomerate bands. Nevertheless, for the evaluation of the potential triggering mechanisms three dimensional situations can be reduced to two dimensional types. In the case of Rufiberg, this is because the overpressure that acts on the potential slip surface builds up from below the landslide. It is not important, if the groundwater in the bedrock was flowing laterally or in a downslope direction.

A simple infinite slope model has been made to estimate the critical height of the hydraulic potential on the slip surface by the use of Equation 2.19 simplified to 7.1.

$$SF = \frac{c' + ((\gamma z_2 \cos^2 \alpha - (h\gamma_w)) \tan \varphi'}{\gamma z_2 \cos \alpha \sin \alpha} \tag{7.1}$$

The following soil paramaters were used:

Cohesion c':	16 kN
Friction angle φ':	21°
Unit weight γ:	18 kN/m^3
Slope angle α:	30°
Slip surface depth z_2:	2 m
Seepage direction λ:	90°, slope parallel

Table 7.4:

The parameters are based on laboratory analyses of an undisturbed sample (nr. 47600, 64-78 m depth, PI = 21%, permeability 2.2 10^{-10}m/s) performed by Maries (2011) and the correlation Tables of Dysli and Steiner (2011) (Table 3.1 for friction angle and Table 3.6 for cohesion). If a soil thickness of 2 m and slope parallel seepage are assumed, the slope becomes unstable when

a hydraulic potential on the slip surface of about 3 m is reached (corresponds to 1 m above the ground, see Figure 7.22).
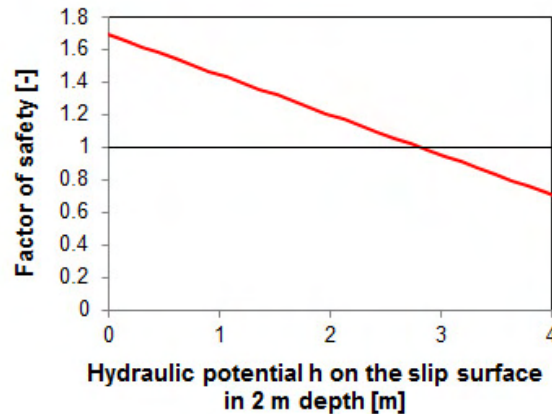
Figure 7.22: *Factor of safety for a confined aquifer at Rufiberg. The factor of safety value plotted is against the hydraulic potential on the slip surface for an infinite slope model (see Equation 7.1).*

The hydraulic potential h on the slip surface depends on the seepage direction λ. If slope parallel seepage is assumed, h on the slip surface is equal to h measured in the drill holes (see Figures 7.23 and 2.9.6b). The maximum measured h was 0.8 m below the ground surface during Event 5 an 15. Thus the potential should rise 1.8 m higher than during Events 5 and 15 to become critical.
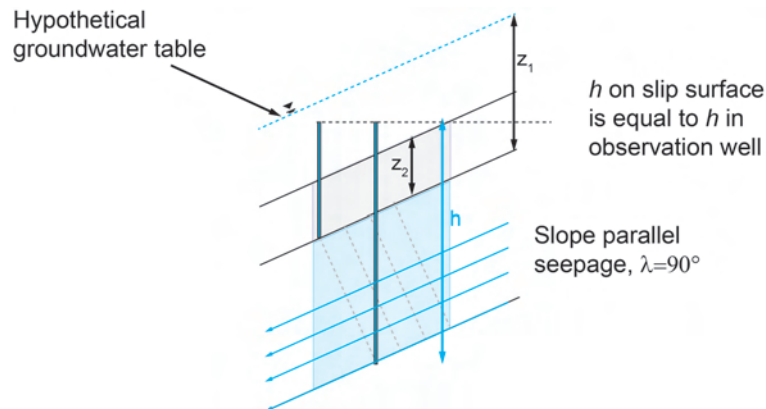
Figure 7.23: *The hydraulic potential on the slip surface is equal to the hydraulic potential in the drill holes if slope parallel seepage is assumed.*

During precipitation events, the hydraulic potential was approximately slope parallel in BH 4,5 and BH6u and the thickness of the colluvium is assumed to be more or less constant and very thin with respect to the length of the slope. Therefore, it is assumed that an infinite slope model can be used to obtain a rough idea of the forces acting on the slip surface. The unknown parameter is the extension of the fractures and thus the extension and exact location of the overpressure acting on the slip surface. In the three boreholes which cover a length of 2 m of the slope, an overpressure was measured. Thus it is possible that the extension of the overpressure acting below the slip surface is in a range of square meters. Thus it can be concluded that the pore water pressure that may build up from below a potential landslide on the Rufiberg cannot be neglected for slope stability analyses, unless it exists a subaerial bedrock outflow that prohibits

the formation of higher overpressure than measured in the year 2011.

Especially if snowmelt and strong rainfall coincide or when several strong rainfalls occur in a few days, the draining capacity of the bedrock may not be sufficient and most likely large pore water pressure can build up from below the potential slip surface. This explains the "fountain like water" extruding from the Rufiberg slope that was observed by Sigi Weber in August 2005.

As seen on the map Figure 7.3, the geological setting with a succession of conglomerate/sandstone bands altering with marlstone dipping approximately 30° towards SE is typical for the entire region. Therefore it is assumed that the triggering mechanisms described on the Rufiberg test site are representative for the entire region.

Chapter 8

Application of the classification

In this chapter, the hydrogeological classification is applied on seven landslides which are described based on literature. Three of those landslides are located in the Swiss Alps, three in the Jura Mountains and one in the French Sothern Alps. A tectonic map of Switzerland with the location of these landslides (and the three case studies presented in Chapters 5, 6 and 7) is shown on Figure 8.1.
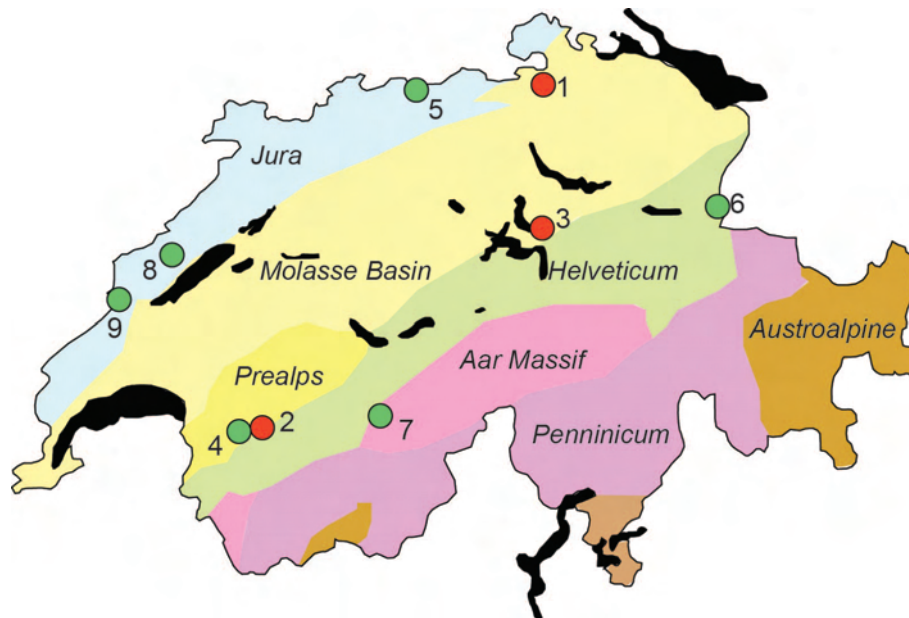
Figure 8.1: Tectonic map of Switzerland showing the location of the three case studies and additional discussed landslides. 1: Rüdlingen, 2: Pont Bourquin, 3: Rufiberg, 4: La Frasse, 5: Steinernase, 6: Triesenberg, 7: Wiler triggering experiment, 8: Travers, 9: La Vraconnaz.

8.1 La Frasse landslide (5H)

The La Frasse landslide is located in the Western Prealps of Switzerland between the villages Aigle and Le Sépey (mean Swiss coordinates: 569200/134000, mean altitude: 1000 m a.s.l.). It is 2000 m long, 500-1000 m wide and the presently active slide is 40-80 m deep. The slope angle is about 11° in the upper part and 20° in the lower part. The landslide has been active for millennia. The long term average velocity is 10-15 cm/year, but during crisis (e.g. 1910-1914, 1966, 1981-1982, 1993-1994) the landslide movement was accelerated up to 1 m per week (Tacher

et al., 2005).
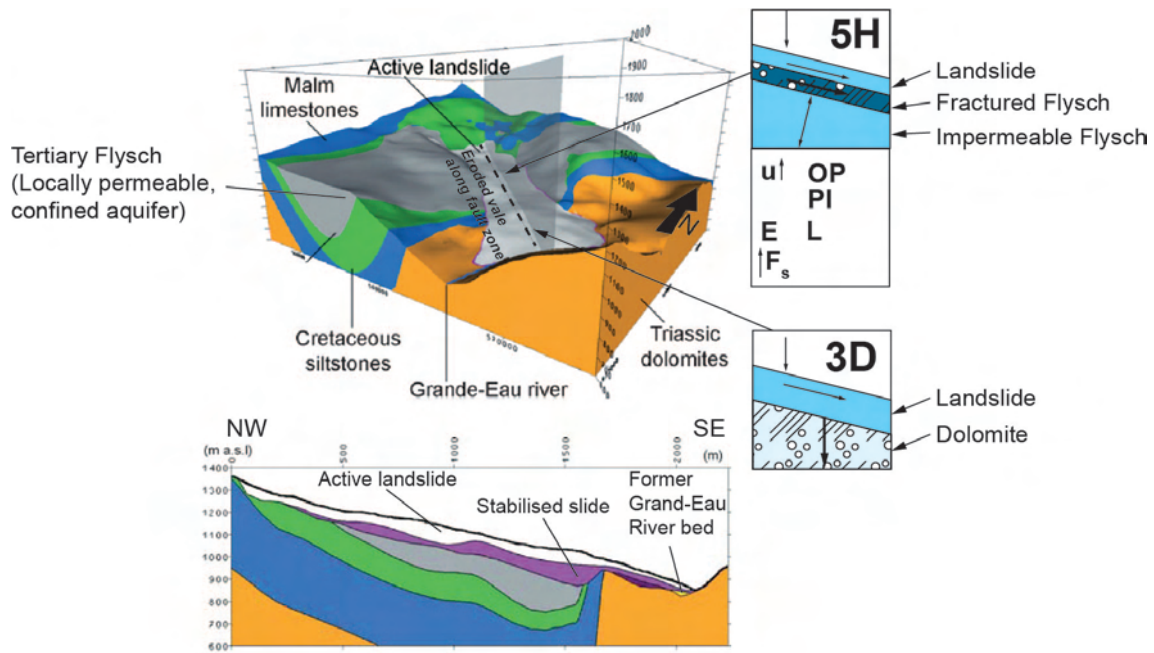
Figure 8.2: *3D model and cross section of the La Frasse landslide. Modified after Tacher et al. (2005).*

The landslide is crossing a syncline of Mesozoic sediments composed of Triassic dolomites, Malm limestone, upper Cretaceous siltstone, and in the core Tertiary Flysch of the Simmen nappe (see Figure 8.2). The Flysch is composed of sandstones and clay schist which gets heavily weathered to plastic black clay with sandy blocks. The deeper inactive landslide mass is composed mainly of Flysch and the upper active 40 - 80 m are composed mainly of moraine. During glaciation periods a vale was eroded along weak fault zones perpendicular to the strike of the syncline. 14'000 years ago, the glacier retreated and the weak Flysch material had no longer a barrier at the toe, neither the compact Mesozoic sediments nor the ice.

The landslide mass is very heterogeneous with locally confined groundwater bodies. It is surrounded by in-situ Flysch. Preferential water circulation occurs along the main slip surface and in the fractured Flysch mass. Groundwater exfiltrates locally from the fractured Flysch and the slide is fed laterally by the in-situ Flysch rather than by direct infiltration from the surface. The carbonate bedrock in the lower part of the landslide is unsaturated and has a draining effect. At the toe, the Grand-Eau River is draining and eroding the landslide. The landslide activity does not show an important reaction to strong precipitation, it is rather past rainfall that influences in a smoothed way the velocity of the actual landslide.

The up-slope part of the La Frasse landslide can by classified as 5H. The Flysch, which is generally low permeable, is fractured. Thus preferential flow occurs through more permeable fractured Flysch layers. Locally, confined groundwater patches may be formed in the fractured Flysch. The lower part of the landslide, where the dolomite has a draining function, is classified as type 3D. But 5H is the dominant type for the acceleration of the La Frasse landslide. The acceleration mechanisms which should be taken into account according to the classification are: increasing pore water pressure, seepage force, liquefaction, overpressure and mechanisms related to a high plasticity index. Seepage erosion may play a minor role due to the fine grained moraine material.

The application of the classification to the La Frasse landslide showed that large deep seated landslides may be divided in different saturation-permeability types. This helps to illustrate different parts of the landslide where several mechanisms are important. The question may arise, how this conceptual model of the La Frasse landslide would look like, if not data from tracer experiments and observation wells would be available. It is not sure if then the Flysch would have been identified as aquifer and the dolomite as sink for the groundwater. It would have been difficult to know, if semi-confined aquifers and subsequent overpressure act as triggering mechanisms. Nevertheless, first conceptual model could have been made with explanations of the assumptions for the permeability and saturation stages of the different units and possible sources of the groundwater in the landslide could have been defined.

8.2 Steinernase landslide (5D)

The Steinernase landslide is located along the River Rhine between the villages Stein and Mumpf in canton Aargau (mean Swiss coordinates: 637000/266000, mean altitude: 300 m a.s.l.). It is about 10 m deep and 1 km long. The landslide accelerates after rain events. A delayed reaction after long-term rainfall is not observed. It is particularly active in winter time. Movements of several decimeters per year are measured.
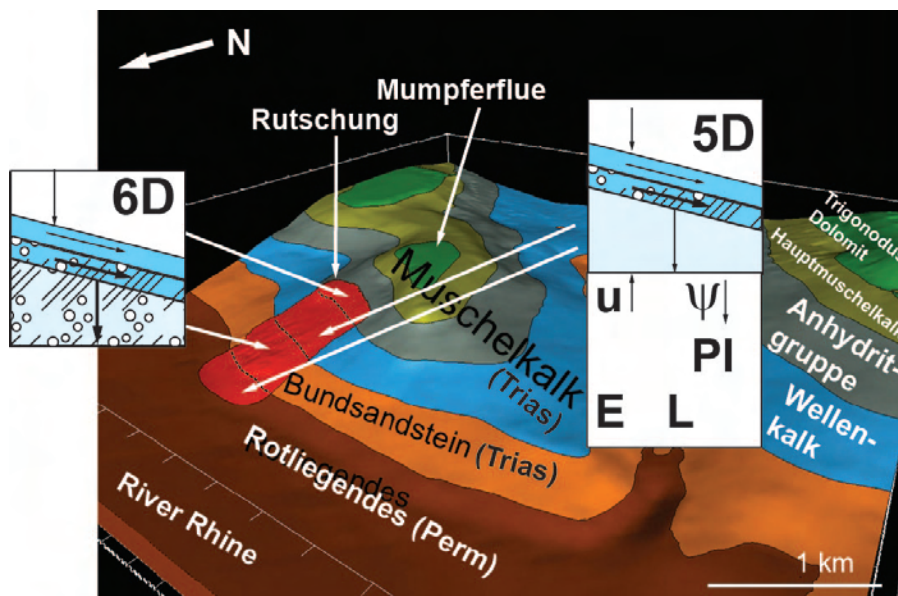
Figure 8.3: *Geological 3D-model of the area around the Steinernase landslide. Modified after Parriaux et al. (2008).*

The landslide shows several internal slip surfaces and is composed mainly of low permeable colluvium. At the toe, permeable alluvium drains the slope into the River Rhine. In the upper part, the landslide is underlain by anhydrite which is permeable and which acts rather as a drain for the slope. In the middle part the landslide is underlain by Triassic sandstone which is permeable due to weathering and joints. The toe of the landslide is underlain by low permeable Permian sand- and siltstone. Figure 8.3 shows a 3D geological model of the area(Parriaux et al., 2008).

The watershed is small and the hydrogeological catchment is equal to the hydrological catchment. The water in the landslide originates from in-situ infiltration at the surface (Parriaux

et al., 2008). The convex shape and hollow structure of the slope favours the accumulation and infiltration of water in the area of the landslide. Little surface runoff is observed. Observations of springs and groundwater in drill holes showed that dominant water flow occurs along the weathered bedrock and the slip surface (Parriaux et al., 2008). Preferential flow occurs along pipes in the landslide body, along tree roots and most likely also along the weathered bedrock. High sulphate concentration in springs located in the lower part of the landslide shows that the water was in contact with anhydrite (in the area of the head scarp of the landslide).

The Steinernase landslide is considered as 5D type. The groundwater flow occurs along more permeable layers and conduits between a low permeable moraine and low permeable bedrock. Triggering or acceleration mechanisms are increase in pore water pressure, seepage forces, seepage erosion and mechanisms related to high plasticity. Furthermore, the low activity in the summer season is explained by the evapotranspiration of the trees, which decreases the saturation of the soil. Therefore also the decreasing suction during the winter season should be considered as an important mechanism in the Steinernase landslide. The upper part underlain by anhydrite and the middle part underlain by permeable sandstone are considered as type 6D because the underlying lithologies (evaporites and sandstone) are more permeable than the Wellenkalk and the Permian sediments. But this does not change in terms of triggering or accelerating mechanisms.

The example of the Steinernase landslide shows that even if the landslide is assumed to be saturated to large parts, the decreasing suction may be taken into account as an important triggering mechanism. It is possible, that in summer, the landslide is a mixture of types 5A and 5D. This shows that the classification can be used to illustrate seasonal changes in saturation.

8.3 Triesenberg (3F)

The Triesenberg landslide is located along the Rhine valley in the principality of Lichtenstein (mean Swiss coordinates: 760000/221000, altitude: 1500 m a.s.l.). It covers an area of 5 km^2, is 2300 m long and 1500 - 3200 m wide. The mean slope angle is 24° and the landslide has a mean velocity of 0-3 cm/year (François et al., 2007).

Figure 8.4 shows a geological 3D-model of the area and a section along the landslide. The landslide consists of two main parts: 1) An ancient deep seated landslide in the upper part. 2) An active 10 - 20 m deep landslide which is underlain by a prehistoric 80 m deep landslide that was activated after glacial retreat in the lower part. The slip surface of the active landslide is very distinct and about 1 m thick. The landslide mass consists of Flysch components and a clayey silt matrix. It is underlain by Austro-Alpine Triesen Flysch. The Flysch is mainly composed of clayey shale with layers of limestone and sandstone. Above the Flysch (see Figure 8.4) is the tectonic Arosa zone which and permeable sandstones.

About 100 springs are observed on the Triesenberg landslide. At the top of the landslide, the water table lies about 20 - 30 m below the ground surface whereas at the bottom, it reaches almost the ground surface. Tracer tests showed that the Valüra Valley groundwater flows partly through the Arosa zone and the sandstones above the Flysch. Therefore the Triesenberg groundwater basin is much larger than the topographic watershed. About 50% of the groundwater observed in the Triesenberg landslide originates in the Valüna valley. Measurements of spring flux and groundwater levels showed that snow melt and rainfall events in the Valüna valley reach the landslide with a delay of several days.

The ancient Triesenberg landslide is classified as 3F type, whereas the lower active landslide
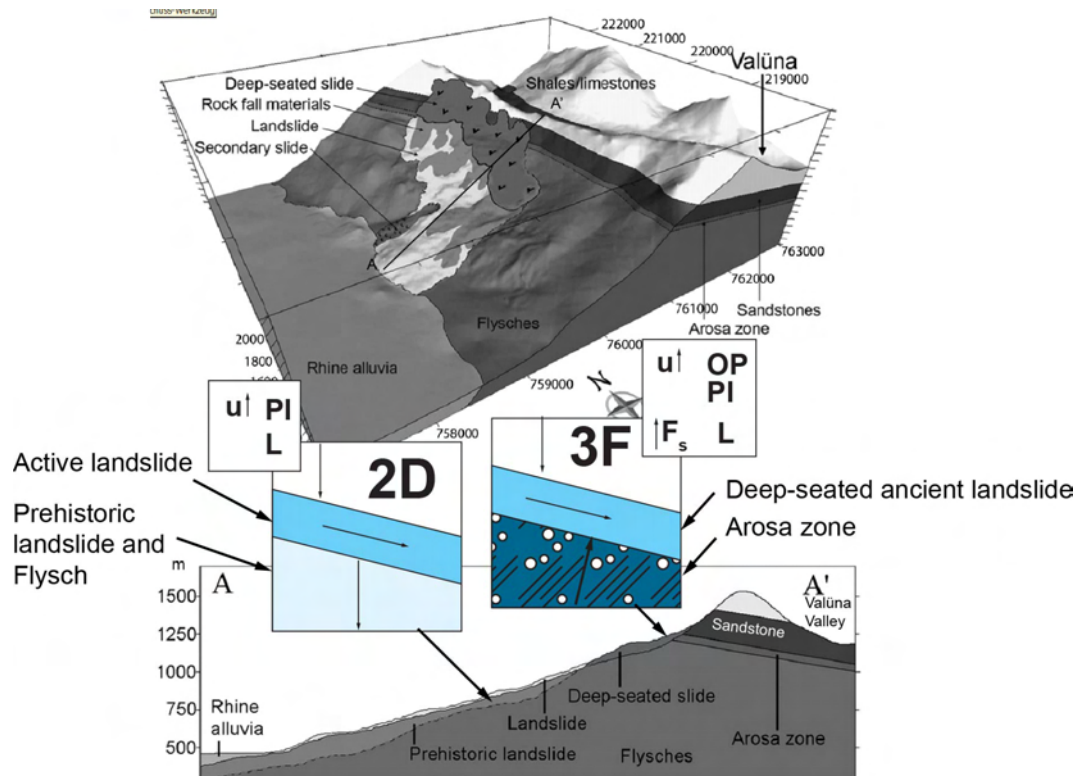
Figure 8.4: *Geological 3-D model and section along the Triesenberg landslide François et al. (2007).*

is classified as a 2D type. In the area of the ancient landslide, water is exfiltrating from the bedrock and is feeding the landslide mass. The active landslide, which is located further downslope with respect to the ancient landslide, is feed by lateral water flow through the unconsolidated sediment. Water pressure variations in the slope have been described as major cause of the movements (François et al., 2007).

According to Cruden and Varnes (1996), the Triesenberg landslide could be classified as very slow earth flow like also the La Frasse and the Steinernase landslide. But by applying the hydrogeological calssification, it can be seen that the triggering mechanisms are different for the three landslides: in La Frasse, over pressure is important, in Steinernase positive pore water pressure and suction, in the active Triesenberg landslide positive pore water pressure and in the ancient Triesenberg landslide it was also over pressure. This shows how the hydrogeological classification can be used to compare different landslides.

8.4 Wiler triggering experiment (4D)

In the frame of the TRAMM project, a landslide triggering experiment was carried out in the year 2007 on a forested north facing slope in the Lötschental, VS. The test site was located above the village Wiler (mean Swiss coordinates: 627300/138700, altitude: 1700 m a.s.l.) and the slope angle was 35-40°. The bedrock in the area consists of pre-hercynian crystalline rocks from the Aar massive. The test site was located in heavily fractured chlorite-gneiss dipping 60-80° towards SE into the slope. The bedrock was covered with moraine and stratified lacustrine clayey deposits (Or et al., 2007). The thickness of the unconsolidated sediment was approximately 1 m followed by a 5-25 m thick layer of weathered and fractured bedrock. The aim of the exper-

179

iment was to trigger a shallow landslide with a volume of several tens or hundreds of cubic metre.

No important springs could be observed around the test site and it was assumed that no bedrock exfiltration occurs in the area. The unconsolidated sediment was fed by in-situ infiltration at the surface. The soil showed a large infiltration capacity. The hydraulic conductivity of the upper 40 cm of unconsolidated sediment was between $6 \cdot 10^{-4}$ and $2 \cdot 10^{-5}$ m/s. Due to fractures, the permeability of the bedrock was assumed to be very large.

Even with intense artificial rainfall of 30 mm/h and a water-filled trench above the test site, the slope remained stable. ERT data showed that a large part of the added water (mixed with salt to enhance the resistivity contrast) infiltrated into the bedrock. It was not possible to saturate the slope. Thus it is assumed that the draining capacity of the fractured and weathered bedrock and the unconsolidated sediment was equal to or larger than the sprinkling and infiltration intensity. It was estimated that 70% of the water was drained laterally in the unconsolidated sediment and 30% percolated into the bedrock. In the unconsolidated sediment, a flow velocity of 30 m/h was measured along preferential flow paths.

The Wiler test site is classified as type 4A (see Figure 8.5): Permeable colluvium over permeable bedrock, both unsaturated.The triggering experiment may be classified as 4D because the unconsolidated sediment was partly saturated. The triggering experiment could correspond to a very heavy rainfall event which occurs every several hundred years. In the case of 4D, pore water pressure, seepage forces and seepage erosion should be taken into account as triggering mechanisms.
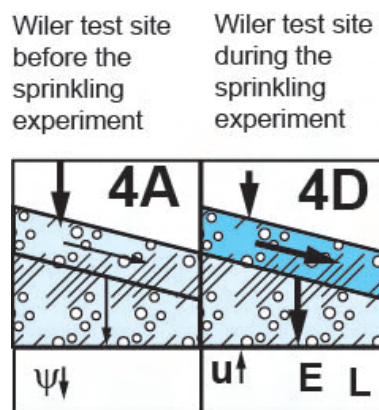
Figure 8.5: *The classification can be used to illustrate the changing saturation during the Wiler sprinkling experiment.*

It is interesting to compare the conceptual models obtained with the classification for the two experiments in Wiler and in Rüdlingen. It can be seen that the initial saturation-permeability types were the same (4A), but in Rüdlingen, the bedrock was more saturated than in Wiler during the experiment.

8.5 Travers landslide (5H)

The Travers landslide is located on a generally slowly creeping slope. A first landslide occurred in 1977 and was reactivated in 1984 and 1995. The main landslide occurred 2006 after a period

of heavy rainfall (Krähenbühl, 2007). The landslide is situated above the village Travers (mean Swiss coordinates: 542300/198400, altitude: 750 m a.s.l.). It is 300 m long and 10 m thick. The maximum slope angle is 25°. It is mainly composed of moraine material and the slip surface is in weathered Molasse bedrock (see Figure 8.7)
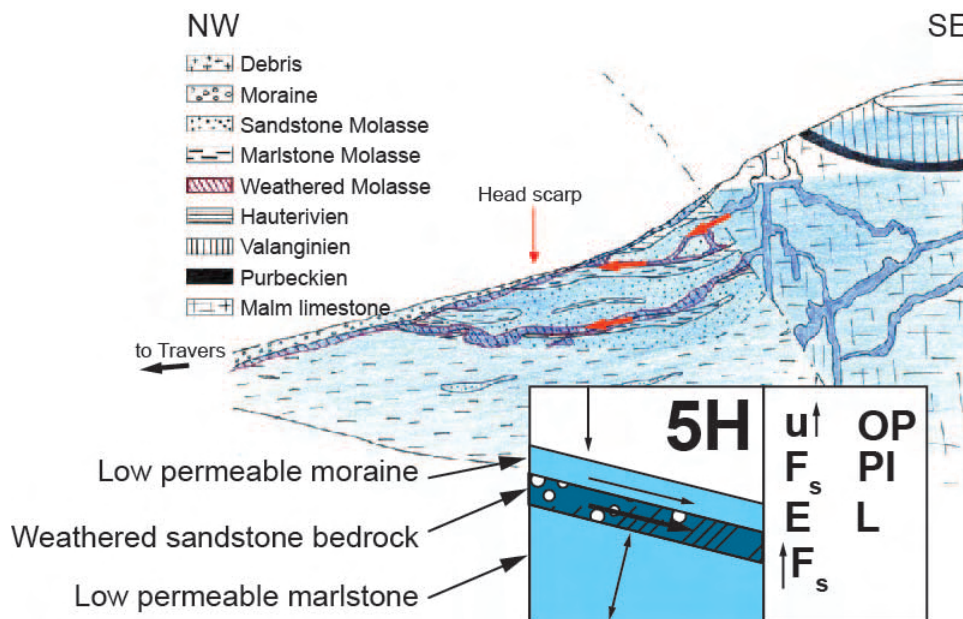
Figure 8.6: Conceptual hydrogeological model of the Travers landslide. From Krähenbühl (2007).

Above the landslide, karstic Malm limestone is outcropping. Meteoric water infiltrates into the karst caves and accumulates at the fault zone between the Malm limestone and the lower permeable Molasse (see Figure 8.7). A high hydraulic potential builds up and water infiltrates from the karst into the weathered sandstone layers in the Molasse. Through this sandstone layers, water arrives at the low permeable moraine cover. High pore water pressure builds up below the landslide. This process is amplified after heavy rainfall and snowmelt.

In 2006, liquefaction was observed in the sandy weathered Molasse layer. This was described as initiation of the landslide. Subsequently, liquefaction destabilized the overlying moraine (Krähenbühl, 2007).

This landslide is classified as type 5H. Altered sandstone layers in the Molasse are permeable and marlstone Molasse is not permeable. The Molasse is overlain by low permeable moraine. Confined aquifers build up in the weathered bedrock below the moraine. By applying the classification it can be seen that liquefaction and overpressure, processes which were both observed in the field, should be considered.

8.6 La Vraconnaz landslide (5H)

The la Vraconnaz landslide is an example for a peat flow that was triggered in September 1987 after extraordinary heavy rainfall (Parriaux, 2007). It is located in the Jura Mountains at 1090 m a.s.l. next to the village St-Croix in the canton of Vaud. The flow occurred in flat terrain with a slope angle of only 2° and affected about 15 hectares. The shallow slip surface is located in a 1 - 3 m thick gyttja formation which underlays a 10 - 30 cm thick layer of low permeable peat.

Gyttja is a dark soil rich in decomposed organic matter and carbonate precipitates formed under nutrient-rich conditions. This formation is more permeable than the overlaying peat. Gyttja contains only very little amount of clay and is low cohesive. Below this formation follows an impermeable layer composed of lacustrine deposits and moraine. The gyttja formation was feed laterally by groundwater from a karstic Cretaceous aquifer.
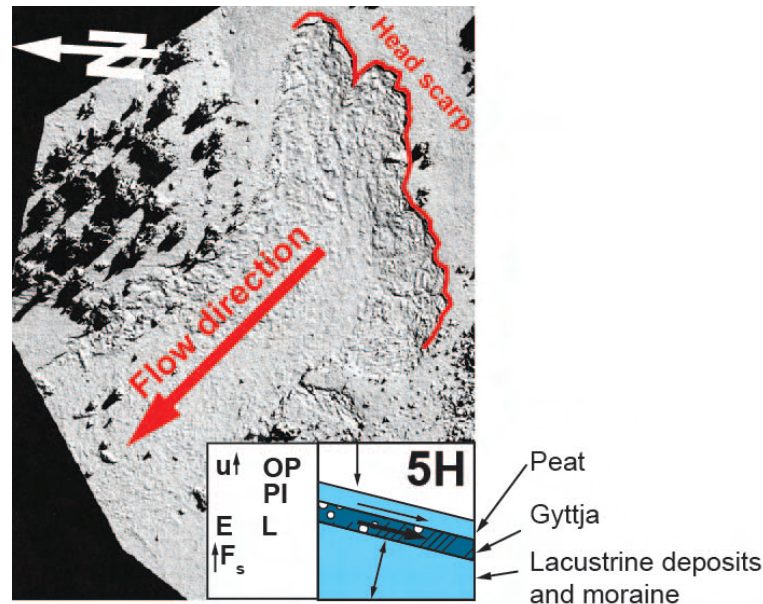
Figure 8.7: *Aerial photograph from the upper part of the Vraconnaz peat flow (Parriaux, 2007).*

This geological setting led to a confined aquifer (gyttja) between two impermeable layers (peat and lacustrine sediments). High pore water pressure and overpressure was building up in the gyttja formation which triggered the flow and led to liquefaction. The triggering of this peat flow is classified as 5H.

The Vracconaz landslide is a peat flow (Hungr et al., 2001) and the Travers landslide can be classified as an earth slide (Cruden and Varnes, 1996), thus two morphologically completely different phenomenon. But by applying the hydrogeological classification it can be seen that this two landslides are classified as the same saturation-permeability type (5H) and that the triggering mechanisms may be similar. In both landslides overpressure from below the landslide did build up. This shows that the hydrogeological classification can be useful as a complementary to the commonly used geomorphological landslide classifications (see Section 2.3.2) in order to establish conceptual hydrogeological models. But it should be clear that the hydrogeological classification is not suitable to distinguish different landslide according to the type of movement, morphology or material.

8.7 Super-Sauze mudslide (1E-3E)

The Super-Sauze mudslide has been active since the 1970s and is located in the French South Alps in black marls (De Montety et al., 2007). These grey clayey schist are very finely laminated and highly tectonised. Above the landslide is the calcareous Klippe of Lan that was overthrust along basal gypsum horizons. The landslide initiated at the interface between 3-15 m thick moraine and black marls and is composed of a silty-sand matrix mixed with moraine debris. It is 850 m long, 130 m wide, located between 2100 and 1740 m a.s.l. and the average slope angle

is 25°. The measured velocity is 0.01 - 0.4 metres per day.
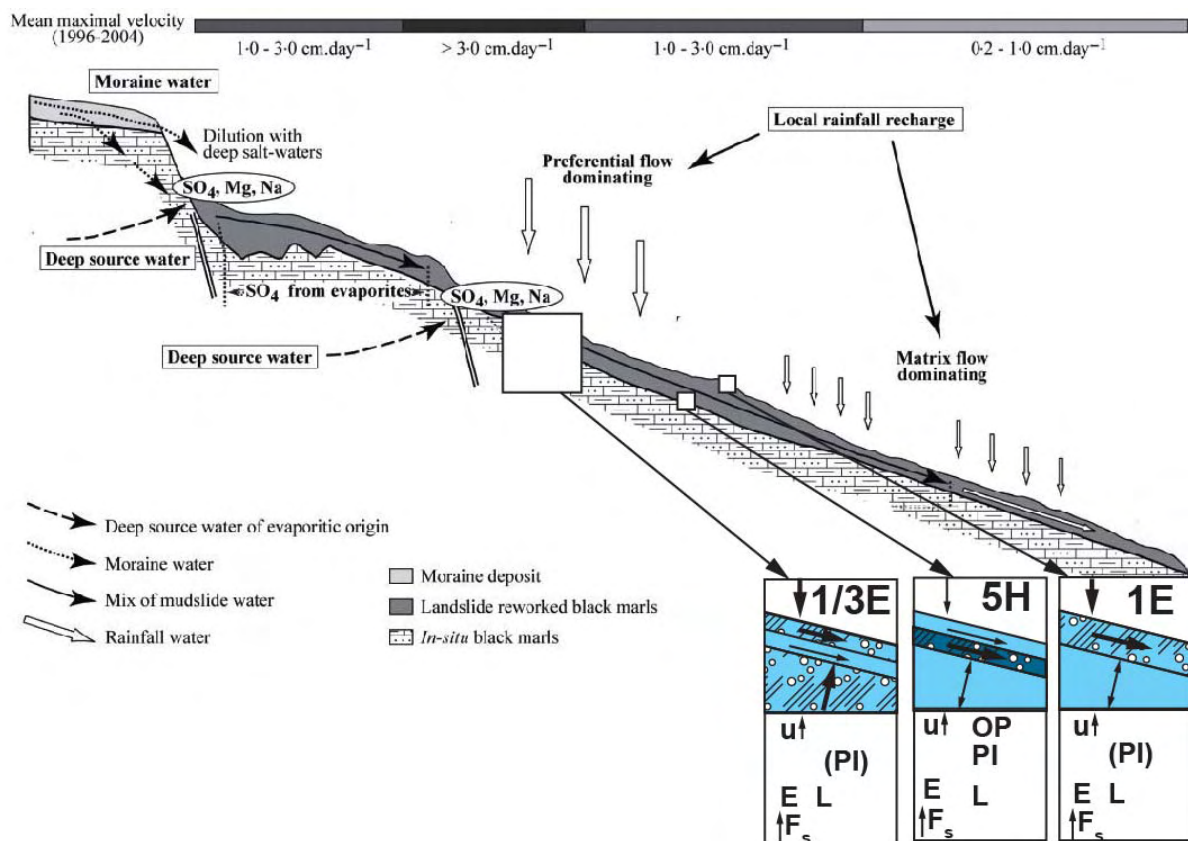
Figure 8.8: *Hydrogeological conceptual model of the Super-Sauze landslide. Zones of saline water correlated with high landslide velocity (De Montety et al., 2007). Depending on the scale and the location, different permeability-saturation types can be defined for this complex landslide.*

The Super-Sauze landslide can be divided into several units. An upper unit present in the western part of the landslide is 5 - 9 m thick and very wet and muddy. The groundwater in this unit responds rapid to rainfall events due to bypass through the crack system. Sprinkling experiments showed that important hydrological features are preferential infiltration through fractures and the formation of perched water bodies (Debieche et al., 2011). Below this upper layer follows a rather stiff and impervious 10 m-thick unit. This unit is recharged with slow infiltration through matrix porosity. Furthermore, locally confined aquifers were observed (De Montety et al., 2007). Hydrochemical analyses of springs from fractured bedrock and moraine aquifer showed that the groundwater in the landslide is not only recharged by rainfall. Saline water that was in contact with the gypsum formation located above the landslide circulates along major faults, bedding planes and schistosity in the black marls. Water with high salinity was observed in the part with the highest activity.

Figure 8.8 shows the hydrogeological conceptual model of the Super-Sauze landslide. In the scale of the sprinkling experiment (Debieche et al., 2011), the landslide can be defined as type 1E: a shallow fractured layer where preferential flow occurs above a low permeable layer. If the landslide is examined in a larger scale, fracture flow in deeper units (3E) and local confined aquifers (5H) are observed in the heterogeneous landslide body. Nevertheless, confined aquifers are assumed to be a rather local phenomenon and thus the landslide is classified as 1E-3E (Figure

8.8).

This example of Super-Sauze landslide showed that the application of the classification depends on the considered scale. Furthermore, it showed that initially low permeable material becomes permeable due to fractures. Therefore the triggering mechanisms related to high plasticity may also be taken into account for permeable layers.

Super-Sauze is an example that shows how important hydrochemical analyses are to trace the origin of groundwater. The knowledge obtained by chemical water analyses influences strongly the definition of the saturation-permeability type for the conceptual hydrogeological model. Other examples were hydrochemical analyses proved to be important methods to trace the groundwater origin from the bedrock are La Clapière, Maritimes Alps, France and Séchilienne, Belledone Alpine massif, France (Guglielmi et al., 2002).

8.8 Criticality

As mentioned in Section 3.7, the term "criticality" is used to define if a slope is in a critical equilibrium stage according to the hydrogeology (permeability contrast and saturation of the landslide and the substratum). Figure 8.9 shows the criticality for the seven landslides described in this section and the three case studies. None is triggered in unsaturated conditions. About half of the landslides are related to confined aquifers. The described landslides occur in medium or high critical areas except of the Wiler triggering experiment and the lower part of La Frasse landslide.

The conceptual model of the La Frasse landslide showed that the relevant triggering mechanism (overpressure) acts in the upper part of the slope, whereas the lower part of the landslide is underlain by unsaturated permeable dolomite which has a rather stabilising effect on the slide.

The classification shows that the slope of Wiler triggering experiment is not very critical to landslides. This corresponds with the findings of the experiment that the slope remained stable during sprinkling. The area around the Wiler triggering experiment is not a landslide-prone area. It is possible that if the classification was applied previously to the Wiler triggering experiment, it would have been seen that the triggering of a landslide on this slope is particularly difficult.

The application of the classification in this chapter showed on the one hand some points which should be considered. For example suction decrease may play a role in landslides even they are to large parts saturated (Steinernase). Or clayey high-plasticity layers my become permeable due to fractures and thus mechanisms related to high plasticity may also play a role in high permeable layers (Pont Bourquin, Supere-Sauze). And morphologically completely different landslides may have equal triggering mechanisms (Travers and La Vraconnaz landslides). On the other hand it illustrated the variety of the use of the classification: comparing several landslides, triggering experiments and different parts and scales in complex landslide. As a next step, the classification should be applied for slopes or landslides from which less knowledge is available. The application of the classification is discussed in more detail in the next chapter.
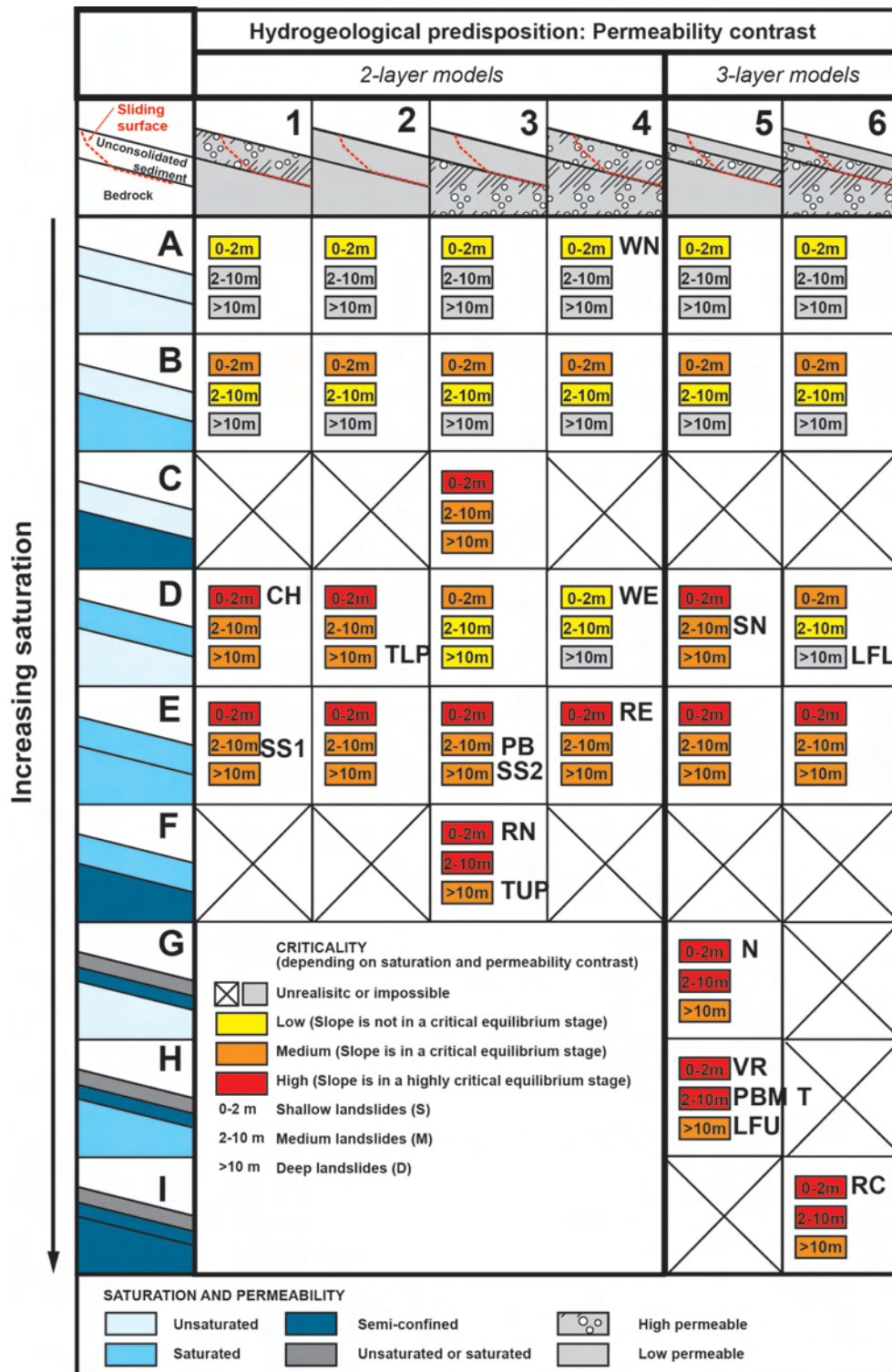
Figure 8.9: *Table showing the criticality of the discussed slopes, landslides and landslide parts according the hydrogeological predisposition (permeability contrast) and the time dependant saturation. WN: Wiler (natural situation), CH: example from Chigira (2002) (Section 3.3.4), TLP: Trisenberg landslide (lower part), WE: Wiler (experiment), SN: Steinernase landslide, LFL: La Frasse landslide (lower part), RE: Rüdlingen experiment, RN: Rüdlingen (natural landslides), PB: Pont Bourquin landslide (upper and lower part), TUB: Triesenberg landslide (upper part), N: example from Rogers and Selby (1980), PBM: Pont Bourquin landslide (middle part), LFU: la Frasse landslide (upper part), RC: Rufiberg slope (above conglomerate), T: Travers landslide, VR: La Vraconnaz landslide, SS1: upper layer in Super-Sauze landslide, scale of the sprinkling experiment, SS2: deeper layer in Super-Sauze landslide, scale of the entire landslide.*

Chapter 9

Discussion

In this chapter, the application of the developed hydrogeological classification is discussed. Innovative aspects of the new classification concept are shown and compared with existing classifications. Furthermore, limitations of the classification are analysed. As an outlook, the application of the classification for entire regions is discussed.

9.1 Application of the classification

The classification proposed in this thesis is a tool to simplify the geology and hydrogeology of slopes and landslides in order to construct conceptual models. The presented classification is based on the assumption that the slip surface of the landslide develops between two geological layers. In some cases, an intermediate third layer (for example weathered bedrock) has to be taken into account. The classification is not suitable for rockfalls. It is applicable for sliding and flowing type landslides in any geological and hydrogeological setting. The classification may be used for shallow, medium and deep seated landslides. Generally, shallow landslides can be classified easier. This is because the hydrogeology of large and deep-seated landslides, for example La Frasse or Triesenberg landslides tends to be more complex than of shallow landslides. Even though in the present study the classification was applied for landslides in the Alps, it can be used in all parts of the world where landslides occur. This is because the parameters used in the classification (permeability and saturation) and the resulting triggering mechanism can be described for any geological, hydrogeological and climate conditions in the world. Furthermore, the classification may be applied for natural landslides as well as for triggering experiments.

Based on the two parameters "saturation" and "permeability contrast", 18 "permeability contrast-saturation types" have been defined for a two layer model and additional 11 types for a three layer model. 29 types might seem a lot, but several types are similar with regard to the potential triggering mechanisms. Several types could be grouped, for example the unsaturated triggered landslides or the landslides where overpressure may play a role. More than half of the analysed landslides occur above confined aquifers and none of the analysed landslide occurs in unsaturated conditions. One might ask why unsaturated conditions are taken into account in the classification. This is because it is known that in some cases of shallow landslides, the decrease of suction is sufficient for the triggering (Iverson et al., 1997; Fourie et al., 1999; Godt et al., 2009). Furthermore, the classification can be used to discuss the changing saturation of a slope during a rainfall or snowmelt event. Therefore it is important to also consider unsaturated conditions (as initial stage).

The application of the presented hydrogeological classification for different landslides has shown that the definition of a permeability-saturation type may depend on:

- the part of the landslide (upper part or lower part of the slope)

- the considered moment (before or after a rainfall event)

- the scale and detailedness (mechanism of entire landslide or local processes, especially for large and deep-seated landslides)

Even though a landslide may be composed of several permeability-saturation types, in most cases one type can be defined as the most relevant for the triggering.

The classification can be applied for:

1. The construction of a conceptual hydrogeological model of a landslide. The classification helps to create an overview of the determining hydrogeological characteristics and potential triggering mechanisms of a landslide. This can yield the base for numerical modelling and the planning of mitigation measures.

2. Comparing different parts of a landslide. For example on the La Frasse and the Pont Bourquin landslide, it can be seen that the slope-upward part and the middle part, respectively, are more important for the triggering and the slope downward parts have rather stabilising effects.

3. Discussing the saturation before and after a rain or snowmelt event. It should be clear whether the saturation after a usual event or after an extraordinary event is analysed. It is possible to evaluate rain events with different return periods. Furthermore, due to variations of the saturation, a slope may change the position in the classification in time. Nevertheless, one saturation-permeability contrast type is determinant for the moment of the triggering.

4. Comparing the hydrogeology of different landslides. For example in Rüdlingen, the classification may be used to compare the natural triggering mechanisms occurring in the region with the triggering mechanisms observed during the experiment. An other example are the two landslides La Frasse and Triesenberg, which are both deep seated and slow moving. The La Frasse landslide is more active in the upper part where bedrock exfiltration and overpressure are important processes. The Triesenberg landslide is more active in the lower part which is underlain by low permeable bedrock. Thus, the application of the classification helps to see the different mechanisms. The comparison of the Rüdlingen and the Wiler experiments shows that the permeability contrast class is the same. But the saturation was different and thus the potential triggering mechanisms and the criticality were different.

5. Estimating the criticality of a slope or an entire region to shallow, medium and deep seated landslides.

The hydrogeological classification can be applied with different amount of details. This means that depending on the available knowledge about the hydrogeology and geology of a slope, the parameters permeability, saturation and plasticity as well as the number and thickness of the geological layers have to be estimated to create a basic conceptual model. In such a case, large uncertainty may exist. If a more precise conceptual model is needed, for example for complex landslides, several investigations may be necessary to evaluate the parameters of interest. This allows to apply the hydrogeological classification in more detail, for example to distinguish different parts of a landslide. The permeability-saturation type firstly defined (before detailed

investigations were performed) may then be confirmed or abandoned.

In this study several methods have been used to establish detailed conceptual models of the investigated landslides and slopes. Figure 9.1 summarises the importance and the costs of the used methods. The most adequate method to obtain information about the origin and flow path of groundwater in the landslides is hydrochemical analyses. Analyses of major ions from spring water on landslides are not very costly. Groundwater sampling from boreholes are more expensive because drilling work is necessary, which can be very cost intensive, especially in steep or remote slopes. Isotope analyses, which provide additional information about the origin of groundwater, are more costly than hydrochemical analyses. To define the saturation patterns in the landslide and substratum, mapping of hydrogeological features like swamps and springs, groundwater measurements in observation wells and ERT monitoring prove to be helpful. Knowledge about the permeability of the different geological layers is provided by infiltration tests and observations of fractures and joints on outcrops. Simple infiltration tests are not costly and can be performed in hand made auger holes. To define the thickness of the layers more precisely, drilling and electric resistivity tomography prove to be helpful. Knowledge about the presence of weathered bedrock is obtained from drilling and field observations (mapping). It is clear that drill holes provide very important geological and hydrogeological information, but they are very costly and often complicate to perform on landslides due to the bad accessibility. Therefore, some of the knowledge found from drilling can primarily be obtained by cheaper methods such as mapping and ERT.
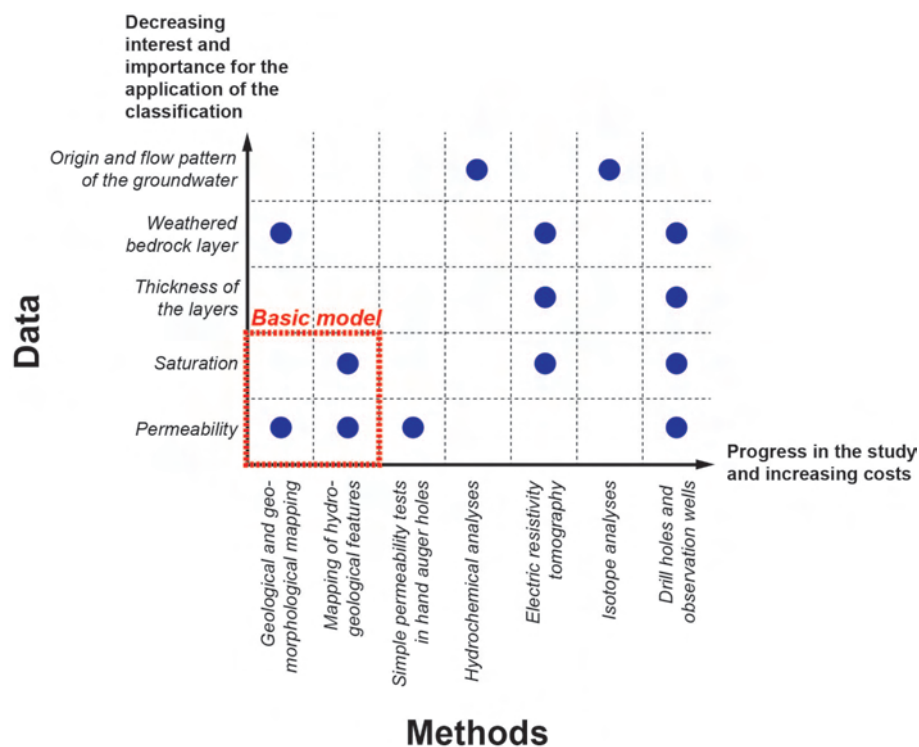
Figure 9.1: Interest and costs of different field methods which are necessary to obtain the required data for the construction of conceptual hydrogeological models of slopes and landslides. The red square indicates the required investigations to create a basic conceptual model.

The hydrogeological classification is applied in the present study after detailed conceptual models of the landslides were established. In this sense it is interesting to see how the studied landslides

and slopes (Chapters 5, 6 and 7) and described landslides (Chapter 8) are categorised and to see if the classification is build up logically. Furthermore, the application of the classification helps to discuss the landslide triggering mechanisms observed in the three case studies. Nevertheless, the idea of the classification is to also apply it for slopes and landslides where less information is available.

9.2 Innovative aspects of the new classification

Existing landslide classifications often describe the observed morphology. The most noted classifications belong to Hutchinson (1988), Cruden and Varnes (1996), Leroueil et al. (1996) and Hungr et al. (2001). The classification from Hutchinson (1988) focusses on morphology and slope movements in relation to landslide mechanism and material. The author defined eight classes: rebound, creep, sagging of mountain slopes, landslides, debris movements of flow-like form, topples, falls and complex slope movements. For each class he defined specific types but the hydrogeology (for example positive pore water pressure and seepage erosions) was only taken into account for certain types. Hutchinson (1988) stated that it would be interesting to know the condition of the failure of slopes by applying a classification. But in his classification it is not very clearly laid out in which cases the groundwater plays which role.

The classification from Cruden and Varnes (1996) is based on the type of material (earth, debris, rock) and movement (fall, topple, slide, spread, flow) of landslides and considers also the activity and velocity. With the parameter "water content" the hydrogeology of the landslide is marginally taken into account. Different processes that are involved in slope movements are described but not directly included in the classification. These are 1) increased shear stresses, 2) low strength and 3) reduced material strength. These processes include a continuous series of events from cause to effect. These are removal of support, imposition of surcharge, earthquakes, tectonics and material and mass characteristics. Water may influence those processes in many ways but in the classification from Cruden and Varnes (1996), the hydrogeological mechanisms are not grouped.

The geotechnical classification from Leroueil et al. (1996) considers three axis: movement type (the same as Cruden and Varnes (1996)), materials (subclasses of rock and saturated/unsaturated soil) and movement stages. The mechanical phenomena, controlling laws and parameters involved are very different from one stage to another. Four movement stages are defined: 1) pre-failure, characterised by changes in stress, creep are progressive failure that lead to the deformation, 2) onset of failure, characterised by the formation of a continuous shear surface through the entire soil mass, 3) post-failure, includes landslide movements from just after failure until it stops and is characterised by an increase of the displacement rate followed by a progressive decrease in velocity, and 4) occasional reactivations, occur when a soil mass slides along one or several pre-existing shear surfaces. Triggering factors, including hydrogeological mechanisms, are also taken into account in this classification. For example for a "reactivated slide in clay shale", the triggering factors are increase in pore pressure, increase in shear stresses and seismic loading. Nevertheless, the approach of this classification does not put focus on hydrogeological parameters and mechanisms.

Hungr et al. (2001) made a classification for landslides of the flow type. He defined 11 landslide types based on material type, water content, presence of excess pore-pressure, liquefaction at the source of the landslide, presence of a defined recurrence paths (channel) and deposition area (fan), velocity and peak discharge of the event. These types are: non-liquefied sand (silt, gravel, debris) flow, sand (silt, debris, rock) flow slide, clay flow slide, peat flow, earth flow, debris flow,

mud flow, debris flood, debris avalanche, and rock avalanche. The hydrology and triggering mechanisms were taken into account firstly by defining the saturation or plastic/liquid limits of each landslide type and secondly by describing "special conditions" such as pore pressure, liquefaction and increasing water content for certain types. But the author did not take into account the hydrogeology of the substratum or mechanisms related to seepage force, seepage erosion und overpressure.

Author	Main parameters (Input)	Main types (Outcome)
Hutchinson (1988)	Morphological parameters Geotechnical parameters	8 classes >30 specific types
Leroueil et al. (1996)	Geotechnical characterisation	4 movement stages
Cruden and Varnes (1996)	Material Type of movement	15 main types additional descriptions
Hungr et al. (2001)	Material Water content Velocity	11 landslides of the flow type
The present classification	Permeability contrast Saturation	29 types 8 triggering mechanisms Origin of groundwater

Table 9.1: *Summary of the input parameters and output information of the 4 most used classifications compared with the present classification.*

Table 9.1 shows the input parameters and the outcome of these four in literature most commonly cited classifications and the presented hydrogeological classification. The classifications from Hutchinson (1988), Cruden and Varnes (1996), Leroueil et al. (1996) and Hungr et al. (2001) are very useful to describe existing landslides after their rupture. But they can not be applied for slopes that could fail in future. An advantage of the hydrogeological classification proposed in this work is that it can also be applied to estimate if a slope is in a critical equilibrium stage according to the hydrogeology (saturation and permeability contrast). This could be useful for hazard mapping. In the proposed classification, focus is put on the hydrogeologically important parameters permeability contrast, saturation and plasticity. The advantage of using the permeability contrast (of two orders of magnitude) instead of absolute values is that 1) the substratum is taken into account and 2) the contrast gives hints about the groundwater flow and formation of positive pore water pressure. Often, the permeability contrast is a parameter that may be estimated in the field. For example at Rufiberg, outcrops of conglomerate showed that this lithology is heavily fractured and thus permeable, whereas ponding water on the slope showed that the unconsolidated sediment is low in permeability. It is assumed that the parameters permeability contrast, plasticity and saturation cover the main hydrogeological characteristics of landslides in space and time which allows defining the potential hydrogeological triggering mechanisms. A new aqspect of the presented classification is that the origin of the groundwater in landslides and the potential triggering mechanism related to the hydrogeology can be directly evaluated. Furthermore, with the parameter "saturation", transient aspects can be taken into account, because the saturation changes in time. Thus, the classification may be a good starting point to discuss the changes of the saturation in time. This can be illustrated by compared the types before and after a snowmelt or a rainfall event occurred.

The presented classification provides a tool to **evaluate potential hydrogeological triggering mechanisms** based on the hydrogeological parameters saturation and permeability contrast

before expensive investigations, calculations and numerical modelling are conducted. It thus can be applied to complement existing landslide classifications.

9.3   Limitations of the classification

The application of the presented classification may be more difficult for complex and large landslides where several triggering processes are involved. Difficulties may arise if the geology of a landslide and the surrounding area is very heterogeneous. In such cases, it may not be possible to classify the entire landslide as a single type. Several types have to be defined for different parts of the landslide. But this may allow to evaluate which part of the landslide acts as an accelerator of the movement and which part rather stabilises the slope.

If the geology of the region of a landslide is complex and no outcrops are observed, the evaluation of the parameters saturation and permeability contrast may be complicated and the uncertainty is large. Detailed investigations (for example drilling) of the landslide may be necessary.

Additional difficulties may arise if the hydrogeology of a landslide is dominated by lateral water flows in three dimensions. In such a case the model has to be reduced to two dimensions. This is possible under the assumption that 1) the boundary between two layers (permeability contrast) is parallel to the slope, 2) the contrast between the two layers is crucial and 3) only the permeability and saturation in these two layers has to be taken into account. Thus, it is not important whether the water in the bedrock flows laterally along the slope or parallel downslope. For example Rufiberg is a 3D situation, because the permeable conglomerate layers cross the slope horizontally and water flow occurs laterally from the sides. Since groundwater pressure is build up locally below the potential landslide, it is mainly important that the groundwater in the bedrock is confined. To describe the triggering, it is not important from which direction the aquifer in the bedrock was fed. Thus it is possible to simplify complex 3D geological settings into 2D problems.

A difficulty may be that, based on the two parameters permeability contrast and saturation, the hydraulic gradient is not known and thus the flow direction is unknown. In this case it is difficult to know when upward seepage occurs. It is assumed that a confined aquifer below the landslide favours upward seepage. Furthermore theoretically the landslide may liquefy when it is saturated, but it is assumed that the risk for liquefaction is higher when the substratum is also saturated or confined.

A limitation point of the presented classification may be that the defined saturation-permeability type always depends on the geological interpretations which have an inherent uncertainty. It is not always evident which permeability contrast should be taken into account. For example, the existence of a weathered bedrock layer is not always evident. But the application of the hydrogeological classification has shown that, for the judgement of a landslide, this has rather little influence because the potential triggering mechanisms and the criticality for a landslide are equal for several types. For example the types 5G, 5H and 5I show the same triggering mechanisms. And the criticality does not change if 2 or 3 layers are assumed in the case of 3F and 6I. The criticality for landslides does, for example, not depend on whether a weathered layer is present or not. Thus, the classification still shows a certain robustness even when a large spectrum of interpretation is possible.

9.4   Perspective

It would be interesting to apply the classification for entire areas with the intention to make landslide susceptibility maps that include the potential hydrogeological triggering mechanisms. For this purpose, a minimum knowledge about thickness, permeability and saturation of the different geological layers is needed. For example, in the area of the Rüdlingen triggering experiment, the bedrock (Lower Freshwater Molasse) is draining the unconsolidated sediment (type 3A-4A). Whereas further upslope of the test site (Upper Marine Molasse), numerous springs yield evidence for the presence of water in permeable sandstone layers (type 3E-3F). If such observations are consistent in the entire region, a map could be made that indicates the different mechanisms which are dominant for the two geological lithologies. In the vicinity of Wiler, the geology does not change significantly along the entire north facing slope of the Lötschental (type 4A). In this case, the classification may be a useful tool to define the susceptibility of the entire slope.

Furthermore, it would be interesting to include the hydrological water balance into the classification to make quantitative analyses of the saturation of a slope. This would be a promising approach to assess the landslide susceptibility of a slope for rain events with a distinct intensity and duration.

Common susceptibility and hazard maps include past phenomena and location, probability and intensity of future events. But as far as known by the author, no maps include the triggering mechanism of the landslide. Taking into account the triggering mechanisms could be helpful for the planning of future investigations and mitigation work. This could be done for example by superposing a map that shows the triggering mechanisms and existing susceptibility or hazard maps. Furthermore, different susceptibility maps could be made for precipitation events with different return periods (for example 30, 100 and 300 years). The triggering experiments conducted at Wiler and Rüdlingen, for example, would be events which occur only every 300 years because during normal events, no saturation is reached.

Chapter 10

Conclusions

In this study, a classification for the hydrogeological characterisation of landslides and for the evaluation of potential triggering mechanisms related to groundwater has been developed. Furthermore, two landslides and a slope prone to slide (Rüdlingen, Pont Bourquin and Rufiberg) were investigated with several field methods. Detailed hydrogeological conceptual models were made and the proposed classification was applied to these three case studies. The main findings of this work are:

1) For studying the hydrogeology of landslides, it is important to take into account the hydrogeological characteristics of the substratum (which is usually the bedrock). If the substratum is permeable and unsaturated, it may act as a drain for the overlaying landslide which rather stabilises a slope, whereas a permeable and saturated substratum may provoke the triggering of landslides. On the one hand, fractures and weathered layers in the bedrock favour rapid water flow which can lead to exfiltration from the bedrock into the overlaying landslide. On the other hand, hydraulic overpressure can build up below a low permeable landslide. Thus it is essential to know from where the groundwater in the landslide is coming for the planning of mitigation work. The following main hydrogeological characteristics are found for the three investigated landslides and slopes:

- During the triggering experiment in Rüdlingen, large joints and weathered bedrock layers were efficiently draining the slope and it was difficult to establish and maintain positive pore water pressure in the unconsolidated sediment.

- In the Pont Bourquin landslide, the triggering is influenced by groundwater flow through fractures in the heavily tectonised black shale lithology and by local confined aquifers that build up in the heterogeneous and generally low permeable and highly plastic landslide mass.

- At Rufiberg, overpressure builds up in bedrock fractures below the low permeable unconsolidated sediment which may influence the triggering of landslides.

2) The proposed classification gives an overview of relevant hydrogeological characteristics of landslides. The classification is a tool to illustrate the origin of the groundwater in the landslide and to evaluate the potential triggering mechanisms related to groundwater. It is a tool to construct conceptual hydrogeological models of slopes. The following main conclusions are made:

- In the classification, 6 different "permeability contrast" types were defined for slopes composed of two or three parallel geological layer (hydrogeological predisposition of a slope).

- Taking into account the varying "saturation" of the different geological layers, a total of 29 types was defined. The classification may be used to illustrate the changing saturation of the landslide and the substratum in time.

- It is possible to construct basic conceptual hydrogeological landslide models with the two parameters permeability and saturation.

- Complex landslides may be composed of several permeability-saturation types, whereof the one, which is the most relevant for the triggering stage, has to be determined.

- Seven hydrogeological triggering mechanisms are defined: decreasing suction, increasing pore water pressure, seepage erosion, upward seepage, liquefaction, overpressure, and mechanisms related to high plasticity. The classification yields for each "saturation-permeability contrast" type the potential hydrogeological triggering mechanisms. It is necessary to evaluate different potential triggering mechanisms for a better understanding of the landslide and for the planning of mitigation work.

- Based on the "saturation-permeability contrast" type and the triggering mechanisms, it can be defined, if a slope is in a critical equilibrium stage for shallow, medium and deep seated landslides. The three investigated landslides are triggered in "high critical" zones according to the classification.

3) The most appropriate methods applied in the present study to investigate the origin and flow paths of groundwater were 1) hydrochemistry, 2) groundwater monitoring in observation wells and 3) electric resistivity tomography monitoring. The combination of hydrogeological and geophysical methods in landslide research is very promising. In some cases it may be impossible to define the origin of groundwater without cost intensive drill holes.

The classification can not exactly predict when and where a rapid landside is triggered or when a permanent landslide experiences a crisis or reactivation. But the classification provides a tool to choose realistic hypotheses for the construction of conceptual hydrogeological models of slopes and landslides. This is a good starting point for more sophisticated methods such as numerical modelling. Furthermore, the classification could provide an easy applicable and economic tool to evaluate landslide susceptibility and mechanisms in entire regions which could improve hazard mapping and support the planning of further investigations and mitigation measures.

Bibliography

AMANN, F.; DONATSCH, G.; BONANOMI, Y.; MOSER, M. (2006) Kinematik und Bewegungsmechanismus der tiefgründigen Instabilität Cuolm Da Vi (Graubünden, Schweiz). *Bull. angew. Geol.*, Volume 11/2:117–131.

ANDERSON, S.P.; DIETRICH, W.E.; MONTGOMERY, D.R.; TORRES, R.; CONRAD, M.E.; LOAGUE, K. (1997) Subsurface flow paths in a steep, unchanneled catchment. *Water Resour. Res.*, Volume 33(12):2637–2653.

ASANO, Y.; UCHIDA, T.; OHTE, N. (2003) Hydrologic and geochemical influences on the dissolved silica concentration in natural water in a steep headwater catchment. *Geochimica et Cosmochimica Acta*, Volume 67(11):1973 – 1989.

ASKARINEJAD, A.; CASINI, F.; KIENZLER, P.; TEYSSEIRE, P.; SPRINGMAN, S. (2010a) Mountain risks: two case histories of landslides induced by artificial rainfall on steep slopes. *Conference 'Mountain Risks: Bringing Science to Society', Florence, Italy, 24.-26.11.2010.*, pages 201–206.

ASKARINEJAD, A. (2009a) First Rüdlingen sprinkling experiment: Volumetric changes and water retention hysteresis. *3rd TRAMM Meeting, 12. November 2009, ETH Zürich.*

ASKARINEJAD, A. (2009b) A method to locate the slip surface and measuring subsurface deformations in slopes. *4th Intern. Young Geotechnical Engineers' Conf., Alexandria, Egypt*, pages 171–174.

ASKARINEJAD, A.; AKCA, D.; SPRINGMAN, S. (2009) The Rüdlingen Landslide Experiment. 17. March 2009 (Film, IGT/IGP/ETH Zürich).

ASKARINEJAD, A.; CASINI, F.; KIENZLER, P.; SPRINGMAN, S. (2010b) Comparison between the in situ and laboratory water retention curves for a silty sand. E. Alonso; A. Gens, editors, *Proceedings of the 5th International Conference on Unsaturated Soils. Barcelona, Spain 6-8 September 2010.*

BADOUX, H.; GABUS, J.; MERCANTON, C. (1990) Geologischer Atlas der Schweiz, 1:25'000, Blatt 1285 Les Diablerets.

BALDERER, W. (1990) Hydrogeologische Charakterisierung der Grundwasservorkommen innerhalb der Molasse der Nordschweiz aufgrund von hydrochemischen und Isotopenuntersuchungen. *Steir. Beitr. z. Hydrogeologie*, Volume 41:35–104.

BERNER, C. (2004a) *Der Bergsturz von Goldau. Geologie, Ausbreitung und Dynamik des grössten historischen Bergsturzes der Schweiz.* Master thesis, ETH Zürich.

BERNER, C. (2004b) Geologisches Gutachten Rufihof Arth SZ, 9. März 2004. Technical report, ETH Zürich.

BERWERT-LOPES, J.; SPICHTIG, F. (2006) Unwetter 22./23. August 2005, Ereignisdokumentation, Bericht.

BEVEN, K.; GERMANN, P. (1982) Macropores and water flow in soils. *Water Resour. Res.*, Volume 18(5):1311–1325.

BEZZOLA, G.; HEGG, C. (2007) Ereignisanalyse Hochwasser 2005, Teil 1 - Prozesse, Schäden und erste Einordnung. Bundesamt für Umwelt BAFU, Eidgenössische Forschungsanstalt WSL. Umwelt-Wissen Nr. 0707.215 S.

BEZZOLA, G.; HEGG, C. (2008) Ereignisanalyse Hochwasser 2005, Teil 2 - Analysen von Prozessen, Massnahmen und gefahrengrundlagen. Bundesamt für Umwelt BAFU, Eidgenössische Forschungsanstalt WSL. Umwelt-Wissen Nr. 0825: 429 S.

BIANCHETTI, G.; CRESTIN, G. (2004) Le glissement de Montagnon (Leytron, canton du Valais, Suisse). *INTERREG*A - Project RISKYDROGEO - Workshop du CREALP à Sion (5-7 Mai 2004)*.

BILGOT, S. (2011) *Coupling Field Methods and Three Dimensional GIS-Based Modelling for Landslide Hazard Assessment and Mapping*. PhD thesis, EPFL.

BISHOP, A. (1959) The principle of effective stress. *Tek. Ukeblad*, Volume 106(39):859–863.

BOGAARD, T.; GUGLIELMI, Y.; MARC, V.; EMBLANCH, C.; BERTRAND, C.; MUDRY, J. (2007) Hydrogeochemistry in landslide research: a review. *Bulletin de la Societe Geologique de France*, Volume 178(2):113–126.

BOLLINGER, D.; HEGG, C.; H.R., K.; LATELTIN, O. (2000) Ursachenanalyse der Hanginstabilitäten 1999. *Bull. angew. Geol.*, Volume 5(1):5–38.

BONNARD, C.; NOVERRAZ, F.; PARRIAUX, A. (1987) Origin of groundwater likely to affect a large landslide. *Proceed. IXe Conférence européenne de Mécanique des sols et fondations, 1987*.

BONNARD, C. (2006) Evaluation et prédiction des mouvements des grands phénomènes d'instabilité de pente. *Bull. angew. Geol.*, Volume 11/2:89–100.

BORGA, M.; DALLA FONTANA, G.; GREGORETTI, C.; MARCHI, L. (2002) Assessment of shallow landsliding by using a physically based model of hillslope stability. *Hydrological Processes*, Volume 16(14):2833–2851.

BORJA, R.; WHITE, J. (2010) Continuum deformation and stability analyses of a steep hillside slope under rainfall infiltration. *Acta Geotechnica*, Volume 5:1–14, 10.1007/s11440-009-0108-1.

BOSCHETTI, T.; CORTECCI, G.; TOSCANI, L.; IACUMIN, P. (2011) Sulfur and oxygen isotope compositions of Upper Triassic sulfates from northern Apennines (Italy): paleogeographic and hydrochemical implications. *Geologica Acta*, Volume 9(2):129–147.

BRAMMER, D.D.; MCDONNELL, J.J. (1996) An Evolving Perceptual Model of Hillslope Flow at the Miami Catchment. *Advances in Hillslope Processes*, Volume 1:35–60.

BROENNIMANN, C.; TACHER, L. (2009) Water related triggering mechanisms of shallow landslides: Numerical modelling of hydraulic flows in slopes verified with filed experiments. *European Geosciences Union General Assembly, Vienna, Austria, 19 -24 April 2009*.

BUDHU, M.; GOBIN, R. (1996) Slope Instability from Ground-Water Seepage. *Journal of Hydraulic Engineering*:415–417.

CALCATERRA, D.; SANTO, A. (2004) The January 10, 1997 Pozzano landslide, Sorrento Peninsula, Italy. *Engineering Geology*, Volume 75(2):181 – 200.

CARVALHO VIEIRA, B.; FERREIRA FERNANDES, N. (2004) Landslides in Rio de Janeiro: The role played by variations in soil hydraulic conductivity. *Hydrological Processes*, Volume 18:791–805.

CASCINI, L.; CALVELLO, M.; G.M., G. (2008a) Modelling the transient groundwater regime for the displacements analysis of slow-moving active landslides. *Chen et al. (eds) © 2008 Taylor & Francis Group, London, ISBN 978-0-415-41196-7.*

CASCINI, L.; CUOMO, S.; GUIDA, D. (2008b) Typical source areas of May 1998 flow-like mass movements in the Campania region, Southern Italy. *Engineering Geology*, Volume 96(3-4):107 – 125.

CASCINI, L.; GULLÀ, G.; GIUSEPPE, S. (2006) Groundwater modelling of a weathered gneissic cover. *Can. Geotech. J.*, Volume 43:1153–1166.

CASINI, F.; JOMMI, C.; SPRINGMAN, S. (2010) A laboratory investigation on an undisturbed silty sand from a slope prone to landsliding. *Granular Matter*, Volume 12:303–316.

CHIGIRA, M. (2002) Geologic factors contributing to landslide generation in a pyroclastic area: August 1998 Nishigo Village, Japan. *Geomorphology*, Volume 46:117–128.

CHING-CHUAN, H.; YIH-JANG, J.; LIH-KANG, H.; JIN-LONG, L. (2009) Internal soil moisture and piezometric responses to rainfall-induced shallow slope failures. *Journal of Hydrology*, Volume 370(1-4):39 – 51.

CLEMENS, T.; HÜCKINGHAUS, D.; LIEDL, R.; SAUTER, M. (1999) Simulation of the development of karst aquifers: the role of the epikarst. *International Journal of Earth Sciences*, Volume 88:157–162.

CLEMENS, T.; HÜCKINGHAUS, D.; SAUTER, M.; LIEDL, R.; TEUTSCH, G. (1997) Modelling the genesis of karst aquifer systems using a coupled reactive network model. *Hard Rock Hydrosystems. Proceedings of Rabat Symposium S2.*

COLOMBO, L. (2009) *Large shear box fro analyzing strength mobilisation in unsaturated conditions.* Master thesis, Politecnico di Milano.

COROMINAS, J.; MOYA, J.; LEDESMA, A.; LLORET, A.; GILI, J. (2005) Prediction of ground displacements and velocities from groundwater level changes at the Vallcebre landslide (Eastern Pyrenees, Spain). *Landslides*, Volume 2:83–96, 10.1007/s10346-005-0049-1.

CRUDEN, D. (1991) A simple definition of a landslide. *Bulletin of the International Association of Engineering Geology*, Volume 43:27–29.

CRUDEN, D.; VARNES, D. (1996) Landslide Types and Processes. *Landslides Investigation and Mitigation (Turner A.K., Schster R.L. eds). Transp. Res. Board Spec. Rep. 247, National Research Council, National Acamedy Press, Washington D.C*:36–75.

DE GAFF, J.V. (1978) Regional Landslide Evaluation: Two Utah Examples. *Environnemental Geology*, Volume 2(4):203–214.

DE MONTETY, V.; MARC, V.; EMBLANCH, C.; MALET, J.P.; BERTRAND, C.; MAQUAIRE, O.; BOGAARD, T. (2007) Identifying the origin of groundwater and flow processes in complex landslides affecting black marls: insights from a hydrochemical survey. *Earth Surface Processes and Landforms*, Volume 32(1):32–48.

DEBIECHE, T.H.; BOGAARD, T.; MARC, V.; EMBLANCH, C.; KRZEMINSKA, D.; MALET, J.P. (2011) Hydrological and hydrochemical processes observed during a large-scale infiltration experiment at Super-Sauze mudslide (France). *Hydrological Processes*, Volume Published online in Wiley Online Library.

DEMANET, D. (2000) *Tomographies 2D et 3D à partir de mesures géophysiques en surface et en forage*. PhD thesis, Université de Liège, Faculté des Sciences Appliquées.

DI CRESCENZO, G.; SANTO, A. (2005) Debris slides-rapid earth flows in the carbonate massifs of the Campania region (Southern Italy): morphological and morphometric data for evaluating triggering susceptibility. *Geomorphology*, Volume 66(1-4):255 – 276.

DILLEY, M. (2005) *Natural disaster hotspots: a global risk analysis*. The World Bank.

DUNCAN, J.; WRIGHT, S. (2005) *Soil Strength and Slope Stability*. John Wiley and Sons, Inc.

DYSLI, M.; STEINER, W. (2011) *Correlations in soil mechanics*. Pressses polytechniques et universitaires romandes.

EBEL, B.; LOAGUE, K.; VANDERKWAAK, J.; DIETRICH, W.; MONTGOMERY, D.; TORRES, R.; ANDERSON, S. (2007) Near-surface hydrologic response for a steep unchanneled catchment near Coos Bay, oregon: 2. Physics-based simulations. *American Journal of Science*, Volume 307:709–748.

EBERHARDT, E.; THURO, K.; LUGINBUEHL, M. (2005) Slope instability mechanismus in dipping interbedded conglomerates and weathered marls - the 1999 Rufi landslide, Switzerland. *Engineering Geology*, Volume 77:35–56.

EINSIEDL, F. (2005) Flow system dynamics and water storage of a fissured-porous karst aquifer characterized by artificial and environmental tracers. *Journal of Hydrology*, Volume 312:312–321.

ENGLER, A. (1919) *Untersuchungen über den Einfluss des Waldes auf den Stand der Gewässer, 12*. Kommissionsverlag von Beer & Cie: Zürich.

EVERETT, A. (1979) Secondary permeability as a possible factor in the origin of debris avalanches associated with heavy rainfall. *Journal of Hydrology*, Volume 43(1-4):347 – 354.

FEISSLI, V. (2010) Géotypes dans les glissements de versants: Pont-Bourquin. Projet ENAC.

FETTER, C. (2001) *Applied hydrogeology*. LinkUpper Saddle River : Prentice Hall.

FIFER BIZJAK, K.; ZUPANCIC, A. (2009) Site and laboratory investigation of the Slano blato landslide. *Engineering Geology*, Volume 105:171–185.

FORD, D.; WILLIAMS, P. (2007) *Karst Hydrogeology and geomorphology:*. John Wiley and Sons, Ltd.

FOURIE, A.; ROWE, D.; BLIGHT, G. (1999) The effect of infiltration on the stability of the slopes of a dry ash dump. *Géotechnique*, Volume 49:1–13.

FRANÇOIS, B.; TACHER, L.; BONNARD, C.; LALOUI, L.; TRIGUERO, V. (2007) Numerical modelling of the hydrogeological and geomechanical behaviour of a large slope movement: The Triesenberg landslide (Liechtenstein). *Canadian Geotechnical Journal*, Volume 44:840–857, sols 02-2007.

GAMBAZZI, F.; SUSKI, B. (2009) Electrical Resistivity Tomography Ruedlingen, Presentation at CCES TRAMM Meeting.

GEOLEP; GEOMOD (2007) Entreprise de correction fluviale du Glissement de La Frasse, Assainissement: Projet d'ouvrage 2006, Modèles hydrogéologiques et géomécaniques. Technical report.

GHIASSIAN, H.; GHAREH, S. (2008) Stability of sandy slopes under seepage conditions. *Landslides*, Volume 5:397–406.

GODT, J.; BAUM, R.; LU, N. (2009) Landsliding in partially saturated materials. *Geophysical Research Letters*, Volume 36:L02403.

GRONDIN, Y.; TURBERG, P.; PARRIAUX, A.; MEULI, R. (2011) Fully 3D measurements of complex rock fracture apertures by X-ray computed tomography. *Geosphere*, Volume (under revision).

GUGLIELMI, Y.; VENGEON, J.; BERTRAND, C.; MURDY, J.; FOLLACCI, J.; GIRAUD, A. (2002) Hydrogeochemistry: an investigation tool to evaluate infiltration into large moving rock masses (case study of La Clapière and Séchilienne alpine landslides). *Bull. Eng. Geol. Env.*, Volume 61:311–324.

GUZZETTI, F.; CARRARA, A.; CARDINALI, M.; REICHENBACH, P. (1999) Landslide hazard evaluation: a review of current techniques and their application in a multi-scale study, Central Italy. *Geomorphology*, Volume 31(1-4):181 – 216.

HANTKE, R. (2006) Geologischer Atlas der Schweiz, 1:25'000, Blatt 1151 Rigi.

HANTKE, R. (1967) Geologische Karte des Kantons Zürich und seiner Nachbargebiete 1:50'000.

HARP, E.L.; WELLS, W.G.; SARMIENTO, J. (1990) Pore pressure response during failure in soils. *Geological Society of America Bulletin*, Volume 102:428–438.

HILKER, N.; BADOUX, A.; HEGG, C. (2009) The Swiss flood and landslide damage database 1972 - 2007. *Natural Hazards and Earth System Science*, Volume 9(3):913–925.

HOEFS, J. (2009) *Stable Isotope Gochemistry. 6th Edition.* Springer Berlin / Heidelberg.

HOEK, E.; BROWN, E. (1997) Practical Estimates of Rock Mass. *Int. J. Rock Mech. Min. Sci.*, Volume 34:1165–1186.

HOELTING, B.; COLDEWEY, W.G. (2009) *Hydrogeologie Einführung in die Allgemeine und Angewandte Hydrogeologie.* Spektrum Akademischer Verlag.

HOFMANN, B.; KNILL, M. (1996) Geochemistry and gneisis of the Lengenbach Pb-Zn-As-Tl-Ba-mineralisation, Binn Valley, Switzerland. *Mineral. Deposita*, Volume 31:319–339.

HUNGR, O.; EVANS, S.; BOVIS, M.; HUTCHINSON, J. (2001) A review of the classification of landslides of the flow type. *Environ. & Eng. Geosci.*, Volume VII (3):221–238.

HUSTRULID, W.A.; MCCARTER, M.K.; VAN ZYL, D.J. (2000) *Slope stability in surface mining.* Society for Mining, Metallurgy, and Exploration, Inc. (SME).

HUTCHINSON, J. (1988) General report: Morphological and geotechnical parameters of landslides in relation to geology and hydrogeology. *State of the art Report. Proc. V Intl. Symposium on Landslides, Lausanne*, Volume 1:3–35.

IVERSON, R.M. (2000) Landslide Triggering by Rain Infiltration. *Water Resour. Res.*, Volume 36:–.

IVERSON, R.M.; MAJOR, J.J. (1986) Groundwater Seepage Vectors and the Potential for Hillslope Failure and Debris Flow Mobilization. *Water Resources Research*, Volume 22(11):1543–1548.

IVERSON, R.; REID, M.; R.G., L. (1997) Debris-Flow Mobilization from Landslides. *Annu. Rev. Earth Plnet. Sci.*, Volume 25:85–138.

JABOYEDOFF, M.; PEDRAZZINI, A.; LOYE, A.; OPPIKOFER, T.; GÜELLIPONS, M.; LOCAT, J. (2009) Earth flow in a complex geological environment: the example of Pont Bourquin, Les Diablerets (Western Switzerland). *Landslide Processes: from geomorphological mapping to dynamic modelling, Strasbourg*, pages 131–137.

JOHNSON, K.; SITAR, N. (1990) Hydrologic conditons leading to debris-flow initiation. *Can. Geotech. J.*, Volume 27:789–801.

JONGMANS, D.; GARAMBOIS, S. (2007) Geophysical investigation of landslides : a review. *Bulletin de la Societe Geologique de France*, Volume 178(2):101–112.

KATSURA, S.; KOSUGI, K.; MIZUTANI, T.; OKUNAKA, S.; MIZUYAMA, T. (2008) Effects of bedrock groundwater on spatial and temporal variations in soil mantle groundwater in a steep granitic headwater catchment. *Water Resour. Res.*, Volume 44(9):W09430–, URL 0.

KATSUYAMA, M.; OHTE, N.; KABEYA, N. (2005) Effects of bedrock permeability on hillslope and riparian groundwater dynamics in a weathered granite catchment. *Water Resour. Res.*, Volume 41(1):W01010–.

KAUER, S. (2010) *Monitoring Soil Moisture Dynamics on a Hillslope Prone to Slide - A Hydrologic Process Study on the Rufiberg Test Site (Switzerland)*. Master thesis, ETH Zürich.

KELLER, B.; BLÄSI, H.; PLATT, N.; MOZLEY, P.; MATTER, A. (1990) Nagra, Technischer Bericht 90-41, Sedimentäre Architektur der Distalen Unteren Süsswassermolasse und ihrer Beziehung zur Diagenese und den petrophysikalischen Eigenschaften am Beispiel der Bohrung Langenthal. Technical report, Geologisches Institut der Universität Bern.

KIENZLER, P. (2008) Overlandflow versus precipitation intensity, Annual TRAMM Meeting, 5. Dec. 2008.

KIENZLER, P.M. (2007) *Experimental study of subsurface stormflow formation*. PhD thesis, ETH Zürich.

KIENZLER, P.M.; NAEF, F. (2008) Subsurface storm flow formation at different hillslopes and implications for the "old water paradox". *Hydrological Processes*, Volume 22(1):104–116.

KIRKBY, M. (1978) *Hillslope Hydrology*. John Wiley and Sons.

KJEKSTAD, O.; HIGHLAND, L. (2009) *Landslides: Disaster Risk Reduction*, chapter Economic and Social Impacts of Landslides.

KOSUGI, K.; KATSURA, S.; KATSUYAMA, M.; MIZUYAMA, T. (2006) Water flow processes in weathered granitic bedrock and their effects on runoff generation in a small headwater catchment. *Water Resour. Res.*, Volume 42(2):W02414–.

KRÄHENBÜHL, S. (2007) *Prévision de la sensibilité locale d'un versant aux mouvements de terrain par l'analyse des indices topographiques, géologiques et hydrogéologiques - Cas du glissement de terrain de Travers (Canton de Neuchâtel, Suisse)*. Master thesis, EPF Lausanne.

LAMBE, W.T.; WHITMAN, R.V. (1979) *Soil Mechanics, SI Version*. John Wiley and Sons.

LATELTIN, O.; TRIPET, J.P.; BOELL, A.; BONNARD, C.; HANSEN, J.; KRUMMENACHER, B.; LOAT, R.; LOUP, B.; ROUILLER, J.D.; SCHNEIDER, J.F.; SCHRENK, K.; SUTER, C.L.; DELLA VALLE, G.; VULLIET, L.; ZUFFI, D. (1997) Naturgefahren, Empfehlungen 1997, Berücksichtigung der Massenbewegungsgefahren bei raumwirksamen Tätigkeiten. Bundesamt für Raumplangung BRP and Bundesamt für Wasserwirtschaft BWW and Bundesamt für Umwelt, Wald und Landschaft BUWAL.

LEROUEIL, S.; VAUNAT, J.; PICARELLI, L.; LOCAT, J.; FAURE, R.; LEE, H. (1996) A geotechnical characterization of slope movements. *Proc. 7th Int. Symp. Landslides, Trondheim*, Volume 1, Balkema, Rotterdam, pages 53–74.

LINIGER, M. (2006) Die Herausforderung der Gefahrenprognose bei Massenbewegungen: Rutsch und Sturzprozesse. *Bull. angew. Geol.*, Volume 22/2:75–88.

LOURENCO, S.D.; SASSA, K.; FUKUOKA, H. (2006) Failure process and hydrologic response of a two layer physical model: Implications for rainfall-induced landslides. *Geomorphology*, Volume 73:115–130.

LOWRIE, W. (2000) *Fundamentals of Geophysics*. Cambridge University Press.

LU, N. (2010) Class handout: Hillslope Hydrology and Stability, November 29th - December 11th 2010, EPFL.

LUTZ, T.; PARRIAUX, A.; TISSIERES, P. (1987) Traçage au Gouffre du Chevrier (Préalpes Vaudoises) et méthode d'identification de l'uranine à faible concentration. *Bulletin du Centre d'hydrogéologie de l'Université de Neuchâtel*, Volume 7.

MAGNIN, O.; BERTRAND, Y. (2005) Guide Sismique réfraction. Technical report, Laboratoire Central des Ponts et Chaussées, 58, boulevard Lefebvre, 75732 Paris Cedex 15.

MAINSANT, G.; LAROSE, E.; BROENNIMANN, C.; JONGMANS, D.; MICHOUD, C.; JABOYEDOFF, M. (2011) Ambient seismic noise to monitor clay landslide: toward failure prediction. *Journal of Geophysical Research*, Volume (under revision).

MANDIA, Y. (1991) *Typologie des aquifèrs evaporitiques du trias dans le bassin lémanique du Rhone (Alpes occidentales)*. PhD thesis, EPF Lausanne.

MARÉCHAL, J.; ETCHEVERRY, D. (2003) The use of 3H and 18O tracers to characterize water inflows in Alpine tunnels. *Applied Geochemistry*, Volume 18:339–351.

MARIES, G. (2011) *Strength and geophysical profiling of a study site at Rufiberg, Canton Schwyz, CH*. Master thesis, Institute of Geophysics and Institute of Geotechnical Engineering, Swiss Federal Institute of Technology Zürich.

MATHEWSON, C.C.; KEATON, J.R.; SANTI, P.M. (1990) Role of Bedrock Ground Water in the Initiation of Debris Flows and Sustained Post-Flow Stream Discharge. *Bulletin of the Association of Engineering Geologists*, Volume XXVII(1):73–83.

MATSUSHI, Y.; MATSUKURA, Y. (2007) Rainfall thresholds for shallow landsliding derived from pressure-head monitoring: cases with permeable and impermeable bedrocks in Boso Peninsula, Japan. *Earth Surface Processes and Landforms*, Volume 32(9):1308–1322.

MATTER, A.; PETERS, T.; BLÄSI, H.; MEYER, J.; ISCHI, H.; MEYER, C. (1988) Nagra, Technischer Bericht 86-01, Sondierbohrung Weiach, Geologie. Technical report, Geologisches Institut der Universität Bern and Mineralogisch-petrographisches Institut der Universität Bern and Geotest AG, Zollokofen.

MATTI, B. (2008) *Geological Heterogeneity in Landslides: Characterization and Flow Modelling*. PhD thesis, EPFL.

McDONNELL, J.; SIVAPALAN, M.; VACHÉ, K.; DUNN, G.; HAGGERTY, R.; HINZ, C.; HOOPER, R.; KIRCHNER, J.; RODERICK, M.; SELKER, J.; WEILER, M. (2007) Moving beyond heterogenity and process complexity: A new vision for watershed hydrology. *Water Resour. Res.*, Volume 43:W07301.

MIKOS, M.; CETINA, M.; BRILLY, M. (2004) Hydrologic conditions responsible for triggering the Stoze landslide, Slovenia. *Engineering Geology*, Volume 73(3-4):193–213.

MONTGOMERY, D.R.; DIETRICH, W.E. (1994) A physically based model for the topographic control on shallow landsliding. *Water Resour. Res.*, Volume 30(4):1153–1171.

MONTGOMERY, D.R.; DIETRICH, W.E.; HEFFNER, J.T. (2002) Piezometric response in shallow bedrock at CB1: Implications for runoff generation and landsliding. *Water Resour. Res.*, Volume 38:–.

MONTGOMERY, D.R.; DIETRICH, W.E.; TORRES, R.; ANDERSON, S.P.; HEFFNER, J.T.; LOAGUE, K. (1997) Hydrologic response of a steep, unchanneled valley to natural and applied rainfall. *Water Resour. Res.*, Volume 33:–.

MONTGOMERY, D.; SCHMIDT, K.; DIETRICH, W.; McKEAN, J. (2009) Instrumental record of debris flow initiation during natural rainfall: Implications for modeling slope stability. *Journal of Geophysical Research*, Volume 114:F01031. 16 p.

NORDSTROM, D.K.; WRIGHT, W.G.; MAST, M.A.; BOVE, D.J.; O., R.R. (2005) Aqueous-Sulfate Stable Isotopes - A Study of Mining - Affected and Undisturbed Acidic Drainage. *Integrated Investigations of Environmental Effects of Historical, Mining in the Animas River Watershed, San Juan County, Colorado, Professional Paper 1651, U.S. Department of the Interior, U.S. Geological Survey*.

NOVERRAZ, F.; BONNARD, C.; DUPRAZ, H.; HUGUENIN, L. (1998) *Grands glissements de versants et climat, Rapport Final PNR 31*.

NUTH, M. (2009) *Constitutive Modelling of Unsaturated Soils with Hydro-Geomechanical Couplings*. PhD thesis, EPFL.

OCHIAI, H.; OKADA, Y.; FURUYA, G.; OKURA, Y.; MATSUI, T.; SAMMORI, T.; TERAJIMA, T.; SASSA, K. (2004) A fluidized landslide on a natural slope by artificial rainfall. *Landslides*, Volume 1:211–219.

ONDA, Y.; KOMATSU, Y.; TSUJIMURA, M.; FUJIHARA, J.i. (2001) The role of subsurface runoff through bedrock on storm flow generation. *Hydrol. Process.*, Volume 15(10):1693–1706.

ONDA, Y.; TSUJIMURA, M.; TABUCHI, H. (2004) The role of subsurface water flow paths on hillslope hydrological processes, landslides and landform development in steep mountains of Japan. *Hydrol. Process.*, Volume 18(4):637–650.

OOSTERBAAN, R.; NIJLAND, H. (1994) *Drainage Principles and Applications*, chapter 12 Determining the saturated hydraulic conductivity. International Institute for Land Reclamation and Improvement (ILRI), Wageningen, The Netherlands, publication 16, second revised edition.

OR, D.; BADOUX, A.; BHANDARI, A.; CANONE, D.; CREMONINO, P.; GÜELL I PONS, M.; HOLLINGER, K.; BARON, L.; KILCHMANN, R.; LEHMANN, P.; LOCHER, D.; SCHWARZ, M.; TACHER, L. (2007) Characterization of the Wiler foield site. Technical report, LASEP, WSL, IGT, UNIL and GEOLEP.

PALACKY, G. (1987) Resistivity characteristics of geological targets. M. Nabighian, editor, *Electromagnetic Methods in Applied Geophysics Investigations in geophysics*, Volume 3, Society of Exploration Geophysicists, Tulsa, OK, pages 53–129.

PARRIAUX, A. (2007) Slope Stability. Lecture Notes.

PARRIAUX, A.; BONNARD, C.; TACHER, L. (2010) *Rutschungen: Hydrogeologie und-Sanierungsmethoden durch Drainage. Leitfaden. Bundesamt für Umwelt, Bern. Umwelt-Wissen Nr.1023: 128 p.*

PARRIAUX, A. (2011) Vulnérabilité des infrastructures géotechniques au changement climatique et mesures d'adaptation selon le contexte géographique. World Road Association. Technical report.

PARRIAUX, A.; TACHER, L.; LOCHER, D.; LALOUI, L.; FERRARI, A.; BONNARD, C. (2008) Geologische, hydrogeologische und geomechanische Modellierung des Erdrutsches bei Stein-Mumpf (AG), Schlussbericht. Technical report, GEOLEP and LMS.

PETLEY, D. (2008) The global occurrence of fatal landslides in 2007. *Geophysical Research Abstracts, Vol. 10., EGU General Assembly 2008.*

PETLEY, D. (2010) An analysis of fatal landslides in the Asia-Pacific region for 2006 to 2008. Dave's Landslide Blog. URL `http://daveslandslideblog.blogspot.com/2010/02/analysis-of-fatal-landslides-in-asia.html`.

PETRASCHECK, A.; BERWERT-LOPES, J.; MANI, P.; ZARN, B. (1998) Ereignisdokumentation Sachseln, Unwetter vom 15. August 1997, In Zusammenarbeit mit dem Tiefbauamt und dem Oberforstamt des Kantons Obwalden.

PETRASCHECK, A.; HEGG, C. (2002) Hochwasser 2000 - Les crues 2000. Ereignisanalyse/Fallbeispiele - Analyse des événements/Cas exemplaires. Berichte des BWG, Serie Wasser. Nr. 2.

POPESCU, M. (1996) From landslide causes to landslides remediation. *Landslides: 7ème Congreès International de l'IAEG/AIGI, Balkema, Rotterdam, Netherland*, pages 75–94.

RICKLI, C. (2001) Vegetationswirkungen und Rutschungen, Untersuchung zum Einfluss der Vegetation auf oberflächennahe Rutschprozesse anhand der Unwetterereignisse in Sachseln OW am 15. August 1997.

RICKLI, C.; BUCHER, H. (2003) Oberflächennahe Rutschungen, ausgelöst durch die Unwetter vom 15.-16.7.2002 im Napfgebiet und vom 31.8.-1.9.2002 im Gebiet Appenzell - Projektbericht zuhanden des Bundesamtes für Wasser und Geologie BWG.

RICKLI, C.; KAMM, S.; BUCHER, H. (2008) Ereignisanalyse Hochwasser 2005, Teilprojekt, Flachgründige Rutschungen, Projektbericht.

ROGERS, N.; SELBY, M. (1980) Mechanisms of shallow translational landsiding during summer rainstorm: North Island, New Zealand. *Geografiska Annaler*, Volume 62 A((1-2)):11–21.

RONCHETTI, F.; BORGATTI, L.; CERVI, F.; GORGONI, C.; PICCININI, L.; VINCENZI, V.; CORSINI, A. (2009) Groundwater processes in a complex landslide, northern Apennines, Italy. *Natural Hazards and Earth System Science*, Volume 9(3):895–904.

SCHOENEICH, P.; TERCIER, J.; HURNI, J.P.; ORCEL, C.; ORCEL, A. (1996) Les crises catastrophiques du glissement des Parchets (Préalpes vaudoises, Suisse): indices d'une augmentation des précipitations extrêmes entre 2000 et 1500 14C BP. *Quaternaire*, Volume 7:97–109.

SCHROTT, L.; SASS, O. (2008) Application of field geophysics in geomorphology: Advances and limitations exemplified by case studies. *Geomorphology*, Volume 93:55–73.

SCHUDEL, B.; BIAGGI, D.; DERVEY, T.; KOZEL, R.; MÜLLER, I.; ROSS, J.H.; SCHINDLER, U. (2002) Einsatz künstlicher Tracer in der Hydrogeologie - Praxishilfe. Berichte des BWG, Serie Geologie Nr. 3. Technical report.

SIDLE, R.C.; OCHIAI, H. (2006) *Landslides: Processes, Prediction, and Land Use*. Number 18 in Water Resources Monograph.

SOILMOISTURE-EQUIPMENT-CORP (2008) *Operating Instructions 2800K1 Guelph Permeameter*. URL http://www.soilmoisture.com.

SOWERS, G. (1979) *Introductory Soil Mechanics and Foundations: Geotechnical Engineering, 4th ed.*

SPRINGMAN, S.; KIENZLER, P.; CASINI, F.; ASKARINEJAD, A. (2009) Landslide triggering experiment in a steep forested slope in Switzerland. M.H. et al., editor, *Proceedings of the 17th International Conference on Soil Mechanics and Geotechnical Engineering*.

SPRINGMAN, S.; MAYOR, P. (2008) *Bodenmechanik. Teil-II. Frühlingssemester 2008*. URL http://geotip.igt.ethz.ch.

SPÖTL, C.; LONGSTAFFE, F.; RAMSEYER, K.; KUNK, M.; WIESHEU, R. (1998) Fluid-rock reactions in an evaporitic mélange, Permian Haselgebirge, Austrian Alps. *Sedimentology*, Volume 45:1019–1044.

TACHER, L. (2010) Hydrogéologie. Haut Ecole d'Ingénierie et de gestion du Canton de Vaud.

TACHER, L.; BONNARD, C.; LALOUI, L.; PARRIAUX, A. (2005) Modelling the behaviour of a large landslide with respect to hydrogeological and geomechanical parameter heterogeneity. *Landslides*, Volume 2:3–14.

TAKE, W.A.; BOLTON, M.D.; WONG, P.C.P.; YEUNG, F.J. (2004) Evaluation of landslide triggering mechanisms in model fill slopes. *Landslides*, Volume 1:173–184, 10.1007/s10346-004-0025-1.

TERZAGHI, K. (1925) *Erdbaumechanik*. Franz Deuticke.

THIELEN, A. (2007) *Einfluss der Bodensättigung aud die Stabiliät von Hängen*. PhD thesis, ETHZ.

THURO, K.; RICK, B.; BOLLINGER, D. (2006) Die Bergstürze am Rossberg und die Massenbewegungen in Folge des Unwetters vom August 2005 - ein Exkursionsfüher. *Bulletin für angewandte Geologie*, Volume 11/2:45–56.

TOPP, G.; DAVIS, J.; ANNAN, A. (1980) Electromagnetic determination soil water content: measurements in coaxial transmission lines. *Water Ressources Research*, Volume 16(3):574–582.

TULLEN, P. (2002) *Méthodes d'analyse du fonctionnement hydrogéologique des versants instables.* PhD thesis, Lausanne.

UCHIDA, T.; ASANO, Y.; OHTE, N.; MIZUYAMA, T. (2003) Seepage area and rate of bedrock groundwater discharge at a granitic unchanneled hillslope. *Water Resour. Res.*, Volume 39(1):1018–.

UCHIDA, T.; KOSUGI, K.; MIZUYAMA, T. (2002) Effects of pipe flow and bedrock groundwater on runoff generation in a steep headwater catchment in Ashiu, central Japan. *Water resources research*, Volume 38(7):24.1–24.14.

UHLENBROOK, S.; SIEBERT, J.; LEIBUNDGUT, C.; RODHE, A. (1999) Prediction uncertainty of conceptual rainfall-runoff models caused by problems to identify model parameters and structure. *Hydrological Sciences Journal*, Volume 44:779–797.

VAN ASCH, T.W.; MALET, J.P.; VAN BEEK, L.P.; AMITRANO, D. (2007) Techniques, issues and advances in numerical modelling of landslide hazard. *Bulletin de la Societe Geologique de France*, Volume 178(2):65–88.

VAN ASCH, T.; BUMA, J.; VAN BEEK, L.P.H. (1999) A view on some hydrological triggering systems in landslides. *Geomorphology*, Volume 30(1-2):25 – 32.

WANG, G.; SASSA, K. (2003) Pore-pressure generation and movement of rainfall-induced landslides: effects of grain size and fine-particle content. *Engineering Geology*, Volume 69(1-2):109 – 125.

WEILER, M.; MCDONNELL, J.J.; TROMP-VAN MEERVELD, I.; UCHIDA, T. (2006) *Subsurface Stormflow.* John Wiley & Sons, Ltd.

WIECZOREK, G. (1996) *Landslides Investigation and Mitigation (Turner A.K., Schster R.L. eds). Transp. Res. Board Spec. Rep. 247, National Research Council, National Acamedy Press, Washington D.C*, chapter Landslide Triggering Mechanisms. pages 76–90.

WILSON, C.; DIETRICH, W. (1987) The contribution of bedrock groundwater flow to storm runoff and high pore pressure development in hollows. *Erosion and Sedimentation in the Pacific Rim (Proceedings of the Corvallis Symposium).*

Appendix A

Additional materials Rüdlingen

A.1 Lithological description of the 23 m-deep drill hole

Figures A.1 and A.2 show the lithological profile of the 23 m-deep drill hole. The profiles include the following parameters: Rock and soil type, strength and consistency of the material, observations of water circulations and joints, estimation of plasticity, and description of colour, components and structure. For the legend of the lithologies see Figure 5.8.

Drillhole RK1

Coordinates: 684'946/269'226   Altitude: 389 m asl   Date: 3.-6. Mars 2009

14 cm diameter, dry drilling

10 cm diameter, wet drilling

Depth	Rock- or Soiltype	Strength (hammer blows), consistency for soils	Water, joints	Plasticity
0m	Sandy silt with little gravel	weak-stiff		
1m	Silty fine-grained sand with rocks			
2m			2.2 m: oxidated, Watercirculation	
3m	Little silty fine-grained sand	very weak		low plasticity
	Fine-/medium-grained sandstone	strong (10 x)	3.9 m: loss of water	
4m		very weak	4.2 - 4.35 m: humid, joint 75°	
5m		very weak		
			5.7 m: strongly oxidated, ochre-reddish layer, 3 cm	
6m				
7m	Medium-grained sandstone	weak	humid	
		strong (4-10 x)		
		very weak	7.6 m: red-orange-ochre oxidated, water circulation	
		extreamly weak		
8m		strong (10x)		
		weak (1-4x)	8.65-8.75 m: vertical joint	
9m	Medium-grained sandstone	weak	humid	
10m				
	Medium-grained sandstone	weak	humid	
		strong (5x)	10.65 - 11m: red, yellow, beige, oxidated	
11m	Medium-grained sandstone	weak	very humid	
12m	Fine-/medium-graine sandstone	weak	very humid	
13m		weak-strong		
			very humid	
14m		very strong		
15m		very strong	humid	
16m	Sandy silt, silty fine-/medium-grained sand	stiff, very weak	little humid	not plastic
17m	Fine-grained sandstone	very strong		
	(Fine-grained sandstone, siltstone)			
18m	Medium-grained sandstone	extremely strong	17.8 - 18.15 m: water loss (joints)	
		extremely strong	18.15 m: water ponds	
	Clayey silt	weak humid	altered, water circulation, brown-red	plastic
19m	Clayey silt, fine-grained sand layers	stiff	Water retaining horizon?	plastic
		strong		
		weak	19.65 m: water ponds	plastic
		weak	orange spots, water circulation	
20m		strong		
		weak-strong		very brittle
		partly very strong	20.5 - 21 m: water loss	less brittle
21m				
	Fine-grained sand and silt	very weak	red spots, very wet, water circulation?	little plastic
22m		stiff	Dry, water retaining horizon?	brittle
				brittle, partly plastic
23m		strong	dry	

Figure A.1: Detailled core descriptions I

Drillhole RK1

Coordinates: 684'946/269'226   Altitude: 389 m asl   Date: 3.-6. Mars 2009

Filling — 14 cm diameter, dry drilling; 10 cm diameter, wet drilling

Depth	Colour	Components (d: diameter), organic matter	Structure, comments
0m	brown	-Sandstone: d=3 cm; -roots, wood	
1m–2m	light brown, dark beige	-Altered greenish sandstone rocks: d=15 cm; -Sandstone pebbles: very angular, some rounded, d=3 cm; 1.2 m: wood	-inhomogeneous, silty or sandy layers; -1.8 m: gray medium-grained sandlayer
3m	dark beige		homogeneous
4m	light gray	Feldspar, quartz, glimmer	homogeneous, horizontal layerig (breaks horizontally)
	dark beige, light brown		no layering, same lithology like gravels in colluvium
5m	brown	Constant grain size	homogeneous, horizontal layering, (breaks horizontally)
7m	dark beige, light brown	Constant grain size	homogeneous, horizontal layering, (breaks horizontally)
	gray	Constant grain size	homogeneous, breaks horizontally
8m			homogeneous, horizontal layering, (breaks horizontally)
9m	brown	Constant grain size	homogeneous, but breaks, crumbles in unstructured parts
10m	brown	Constant grain size; 10.6 - 10.65 m: organic matter, black	homogeneous, but breaks, crumbles in unstructured parts
11m	dark beige	-Constant grain size; -little organic matter, black	very homogeneous, breaks very horizontally in 0.5 - cm thick layers
12m	light brown	Constant grain size	homogeneous, less layered
	light brown		strongly layered
	light brown		homogeneous, less layered
13m	brown		strongly layered
	brown		homogeneous, less layered
14m			massive, compact and less layered
15m	dark beige		less layered
16m	dark olive, dark gray, dark brown		Layers < 1cm of fine-middle sand, crumbles
17m	light gray		massive
	light gray, light green		
18m	dark beige		homogeneous, massive, no layers, well cemented
	light gray		homogeneous, little layered, crumbles
	brown		clayey silt with finesand layers, paleosoil
	red-gray-beige		
19m	beige	Organic matter (black spots)	layered, crumbles, like RKB2
	ochre, greenish		does not crumble
	brown-red		
	ochre-beige		
20m	gray-green, ocre-beige		no layers, crumbles
	gray		
	brown-red, ochre-beige	black spots, especially along micro-fissures	
21m	red, beige		20.5 m: red, iron?
22m	brown-red, orange, dark beige		Finesand layers: rot-ocre-beige, 1-10 cm thick; Silt layers: dark beige, 0.5 cm thick
	beige-red spots, light gray, light beige-orange spots		
23m	dark beige, grey-lihgt		1-cm layers, inhomogeneous
	beige, red spots		

Figure A.2: *Detailed core descriptions II*

A.2 Water pressure data from the 23 m-deep drill hole

Figure A.3 shows the entire pore pressure records from Mars 2009 until summer 2011. During the landslide triggering experiment, no meaningful water pressure variations were monitored (see Figure A.4). Variations in 21.3 m depth are artefacts. Also the rapid variations between 20 and 40 cm recorded in 2.3 m look corrupt. This sensor was installed in the weathered bedrock. It would be surprising, if no groundwater table established in this piezometer as the sprinklers were installed next to the drill hole. It could be that the sensor was installed too high and a temporal groundwater table was formed just below the sensor. Due to efficient draining of permeable weathered sandstone layers or joints, the groundwater level was inhibited to rise. The sensor at 2.3 m depth was removed after the landslide triggering experiment. The other three sensors were kept for two years of monitoring. The 11 March 2011, the water in the observation wells at 18.7 and 21.3 m depth was removed with a hand sampling tool. In the following, the water pressure record will be described for each sensor.
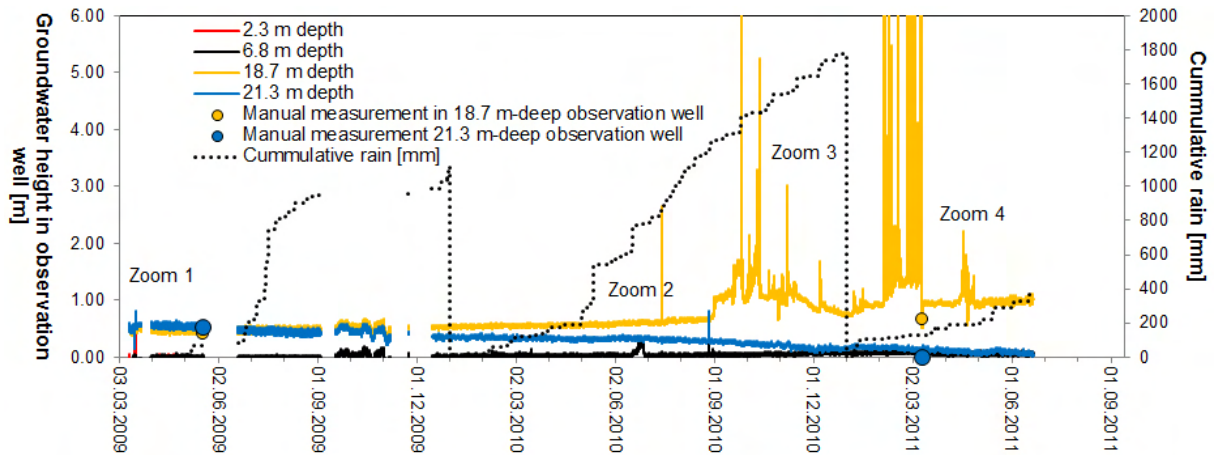
Figure A.3: *Entire record from the water pressure sensors in the 23 m deep drill hole, from March 2009 - August 2011.*

A.2.1 Sensor at 6.8 m depth

The sensor at 6.8 m depth was installed in a non-cemented sandstone layer. No water signals were monitored except for 11 days between 18. - 29.6.2010 (see Zoom 2, Figure A.5). During 5 days, the groundwater pressure was continuously rising up to 14 cm followed by 6 daily pulses up to 32 cm. The peak of those pulses at any one time was reached around midday followed by a drop of up to 13 cm each. After 11 days the pore water pressure value dropped again to 0 m.

It is possible that joints are efficiently draining the groundwater in this layer. Only if the bedrock and the joints are saturated up to this level, groundwater variations can be observed like it as the case end of June 2010. Nevertheless, only a single event was recorded in two years. It is possible that the recorded event was an artefact.

A.2.2 Sensor at 18.3 m depth

The sensor at 18.7 m depth was installed at the interface of the sandstone to the marlstone, because this is a very coloured horizon and the marlstone was assumed to be an impeding layer above which a groundwater table can be formed. The sensor showed a continuous water pressure

of 0.5 m until beginning of September 2010, when it started rising (see Figure A.6. Four periods of fluctuating water table are observed: 1 September - 16 November 2010, 7 - 16 January 2011, 5 February - 11 March 2011 and 17 - 28 April 2011. The water level rose up to 1.5 - 2 m above the sensor (the peaks that rose further are interpreted as artefacts). For several reasons, it was assumed that the data could be corrupt: No correlation with rain events could be made. On the 30 October 2010, a sudden drop and rise in groundwater can be observed. After pumping on the 11 March 2011, the water level remained low (see Figure A.7). Thus interpretations remain very hypothetical.

It is possible that during drilling some clogged fractures in the bedrock were washed out so that they could efficiently drain the bedrock. After 1.5 years, those fractures again clogged (partly) so that a positive pore water pressure could build up above impeding layers. This opening and closing from fractures could also be related to large-scale movements in the bedrock. But this is very hypothetical and will therefore no be discussed in more detail.

A more realistic interpretation is that at the level of 0.5 m above the sensor (water level that was constant for 1.5 years), a fracture is constantly draining the piezometer. The rise in groundwater after pumping the 11 March 2011 showed that groundwater flows into the piezometer. It is possible that it underlies periodical fluctuations. At the location of the test site, the bedrock is draining the unconsolidated sediment. It is very unlikely that the deep groundwater in the bedrock will rise up to the boundary between the bedrock and the unconsolidated sediment und thus it has no effect on the landslide triggering.

A.2.3   Sensor at 21.3 m depth

This sensor is installed in a sandy layer within the marlstone which was orange coloured, indicating water circulations. The measured water table showed a continuous decrease from 0.5 m water pressure after drilling to 0 m water pressure in summer 2011.

This could be water that was trapped after the drilling which was then slowly draining during two years through the very low permeable marlstone. By dividing the water volume which was drained (0.00016 m^3) by the surface of the piezometer tube (0.315 m^2) and the draining time (66700000 sec), a hydraulic conductivity k in the order of magnitude 10^{-12} m/s can be estimated. The water level was confirmed by manual piezometric measurements.
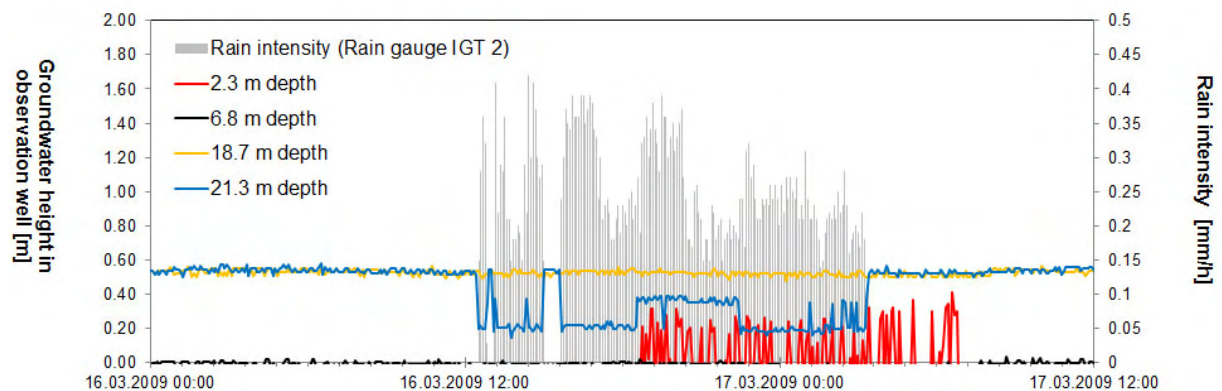
Figure A.4: *Zoom 1: Monitoring in 23 m-deep drill hole during the second sprinkling experiment in March 2009. Acquisition interval was 5 min. The variations recorded in 21.3 and 2.3 m depth are most likely corrupt.*
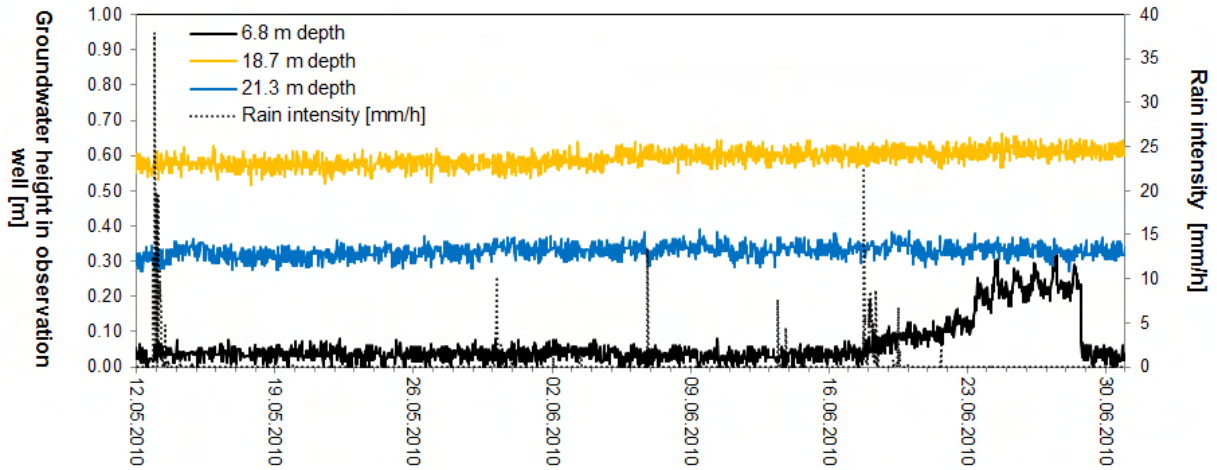
Figure A.5: *Zoom 2: Event recorded in 6.8 m depth at end of June 2010.*
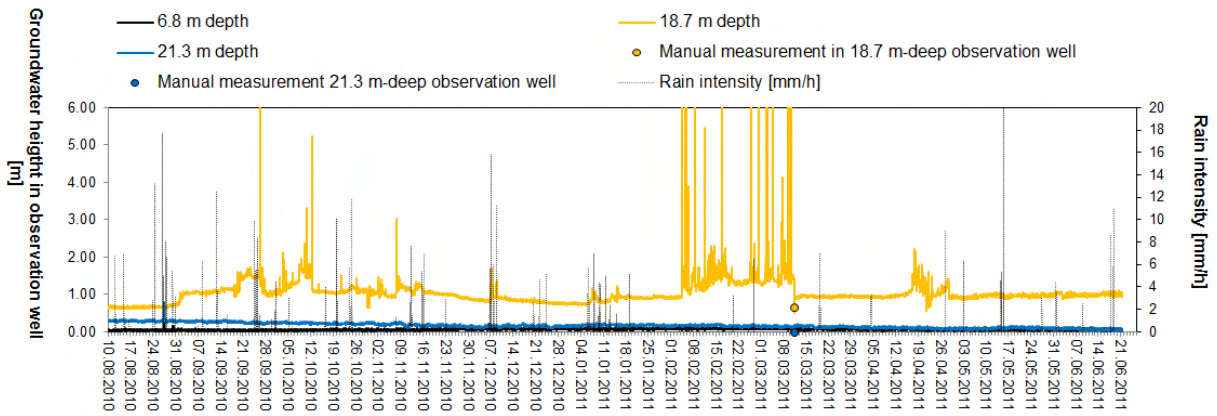
Figure A.6: *Zoom 3: Monitored events August 2010 - June 2011 recorded in 18.7 m depth.*
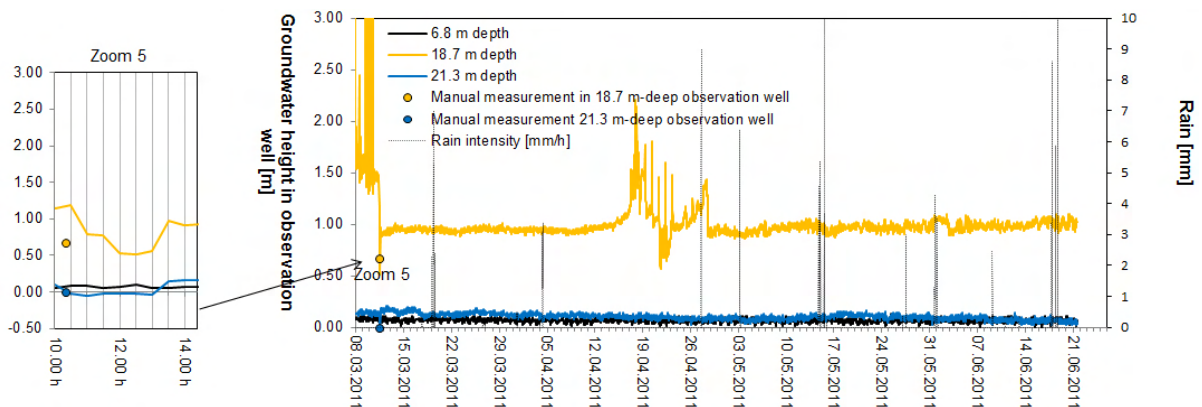
Figure A.7: *Zoom 4: Reaction in 18.7 m deep observation well after pumping test performed on 11.03.2011.*

A.3   Hydrogeochemistry in the drill hole

With a manual water sampler two samples for hydrochemical analyses were extracted from the piezometers at 18 m and 21 m depth. The temperature of the samples was 12.8 °C and the water conductivity was 519 and 699 μS/cm at 18 m and 21 m depth, respectively. Table A.1 shows the concentration of major elements.

The groundwater is rich in HCO_3^- and Ca^{2+}. It is similar to the groundwater of type Ca-(Mg)-HCO3 found in gravel in nearby village Weiach, Canton Aargau, which shows a total mineralisation of 560-623 mg/l and SO_4^{2-} of 23-26 mg/l (Balderer, 1990). The mineralisation of the two water samples is slightly different. The sample from 21.3 m depth contains more Mg^{2+} and NO_3^- than the sample from 18.7 m depth. This leads to the assumption that the two aquifers are not directly connected but separated by an impeding layer. This consists with the observations during drilling. It is possible that the water in the deeper piezometer showed a higher mineralisation because it was stored since the drilling. The higher concentration in Mg^{2+} and NO_3^- could result from magnesium nitrate, which is used as fertilizer. The absence of this component in 18.3 m depth may indicate a shorter residence time of the groundwater than in the deeper piezometer.

Sample depth	Date	Na^+ mg/l	K^+ mg/l	Mg^{2+} mg/l	Ca^{2+} mg/l	F^- mg/l	Cl^- mg/l	NO_3^- mg/l	SO_4^{2-} mg/l	HCO_3^- mg/l	Temp °C	Cond μS/cm
18 m	11.3.211	9.03	4.82	20.30	96.30	0.29	11.05		30.09	366.00	12.9	519
23 m	11.3.211	13.76	6.44	44.60	93.90	0.36	20.12	46.15	32.94	415.00	12.8	699

Table A.1: *Analyses of mayor elements of water samples from the observation well at 18 m and 21 m depth. The different concentrations show that the samples originate from different groundwater.*

A.4 Description of the landslide

During the first experiment, small vertical movements of 0.5 - 5 cm were measured with photogrammetry (Askarinejad, 2009a). The accuracy of the monitored movements is about 1.5 cm. In the horizontal direction, slope upward movements of a few mm could be observed at some points (see Figure A.8). This was interpreted as swelling of the soil. If a soil thickness of 1.5 m is assumed, the maximum swelling was about 3%.

With the photograph from the photogrammetry camera taken during the second experiment (Askarinejad et al., 2009), the landslide movement was described. The first movements initiated at 3:23 h. First a crack opened along the future head scarp of the landslide. Then the movement propagated downwards until it stopped after approximately 20 seconds. The main movement occurred in 10 seconds and was rather translational. The sliding mass initially moved as a single block and reached a velocity >1 m/s, before it hit the topographic bulge in the lower part of the test site. No liquefaction was observed. The triggered landslide was 17 m long and 7-8 m wide. The slip surface was along the weathered bedrock in a depth between 1 and 2 m. The landslide had a volume of 180 m^2 and is classified as an earth-slide.
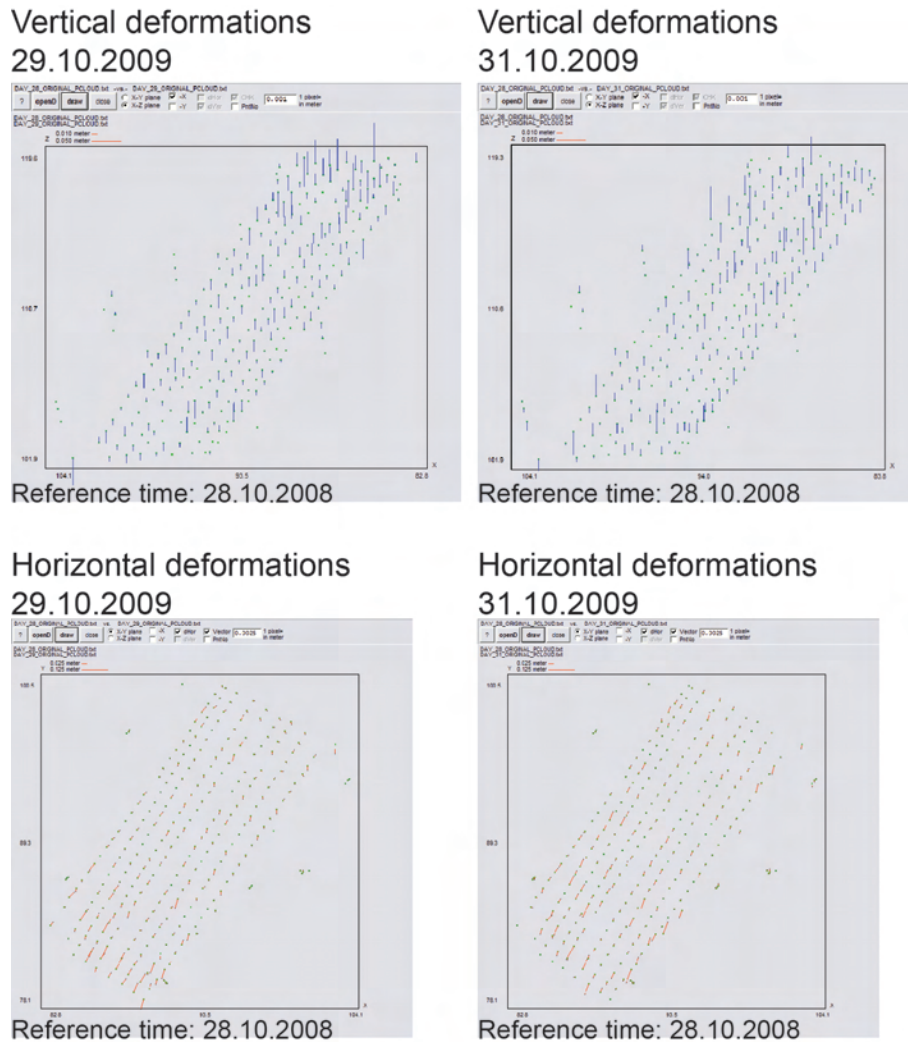
Figure A.8: *Photogrammetry data first experiment. Images from Askarinejad (2009a).*

Appendix B

Additional materials Pont Bourquin

B.1 Protocol seismic refraction

The following table shows the location of the hammer blows and explosives along the three seismic refraction profiles.

Profile name	Blast nr.	Geophone nr.	Distance (m)
Profile P1	1	1	0
	2	4	9
	3	7	18
	4	10	27
	5	13	36
	6	16	45
	7	19	54
	8	22	63
	9	24	72
Profile P3	1	1	0
	2	4	9
	3	7	18
	4	10	27
	5	13	36
	6	16	45
	7	19	54
	8	22	63
	9	24	72
Probile P4	1	2	5
	2	3	10
	3	6	25
	4	9	40
	5	12	55
	6	15	70
	7	18	85
	8	21	100
	9	24	115
	10	27	130
	11	30	145

Table B.1: *Protocol active seismic: Table with all blasts performed along profiles P1, P3 and P4.*

Profile name	Blast nr.	Geophone nr.	Distance (m)
	12	33	160
	13	36	175
	14	39	190
	15	42	205
	16	45	220
	17	48	235
	18	51	250
	19	54	265
	20	57	280
	21	60	295
	22	63	310
	23	66	325
	24	69	340
	25	72	355

Table B.1: *Protocol active seismic: Table with all blasts performed along profiles P1, P3 and P4.*

B.2 Hydrochemical analyses

Nr	Name	Date	Na$^+$ mg/l	K$^+$ mg/l	Mg^{2+} mg/l	Ca^{2+} mg/l	F$^-$ mg/l	Cl$^-$ mg/l	NO$_3^-$ mg/l	SO$_4^{2-}$ mg/l	HCO$_3^-$ mg/l	Si^{4+} mg/l	Sr^{2+} mg/l	Temp °C	Cond μS/cm	pH	Eh mV
		2009															
1.1	Sp25	14.07	1.58	1.32	46.20	216.20		0.80	0.84	452.00	332.70			13.8	1165		
1.2	Sp18	14.07	1.36	1.06	49.00	215.30		0.53	0.35	516.00	274.10			17.4	1099		
2.1	1C	02.09	19.68	3.37	5.90	102.46	0.18	3.87		4.88	383.00			13.6	483		
2.3	PB5	02.09	27.62	34.89	66.00	269.00		1.33		961.79	91.50			11.4	1385		
2.4	Sp25	02.09	19.22	19.19	47.00	188.00	0.14	0.47	0.50	472.38	248.90			14.0	940		
3.2	Sp54	09.10	0.67	0.48	7.02	68.85	0.09	0.71	0.46	27.70	217.90			12.0	314		
3.3	Sp18	09.10	1.78	1.52	75.38	271.51	0.06	1.21	1.03	738.66	254.50			13.1	1256		
4.1	Ch2	03.12	1.36	0.34	1.21	59.16	0.08	0.29	0.17	1.46	187.40				265		
4.2	1A	03.12	5.52	0.31	1.01	14.50	0.08	0.57	0.76	1.38	61.50				84		
4.3	1C	03.12	8.32	1.98	7.66	106.60	0.12	2.37	0.03	5.05	378.30				498		
4.4	1E	03.12	0.94	2.03	2.93	50.50	0.07	1.12	0.30	4.44	170.10				242		
4.5	PB5	03.12	19.06	44.85	46.30	351.40	0.05	0.99	0.10	1099.28	32.82				1703		
4.6	Sp32	03.12	1.43	1.05	73.81	321.90	0.06	0.65	0.33	850.15	298.17				1500		
5.2	1A	23.12	3.99	0.75	1.53	12.63	0.07	1.26	0.79	1.59	51.97			4.6	66		
5.3	1C	23.12	6.13	2.27	6.90	107.20	0.12	2.69	0.05	9.64	372.47			5.5	471		
5.4	1E	23.12	1.12	2.31	3.30	57.40	0.06	1.19	0.05	4.80	192.76			4.4	260		
5.5	PB5	23.12	12.76	36.63	40.40	431.26	0.00	1.25	0.07	1215.32	29.04			7.3	1763		
5.6	Sp32	23.12	1.79	1.33	49.70	245.69	0.00	0.68	1.01	471.27	410.29			6.3	1153		
		2010															
6.1	Ch2	18.01	1.26	0.57	1.10	56.80	0.05	0.89	0.35	2.01	183.10			5.6	241		
6.2	1A	18.01	2.95	0.36	0.93	11.47	0.07	0.92	0.31	1.73	45.60			3.9	71		
6.3	1C	18.01	5.49	1.95	6.30	105.10	0.11	2.69	0.04	10.06	357.60			4.7	484		
6.4	1E	18.01	1.17	2.76	3.10	61.70	0.06	1.24	0.03	4.30	207.60			3.9	288		
6.5	PB5	18.01	10.26	26.73	98.80	433.10	0.03	0.89	0.05	1292.62	225.80			6.8	2080		
6.6	Sp32	18.01	1.75	1.15	41.20	207.85	0.02	0.60	0.77	406.84	294.80			5.1	1155		
7.1	Ch2	23.02	1.27	0.60	1.50	68.80	0.05	0.59	0.23	1.59	215.60			2.4	305		
7.2	1A	23.02	2.02	0.47	1.05	12.20	0.06	1.18	0.39	1.52	43.70			1.4	61.2		
7.3	1C	23.02	4.04	1.77	6.97	106.30	0.09	2.27	0.05	9.06	353.90			2.7	490		
7.4	1E	23.02	1.69	3.34	4.45	63.20	0.08	1.68	0.05	3.34	216.40			2.9	350		
7.5	Sp32	23.02	1.68	1.05	55.93	289.68	0.00	0.62	0.51	596.15	425.40			4.3	1310		

Table B.2: *Chemical water analyses of major ions performed at the laboratory of engineering and environmental geology, EPFL.*

Nr	Name	Date	Na$^+$ mg/l	K$^+$ mg/l	Mg^{2+} mg/l	Ca^{2+} mg/l	F$^-$ mg/l	Cl$^-$ mg/l	NO$_3^-$ mg/l	SO$_4^{2-}$ mg/l	HCO$_3^-$ mg/l	Si^{4+} mg/l	Sr^{2+} mg/l	Temp °C	Cond µS/cm	pH	Eh mV
7.6	PB5	23.02	5.34	14.36	122.50	435.34	0.00	0.99	0.12	1439.68	200.90			1.2	2030		
7.8	Sp18	23.02	1.37	0.87	63.08	264.50	0.00	0.51	0.30	664.74	266.30				1310		
8.1	Ch2	31.03	1.18	5.67	1.00	67.40	0.04	5.67	0.75	1.70	214.10			3.2	290	7.6	
8.1	C27L	31.03	0.60	0.58	24.10	112.90	0.04	0.40	1.00	218.02	192.60			4.0	671		
8.2	1A	31.03	1.68	0.30	0.40	13.40	0.05	0.65	0.50	1.57	47.50			2.5	69	7.4	
8.3	1C	31.03	3.61	1.94	6.00	106.90	0.10	2.41	0.06	9.24	356.10			3.9	487	7.3	
8.4	1E	31.03	1.41	3.97	3.90	65.90	0.07	1.65	0.02	2.05	226.20			3.5	359	6.8	
8.5	PB5	31.03	3.83	9.93	102.69	442.47	0.31	0.71	0.09	1320.19	284.90			4.7	2070	7.3	
8.6	Sp32	31.03	1.16	0.80	28.70	157.30	0.03	0.56	1.03	237.90	325.90			3.3	793	7.4	
8.7	Sp54	31.03	0.52	0.43	8.30	74.60	0.06	0.34	0.84	33.55	231.30			4.9	270	7.5	
9.2	1A	12.05	1.07	0.71	0.00	9.40	0.02	1.33	0.96	2.83	27.00			7.1	43	7.4	
9.3	Ch2	12.05	1.04	0.56	0.60	68.60	0.04	0.89	0.68	0.72	217.00			9.3	281	7.4	
9.4	Sp54	12.05	0.97	1.26	7.40	83.70	0.07	3.32	1.04	34.43	250.00			11.0	373	7.5	
9.5	1C	12.05	3.01	1.60	5.70	105.40	0.09	2.38	0.15	9.77	347.00			8.5	451	7	
9.6	1E	12.05	1.61	6.27	4.10	67.60	0.07	4.98	0.00	1.90	233.00			8.2	363	6.8	
9.7	C44L	12.05	0.58	0.55	5.40	50.20	0.07	0.41	0.51	35.17	138.00			17.7	245	7	
9.8	C36L	12.05	1.45	1.54	39.20	202.40	0.00	1.82	1.94	435.59	258.00			15.5	900	7.1	
9.9	Sp32	12.05	1.29	0.97	36.50	188.80	0.02	0.56	0.82	290.28	383.00			6.2	849	7.1	
9.1	PB5	12.05	2.81	7.97	58.20	288.40	0.00	0.78	0.00	797.28	177.00			8.3	1247	7.2	
10.1	Sp54	02.06	1.01	0.56	6.10	74.00	0.08	1.50	0.97	36.39	212.80			9.8	330		
10.2	C44L	02.06	0.50	0.47	5.80	54.60	0.06	0.16	0.65	33.12	158.00			13.8	305		
10.3	C40L	02.06	0.58	0.57	17.70	97.60	0.05	0.19	1.00	145.00	208.50			12.3	581		
10.4	C36L	02.06	0.76	0.85	31.40	159.00	0.05	0.30	1.24	328.18	232.20			13.2	925		
10.5	Sp32	02.06	1.29	0.91	38.00	209.10	0.02	0.38	1.06	351.13	396.00			7.3	1129		
10.6	C32L	02.06	0.76	0.75	31.00	155.20	0.05	0.33	1.25	326.97	224.50			12.0	896		
10.7	PB5	02.06	3.78	10.59	83.60	401.50	0.08	1.17	0.08	1166.06	240.10			8.1	2050		
10.8	C27L	02.06	0.80	0.83	32.50	155.10	0.06	0.42	1.16	349.39	203.90			11.9	909		
11.1	1A	04.07	0.96	11.09	0.82	8.60		10.00	0.34	4.32	26.80	1.52	0.05	15.5	53	7.0	60
11.2	Sp54	04.07	1.88	5.38	6.40	85.00	0.19	13.92	0.85	34.17	240.80	1.56	0.16	17.0	420	7.4	190
11.3	C44L	04.07	0.87	0.92	11.50	96.80	0.07	0.22	1.02	89.10	245.30	1.04	0.24	19.0	550	7.8	218
11.4	PB39	04.07	1.59	11.77	6.20	102.30	0.15	14.22	5.07	103.88	206.10	1.16	0.36	16.0	478	7.7	255
11.5	Sp32	04.07	1.92	1.32	45.70	242.10		0.40	0.95	423.82	437.10	1.31	0.80	11.0	1344	7.6	254
11.6	PB5	04.07	3.76	11.37	85.97	476.19		1.53		1285.47	316.00	3.02	1.49	10.6	2270	7.7	215
11.7	C12R	05.07	1.79	1.54	57.50	250.30	0.06	0.56		636.82	265.20	0.98	0.50	14.0	1320	7.3	120

Table B.2: *Chemical water analyses of major ions performed at the laboratory of engineering and environmental geology, EPFL.*

Nr	Name	Date	Na$^+$ mg/l	K$^+$ mg/l	Mg^{2+} mg/l	Ca^{2+} mg/l	F$^-$ mg/l	Cl$^-$ mg/l	NO$_3^-$ mg/l	SO$_4^{2-}$ mg/l	HCO$_3^-$ mg/l	Si^{4+} mg/l	Sr^{2+} mg/l	Temp °C	Cond µS/cm	pH	Eh mV
11.8	Sp45M	05.07	1.29	1.40	15.00	111.70	0.16	0.93	0.89	96.06	297.20	0.86	0.29	15.0	600	7.9	124
11.9	C40L	05.07	1.98	1.83	38.20	155.40	0.33	1.64	1.09	359.04	209.20	1.17	0.44	26.0	890	7.9	140
11.1	1E	05.07	2.47	5.20	5.40	72.30	0.17	3.97		15.24	238.90	1.48	0.21	16.0	412	7.6	
11.11	Ch2	05.07	1.91	1.82	2.20	95.00	0.12	2.24	0.18	3.21	305.00	2.00	0.26	15.0	430	7.9	100
12.1	Sp32	28.07	1.78	1.26	48.70	278.30	0.00	0.42	1.01	455.08	484.22	1.11	0.90	10.0	1456	6.8	280
12.2	CrR	28.07	0.75	10.90	5.18	30.20	0.04	10.43	0.39	13.32	102.72	1.25	0.10	10.0	197	7.3	234
12.3	SpA	28.07	0.50	1.12	3.69	25.40	0.04	1.28	0.29	9.19	87.35	1.23	0.06	10.0	154	6.2	268
12.4	Sp49R	28.07	0.93	1.45	19.27	144.40	0.04	0.98	0.15	102.30	401.50	1.49	0.29	12.0	230	6.3	230
13.1	Spr32	19.08	1.60	26.58	47.30	260.00	0.02	23.36	1.14	481.45	440.80		0.83		1360	6.9	284
13.2	CrR	19.08	0.56	5.09	4.80	27.10	0.03	5.42	0.45	14.39	93.30		0.08		169	7.4	256
14.1	Sp49R	25.08	0.99	0.91	18.20	144.70	0.03	0.60	0.25	102.55	409.30		0.23		760	7.14	304
14.2	CrR	25.08	0.68	0.62	5.20	30.70	0.02	0.59	0.48	13.62	107.60		0.08	12.0	188	7.9	392
14.3	Sp32	25.08	1.85	1.48	48.90	272.00	0.02	0.80	1.10	497.05	459.00		0.81	12.3	1426	7.2	310
14.4	Sp25	25.08	1.99	13.74	71.70	390.00	0.00	12.78	0.38	914.10	411.10		0.83	12.0	1932	7.1	305
		2011															
15.1	Sp54	15.03	1.71	0.84	9.60	95.70	0.27	2.42	0.67	50.08	280.00			8.2	464		
15.2	Sp49R	15.03	0.71	0.74	15.40	115.30	0.12	0.49	0.77	106.82	295.60			7.7	558		
15.3	Sp49L	15.03	0.85	1.00	10.90	112.10	0.10	0.52	0.55	57.12	329.00			10.0	527		
15.4	Sp45L	15.03	2.12	1.48	74.00	359.00	0.08	0.90	0.15	775.98	460.67			10.2	1692		
15.5	Sp32	15.03	1.64	1.13	61.10	342.50	0.05	0.40	0.55	671.92	491.29			5.1	1555		
15.6	Sp25	15.03	2.22	1.37	76.50	353.90	0.15	1.53	0.72	918.44	286.58			8.1	1638		
16.1	Sp32	15.04	1.72	1.17	64.42	329.54	0.00	0.50	0.56	619.73	512.60			6.1	1538		
16.2	Sp49R	15.04	0.92	0.90	18.24	120.16	0.00	0.88	0.00	97.21	331.70			8.1	598		
16.3	Sp45L	15.04	1.96	1.45	88.38	407.51	0.00	0.59	0.00	943.99	432.00			9.0	1929		
16.4	Sp54	15.04	0.82	0.51	11.67	87.74	0.09	0.93	1.75	29.21	282.30			8.6	432		
16.5	CrR	15.04	0.69	0.33	5.04	29.62	0.00	0.35	0.74	16.01	93.50			3.2	163		
16.6	Sp25	15.04	1.77	1.28	85.59	402.79	0.00	0.67	0.36	956.84	365.40			7.4	1814		
16.7	Sp18	15.04	1.64	1.13	91.63	344.91	0.00	0.85	1.03	944.60	247.10			8.4	1641		
16.8	PB5	15.04	1.91	2.28	84.76	399.60	0.00	0.92	0.00	950.01	438.80			6.1	1870		
16.9	1E	15.04	1.28	3.55	5.66	63.86	0.06	0.68	0.03	4.83	235.00			5.4	456		
16.1	1C	15.04	2.61	1.60	6.35	104.39	0.14	1.72	0.00	8.37	360.00			6.5	505		
16.11	1A	15.04	0.50	0.00	0.52	6.04	0.09	0.72	0.93	2.44	16.80			5.1	36		
16.12	Ch2	15.04	0.65	0.63	1.72	70.75	0.03	0.35	0.53	0.53	235.00			6.9	330		

Table B.2: Chemical water analyses of major ions performed at the laboratory of engineering and environmental geology, EPFL.

219

B.3   Sulphur isotope analyses

Sample name	Location	Sample date	δ^{34}S measured	δ^{34}S V-CDT
15.5	Spring32	15.03.2011	9.922	9.2
			9.52	8.9
16.1	Spring32	15.04.2011	9.539	9.1
			9.448	9.1
16.2	Spring45M	15.04.2011	4.145	3.8
			4.168	3.9
16.3	Spring45L	15.04.2011	5.227	5.1
			5.88	5.9
16.8	PB5	15.04.2011	10.659	10.9
			10.32	10.6
16.6	Spring25	15.04.2011	9.711	10.1
			9.96	10.5

Table B.3: *Results from $\delta^{34}S$ measurements performed at the Institute of Mineralogy and Geochemistry, University of Lausanne.*

B.4 Manual extensometer measurements
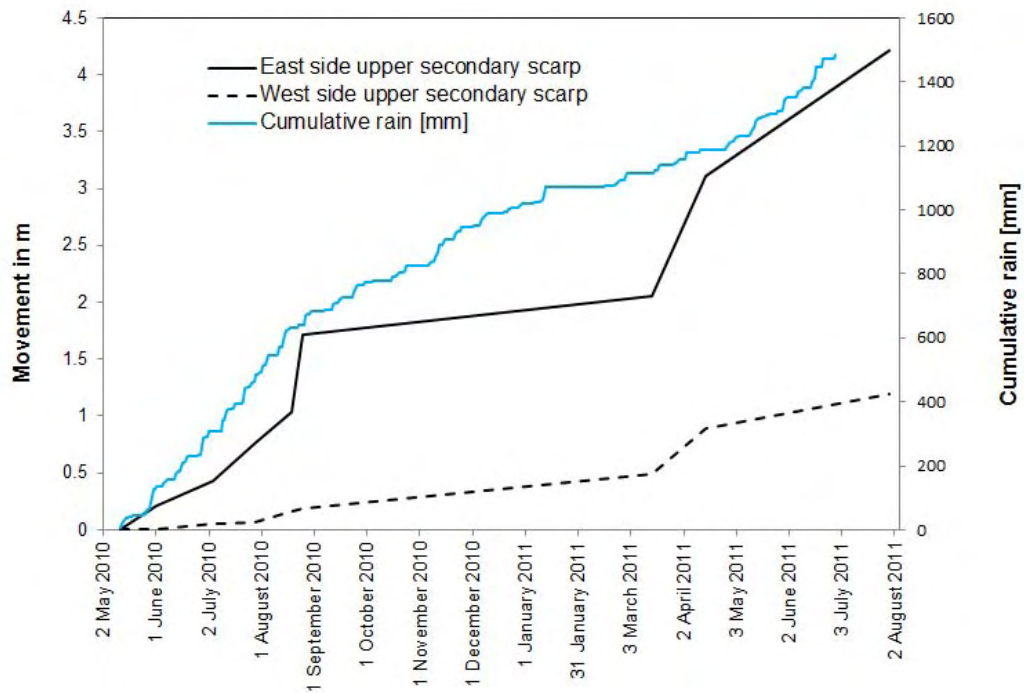
Figure B.1: *Each two rods were installed the western and eastern side of the upper secondary scarp of the Pont Bourquin landslide to measure manually the superficial movement of the Pont Bourquin landslide. In 2010, the landslide accelerated in July after heavy rainfalls and in 2011 in April after snowmelt. For the description of the method, see Section 4.14.*

Appendix C

Additional materials Rufiberg

C.1 Photographs of the drill hole clusters

Figure C.1: *Cluster 1 with boreholes 1 - 3 and Cluster 2 with boreholes 4 - 6. Cluster 2 is located 20 m downslope of cluster 1. Borehole 6 is equipped with 2 piezometers. All others are equipped with 1 piezometer.*

C.2 Hydrogeochemical analyses

Sample	Date	Na^+ mg/l	K^+ mg/l	Mg^{2+} mg/l	Ca^{2+} mg/l	F^- mg/l	Cl^- mg/l	NO_3^- mg/l	SO_4^{2-} mg/l	HCO_3^- mg/l	Temp °C	Cond μS/cm
Spring 17/18	19.05.2010	0.35	0.83	2.00	41.80	0.03	0.42	0.90	1.64	134.80		193
Colluvium	19.05.2010	0.36	0.87	3.30	25.30	0.03	0.24	0.29	1.21	97.20		139
Colluvium	19.05.2010	1.09	0.21	0.40	8.60	0.02	4.07	15.22	3.57	8.66		43
Creek	19.05.2010	0.35	0.53	8.90	51.00	0.04	0.45	4.63	3.45	197.40		271
Spring 17/18	24.11.2010	6.41	62.55	23.00	93.00	0.15	59.88	0.10	22.18	395.00		546
BH1	12.03.2011	17.89	1.93	22.70	84.30	0.17	1.02		16.32	403.10	4.1	563
BH4	12.03.2011	6.61	2.73	9.70	97.00	0.12	7.06	2.76	26.26	321.60	6.7	486
BH5	12.03.2011	5.09	1.29	12.80	81.60		1.22	0.60	9.71	316.20	4.1	427
Spring 17/18	12.03.2011	0.50	0.63	4.00	67.80	0.02	0.48	0.60	1.70	225.70	5.7	303
BH1	02.07.2011	12.70	1.50	21.84	75.79	0.13	0.98		5.81	390.80	8.3	519
BH4	02.07.2011	5.06	2.26	11.84	79.80	0.16	3.52		17.28	279.00	17.2	452
BH5	02.07.2011	3.29	0.92	11.48	66.82	0.11	0.64		4.40	262.00	9	379
Spring 17/18	02.07.2011	0.36	0.54	4.94	63.00	0.06	0.10		1.09	223.38	17.4	327

Table C.1: *Chemical water analyses of major ions.*

CORNELIA BRÖNNIMANN

Address: Dorngasse 4, 3007 Bern
Email: c.broennimann@gmx.net
Mobile: 0041 79 321 45 67
Age: 31, **Nationality:** Swiss

PROFESSIONAL EXPERIENCES

9/2008 – 8/2011   **PhD Thesis and Assistance, Laboratory of Engineering and Environmental Geology, EPF Lausanne, Switzerland**
- Subject of the thesis: Effect of groundwater on landslide triggering
- Geomorphological, geological and hydrogeological mapping of landslides
- Monitoring of landslides, combination of hydrogeological and geophysical methods and laser scanning
- Planning and leading of drilling campaigns in steep terrain
- Installation and realisation of a real-scale landslide triggering experiment
- Numerical groundwater flow modelling
- Assistance for hydrogeological master courses

2/2008 – 6/2008   **Work experience, Ministerio de Minas y Petróleo, Quito, Ecuador in collaboration with Hochschule für Technik, Rapperswil, Switzerland**
- Fieldwork and mapping of landslides around Quito, development of natural hazard maps, computer simulations of landslides, development of sanitation programs
- Become familiar with natural hazards and political difficulties in Ecuador

2/2007 – 2/2008   **Employment, Geology Office Matousek, Baumann und Niggli AG, Baden, Switzerland**
- Planning and realization of historical and technical investigations of contaminated sites (leading fieldwork, writing offers and reports)
- Responsibility for sampling for the national ground water survey project *NAQUA*

12/2006 – 1/2007   **Work experience, GEOTEST AG, Bern, Switzerland**
- Fieldwork along traffic routes and in mountain regions at risk to natural hazards (rock falls, landslides, debris flows)

CONTINUING EDUCATION

11/2011   **Workshop:** Disaster risk reduction in international development, University of Lausanne, Switzerland

2/2011   **Zertifikatslehrgang:** Protection measures against natural hazards, ETHZ, Switzerland

11/2010   **Zertifikatslehrgang:** Field measuring methods and monitoring, ETHZ, Switzerland

6/2010   **Intensive Course:** Mountain Disaster Risk Management, Barcelonnette, France

9/2009   **International School:** Landslide Risk Assessment and Mitigation, Salerno, Italy

8/2009   **International Summer School:** Rockslides and Related Phenomena, Kyrgyzstan

6/2009   **Intensive Course:** Multi-technique landslide investigation for hazard assessment, les Diablerets, Switzerland

Lausanne, November 2011

EDUCATION

10/2006	**Master in Earth sciences, ETH Zurich, Switzerland**
	• Specialisations: Engineering geology, Sedimentology, Structure geology, Petrology
2006	**Master Thesis in Limnogeology: *Climate variability in the younger Holocene – the sediments of Lake Engstlen, Swiss Alps***
	• Evaluation of the work: 6/6
	• Drilling-campaign on the frozen lake, dating of sediment samples, chemical and physical sediment analyses
	• Reconstructions of past climate changes and events such as earthquakes, landslides and heavy rainfalls during the Holocene
1/2006 - 2/2006	**International Research Project in Limnogeology: Environmental changes, Lago Peten-Itza, Guatemala**
	• Responsibility for the organization of the sediment laboratory
	• Analysing first sediment samples during night shift in an international team
9/2004	**Marine research cruise in a Russian team, Mediterranean Sea**
	• Analysing side scan sonar data of Submarine Landslides in the Eivissa Channel
7/2004 – 8/2004	**Geological Mapping, Lukmanierpass, Swiss Alps**
	• Mapping a N-S profile along the structurally complex Piora-Zone

VOLUNTEERING

Since 2007	**Leader for ski touring, Youth Organization of Swiss Alpine Club Section Bern**
	• Organisation and leading of ski touring weekends and camps for young people
10/2000 – 3/2001	**Guide for horse trekking in New Zealand**
	• Responsibility for groups on horse treks

LANGUAGES

German:	Mother Tongue
English:	Advanced (lived and worked for 6 months in New Zealand)
French:	Advanced (lived and worked for three years in Lausanne)
Spanish:	Basic knowledge (lived and worked for 6 months in Ecuador)

IT-KNOWLEDGE

GIS (ArcGIS), MS-Office, Adobe Illustrator/Photoshop, Surfer, RES2DINV, LaTex, Feflow

PRIVATE INTEREST

Mountaineering, hiking, travelling, horse riding

Lausanne, November 2011